



Fakultät für Chemie

# **Novel Silicon Complexes of bidentate *N*-Heterocyclic Imines: Silyliumylidene Ions and Beyond**

**Franziska Hanusch**

Vollständiger Abdruck der von der Fakultät für Chemie der Technischen Universität München zur Erlangung des akademischen Grades einer

**Doktorin der Naturwissenschaften (Dr. rer. nat.)**

genehmigten Dissertation.

Vorsitz: Prof. Dr. Angela Casini

Prüfer\*innen der Dissertation: 1. Prof. Dr. Shigeyoshi Inoue  
2. Priv.-Doz. Dr. Alexander Pöthig

Die Dissertation wurde am 10.01.2022 bei der Technischen Universität München eingereicht und durch die Fakultät für Chemie am 03.03.2022 angenommen.

Diese Arbeit wurde in der Zeit von Februar 2016 bis März 2020 im Rahmen der Professur für Siliciumchemie der Technischen Universität München unter Betreuung von Herrn Prof. Dr. Shigeyoshi Inoue durchgeführt.

## Acknowledgements

Mein erster Dank gilt meinem Doktorvater,

Herrn *Prof. Dr. Shigeyoshi Inoue*,

für die Aufnahme in seine Arbeitsgruppe und die Bereitstellung des Promotionsthemas. Er hat mich mit seiner Leidenschaft für die Hauptgruppenmetallchemie angesteckt und mir die Einarbeitung in das anfangs für mich neue Gebiet mit seiner immer freundlichen und entspannten Art sehr leicht gemacht. Durch sein Vertrauen konnte ich die Arbeiten an meiner Promotion, aber auch darüber hinaus, mit großen Freiheiten gestalten und nicht nur als Chemikerin an den immer neuen Aufgaben wachsen. Danke, dass ich ein Teil dieser Gruppe sein darf, die mir sehr ans Herz gewachsen ist.

Daneben danke ich der gesamten Arbeitsgruppe des AK Inoue für die immer ereignisreiche und spannende Laborzeit. Meinen Freunden und liebsten Kollegen, den „drei von der Tanke“ *Philipp Frisch, Richard Holzner und Dominik Reiter* gebührt ein ganz besonderer Dank. Ohne euch Burschen und das allgegenwärtige „blede Gschwätz“ wäre die Laborzeit nicht mal halb so schön gewesen. Die besten Diskussionen (ob wissenschaftlich oder nicht) und die meiste Hilfe während der letzten vier Jahre kam eindeutig von Euch.

Auch bei der „next generation“ *Lisa Groll, Florian Tschernuth, Teresa Eisner* (und der ‚über-next Generation‘) möchte ich mich für die entspannte Atmosphäre und die vielen kleineren und größeren Späße bedanken. Hier ganz besonders bei meiner Reihenkollegin *Ramona Baierl*. Danke für die vielen Kaffeepausen, Feierabendbiere und Eure Unterstützung.

Als Teil der Kooperation mit der WACKER Chemie AG möchte ich mich selbstverständlich für die immer gute und sehr konstruktive Zusammenarbeit im Rahmen des Projektes bedanken. Die stets unkomplizierte und strukturierte Arbeitsatmosphäre bei Treffen und Symposien war eine große Hilfe bei der Fertigstellung dieser Arbeit. Herrn *Dr. Thomas Renner*, Herrn *Dr. Richard Weidner*, Frau *Dr. Elke Fritz-Langhals*, Herrn *Dr. Jan Tillmann* und Herrn *Dr. Nicklas Wienkenhöver* möchte ich speziell für die zahlreichen fachlichen Diskussionen danken.

Ein zusätzlicher Dank gilt Herrn *Prof. Dr. Dr. h.c. Bernhard Rieger* und *Dr. Carsten Troll* und dem ganzen Team des WACKER-Lehrstuhls für Makromolekulare Chemie für die tatkräftige Unterstützung beim Aufbau unserer Arbeitsgruppe und die vielen technischen Kniffe aber auch für den großzügigen Umgang mit ihrem Equipment.

Natürlich wäre meine Arbeit nicht die, die sie geworden ist ohne die hands-on Hilfe all der guten Geister der Labore. Zuerst einen Dank an meine motivierten und fleißigen Studenten, *Thilo, Florian, Lilly, Leon(1), Leon(2), Elena* und *Tobias*, die mir nicht nur ihre synthetischen Fähigkeiten geliehen haben, sondern auch immer halfen einen neuen Blick auf die Chemie zu werfen. Daneben möchte ich natürlich auch allen danken, die mir in Analyse und Technik geholfen haben: *PD Dr. Alexander Pöthig, Dr. Christian Jandl* und *Dr. Philipp Altmann* für die (Einsteiger-) Ausbildung in Kristallographie und die anhaltende Hilfsbereitschaft, *Frau Ulrike Ammari* für die Messung von Elementaranalysen sowie *Dr. Lorenz Schiegerl, Kevin Frankiewicz* und *Maxi Muhr* für die MS-Messungen. Herrn *Prof. Dominik Munz* und Herrn *Prof. Karsten Meyer* möchte ich für die Unterstützung mit theoretischen Berechnungen und Mößbauer Spektroskopien danken.

Die guten Feen aus allen Administrationen will ich natürlich nicht vergessen. Besonders möchte ich mich hier bei *Manuela Donaubauer* und *Melanie Lorenz* für ihre immer offenen Ohren und ihre Hilfe bedanken.

Nicht zuletzt aber wohl am wichtigsten möchte ich bei all meinen Freunden und meiner ganzen Familie bedanken. Insbesondere bei meinen damaligen Betreuern, die zu guten Freunden wurden - danke *Marianne* und *Thomas*, dass ihr mich für die Chemie so begeistert habt und einen ‚*Bob-der-Baumeister*‘ aus mir gemacht habt.

Den größten Anteil haben natürlich meine Eltern, denn ohne die andauernde Unterstützung meiner Mutter *Gabriele* und meines Vaters *Xaver* wäre das Studium und die abschließende Promotion nicht möglich gewesen. Ihr habt mich auf dem ganzen Weg begleitet, seit ich mir als 7-Jährige in den Kopf gesetzt hatte Wissenschaftlerin zu werden – Danke für Alles.

Meinem Ehemann *Florian* will ich noch darüber hinaus für so Vieles danken. Du hast mich durch das Studium und die Promotion begleitet und mich in der ganzen Zeit durch Deine liebevolle und lebensfrohe Art geerdet und motiviert. Danke für jeden Tag, den wir gemeinsam gegangen sind und noch gehen werden. Du machst mich glücklich.

---

*“We are dwarfs standing on the shoulders of giants so that we can see more and farther than they can – not thanks to our own vision or size, of course, but because the height of the giants lifts us up.”*

*Bernhard von Chartres*

*“~~Hobbits~~ Tretels really are amazing creatures elements. You can learn all there is to know about their ways in a month, and yet after a hundred years they can still surprise you.”*

*Adapted from Gandalf*

## List of Abbreviations

(AT-)IR	Attenuated total reflectance infrared
Ad	1-adamantyl   C <sub>10</sub> H <sub>15</sub>
Ar	aryl
aq.	aqueous
Bbt	2,6-bis[bis(trimethylsilyl)methyl]-4-[tris(trimethylsilyl)methyl]-phenyl   2,6-bis[CH(TMS) <sub>2</sub> ]-4-[C(TMS) <sub>3</sub> ]-C <sub>6</sub> H <sub>2</sub>
bipyr	4,4'-bipyridinyl   (NC <sub>5</sub> H <sub>4</sub> )
Bu	butyl   C <sub>4</sub> H <sub>9</sub>
cAAC	cyclic alkyl amino carbene
cf.	latin confer/conferatur: "compare"
CGMT	Carter-Goddard-Malrieu-Trinquier
cod	cycloocta-1,5-diene   C <sub>8</sub> H <sub>12</sub>
Cp	cyclopentadienyl   C <sub>5</sub> H <sub>5</sub>
Cp*	pentamethylcyclopentadienyl   C <sub>5</sub> Me <sub>5</sub>
δ	chemical shift [ppm]
D	donor
DABCO	1,4-diazabicyclo[2.2.2]octane   N <sub>2</sub> (C <sub>2</sub> H <sub>4</sub> ) <sub>3</sub>
DFB	difluorobenzene   C <sub>6</sub> H <sub>4</sub> F <sub>2</sub>
DFT	density functional theory
Dip	diisopropylphenyl   2,6- <i>i</i> Pr <sub>2</sub> -C <sub>6</sub> H <sub>3</sub>
DMAP	4-dimethylaminopyridine   NC <sub>5</sub> H <sub>4</sub> N(CH <sub>3</sub> ) <sub>2</sub>
DME	dimethoxyethane   CH <sub>3</sub> OCH <sub>2</sub> CH <sub>2</sub> OCH <sub>3</sub>
<i>e.g.</i>	latin exempli gratia: "for example"
EPR	electron paramagnetic resonance
equiv. / eq.	equivalent
ESI-MS	electrospray ionization
etc.	latin et cetera: "and so on"
FLP	frustrated Lewis pair
h	hour
HMBC	heteronuclear multiple bond correlation
HMPA	hexamethylphosphoramide

---

HOMO	highest occupied molecular orbital
<i>i.e.</i>	latin id est: “that is”
IBO	intrinsic bond-orbital
IDip	1,3-bis(2,6-diisopropylphenyl)imidazolin-2-ylidene
IG	invers gated
IMe <sub>2</sub> iPr <sub>2</sub>	1,3-diisopropyl-4,5-dimethylimidazolin-2-ylidene
IMe <sub>4</sub>	1,3,4,5-tetramethylimidazolin-2-ylidene
IMes	1,3-bis(2,4,6-trimethylphenyl)imidazolin-2-ylidene
in situ	latin: “on site”
<i>i</i> Pr	<i>iso</i> -propyl   HC(CH <sub>3</sub> ) <sub>2</sub>
IUPAC	International Union of Pure and Applied Chemistry
KHMDS	potassium(K) hexamethyldisilazide   KN(SiMe <sub>3</sub> ) <sub>2</sub>
λ	wavelength [nm]
L	ligand
LIFDI	liquid injection field desorption ionization
LUMO	lowest unoccupied molecular orbital
M.P.	melting point
Mes	mesityl   2,4,6-Me <sub>3</sub> -C <sub>6</sub> H <sub>2</sub>
min	minute
MS	mass spectrometry
Nacnac	β-diketiminato
Naph	naphthalene   C <sub>10</sub> H <sub>8</sub>
NBO	natural bond order
NHC	<i>N</i> -heterocyclic carbene
NHI	<i>N</i> -heterocyclic imine
NHSi	<i>N</i> -heterocyclic silylene
NMR	nuclear magnetic resonance
OER	oxygen evolution reactions
OTf	triflate   O <sub>3</sub> SCF <sub>3</sub>
OTs	<i>para</i> -toluenesulfonate   O <sub>3</sub> S-C <sub>7</sub> H <sub>7</sub>
Ph	phenyl   C <sub>6</sub> H <sub>5</sub>

---

PIL	phosphorane iminato ligand   $R_3PN^-$
ppm	parts per million
pyr	pyridine   $C_5H_5N$
R	substituent / functional group
red.	reduction
r.t.	room temperature
S/T gap	singlet-triplet gap
SC-XRD	single crystal X-ray diffraction
SOMO	singly occupied molecular orbital
<i>t</i> Bu	<i>tert</i> -butyl   $C(CH_3)_3$
<i>m</i> Ter	<i>meta</i> -terphenyl   <i>meta</i> -dimesitylbenzene   1,3-Mes- $C_6H_4$
THF	tetrahydrofuran   $C_4H_8O$
Tipp	triisopropylphenyl   2,4,6- <i>i</i> Pr <sub>3</sub> - $C_6H_2$
TMS	trimethylsilyl   $Si(CH_3)_3$
vdW	van der Waals
vide supra	latin: "see above"
VSEPR	valence shell electron pair repulsion
vt	variable temperature
WBI	Wiberg bond index
wt%	weight percent
Xant	xanthene   $CH_2(C_6H_4)_2O$

## Publication List

Partial results of the present work have been published in the following articles:

### **A Zwitterionic Heterobimetallic Au–Fe Complex Supported by Bis(*N*-Heterocyclic Imine) Silyliumylidene**

F. Hanusch, D. Munz, J. Sutter, K. Meyer, S. Inoue  
*Angew. Chem. Int. Ed.*, **2021**, *60*, 23274–23280.

### **Modification of bidentate bis(*N*-heterocyclic imine) ligands for low-valent main group complexes**

S. V. Hirmer, F. S. Tschernuth, F. Hanusch, R. Baierl, M. Muhr, S. Inoue  
*Mendeleev Commun.*, **2022**, *32*, 1–4. *Accepted Article*

### **Isolation and Reactivity of Chlorotetryliumylidenes Using a Bidentate Bis(*N*-heterocyclic imine) Ligand**

F. S. Tschernuth, F. Hanusch, T. Szilvási, S. Inoue  
*Organometallics*, **2020**, *39*, 23, 4265–4272.

### **Silyliumylidenes and Silylones: Low-valent Silicon Species in Small Molecule Activation**

S. L. Powley, F. Hanusch and S. Inoue in *Catalysis with Earth-abundant Elements* CHAPTER 10  
*The Royal Society of Chemistry*, **2021**, pp. 284–308.

Publications beyond the scope of this thesis:

### **Isolation of Cyclic Aluminium Polysulfides by Stepwise Sulfurization**

H. Xu, C. Weetman, F. Hanusch, S. Inoue  
*Chem. Eur. J.* **2021**, e202104042.

### **Bis(perfluoropinacolato)silane: A Neutral Silane Lewis Superacid Activates Si–F bonds**

F. Tschernuth, T. Thorwart, L. Greb, F. Hanusch, S. Inoue  
*Angew. Chem. Int. Ed.*, **2021**, *60*, 25799–25803.

### **Application of Ferrocene-Bridged *N*-Heterocyclic Carbene Stabilised Bis-Phosphinidenes in Sn(II) Complexation**

R. Baierl, A. Kostenko, F. Hanusch, S. Inoue  
*Dalton Trans.*, **2021**, *50*, 14842–14848.

### **An Isolable Three-Coordinate Germanone and Its Reactivity**

X. Zhao, T. Szilvási, F. Hanusch, S. Inoue  
*Chem. Eur. J.*, **2021**, *27*, 15914–15917.

### **Recent advances of group 14 dimetallenes and dimetallynes in bond activation and catalysis**

F. Hanusch, L. Groll, S. Inoue  
*Chem. Sci.* **2021**, *12*, 2001–2015.

### **Dialumenes – Aryl vs. Silyl Stabilization for Small Molecule Activation and Catalysis**

C. Weetman, A. Porzelt, P. Bag, F. Hanusch, S. Inoue  
*Chem. Sci.* **2020**, *11*, 4817–4827.

### **An Air-stable Heterobimetallic Si<sub>2</sub>M<sub>2</sub> Tetrahedral Cluster**

G. Dübek, F. Hanusch, D. Munz, S. Inoue  
*Angew. Chem. Int. Ed.* **2020**, *59*, 5823–5829.

### **NHC-Stabilized Silyl-Substituted Chlorosilylene**

G. Dübek, F. Hanusch, S. Inoue  
*Inorg. Chem.* **2019**, *58*, 15700–15704.

**N-Heterocyclic Carbene-Stabilized Germanium and Tin Analogues of Heavier Nitriles: Synthesis, Reactivity, and Catalytic Application**

V. Nesterov, R. Baierl, F. Hanusch, A. E. Ferao, S. Inoue  
*J. Am. Chem. Soc.* **2019**, *141*, 14576-14580.

**NHI- and NHC-Supported Al(III) Hydrides for Amine–Borane Dehydrocoupling Catalysis**

C. Weetman, N. Ito, M. Unno, F. Hanusch, S. Inoue  
*Inorganics* **2019**, *7*, 92.

**Three-Coordinate Boron(III) and Diboron(II) Dications**

D. Franz, T. Szilvási, A. Pöthig, F. Deiser, S. Inoue  
*Chem. Eur. J.* **2018**, *24*, 4283-4288.

**Conference Contributions****A Novel Bis-NHI-Stabilized Silyliumylidene and its Reactivity towards Transition Metals**

F. Hanusch and S. Inoue

Poster (Awarded Poster Price)

The 7th Asian Silicon Symposium (ASIS-7), Singapore, July 2019

**Novel Bis-NHI-Stabilized Tetryliumylidenes and Their Reactivity**

F. Hanusch and S. Inoue

The 9<sup>th</sup> European Silicon Days (ESD), Saarbrücken, Germany, September 2018

## Abstract

Within the last two centuries a plethora of chemical transformations and processes changed the face of our planet in the context of and alongside with the industrialization of the western world. This development brought prosperity and wealth, but also left us with new challenges. In the face of climate change, it is of high importance to re-think and refine processes to reduce costs, toxicity, and the environmental load. Among the most abundant and least toxic elements in the earth's crust, silicon attracted much attention. It offers chemistry way beyond the very stable fourfold coordination and oxidation state of +IV. Ligand stabilized, low valent molecular silicon complexes are promising candidates to find application in novel materials as well as being catalysts for chemical transformations.

The here presented doctoral dissertation thesis concludes the studies on bis-*N*-heterocyclic imine (bis-NHI)-stabilized silicon centered complexes and their reactivity. Whereas different bis-NHIs and one mono-NHI ligands could be synthesized, the 2017 published mesityl-substituted and ethylene bridged bis<sup>Et</sup>-NHI<sup>Mes</sup> (**P0**) was chosen as a work horse throughout the thesis.

In the beginning, several halo-silane and silyliumylidene complexes were isolated and fully characterized. The yielded complexes range from five-coordinated [bis-NHISiH<sub>x</sub>Cl<sub>3-x</sub>][Cl] (x = 0 **P4**, 1 **P5**, 2 **P6**) halosilanes, over the four-coordinated [bis-NHISiH<sub>2</sub>]<sup>2+</sup>2[<sup>-</sup>I] dication (**P7**), to three-coordinated [bis-NHISiX][X] (X = Cl **P1**, Br **P2**) silyliumylidenes.

The main part describes the reactivity of [bis-NHISiCl][X] (X = Cl **P1**, OTf **P3**), that was executed to elucidate the electronic structure of the silyliumylidene as well as its suitability to serve as a ligand in coordination chemistry and as precursor for reduction to novel silicon(0) species. Oxidation with heavier chalcogens yielded selectively the corresponding silaacyliumions [bis-NHISiClE][Cl] (E = S **P8**, Se **P9**, Te **P10**). Furthermore, the <sup>77</sup>Se NMR shift of the selenide complex was used to assess the π-acceptor properties of the silyliumylidene, when acting as a ligand in coordination chemistry. Further conversion enabled the isolation and characterization of group 6 and group 11 complexes [bis-NHISiCIM][X] (M = Cr(CO)<sub>5</sub> **P11**, Mo(CO)<sub>5</sub> **P12**, CuCl **P13**, AgCl **P14**, AuCl **P15**, AuMe **P16**; X = Cl, OTf). From the coinage metal compound **P15**, unusual double anion exchange gave rise to novel heterobimetallic silyliumylidene bis-NHICISiAuFe(CO)<sub>4</sub> (**P17**) as an overall neutral, yet zwitterionic species. The electronic structure of complex **P17** was examined *via* computational and spectroscopic methods, suggesting it to be best described as bis-NHICISi<sup>(II)</sup>→Au<sup>(I)</sup>←Fe<sup>2-</sup>(II)(CO)<sub>4</sub>. Follow up reactivity of the compound was tested and functionalization by chloride exchange was proven possible.

Finally, the direct reduction of **P1** to novel silylone  $L_2Si(0)$  was attempted through reductive dehalogenation. Whereas the free silylone bis-NHISi could not be observed, iron silylone complex bis-NHISiFe(CO)<sub>4</sub> (**P21A**) is hypothesized to form upon reaction with  $K_2Fe(CO)_4$ . The complex has a short lifetime and could not be characterized in the time of this thesis. Intramolecular C–H activation stabilizes the elusive iron silylone, forming an isolable silicon hydride species that could be characterized as bis-NHIHSiFe(CO)<sub>4</sub> complex **P21**. Trapping reaction using  $NH_3BH_3$  and an additional equivalent of  $K_2Fe(CO)_4$  afforded [bis-NHISiHFe][HFe(CO)<sub>4</sub>] (**P22**) further validating the intermediate three-coordinated silylone.

Two additional parts describe reactivity studies of [bis-NHISiCl<sub>3</sub>][Cl] (**P4**), [bis-NHISiH<sub>2</sub>Cl][Cl] (**P6**), and [bis-NHISiH<sub>2</sub>][I]<sub>2</sub> (**P7**) towards HCl abstraction and reductive agents, such as  $K_2Fe(CO)_4$ . Whereas the selectively formed product that stems from **P7** could not be identified unambiguously, the reaction with **P4** resulted in the [bis-NHISiClFe(CO)<sub>4</sub>] silyliumylidene iron complex cation with steerable formation of either <sup>-</sup>Cl (**P24**) or <sup>-</sup>HFe(CO)<sub>4</sub> (**P23**) anion.

## Zusammenfassung

In den letzten zwei Jahrhunderten hat eine Fülle von chemischen Umwandlungen und Prozessen unter anderem im Zuge der Industrialisierung der westlichen Welt das Gesicht unseres Planeten verändert. Diese Entwicklung brachte Wohlstand und Reichtum, stellte uns aber auch vor neue Herausforderungen. Angesichts des Klimawandels ist es von großer Bedeutung, Prozesse zu überdenken und zu verfeinern, um die Kosten, die Toxizität und die Umweltbelastung zu reduzieren. Silizium ist eines der am häufigsten vorkommenden und am wenigsten toxischen Elemente der Erdkruste und hat viel Aufmerksamkeit auf sich gezogen. Es bietet synthetische Möglichkeiten, die weit über die sehr stabile Vierfachkoordination und die Oxidationsstufe +IV hinausgehen. In ligandenstabilisierten und niedrigvalenten Molekülkomplexen ist Silizium ein vielversprechender Kandidat für die Verwendung in neuartigen Materialien sowie als Katalysator für chemische Umwandlungen.

Die hier vorgestellte Dissertation umschließt die Untersuchungen zu Bis-*N*-heterozyklischen Imin (NHI)-stabilisierten siliziumzentrierten Komplexen und deren Reaktivität. Obwohl verschiedene Bis-NHIs und ein Mono-NHI-Ligand synthetisiert werden konnten, wurde der 2017 veröffentlichte Mesityl-substituierte und Ethylen-verbrückte bis<sup>Et</sup>-NHI<sup>Mes</sup> (**P0**) als Arbeitspferd für die gesamte Dissertation gewählt.

Zu Beginn wurden mehrere Halogensilan- und Silyliumylidenkomplexe isoliert und vollständig charakterisiert. Die erhaltenen Komplexe reichen von fünffach koordinierten [bis-NHISiH<sub>x</sub>Cl<sub>3-x</sub>][Cl] (x = 0 **P4**, 1 **P5**, 2 **P6**) Halosilanen über ein vierfach-koordiniertes [bis-NHISiH<sub>2</sub>]<sup>2+</sup>2[I]<sup>-</sup> Dikation (**P7**), bis hin zu dreifach-koordinierten [bis-NHSiX][X] (X = Cl **P1**, Br **P2**) Silyliumylidenen.

Der dritte Teil beschreibt die Reaktivitätsuntersuchungen von [bis-NHSiCl][X] (X = Cl **P1**, OTf **P3**), um die elektronische Struktur des Silyliumylidens sowie seine Eignung als Ligand in der Koordinationschemie und als Vorstufe für die Reduktion zu neuartigen Silicium(0)-Spezies aufzuklären. Die Oxidation mit schwereren Chalkogenen führte selektiv zu den entsprechenden Silaacyliumionen [bis-NHSiClE][Cl] (E = S **P8**, Se **P9**, Te **P10**). Darüber hinaus wurde die <sup>77</sup>Se-NMR-Verschiebung des Selenidkomplexes genutzt, um die π-Akzeptoreigenschaften des Silyliumylidens zu bewerten, wenn es als Ligand in der Koordinationschemie fungiert. Eine weitere Umwandlung ermöglichte die Isolierung und Charakterisierung der Gruppe 6- und Gruppe 11-Komplexe [bis-NHSiCIM][X] (M = Cr(CO)<sub>5</sub> **P11**, Mo(CO)<sub>5</sub> **P12**, CuCl **P13**, AgCl **P14**, AuCl **P15**, AuMe **P16**; X = Cl, OTf). Aus der Münzmetallverbindung **P15** entstand durch ungewöhnlichen doppelten Anionenaustausch das neuartige heterobimetallische Silyliumyliden bis-NHIClSiAuFe(CO)<sub>4</sub> (**P17**) als insgesamt

neutrale, aber zwitterionische Spezies. Die elektronische Struktur dieses Komplexes wurde mittels theoretischen und spektroskopischen Methoden untersucht und lässt sich am besten als  $\text{Bis-NHIClSi}^+(\text{II}) \rightarrow \text{Au}^+(\text{I}) \leftarrow \text{Fe}^{2-}(\text{II})(\text{CO})_4$  beschreiben. Die Anschlussreaktivität der Verbindung wurde getestet und eine Funktionalisierung durch Chloridaustausch erwies sich als möglich.

Schließlich wurde die direkte Reduktion von **P1** zu einem neuartigen Silylon  $\text{L}_2\text{Si}(0)$  durch reduktive Dehalogenierung untersucht. Während das freie Silylon Bis-NHISi nicht beobachtet werden konnte, wird angenommen, dass sich der Eisensilylon-Komplex  $\text{Bis-NHISiFe}(\text{CO})_4$  (**P21A**) bei der Reaktion mit  $\text{K}_2\text{Fe}(\text{CO})_4$  bildet. Der Komplex hat eine kurze Lebensdauer und konnte im Rahmen dieser Arbeit nicht charakterisiert werden. Eine intramolekulare C–H-Aktivierung stabilisiert das schwer fassbare Eisensilylon und bildet eine isolierbare Siliciumhydrid-Spezies, die als  $\text{bis-NHIHSiFe}(\text{CO})_4$  (**P21**) charakterisiert werden konnte. Die Abfangreaktion mit  $\text{NH}_3\text{BH}_3$  und einem zusätzlichen Äquivalent  $\text{K}_2\text{Fe}(\text{CO})_4$  ergab  $[\text{bis-NHISiHFe}][\text{HFe}(\text{CO})_4]$  (**P22**), wodurch die Bildung des intermediären dreifach koordinierten Silylon weiter untermauert wurde.

Zwei weitere Teile beschreiben Reaktivitätsstudien an  $[\text{bis-NHISiCl}_3][\text{Cl}]$  (**P4**),  $[\text{bis-NHISiH}_2\text{Cl}][\text{Cl}]$  (**P6**), und  $[\text{bis-NHISiH}_2][\text{I}]_2$  (**P7**) zu HCl-Abstraktion und gegenüber Reduktionsmitteln wie  $\text{K}_2\text{Fe}(\text{CO})_4$ . Während das selektiv gebildete Produkt aus **P7** nicht eindeutig identifiziert werden konnte, ergab die Reaktion mit **P4** das Silyliumyliden-Eisenkomplekation  $[\text{bis-NHISiClFe}(\text{CO})_4]$  mit steuerbarer Bildung von entweder dem  $^-\text{Cl}$  (**P24**) oder  $^-\text{HFe}(\text{CO})_4$ -Anion (**P23**).

## Table of Contents

Acknowledgements.....	I
List of Abbreviations.....	IV
Publication List.....	VII
Abstract.....	IX
Zusammenfassung.....	XI
Table of Contents.....	XIII
1 Introduction .....	1
2 State of the Art .....	3
2.1 <i>N</i> -Heterocyclic Carbenes (NHC) and Imines (NHI).....	3
2.2 Low Coordinate Silicon Species – Fundamentals .....	10
2.3 Silyliumylidenes and Silylones.....	16
2.3.1 Silyliumylidene Ions.....	16
2.3.2 Silylones.....	26
2.3.3 Silyliumylidene and Silylone Metal Complexes.....	37
3 Scope of this Work .....	42
4 Results and Discussion.....	45
4.1 Ligand Synthesis.....	45
4.2 Synthesis and Characterization of bis-NHI-stabilized Silyliumylidenes and Halosilane Complexes.....	47
4.3 Chemistry of bis <sup>Et</sup> -NHI <sup>Mes</sup> SiH <sub>2</sub> X <sub>2</sub> ( <b>P6</b> X = Cl, <b>P7</b> X = I).....	59
4.4 Chemistry of bis <sup>Et</sup> -NHI <sup>Mes</sup> SiCl <sub>2</sub> ( <b>P1</b> ) .....	62
4.4.1 Chalcogens .....	62
4.4.2 Transition metals of Group 12, 10, and 8 .....	66
4.4.3 Transition metals of Group 6.....	67
4.4.4 Transition metals of Group 11 .....	69
4.4.5 Heterobimetallic Silyliumylidene complex bis <sup>Et</sup> -NHI <sup>Mes</sup> ClSiAuFe(CO) <sub>4</sub> ( <b>P17</b> ).....	73
4.4.6 Silylone metal complexes.....	86
4.5 Chemistry of bis <sup>Et</sup> -NHI <sup>Mes</sup> SiCl <sub>4</sub> ( <b>P4</b> ) .....	92
5 Conclusion.....	95
6 Experimental.....	100
7 References .....	122
8 Appendix .....	XIV

## 1 Introduction

Over the last centuries, the advances in chemical science and industry have changed the face of our world. Among the most groundbreaking developments is the high richness of fine chemicals and tailor-made structures in organic- and pharmaceutical chemistry that offer excellent materials for industrial application and everyday life. Organometallic chemistry has grown and evolved in tandem with the ever-increasing demands on structures, purities, and economical efficiency of stock and fine chemicals. Beyond the pure academic eager, organometallic complexes of transition metals have early shown their potential to serve as catalysts in chemical conversions and became quickly indispensable. To date, precious metal catalysts are appreciated for their versatility, reactivity, and high selectivity. Yet, due to drawbacks such as high cost, limited availability, or toxicity, alternative solutions are increasingly sought.

Since the 1980s it became more and more clear that the main group elements are not only by far more abundant than precious transition metals and established part of inanimate nature but could also be brought in unusual coordination and oxidation states, making them main actors in novel classes of reactive organometallic complexes. This so-called renaissance of main group chemistry started with three major reports by West,<sup>[1]</sup> Yoshifuji,<sup>[2]</sup> and Brook<sup>[3]</sup> who were able to stabilize multiply bonded p-block elements in the key compounds  $\text{Me}_2\text{Si}=\text{SiMe}_2$ ,  $2,4,6\text{-}(t\text{Bu})_3\text{-C}_6\text{H}_2\text{-P}=\text{P-}2,4,6\text{-}(t\text{Bu})_3\text{-C}_6\text{H}_2$ , and  $(\text{Me}_3\text{Si})_2\text{Si}=\text{C}(\text{OSiMe}_3)\text{Ad}$  (Ad = 1-adamantyl). These findings disproved the so-called “double-bond-rule”<sup>[4,5]</sup> and opened the door for a today booming research area. When the main group elements revealed their secrets, it became clear that their reactivity is not as limited as was thought when only their most stable oxidation states were considered.

The accessible *d*-orbitals, that put the magic into transition metal chemistry, are lacking in p-block complexes. Therefore, their stabilization is more challenging, but not impossible. One look into well-known principles of organic chemistry demonstrates the importance of *s*- and *p*-orbitals and their ability to hybridize. In direct comparison carbon shows by far the most efficient hybridization, due to its rather low atomic radius and repulsion of the inner electron shells. Going down group 14 the hybridization ability fades tremendously – this trend is the explanatory fundament of the disproven “double-bond-rule”.<sup>[4,6]</sup>

Regardless, many milestones in modern main group chemistry were reached within the past four decades and it is clearly debatable, which ones are the most striking or the most important. Even if one focuses only on low-valent complexes of p-block elements, the realized range of unusual bondings, electronic structures and surprising reactivities, is outstanding.<sup>[7]</sup>

Actually, one can say that the p-block elements are able to mimic the reactivities of transition metals, engaging in small molecule and bond activation, redox catalysis and even hypervalent coordination catalysis.<sup>[8,9]</sup> Within the p-block elements, group 14 and silicon in particular sparks major interest. Firstly because of its lightest sibling carbon and its special position in organic chemistry, secondly because of the passage from non-metal (C) *via* the semi-metals (Si, Ge) to metals (Sn, Pb). Additionally, silicon features a high natural abundance and non-toxic nature.

For these reasons, among others, silicon is often considered the most promising candidate to take on the challenge between the stabilization of low valent complexes and maintaining the highest possible reactivity. Although, there has been great progress in organosilicon chemistry (e.g. the recent leap of a silyliumylidene complex into industrially relevant applicability<sup>[10,11]</sup>), the field is still in its beginning and requires close study.

## 2 State of the Art

### 2.1 N-Heterocyclic Carbenes (NHC) and Imines (NHI)

#### Carbenes

Since their earliest mention in the first half of the 19th century, carbenes have matured from an obscure, unprovable idea, through detectable but elusive transitional states in the 1950s, to the cornerstone of the new synthetic era that we are part of today.<sup>[12]</sup> The great attention is based on the highly reactive electronic nature of a divalent carbon that possesses an electron sextet ( $R_2C:$ ). In consequence, a stereochemically lone pair of electrons dominates the reactivity of carbenes. Due to the hybridized  $sp^2$ - $p$ -orbital structure of the carbon atom, carbenes can exist in two distinct electronic ground states. Although the parent methylene ( $H_2C:$ ) occupies the triplet ground state with two unpaired electrons in the  $sp^2$  and  $p$ -orbital, carbenes can be transformed comparatively easily into the singlet state by modifying the energetic position of the orbitals. Electronegative and/or  $\pi$ -donating heteroatoms in adjacent position to the carbene carbon, for example, increase the  $sp^2$ - $p$ -orbital separation (Figure 1). The same effect can be achieved by shrinking the R–C–R angle. As soon as the spin pairing energy is less than the  $sp^2$ - $p$ -orbital separation energy, the singlet state is preferred.<sup>[13]</sup>

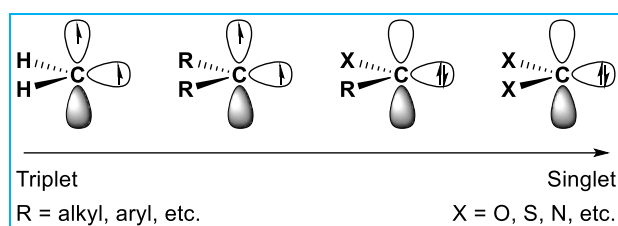


Figure 1: General representation with approximated frontier orbitals of carbenes arranged according to their electronic ground state.

Understanding of the electronic nature is crucial for a deeper understanding of the reactivity of carbenes, however it lagged behind the experimental isolation of the first carbene transition metal complexes. Whereas the first complex of a singlet carbene was isolated already in 1925 (surprisingly without recognizing its carbene nature) as Chugaev's salt<sup>[14]</sup>  $[PtC_8H_{15}N_6]_xCl_x$  (**A**), the breakthrough of the carbene chemistry was sought after 40 more years until the age of Fischer and Schrock carbenes started (Figure 2).<sup>[15]</sup> Ernst Otto Fischer and Richard Royce Schrock could isolate the first transition metal coordination complexes of otherwise elusive singlet (Fischer) and triplet (Schrock) carbenes and became namesakes of the chemistry.

This class of transition metal complexes, often represented by the seminal structures  $(CO)_5W=CMe(OMe)$ <sup>[16]</sup> (**B**) and  $(tBuCH_2)_3Ta=CH(tBu)$ <sup>[17]</sup> (**C**), differ substantially in reactivity according to the electronic ground state of the carbene.

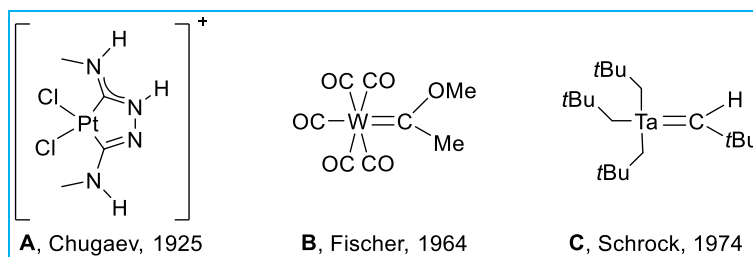


Figure 2: Selected early carbene transition metal complexes.

The singlet carbene donates to the metal center *via* the electron lone pair ( $\sigma$ -donation) and receives  $\pi$ -back donation into the vacant p-orbital. Therefore, electrophilic Fischer carbenes (like **B**) are relatively stable and inert, so that they are mainly found in optical and sensing applications. In contrast, the less stable and nucleophilic Schrock carbenes (like **C**) have been firmly established in catalytic olefin metathesis, for which Schrock (**D**) and Grubbs (**E**) were honored with the Nobel Prize in 2005 (Figure 3).<sup>[18]</sup> The bonding can be described as a triplet-triplet interaction between the metal and the carbene.

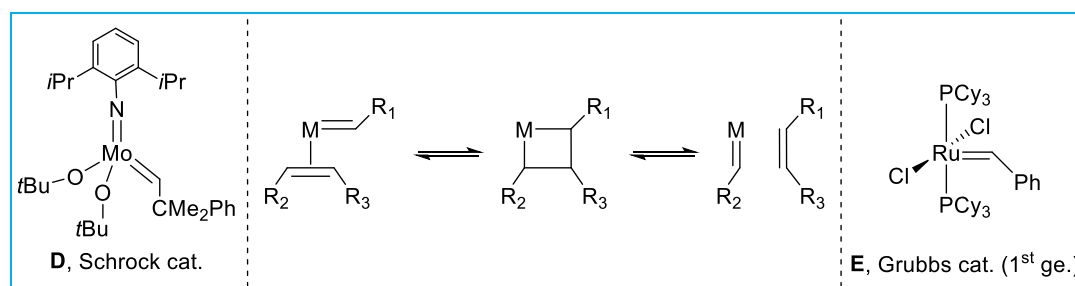


Figure 3: General representation of the catalytic olefin metathesis using Schrock and Grubbs catalysts.

As the chemistry of carbene metal complexes already flourished, persistent carbenes still remained elusive until the early 1990s. Certainly, the early findings regarding the Wanzlick equilibrium in 1960 were promising: *Via* vacuum pyrolysis of 2-trichloromethyl dihydroimidazole derivatives, imidazole-2-ylidene dimers **F** could be generated and the presence of small amounts of the monomeric form **F'** was proposed by reactivity studies (Figure 4, top).<sup>[19]</sup> However, isolation of a stable and 'free' carbene was not achieved until 1988, when Bertrand published the distillable phosphinocarbene **G**<sup>[20]</sup> and shortly after, when Arduengo succeeded in the crystallization of adamantly substituted imidazole-2-ylidene **H**<sup>[21]</sup> (Figure 4, bottom).

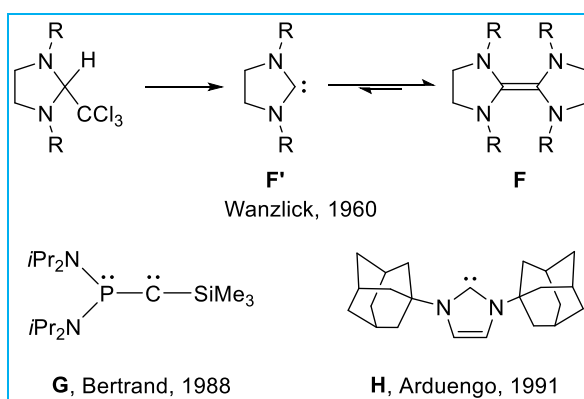


Figure 4. Milestones in carbene chemistry: First isolated persistent carbenes.

In fact, the ‘Arduengo-carbene’ should arouse great interest: It showed that a free carbene could not only be isolated and characterized, but that it could be conveniently prepared in moderate to high scales and stored under inert conditions for long terms. Within no time, the range of so-called NHCs (*N*-heterocyclic carbenes) was extended and their chemistry investigated.

#### NHCs – very special carbenes

Today NHCs are a widely applied and well understood class of ligands that offer not ending possibilities of electronic as well as steric design. In general, they are considered as being a special class of carbenes that are structurally as well as electronically related to Fischer carbene ligands. While the term ‘NHC’ refers to a range of structurally rather diverse carbenes that bear a cyclic design and at least one nitrogen heteroatom, organometallic chemists tend to use it in particular for the so-called ‘Arduengo-type’ imidazoline-2-ylidenes.<sup>[22]</sup> In a 5-membered cyclic core, the carbene carbon is flanked by two adjacent nitrogen intramolecular donor atoms that stabilize the central carbon atom in the formal oxidation state +II (Figure 5).

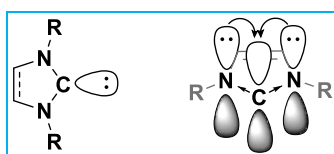


Figure 5. Ground state multiplicity and approximation of frontier orbitals of (Arduengo-type) *N*-heterocyclic carbenes. R = alkyl- or aryl substituent.

Steric protection in varying scaling is gained by two substituents (R; Figure 5) at the nitrogen atoms in 1 and 3 position as well as optional additional substituents on the backbone carbons in 4 and 5 position. The substituents are chosen according to the degree of sterically shielding, and electronically properties to exert the desired effects on possible central atoms. Since the first isolation of so-called ‘bottleable’ carbenes, NHCs have turned the face of metalorganic chemistry tremendously and have made it possible to synthesize easily storable

but still powerful catalysts.<sup>[23]</sup> Nevertheless, they already found widespread application besides being ligands for transition metals and f-block elements: They are valued as organocatalysts and also act as Lewis base ligands in many main group complexes stabilizing otherwise elusive species.<sup>[24]</sup>

The well-balanced counterplay of strong  $\sigma$ -donor ability and possible  $\pi$ -back donation allowed the stabilization of many 'novel' and 'first-of-their-kind' main group species and bonding motifs, that have been reviewed a number of times.<sup>[24]</sup> Here, only some selected examples of NHC-stabilized main group compounds can and should be mentioned. Quite stunningly, in 2008 Robinson observed the first 'naked'  $\text{Si}_2$ -unit with NHC stabilization ( $\text{NHC} \rightarrow \text{:Si}=\text{Si} \leftarrow \text{NHC}$ , **K**) that is considered being the first successful (molecular)  $\text{Si}(0)$  isolation.<sup>[25]</sup> From that point on, species like  $\text{NHC} \rightarrow \text{SiX}_2$  (**M**, X = halogen)<sup>[26-28]</sup> and other reactive monomeric compounds such as bis-NHC  $\rightarrow \text{:Si}$ : (**44**)<sup>[29]</sup> or  $\text{NHC}_2 \rightarrow \text{HSi}^+$  (**9**)<sup>[30]</sup> became accessible. Apart from silicon and group 14, NHC-stabilization gave rise to group 13 multiple bonds (e.g.  $\text{NHC} \rightarrow \text{HB}=\text{BH} \leftarrow \text{NHC}$ , **I**;  $\text{NHC} \rightarrow \text{B} \equiv \text{B} \leftarrow \text{NHC}$ , **N**; and  $(\text{NHC})\text{RAI}=\text{AIR}(\text{NHC})$ , **J**), a stabilized parent borylene ( $\text{NHC} \rightarrow \text{HB} \leftarrow \text{NHC}$ , **L**) and a group 15 formal triple bond ( $\text{NHC} \rightarrow \text{P} \equiv \text{P} \leftarrow \text{NHC}$ , **O**), beyond others.<sup>[24]</sup>

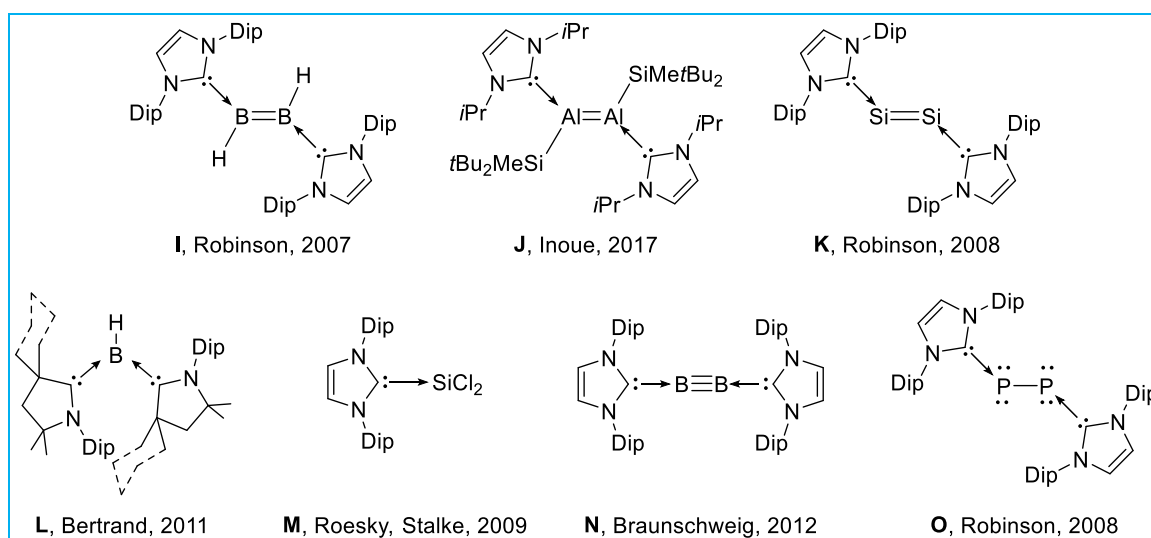


Figure 6. Selected examples of NHC- and cAAC-stabilized low-valent p-block complexes.

### NHI – the stronger donors

In the animate life there are countless processes that involve the coordination of N-based ligands at various metal centers, with hemoglobin being only one, but a striking example. As nature has always served as a good model for synthetic chemistry, it is not surprising that the relative strength and coordinative flexibility of nitrogen has been exploited again and again. When NHCs are extended with an exocyclic nitrogen atom, they form imidazoline-2-imines,

the so-called *N*-heterocyclic imines (NHI).<sup>[31]</sup> In respect to NHC, the properties of these compounds, of course, change drastically. Nitrogen is known for its strong coordinative nature, showing a rather high electronegativity and donor strength, due to the lone pair that is formed in  $sp^3$ - or  $sp^2$ -orbital configuration of trivalent nitrogen-compounds like amines and imines, respectively.

The concept of using iminato-type ligands in organometallic main group- or transition metal chemistry was known before NHI found application. Phosphorane iminato ligands (PILs)  $R_3PN^-$ , for example, are known since 1970, when triphenylphosphine and molybdenum (or tungsten) nitride chloride were boiled in dichloromethane, yielding  $M(NPPh_3)Cl_3$  ( $M = Mo, W$ ).<sup>[32]</sup> The field flourished and produced a large number of structurally diverse transition metal complexes within the next decades. In the beginning of the new millennium, PILs had found also vivid interest in main group chemistry and were reviewed by Dehnicke and Weller.<sup>[33]</sup> Among the most used starting materials for the coordination chemistry of phosphorane imines is the TMS adduct  $R_3P=N-SiMe_3$ . It can be formed from  $Me_3SiN_3$  and  $PR_3$  by Staudinger-type reaction. Actually, this spans the bridge back to NHI, that are also readily available *via* an analogue strategy.<sup>[34]</sup>

NHI and PIL are isoelectronic and can be considered as monodentate but isolobal cyclopentadienyl (Cp) analogues.<sup>[34]</sup> However, obviously the bonding modes and nature are not directly comparable. The iminato ligands show surprisingly short M–N bonds that are interpreted as  $\sigma$ -single bonds, reinforced by polar bond shares. Nevertheless, the mesomeric structures shown in Figure 7 are useful to map the bonding situation on metal centers properly.

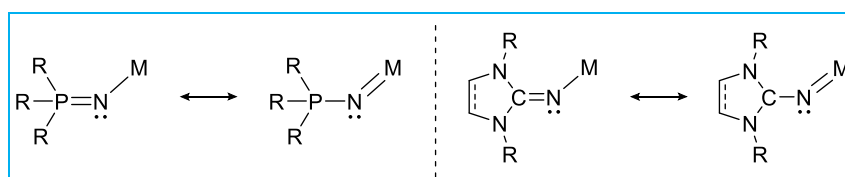


Figure 7. Comparison and mesomeric structures of phosphorane imines and *N*-heterocyclic imines.

It is worth noting that PIL and NHI can form both linear and bent angles to metal centers. However, metals in high oxidation state tend to form linear bonds, whereas changes in the oxidation state, substituents or packing effects result in deviation from the linear bonding mode.<sup>[35]</sup>

It was hypothesized, that replacing phosphines with NHCs in imino ligands could boost stability and catalytic activity of resulting novel NHI–M complexes. The iminato functionality in imidazoline-2-imines involve two main resonance structures that show how they act on

metal centers (Figure 8, right). NHIs are mono anionic ligands that effectively stabilize a formal positive charge within the imidazoline backbone and provide significant enhanced electron-donating properties compared to PILs. Considering the orbital interactions between the NHC and exocyclic imino nitrogen (Figure 8 left), it is apparent, that NHIs are strong  $2\sigma$ - as well as 2-4  $\pi$ -electron donors but avoid  $\pi$ -back donation according to the already filled nitrogen  $p$ -orbital in orthogonal orientation.<sup>[36]</sup>

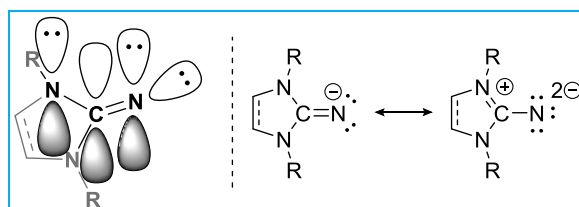


Figure 8. Ground state multiplicity with orbital interaction (left) and mesomeric structures (right) of *N*-heterocyclic imines.

Those properties allowed the isolation of a broad range of main group metal complexes.<sup>[37]</sup> They profit from stabilizing electron donation that balance electron deficiency, and a boosting effect that enhances reactivity. Figure 9 shows selected examples **P-V** isolated within the last decade.<sup>[38,39]</sup>

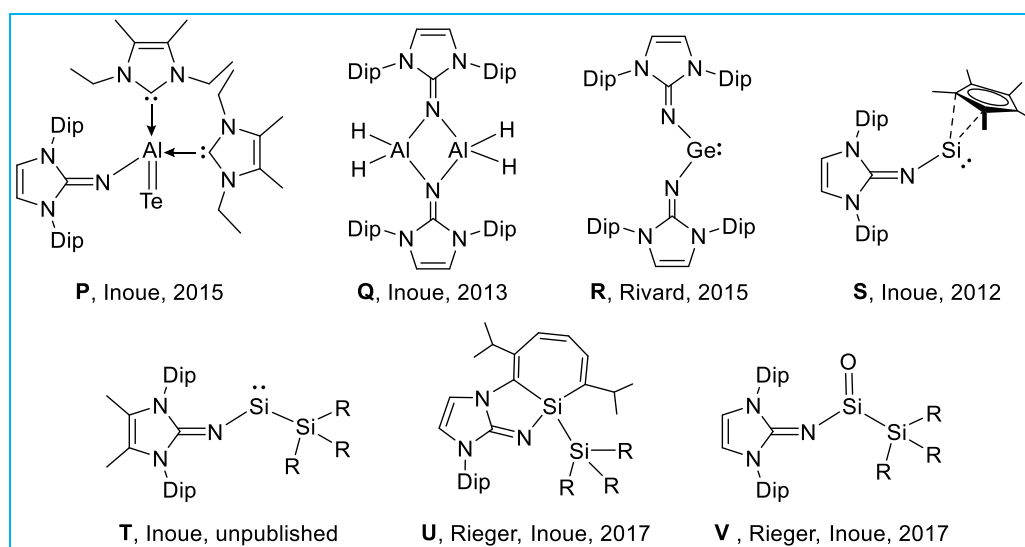
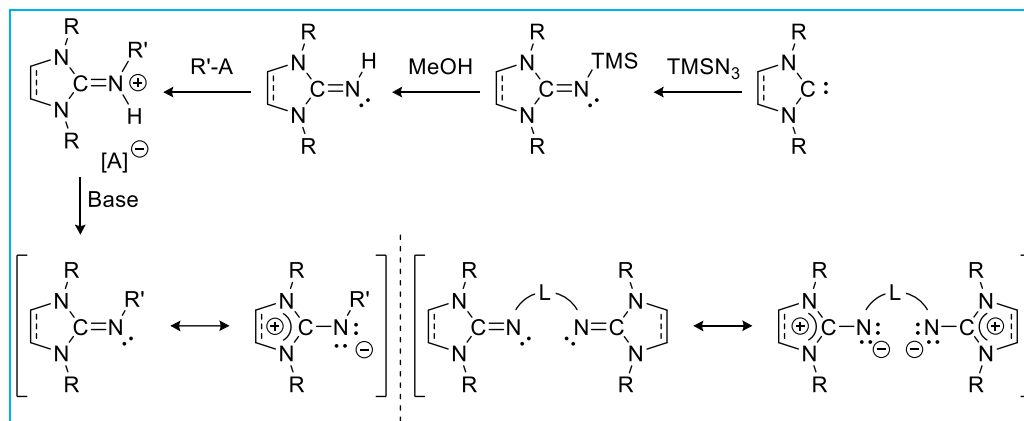


Figure 9. Selected examples of NHI-stabilized low valent main group compounds. (R = tBu, TMS)

The structural variability of NHI is comparable to that of NHC in view of modifications on the imidazoline-body and wingtips, and bridging ability towards multidentate ligands. However, it is superior considering that bridging can not only be performed at the endocyclic imidazoline-N in 1- and/or 3-position, but also *via* the exocyclic imine function.<sup>[40]</sup> Bridging of NHI *via* the imino-nitrogen atoms comes along with a decisive change from anionic imino-ligands towards two neutral and pure donor bis-imine functionality (Scheme 1, bottom, right). Compounds of that bis(imidazoline-2-imine) (bis-NHI)-type offer accumulated charge

delocalization ability and therefore substantially advanced basicity – qualifying them as powerful organosuperbases.<sup>[41]</sup> It should be mentioned, that adding a substituent to the imine nitrogen can also be achieved without the urge of bridging, resulting in an additional class of monodentate, neutral NHI (n-NHI) ligands (Scheme 1, bottom left).



Scheme 1. General synthetic pathway for neutral NHI and mesomeric structures of bridged neutral NHI. L = bridge (e.g. C<sub>2</sub>H<sub>4</sub>, C<sub>6</sub>H<sub>4</sub>, C<sub>3</sub>H<sub>7</sub>), R, R' = aryl, alkyl substituents.<sup>[40,41]</sup>

The first bis-NHI, bridged by an ethylene group was reported by Kuhn in 1998,<sup>[42]</sup> but the procedure suffered from inconvenient multi-step syntheses. In 2007 Tamm showed a refined strategy that yields desired bis-NHI within four synthesis steps, starting from respective free NHC (Scheme 1, top pathway).<sup>[43]</sup>

Whereas the unique properties of bis-NHI are already valued in transition metal chemistry, they are growing exceptionally slowly into the field of main group chemistry. Our group has shown successfully, that novel aryl substituted bis-NHI can effectively be used for stabilization of electron deficient main group species, such as group 13 boron and aluminum cations **W-Y**<sup>[44,45]</sup> and group 14 tetryliumylidenes **Z** and **AA** (Figure 10).<sup>[46]</sup>

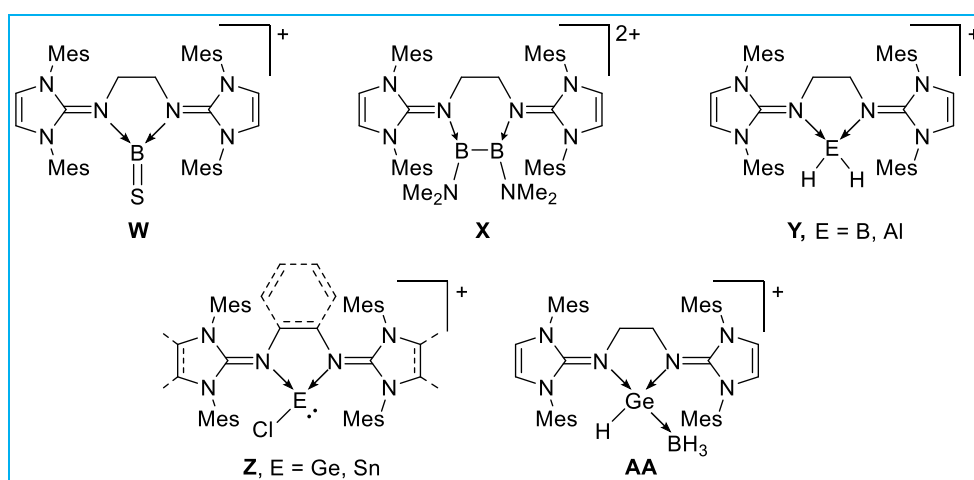


Figure 10. Selected examples of bis-NHI stabilized electron deficient main group cations of group 13 and 14 reported by the Inoue group.

## 2.2 Low Coordinate Silicon Species – Fundamentals

Silicon is the lighter sibling of carbon, but the differences between these group neighbors are so decisive that the first has become the basis of all known life and the synthetically best-known element of all, whereas the latter is forming the second largest part of the inorganic and inanimate earth's crust material (Figure 11).<sup>[47]</sup>

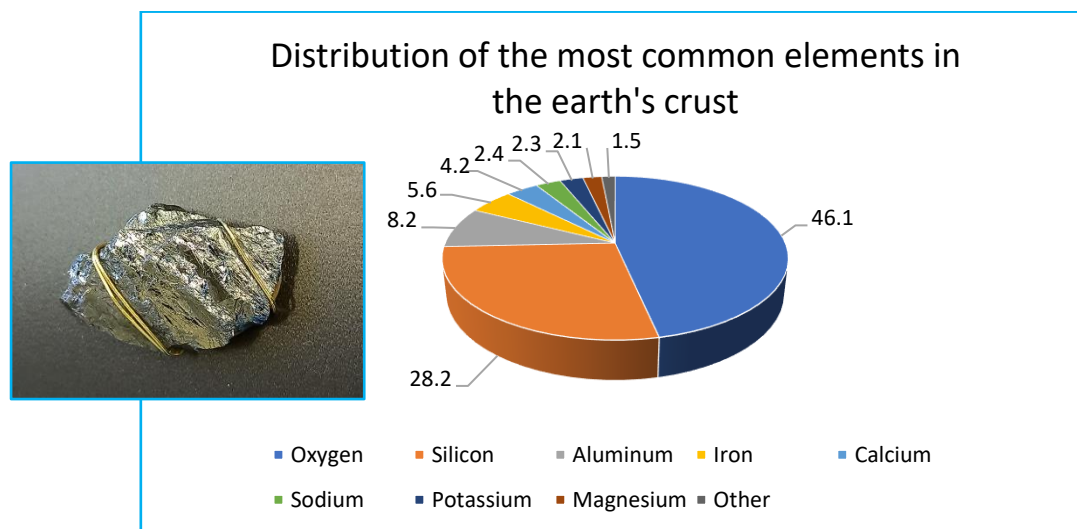


Figure 11. Distribution of the eight most abundant elements in the earth's crust (big) and photograph of a silicon piece wrapped in gold wire (small).

Therefore, when comparing carbon to silicon it is easy to find similarities in naming and structural composition but also unique features that make silicon differ not only from carbon but giving it a special position in modern main group chemistry. The differences between carbon and silicon are already clearly apparent: The increasing size of the atomic orbitals, the higher electron affinity but lower electronegativity, as well as the lower ionization energies, in silicon efficiently divides carbon from the heavier group 14 elements. So, silicon has neither the special hybridization tendency of carbon, nor the stability of the +II oxidation state that the heavy homologs Ge and Sn show. Furthermore, it shows a high stability in the +IV oxidation state and fourfold coordination, and is fairly oxophilic. All these points rationalize the fact that low-coordinate silicon compounds are hard to isolate and to handle. Yet, low-coordinate and low valent silicon species are no longer fleeting curiosities that can only be detected from a distance – rather, they are accessible and isolable subjects of a fascinating field of synthetic chemistry. This section attempts to provide a concise outline of the most common compound classes referred to as 'low valent silicon'.<sup>[48]</sup>

### Silanes – The Starting point

Silanes are not low valent compounds, nevertheless, as the most common starting point for low valent silicon chemistry, they should be briefly described. Within this simplest tetra

coordinated silicon compounds, a structural variety can be found that leads beyond the parent eponym  $\text{SiH}_4$ , named (mono-)silane. Following IUPAC nomenclature, the term silane describes compounds of the form  $\text{Si}_n\text{H}_{2n+2}$ , with Si in the  $sp^3$  hybridization, resembling the carbon class of alkanes. However, also compositions of  $\text{SiR}_4$  (R = alkyl, aryl) and  $\text{SiX}_4$  (X = Cl, Br, I) are coined as alkyl-, aryl-, and halo-silanes, respectively. Methane and mono-silane bare a similar tetrahedral structure, but the bonding enthalpies reveal a quite significant higher stability of the C–H bond ( $416 \text{ kJ mol}^{-1}$ ) compared to the Si–H bond ( $326 \text{ kJ mol}^{-1}$ ) together with an inverse bond polarity.<sup>[49]</sup> In consequence silanes are more reactive than their matching alkanes, as can be easily understood by contrasting methane, which is difficult to activate, with silane, which spontaneously self-ignites in humid air.

### Disilenes and Disilynes

Until the 1970's the stabilization of heavier group 14 multiple bonds (and p-block elements in general) seemed so futile, that the so-called 'classical double bond rule' was established to explain their absence.<sup>[6]</sup> That rule based on the simple observation of the vast richness of first row p-block multiple bonds and the lack of their heavier congeners with lower hybridization ability.

Obviously, this rule was obsolete with the report of  $[\text{ECH}(\text{SiMe}_3)_2]_2$  (E = Ge, Sn) by Lappert<sup>[50]</sup> in 1976 and  $\text{Mes}_2\text{Si}=\text{SiMes}_2$  by West<sup>[1]</sup> in 1981. Looking back, the observation of a stable Si=Si double bond marked the starting point of modern low-valent silicon chemistry. Today it is known that, despite their lower tendency for hybridization, silicon can form multiple bonds in compound classes such as silenes ( $\text{R}_2\text{Si}=\text{CR}_2$ ),<sup>[3]</sup> disilenes ( $\text{R}_2\text{Si}=\text{SiR}_2$ ),<sup>[51]</sup> silynes ( $\text{RSi}\equiv\text{CR}$ ),<sup>[52]</sup> and disilynes ( $\text{RSi}\equiv\text{SiR}$ ).<sup>[53]</sup> Also other heteronuclear multiply bonded silicon compounds ( $\text{R}_2\text{Si}=\text{'M'}$  /  $\text{RSi}\equiv\text{'M'}$ ) are described.<sup>[54]</sup> Due to the wide range of silicon multiple bonds, only disilenes and disilynes are described here as being the direct descendants of alkenes and alkynes.

Looking at the bonding situation in the parent disilene and ethylene in comparison, shows that the bonding situation and structure in  $\text{H}_2\text{Si}=\text{SiH}_2$  is dominated by Pauli repulsion between two  $\text{H}_2\text{Si}$ : moieties in the singlet ground state that leads to trans-bending and/or twisting as described best in the Carter-Goddard-Malrieu-Trinquier (CGMT)-model (Figure 12). With that, the bonding in disilenes can be best described as a double donor-acceptor interaction between occupied  $sp^2$  lone pair orbitals and vacant  $p$ -orbitals. In contrast, the methylene  $\text{H}_2\text{C}$ : moieties are in the triplet ground state, forming covalent and planar ( $\pi$ -)bonds. For disilynes, the bonding situation follows the same concept, with  $\text{HSi}:$  moiety in the doublet ground state, that form one covalent bond additional to the double donor-acceptor interaction.

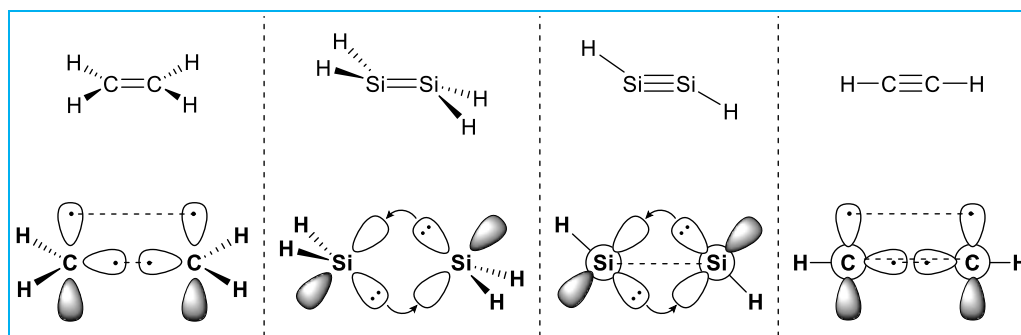


Figure 12. Depiction of parent ethylene, disilene, disilyne, and acetylene and the respective approximation of frontier orbitals.

The reactivity of disilenes and disilynes stems from the availability of the lone pairs within the multiple bond that is dominated by the inert pair effect and ligand influences. However, in general it can be said that multiply bonded silicon compounds are prone to undergo cycloaddition reactions with olefins,  $\text{CO}_2$ , and other heteroatom multiple bonds. Additionally, activation of small molecules like  $\text{H}_2$ ,  $\text{NH}_3$ , etc., *via* bond order reducing addition reactions are common.

Although, there are today numerous isolated examples of group 14 multiply bonded compounds, they remain elusive and reactive species.<sup>[55]</sup>

### Silyl Ions

This three-coordinate silicon compounds can be synthesized either as Lewis acidic silylium cations ( $\text{R}_3\text{Si}^+$ ) or Lewis basic silyl anions ( $\text{R}_3\text{Si}^-$ ). Both of this ionic compound classes can be idealized as the heavier analogues of carbocations and carbanions, respectively (Figure 13). Their structures also resemble those of the carbon analogue with planar shaped silyl cations in  $sp^2$ - $p$  configuration and trigonal pyramidal shaped silyl anions in  $sp^3$  hybridization.

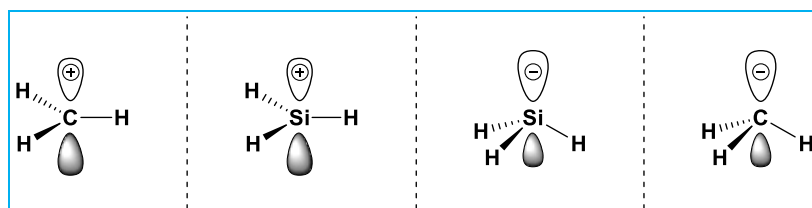


Figure 13. Parent three-coordinate cations  $\text{H}_3\text{E}^+$  and anions  $\text{H}_3\text{E}^-$  of carbon and silicon ( $\text{E} = \text{C}, \text{Si}$ ).

In contrast, the lower electronegativity and higher polarizability of silicon results in a thermodynamic stabilization of the silylium cation, which makes it comparably easy to generate those species in the gas phase. Isolation in the condensed phase, however, requires additional kinetic stabilization of the highly electrophilic vacant orbital. Owing to the “voracious appetite for nucleophiles” of silylium ions, it is challenging to find a set of suitable substituents, counter anion, and solvent that is truly inert towards the silyl cation.<sup>[56]</sup> Even with

careful design, interaction with a broad variety of  $\sigma$ - and  $\pi$ -donors is hardly avoidable, so that the isolation of silylium ions has been targeted for more than 60 years.<sup>[57]</sup> Although the isolation of truly ‘free’ silylium ions remains challenging even until today – the first structurally proven example  $[\text{Mes}_3\text{Si}]^+[\text{H-CB}_{11}\text{Me}_5\text{Br}_6]^- \cdot \text{C}_6\text{H}_6$  was reported only in 2002 by Lambert and Reed<sup>[58]</sup> – understanding of their catalytic capability has developed rapidly.<sup>[59]</sup> 1996, when isolation of silylium-ions was only possible in a solvent or anion coordinated form, Lambert was able to show the first successful application of  $\text{Et}_3\text{Si}^+[\text{B}(\text{C}_6\text{F}_5)_4]^-$  as catalyst in hydrosilylation. In 2005 the first catalytic C–F bond activation was found by Ozerov using the same compound.<sup>[60]</sup> Of course, Si-based Lewis acids are well known catalysts, however, silylium ions outperform them due to their extreme Lewis acidity in difficult conversions such as Diels-Alder cycloadditions, but stand back in Lewis acid catalysis, of all things. The challenging task is to find the ideal balance between exposure and protective shielding of the reactive vacant orbital.

While the reactivity of the silyl cations is mainly determined by the vacant  $3p$ -orbital, the occupation of this orbital reverses the face of the compound towards nucleophilic silyl anions. Silyl anions ( $\text{R}_3\text{Si}^-$ ) – also called silanides – can form direct coordination to their counter cation or stay separated in the ionic form. Their synthesis is commonly achieved by reductive metalation starting from the respective (halo-)silane. Silanides are way scarcer in small molecule activation and catalysis<sup>[61]</sup> but found relevant application in synthetic purpose, as silyl transfer agent and novel building blocks for organosilicon compounds.<sup>[62]</sup>

### Silyl Radicals

Within the group of three-coordinated Si-compounds neutral  $\text{R}_3\text{Si}^\bullet$  radicals are also to be mentioned. They are the silicon version of the well-known  $\text{R}_3\text{C}^\bullet$  carbon radicals, featuring a singly occupied orbital (SOMO) (Figure 14).

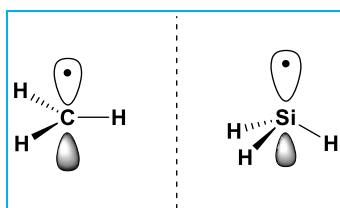


Figure 14. Parent three-coordinate radicals  $\text{H}_3\text{E}^\bullet$  of carbon and silicon ( $\text{E} = \text{C}, \text{Si}$ ) with depicted SOMO.

The structure and electronic nature of  $\text{R}_3\text{Si}^\bullet$  radicals are determined by the  $s$ -character of the SOMO. Whereas the parent carbon radical is planar with  $sp^2$ - $p$ -orbital configuration, the heavier tetrel radicals  $\text{H}_3\text{Si}^\bullet$ ,  $\text{H}_3\text{Ge}^\bullet$ , and  $\text{H}_3\text{Sn}^\bullet$  show increasingly higher  $s$ -character SOMOs and are therefore pyramidalized with rather  $sp^3$ -type orbitals.<sup>[63]</sup> Silyl radicals are observable since the 1960's *via* EPR (electron paramagnetic resonance) spectroscopy but persistent silyl

radicals are only known since the late 1990's by the groups of Matsumoto and Kira.<sup>[64]</sup> The first silyl radical analyzed by single crystal X-ray diffraction (SC-XRD) analysis was a cyclotetrasilanyl radical in 2001<sup>[65]</sup> and the acyclic trisilyl substituted silyl radical  $(t\text{Bu}_2\text{MeSi})_3\text{Si}^\bullet$  in 2002<sup>[66]</sup> by Sekiguchi. The significance of silyl radicals becomes apparent when they are placed in an electrochemical context. Silyl radicals are very promising candidates to undergo one electron reduction towards silyl anions, as well as one electron oxidation, forming silyl cations. Several examples of silyl radical redox couples are known today and have also demonstrated their suitability for battery applications.<sup>[67]</sup> In contrast to common lithium ion batteries, the merit of silyl radicals lies in the highly reversible redox behavior and the high abundance of the elements. Moreover, considering lithium's (self-)ignitability and difficult extinguishability, metal-free organic silyl batteries could offer positive safety aspects in some applications.

### Silylenes

Main group chemists show considerable interest in the chemistry of silylenes, which, in addition to their undeniably diverse and astonishing chemistry, is probably due to the light that shines from the carbenes onto their heavier congener. In fact, the parent silylene  $\text{H}_2\text{Si}:$  is – as carbenes are – a 2-coordinate Si(II) species that bears a lone pair. But in contrast to the triplet methylene ( $\text{H}_2\text{C}:$ ), the parent silylene exists in the singlet electronic ground state, with a singlet-triplet (S/T)-gap of  $16.7 \text{ kcal mol}^{-1}$  (Figure 15, left and middle left).<sup>[68]</sup> In this configuration, singlet silylenes are ambiphilic in nature and mimic the  $d$ -orbitals of transition metals.<sup>[8]</sup> They benefit from donor stabilization through their Lewis acidic vacant  $p$ -orbital, but also react as quite strong Lewis bases *via* their chemically active lone pair (Figure 15, middle).

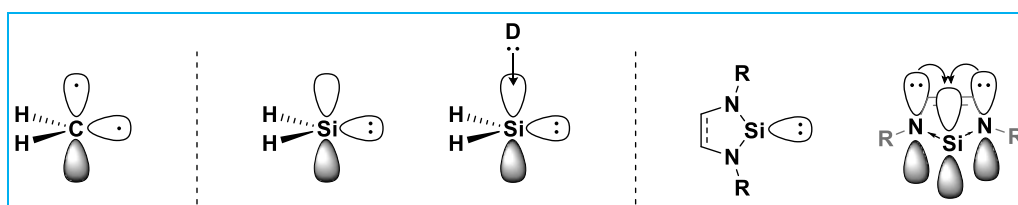


Figure 15. Ground state multiplicity and approximation of frontier orbitals of methylene (left), silylene  $\text{H}_2\text{Si}$  (middle; middle right: additional donor stabilization D = donor molecule) and NHSi (right) for comparison.

As their lighter siblings – the carbenes – also silylenes benefit exceptionally from stabilization *via* intramolecular donor atoms and cyclization of the ligands (Figure 15, right). Knowing that, it is not surprising that the first isolable and 2-coordinate silylene was prepared in 1994 as an *N*-heterocyclic compound, resembling the Arduengo carbene.<sup>[69]</sup> The availability of room temperature stable and bottleable silylenes mark not the first – but maybe most important milestone in silylene chemistry. To date, NHSi – that are by far not limited to the ‘Arduengo-

type' – represent the largest group of known silylenes.<sup>[70]</sup> Elimination of the stabilizing N-donors from the cyclic backbone yields more reactive carbocyclic silylenes, of which the first representative was isolated in 1999 by Kira.<sup>[71]</sup> Whereas all silylenes are considered as highly reactive species that are prone to di- and oligomerization, this holds exceptionally true for acyclic and 2-coordinate silylenes. Until the beginning of the new millennium, only cyclic silylenes were known, which changed in 2003, with the report of  $(\text{TMS}_2\text{N})_2\text{Si}$ : by West.<sup>[72]</sup> With the removal of the cyclic ligand sphere, the R–Si–R angle is no longer forced small by the ligands but can be intentionally widened. According to computational studies, larger R–Si–R angles result in smaller (S/T)-gaps, due to enhancement of the *p*-character of the silicon  $sp^2$ -hybrid orbitals and thus the stabilization of the triplet state.<sup>[73]</sup> The combination of the small S/T-gaps and the transition metal like orbital configuration make 2-coordinate, acyclic silylenes very promising candidates for activation of otherwise chemically rather inert small molecules, such as  $\text{H}_2$ ,  $\text{NH}_3$ , olefins, and  $\text{CO}_2$ . Within the last decade important progress was shown in this field, proving this concept right.<sup>[74]</sup> Although especially acyclic silylenes do show small S/T-gaps it is important to mention, that until today there is no isolable triplet silylene known. Overcoming of the S/T-gap, which is comparatively easy for carbenes, is a remarkable challenging task for silylenes. So far very scarce examples of triplet silylene ( $\text{Si}(\text{Si}t\text{Bu}_3)_2$ ,  $t\text{Bu}_3\text{SiM}$  (M = Li, K)) were proven to exist *via* EPR spectroscopy from frozen glass matrix at 9 and 15 K, respectively.<sup>[75]</sup>

## 2.3 Silyliumylidenes and Silylones

### 2.3.1 Silyliumylidene Ions

#### Bonding and Electronic nature

Silyliumylidenes are often described as a combination of silylenes and silylium ions in terms of their electronic nature and reactivity. This description aims to express that they combine the main reactive features of a positive charge and resulting enhanced Lewis acidity (silylium ion), and a chemically active lone pair with accompanying Lewis basicity (silylene) in themselves.<sup>[76]</sup> Their composition and structure differ of course from these two models, being coordinated by only one covalent substituent. So, silyliumylidenes do have four valence electrons, two vacant orbitals, and are of the general form R–Si<sup>+</sup> (Figure 16, left), but barely any isolable examples are known, that can dispense with the stabilizing effect of one (Figure 16, middle) or two additional intra- or intermolecular donors (Figure 16, right). From calculations it is proposed that this is in good agreement with theoretical findings regarding the non-donor substituted Me–Si<sup>+</sup> by Müller.<sup>[77]</sup> The HOMO was found to be a located lone pair in the *sp*-hybrid orbital, whereas two degenerate *p*-orbitals remain vacant LUMOs. This prompts the methyl-substituted silyliumylidene cation to persist in the singlet ground state with an S/T gap of 222.4 kJ mol<sup>-1</sup>.

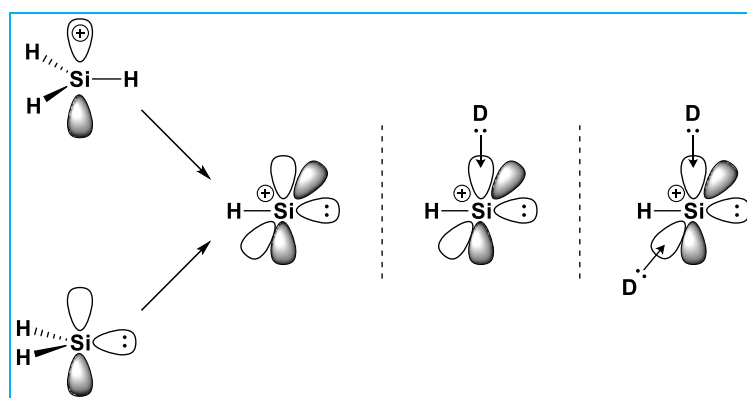


Figure 16. General depiction and approximation of frontier orbitals of silylium ion (left top) and silylene (left bottom) that combine within silyliumylidene ion (middle; middle right: additional donor stabilization D = donor molecule).

Obviously, the use of coordinating Lewis bases ( $\sigma$ -donors, e.g. D = NHC, DMAP, R<sub>3</sub>N), comes with a trade off in reactivity: The system undergoes kinetic as well as thermodynamic stabilization, by partial population of the vacant *p*-orbitals. Whereas the direct electron donation decreases the Lewis acidity, the steric demand decreases the Lewis basicity of the lone pair. Additionally, the covalent bound residue introduces distinct electronic as well as steric properties into the system compared to the parent silyliumylidene (H–Si<sup>+</sup>,  $\Delta E = 0$ ). For example, aryl- (R = Ph<sup>-</sup>,  $\Delta E = 38.2$  kcal mol<sup>-1</sup>) and  $\pi$ -donor (R = H<sub>2</sub>N<sup>-</sup>,  $\Delta E = 46.4$  kcal mol<sup>-1</sup>)

ligands and combination of those ( $R = m\text{Ter}^-$ ,  $\Delta E = 71.8 \text{ kcal mol}^{-1}$ ) can provide valuable stabilization by delocalization of the positive charge and  $\pi$ -electron donation into the vacant  $p$ -orbital (Figure 17). Electropositive ligands, such as silyl-groups show less stabilization energy ( $R = \text{H}_3\text{Si}^-$ ,  $\Delta E = 9.6 \text{ kcal mol}^{-1}$ ).<sup>[77]</sup>

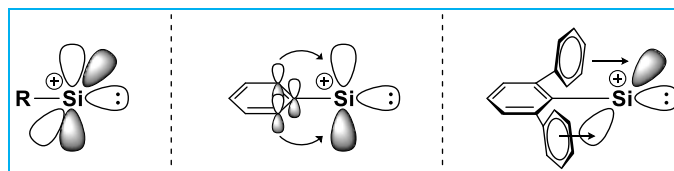


Figure 17. Stabilizing influence of electron donation by aryl and terphenyl ligands on vacant orbitals of silyliumylidenes.

Ligands and substituents with strong  $\pi$ -donor substituent effect, such as halogens ( $R = \text{F}^-$ ,  $\text{Cl}^-$ ,  $\text{Br}^-$ ,  $\text{I}^-$ ), nitrogen binding substituents (e.g.  $R = \text{H}_2\text{N}^-$ ,  $\text{N}_3^-$ ) and ligands (e.g.  $D = \text{H}_3\text{N}$ ,  $R=\text{N}-\text{R}'$ ), or oxygen binding substituents (e.g.  $R = \text{OH}^-$ ,  $\text{O}^{2-}$ ) effectively donate surplus electron density into the orthogonal  $p$ -orbitals and contribute significantly to the stabilization of silyliumylidene ions.

Thus, with careful design, the properties of a silyliumylidene ion can be finely tuned, at least on paper.

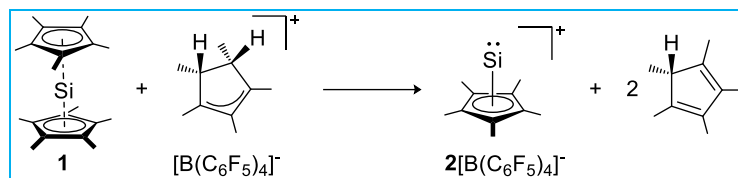
### History and Synthesis – State of the Art

Whereas the coordination of silyliumylidene ions was, for the sake of clarity, previously defined as mono-coordinated with respect to only covalent substituents, in terms of synthesis and structure discussion it makes more sense to count all ligands present in the coordination sphere. Therefore, single donor stabilized silyliumylidene ions are referred to as 2-coordinate and double donor-stabilized silyliumylidenes are referred to as 3-coordinate, respectively.

The smallest non monoatomic silicon species  $\text{HSi}^+$  has been of interest since its spectroscopic discovery in a discharge of He with  $\text{SiH}_4$  by Douglas and Lutz and its identification in the solar spectrum in 1970. Due to this interstellar importance, it has been widely studied theoretically as well as spectroscopically, long before the first derivative could be isolated in the condensed phase.<sup>[76,78]</sup>

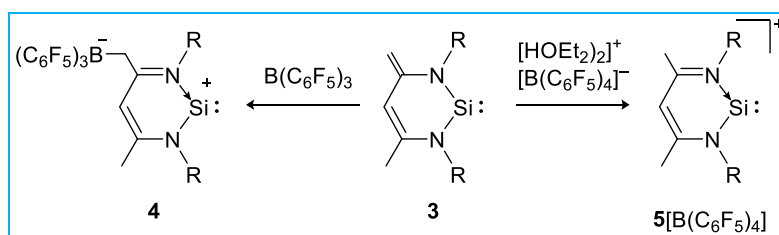
Whereas it remains not possible until today to isolate a truly mono-coordinated and donor-free silyliumylidene ion, the outstanding report of the first isolated silyliumylidene is also the only known example of the donor-free (but  $\eta^5$ -coordinated)  $[\text{Cp}^*\text{Si}^+][\text{B}(\text{C}_6\text{F}_5)_4]$  (**2**) found by Jutzi in 2004.<sup>[79]</sup> **2** was prepared *via* protonation and elimination of one  $\text{Cp}^*$  ligand in  $\text{Cp}^*_2\text{Si}^+$ <sup>[80]</sup> (**1**) using  $[(\text{CH}_3)_5\text{C}_5\text{H}_2][\text{B}(\text{C}_6\text{F}_5)_4]$  (Scheme 2). The structure of  $\text{Cp}^*\text{Si}^+$  (**2**) is found to be slightly distorted pentagonal-pyramidal with weak Si–anion interaction (shortest Si–F distance of

2.99 Å). The Cp\*–Si distance of 1.76 Å is substantially shorter than in the pentamethylsilylocene precursor **1**. The  $^{29}\text{Si}$ -NMR shift of **2** appears in the very high field region at –400.2 ppm and is in good agreement with previously reported  $\pi$ -complexes of di-coordinated Si centers.<sup>[81]</sup>



Scheme 2. Synthesis of Cp\*Si<sup>+</sup> (**2**) starting from SiCp\*<sub>2</sub> (**1**) via protonation of one Cp\*.

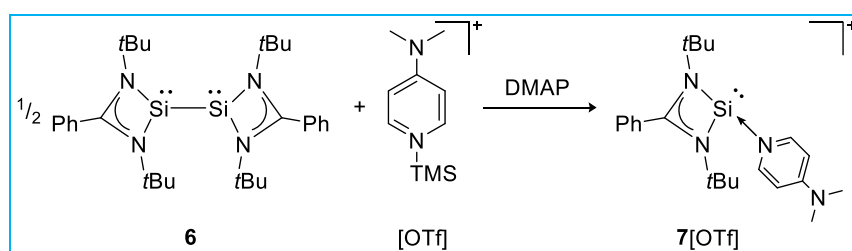
2-fold coordinated silyliumylidene ions are similarly rare as singly coordinated ones, with the  $\beta$ -diketiminato-supported **4** and **5** being the only reported examples up to date. In a straight forward reaction of the zwitterionic *N*-heterocyclic silylene precursor **3** with B(C<sub>6</sub>F<sub>5</sub>)<sub>3</sub> or [H(OEt<sub>2</sub>)<sub>2</sub>][B(C<sub>6</sub>F<sub>5</sub>)<sub>4</sub>], **4** and **5** were afforded, respectively (Scheme 3).<sup>[82]</sup> Both compounds feature a silyliumylidene center but utilization of the borane results in a coordinated anion and an overall neutral (but zwitterionic) species, whereas the borate anion remains separated in **5**. The structure of **5** demonstrates the concept of the  $\beta$ -diketiminato ligand with one nitrogen binding covalent (Si–N 1.76 Å) and one featuring a donor-acceptor interaction (Si–N 1.77 Å). Overall, the compound shows the expected aromatic-like planar 6-membered SiN<sub>2</sub>C<sub>3</sub>-core. The less effective shielding of the Si-nucleus compared to **3** ( $\delta(^{29}\text{Si}) = 88.4$  ppm) leads to a  $^{29}\text{Si}$ -NMR signal at 69.3 ppm.



Scheme 3. Preparation of **4** and **5** starting from **3**. Different pathways (B(C<sub>6</sub>F<sub>5</sub>)<sub>3</sub> / [B(C<sub>6</sub>F<sub>5</sub>)<sub>4</sub>]<sup>–</sup>) lead to either zwitterionic-contact or separated silyliumylidene ion complexes.

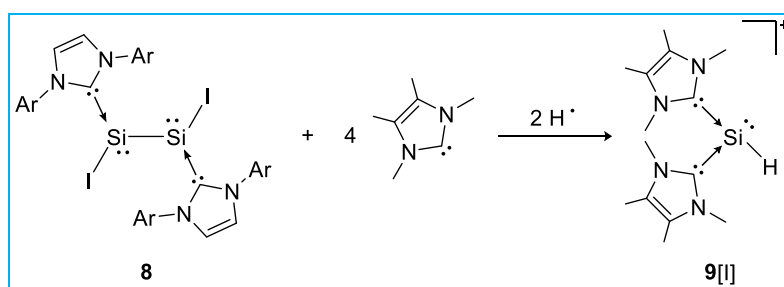
As already mentioned, those examples are exceptions and three-coordinated silyliumylidenes are the standard picture. Among them, the majority features two identical donor ligands with either an aryl or halogen substituent. However, variations for this pattern are also known: In 2013, So reported on the synthesis of amidinate-stabilized and 4-dimethylaminopyridine (DMAP)-coordinated silyliumylidene **7**, which comes with covalent (Si–N 1.85 Å) and donor-acceptor (Si–N 1.86 Å) amidinate-*N* bonds, and one DMAP (Si–N 1.88 Å) donor-acceptor interaction. Compound **7** was formed by reacting interconnected bis-silylene **6** with oxidizing [4-NMe<sub>2</sub>C<sub>5</sub>H<sub>4</sub>NSiMe<sub>3</sub>]OTf and additional two equivalents of DMAP (Scheme 4).<sup>[83]</sup> As usual for

three-coordinated silyliumylidenes, the Si atom in **7** adopts a slightly distorted trigonal pyramidal geometry, which indicates a localized lone pair of electrons with high s-character on a nearly non-hybridized silicon center. Computationally, the lone pair could be found representing the HOMO. The  $^{29}\text{Si}$ -NMR shift of  $\delta = -82.3$  ppm is in consistency with a three coordinated silicon nucleus and, due to Lewis base coordination, upfield shifted compared to its bissilylene precursor **6**. The compounds **4**, **5**, and **7** are purely nitrogen-substituted silyliumylidenes, and thus differ additionally from the previously discussed  $\text{Cp}^*\text{Si}^+$  (**2**) and the following aryl (Ar) and halo (X)-substituted silyliumylidenes.



Scheme 4. Synthesis of DMAP-stabilized 3-coordinate silyliumylidene **7** starting from interconnected bissilylene **6**.

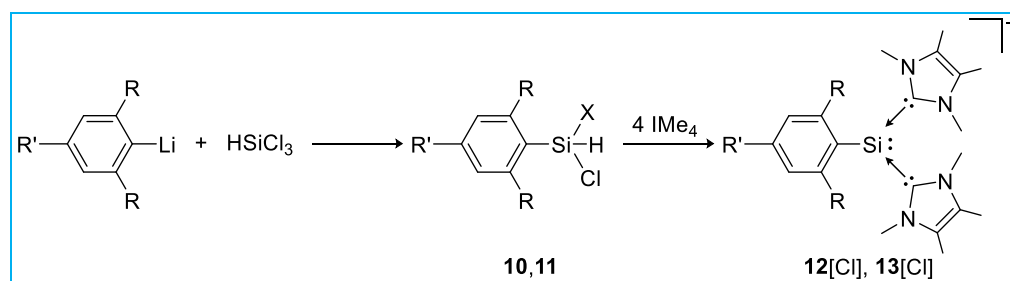
The greatest progress in silyliumylidene chemistry was made using NHCs and cAACs as stabilizing Lewis bases. The structural variety increased with symmetric (same carbene), and asymmetric (different carbene), as well as cyclic (bridged carbene) compounds of aryl-, and halo (X)-silyliumylidenes.<sup>[84,85]</sup> Within this group the donor-stabilized  $(\text{Ime}_4)_2\text{HSi}^+$  (**9**) was isolated in 2017 as first derivative of the parent species (Scheme 5).<sup>[30]</sup> The synthesis strategy of NHC-stabilized silyliumylidenes focuses mainly on straight forward utilization of either Si(II)-precursors such as  $\text{NHC}:\rightarrow\text{SiX}_2$  ( $\text{X} = \text{Cl}, \text{Br}, \text{I}$ ) for  $(\text{NHC})_2\text{XSi}^+$  or base induced H-X abstraction of aryl-substituted silanes to form  $(\text{NHC})_2\text{ArSi}^+$ .<sup>[86]</sup>



Scheme 5. Preparation of  $\text{Ime}_4$ -stabilized parent silyliumylidene iodide **9**, via bond cleavage of interconnected bissilylene **8**.

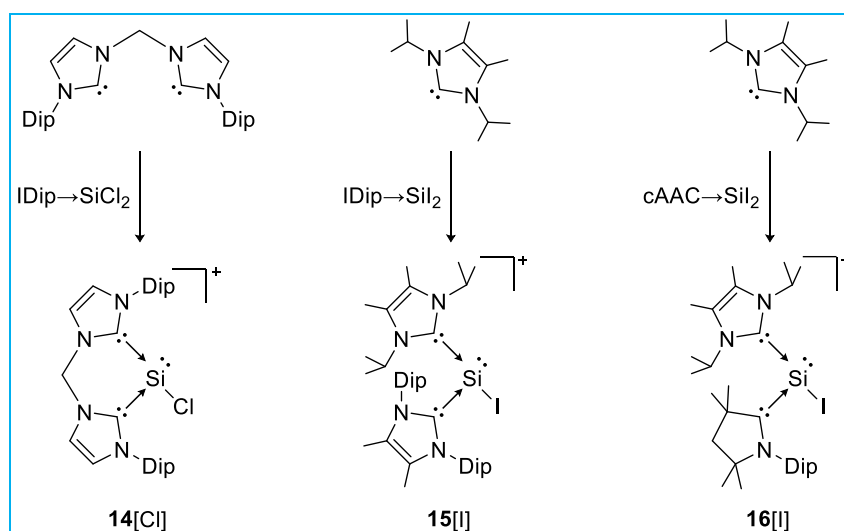
In the case of **9**, the interconnected bissilylene **8** reacts with four equivalents of  $\text{Ime}_4$ , homoleptically cleaving the Si-Si bond and abstracting  $\text{H}\cdot$  from a toluene molecule. Whereas the  $^{29}\text{Si}$  NMR shift of **9** ( $-77.7$  ppm) appears only slightly downfield shifted from **7**, a remarkably downfield shifted single signal at  $\delta = 9.73$  ppm in the  $^1\text{H}$  NMR verifies the presence of 'Si-H' in solution, which could also be found by SC-XRD analysis in the solid state.

In 2014 our group demonstrated that the small tetramethyl-NHC  $\text{IMe}_4$  was suitable for stabilizing aryl-substituted silyliumylidenes  $(\text{IMe}_4)_2m\text{TerSi}^+$  (**12**) and  $(\text{IMe}_4)_2\text{TippSi}^+$  (**13**) (Scheme 6).<sup>[87]</sup> The sterically demanding aryl groups provide the previously described stabilizing effect of charge delocalization and electron donation, leading to a moderate downfield shift in  $^{29}\text{Si}$  NMR with signals at  $\delta = -68.9$  ppm and  $-69.5$  ppm, respectively. **12** and **13** show that aryl groups enable a more conservative synthesis strategy, in which  $\text{SiHCl}_3$  is used as a starting material to generate  $\text{Ar-SiHCl}_2$  *via* salt metathesis. The respective arylsilane can directly be transformed into silyliumylidene species by conversion with three equivalents of  $\text{IMe}_4$  providing the base for reductive HCl abstraction as well as stabilizing  $\text{IMe}_4$  donors. Within a short period of time the structural diversity was expanded by introduction of various aryl groups.<sup>[84,85]</sup>



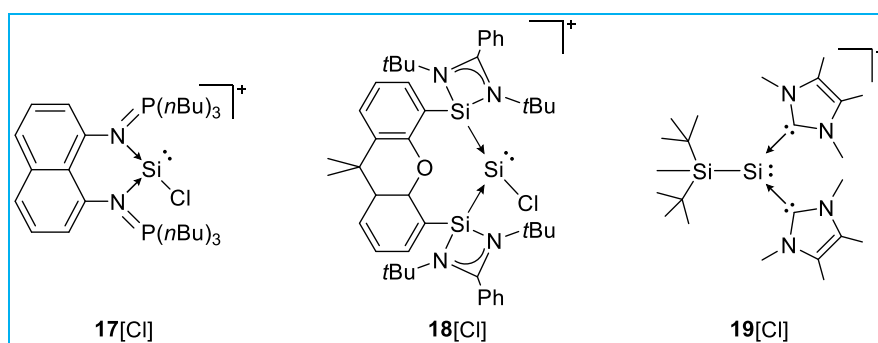
Scheme 6. Synthesis of aryl-substituted and  $\text{IMe}_4$ -stabilized silyliumylidene chlorides **12** ( $\text{R} = \text{Mes}$ ,  $\text{R}' = \text{H}$ ), **13** ( $\text{R} = \text{R}' = i\text{Pr}$ ) *via* reductive dehalogenation of arylsilanes **10** ( $\text{R} = \text{Mes}$ ,  $\text{R}' = \text{H}$ ), **11** ( $\text{R} = \text{R}' = i\text{Pr}$ ).

If halogen (X)-substituted silyliumylidenes are to be achieved – *i.e.* to dispense with the large and aryl ligands – larger and more demanding NHCs are employed, consequently. Compounds **14**,<sup>[29]</sup> **15**,<sup>[88]</sup> and **16**<sup>[89]</sup> display possible strategies to use two NHC with different steric demand (**15**), a mixture of NHC and cAAC (**16**), and a bridged bis-NHC that results in a cyclic silyliumylidene (**14**). In 2013 compounds **14** and **15** were reported by the groups of Filippou and Driess, who both used  $\text{IDip} \rightarrow \text{SiX}_2$ , a relatively easy accessible Si(II)-halide adduct, to treat them with their respective NHC ligand (Scheme 7). Whereas  $\text{IDip} \rightarrow \text{SiI}_2$  reacts with  $\text{IMe}_2i\text{Pr}_2$  under addition,  $\text{IDip} \rightarrow \text{SiCl}_2$  gets stripped of IDip upon complexation with the bis-NHC ligand. In 2016, So used a similar technique for successful isolation of the mixed carbene **16**, starting from  $\text{cAAC} \rightarrow \text{SiI}_2$ .



Scheme 7. Formation of halosilyliumylidene ions **14**, **15**, and **16** via complexation of stabilized  $\text{SiX}_2$  ( $\text{X} = \text{Cl}, \text{I}$ ) synthons.

The  $^{29}\text{Si}$  NMR shifts are in good agreement with aryl-substituted three coordinate silyliumylidenes but occur slightly downfield shifted with  $\delta(^{29}\text{Si}) = -55.3$  ppm (**14**),  $-51.5$  ppm (**15**), and  $-58.4$  ppm (**16**). It is worth noting that besides using NHC for stabilization, also a  $\text{R}_3\text{P}=\text{N}$  supported silyliumylidene (**17**) was reported by Driess in 2012 (Scheme 8, left).<sup>[90]</sup> The bis(iminophosphorane) chelate ligand equipped **17** with diminished Lewis acidity, due to the higher donor strength of the imino-function, thus leading to further downfield shift of the  $^{29}\text{Si}$  NMR signal (compared to other three-coordinate silyliumylidenes) at  $\delta(^{29}\text{Si}) = -3.3$  ppm. Likewise to **14–16**, **17** can be synthesized by treating the bis-iminophosphorane ligand directly with  $\text{IDip} \rightarrow \text{SiCl}_2$ . By using a bridged bis-silylene as donating ligand system in an analogous strategy, Driess 2020 expanded the range of silyliumylidene classes by isolation of **18** (Scheme 8, middle).<sup>[91]</sup> The xanthene-bridged bis-silylene ligand creates a  $\text{Si-Si-Si}$  skeleton describing a  $114.2^\circ$  angle. Whereas the silylene Si resonates at  $\delta = -5.2$  ppm in  $^{29}\text{Si}$  NMR, the central Si atom appears upfield at  $\delta = -71.7$  ppm. Recently our group succeeded in introducing silyl groups for stabilization of silyliumylidene **19** (Scheme 8, right).<sup>[85]</sup> The effect of the electropositive substituent contrasts **19** with a pronounced Lewis acidity and a  $^{29}\text{Si}$  NMR shift of  $\delta = -90.7$  ppm. The synthesis protocol is based on the preparation of  $\text{ArSi}(\text{NHC})_2$  (**12**, **13**), such as that the silyl-group is introduced to  $\text{SiCl}_3\text{H}$  and three equivalents of NHC are added for HCl abstraction and subsequent coordination.

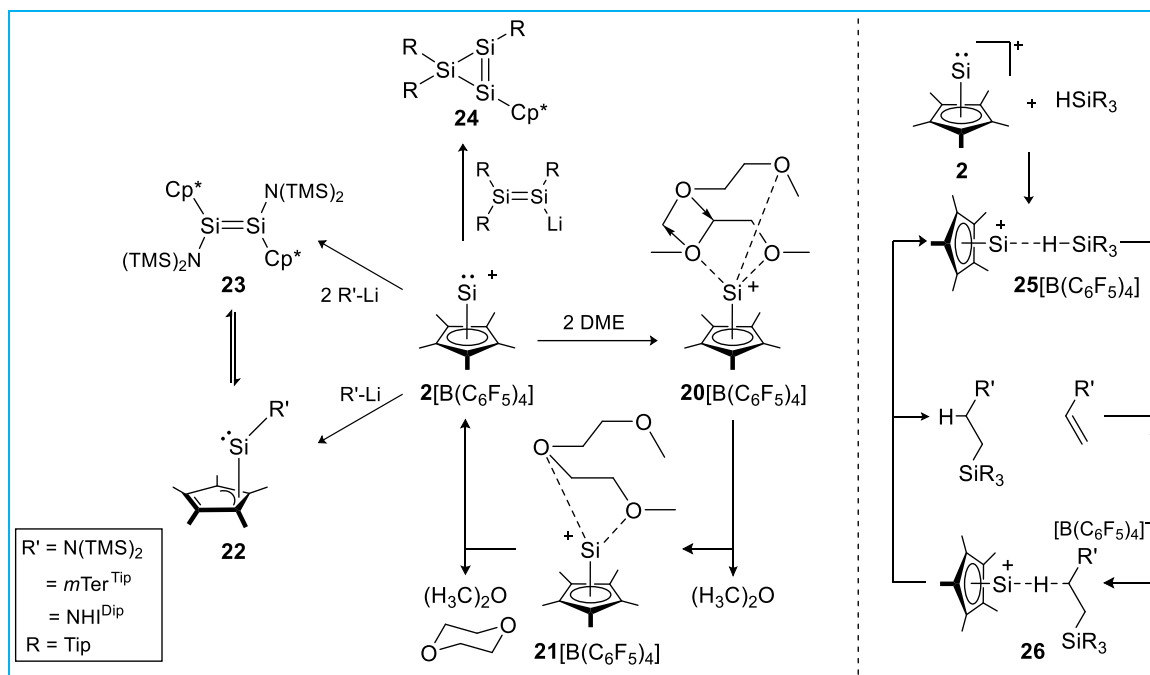


Scheme 8. Non NHC-stabilized silyliumylidene ions **17** and **18**, and silyl-substituted silyliumylidene ion **19**.

### Reactivity (recent advances)

Due to their complex electronic properties, silyliumylidenes can show quite diverse reactivity. Whereas electron withdrawing and small ligands result in Lewis acidic silyliumylidenes, the introduction of strong donors and sterically demanding groups quenches the electrophilicity and pronounces their potential as Lewis bases. Although these ambiphilic and tunable properties are exciting and promising for reactivities, such as small molecule activation and catalytic application, they have long been seen only as reactive intermediates and have been little studied in their own right. Since the role of silyliumylidenes as ligands for transition metal complexes is to be discussed in detail in a separate chapter (see 2.3.3), it will be skipped here.

With its unique structure  $\text{Cp}^*\text{Si}^+$  is an exception and has been studied extensively as outstanding reactivities had been found few years after the seminal report. Dissolving **2** in dimethoxyethane (DME), Jutzi *et al.* observed conversion yielding 2,6-dioxane and dimethylether. Further studies revealed the catalytic activity of the silyliumylidene cation towards the degradation of several oligo(ethyleneglycol) diethers in dichloromethane and a catalyst loading of 5–10 mol%.<sup>[92]</sup> The reaction mechanism, calculated for DME degradation, is proposed to proceed *via* a double DME coordinated intermediate **20** that emits dimethylether after rearrangement of  $\sigma$ - and lone pair electrons of the ether molecules forming **21**. Within two steps the ring ether is formed and released to regenerate **2**. In this study the role of the counter anion is not highlighted and may be considered negligible, however,  $\text{B}(\text{C}_6\text{F}_5)_4^-$  anions and neutral  $\text{B}(\text{C}_6\text{F}_5)_3$  in general are known to show catalytic activity in various chemical transformations including the hydrosilylation of olefins.<sup>[93]</sup> Within the last decade a number of transformations was found for  $\text{Cp}^*\text{Si}^+$  (**2**)<sup>[94]</sup> leading to novel low valent Si-species **22-24** (compiled in Scheme 9, left) but probably most striking is a further catalytic application that was found only recently in 2019 by a research group of WACKER Chemie AG (Scheme 9, right).<sup>[10,11]</sup>

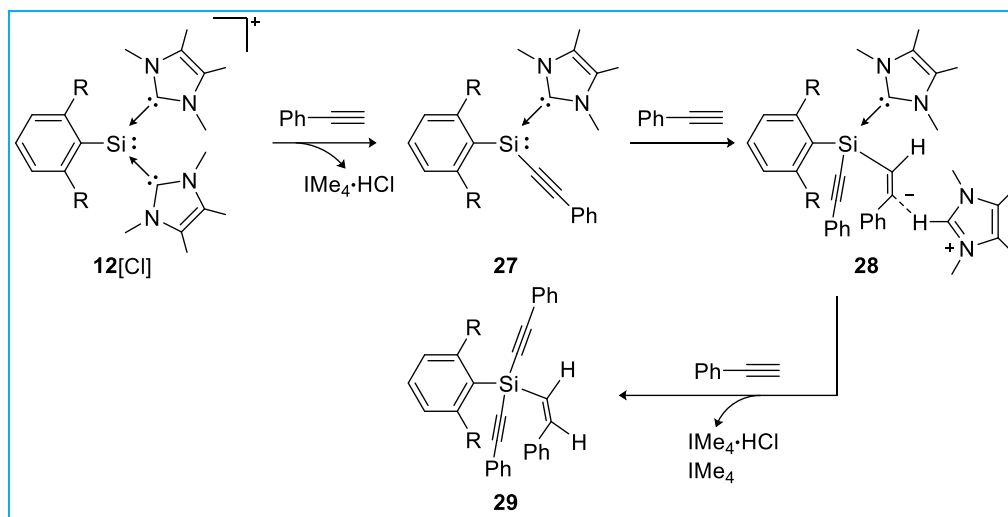


Scheme 9. Example reactivity of **2** towards nucleophiles forming **22-24** and catalytic degradation of ethers via **20** and **21** (left). Proposed mechanism of catalytic hydrosilylation of olefins under industrial suitable conditions (right).

Fritz-Langhals reported on hydrosilylation using **2** in even technical relevant conditions. In this, the mechanism is described with weak interaction of the Si(II) cation with the substrate weakening the Si–H bond of silanes (**25**). In this state the complex is able to undergo insertion of an unsaturated olefin in the Si–H bond (**26**) to form the product. It is of note that this is the first example of hydrosilylation using a low valent main group element that accepts a broad range of substrates and is able to compete to standard Pt(0) catalysts in selectivity, conversion and turnover. With that, the preeminent advantage of low cost and low toxic silicon could mark a turning point in hydrosilylation and with that heading towards the polymerization of polysiloxanes. The matter of the counter anion is more addressed in this study. Using  $2[B(C_6F_5)_4]$  the author states higher activity of the catalyst **2** (0.0013 mol% loading for terminal olefins) compared to non-metal  $[B(C_6F_5)_3]$  (1-5 mol% loading). In addition, the selective activation of  $Me_2SiCl$  (as opposed to the more electron-deficient  $MeSiCl_2$ ) suggests a cationic mechanism as described (Scheme 9). Variation of the anion revealed the efficiency of ion pair separation to be a stronger influence on the catalyst's activity than the anion's nature itself.

Silyliumylidenes of the type  $Ar-Si^+(NHC)_2$  have proven to be active in small molecule activation.<sup>[84]</sup> In 2014,  $mTer-Si^+(IME_4)_2$  (**12**) was shown to react with three equivalents of phenylacetylene ( $HC\equiv C-Ph$ ) yielding the double C–H activated and acetylene-hydrogenated product **29** (Scheme 10).<sup>[87]</sup> Calculated mechanism of the reaction suggests that the first oxidative addition of acetylene is followed by reductive H–Cl abstraction driven by one of the coordinated  $IME_4$  (**27**). Upon C–H activation of the second acetylene molecule, the hydrogen

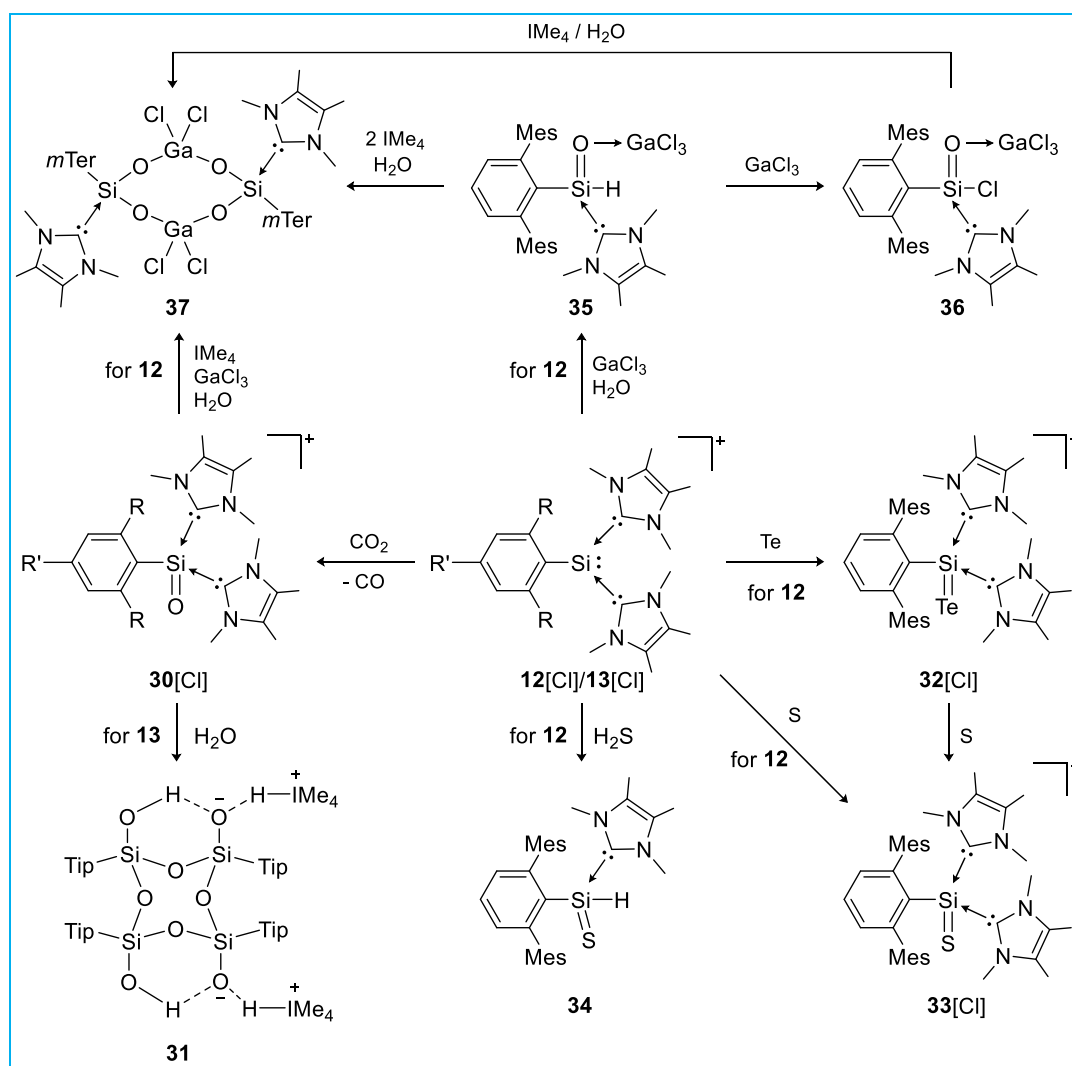
is transferred to the first acetylene substituent (**28**). Intermediate **28** is stabilized by surrounding  $\text{IME}_4\text{HCl}$  and reacts with a further acetylene molecule, whose hydrogen atom is again transferred to the unsaturated double bond. Overall, both NHCs are abstracted as  $\text{IME}_4\text{HCl}$  during the addition and hydrogen-transfer reaction of three phenylacetylene molecules.



Scheme 10. Activation and addition of phenylacetylene by **12** via a three-step mechanism including NHC-HCl abstraction forming **29** (R = Mes).

Furthermore, **13** is oxidized by  $\text{CO}_2$  furnishing CO and a stabilized 'Si=O' derivative, which is present in the form of the heavy silaacylium ion **30**. Controlled addition of small amounts  $\text{H}_2\text{O}$  to **30** enable further oxidation towards cyclotetrasiloxanediol dianion (**31**) (Scheme 11, left bottom).<sup>[95]</sup> A 4-membered ring compound was isolated as stable intermediate in case of R = *m*Ter (**12**).<sup>[95]</sup>

Different from the oxygen case, the heavier silaacylium ions of S (**33**), Se (**12<sup>Se</sup>**), and Te (**32**) are accessible directly from the reaction of **12** and **13** with the elemental chalcogens (Scheme 11, right).<sup>[96]</sup> Going down group 14, a transmetalation series can be initiated, in which the ever-lighter chalcogen replaces the former (**32** and **33**). Introducing an acidic reagent, such as hydrogen sulfide ( $\text{H}_2\text{S}$ ) results in abstraction of  $\text{IME}_4\text{HCl}$  and the neutral thiosilaaldehyde **34** (Scheme 11, bottom middle).<sup>[97]</sup> Whereas the acceptor-free silaaldehyde remained elusive, it could be shown that the Lewis acid-stabilized silaaldehyde **35** is observable via equimolar conversion of **12** with  $\text{GaCl}_3$  and  $\text{H}_2\text{O}$  under release of  $\text{IME}_4\text{HCl}$  (Scheme 11, top middle). Reaction of stable **35** with an excess of  $\text{GeCl}_3$  results in isolable silaaroyl chloride **36**. Treatment of **35** and **36** with additional equivalents of  $\text{IME}_4$  result in formation of gallium silacarboxylate complex **37** (Scheme 11).<sup>[98]</sup>



Scheme 11. Chalcogen activation by **12** (R = Mes, R' = H) / **13** (R = R' = *i*Pr) via oxidation of the *s*-type lone pair yielding **30**, **32**, **33**, and **34** with subsequent hydrolysis and oligomerization of **30** forming **31**

Turning towards nitrogen ligand-stabilized silyliumylidenes **7** and **17**, the so far shown reactivity is more limited. They show for example activation of heavier chalcogens such as elemental sulfur. Moreover, **7** can be transformed into novel low valent Si(II) species via dimerization and trimerization, using the precursor bis-silylene (**6**) or reductive hydride transfer agent K{HB(*i*Bu)<sub>3</sub>}, respectively.<sup>[83,90]</sup>

## 2.3.2 Silylones

Bonding and Electronic nature

Within the last two decades, the low valent silicon family has been extended by donor ligand-stabilized Si(0) compounds. This step into the stabilization of the smallest clusters of elemental silicon atoms, that feature no covalent ligand interactions, represents a major step in understanding the nature of silicon and provides fascinating new building blocks for novel silicon species and imaginable applications. Basically, these compounds can be divided into two types: i) single base stabilized multi nuclear **38**<sup>[25]</sup> and **39**,<sup>[99]</sup> that being “(D→Si<sup>(0)</sup>·)<sub>n</sub>” with n = 2, 3 (Figure 18, left) and ii) double base stabilized mono nuclear “D→:Si<sup>(0)</sup>:←D” complexes (Figure 18, right). Although all of these species are understandably highly reactive and difficult to handle, a clear distinction can be drawn between the first group with stabilizing Si–Si bonding and the second, which must do without these element–element bonds. In 2009, Frenking coined the term silylones for this compound class,<sup>[100]</sup> which is derived from the analog carbon species ‘carbones’ “D→:C:←D” that is known since the first appearance of C(PPh<sub>3</sub>)<sub>2</sub> in 1961 reported by Ramirez and its structural characterization in 1978.<sup>[101–103]</sup>

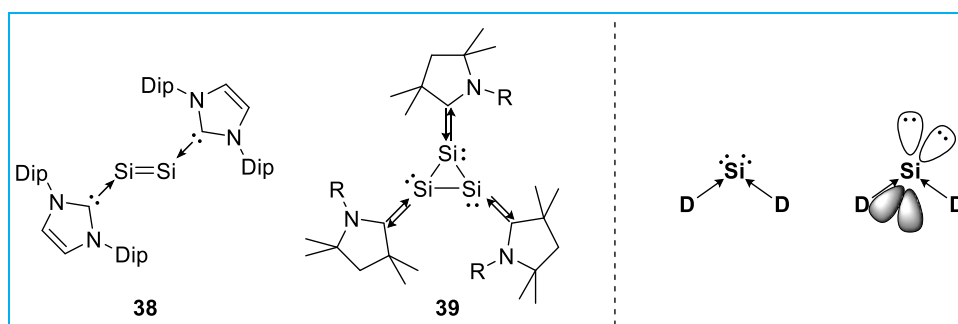


Figure 18. Polynuclear molecular Si<sup>0</sup> compounds **38** and **39** (right) and general representation of silylones with approximated frontier orbitals (right).

Of course, the bonding nature in compounds such as C(PPh<sub>3</sub>)<sub>2</sub> (**40**) needs to be described with at least two mesomeric structures reflecting the interplay between covalent and donor-acceptor interaction present between the central carbon and the phosphine ligands (Figure 19, left). In case of carbon, the favored hybridization questioned the carbone character, although it was proposed by both theory and structural analysis.<sup>[101,102,104,105]</sup> The experimental evidence for the presence of two stereochemically active lone pairs at the carbon center was provided in 1976 *via* the isolation of the geminal dimetallated (ClAu)<sub>2</sub>C(PPh<sub>3</sub>)<sub>2</sub> (Figure 19, right).<sup>[106]</sup>

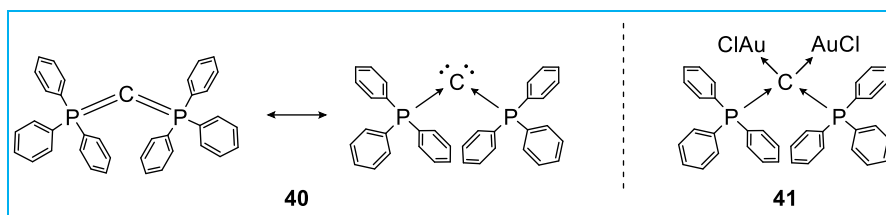


Figure 19. Mesomeric structures of carbene  $(\text{PPh}_3)_2\text{C}$  **40** and bimetallic complex  $(\text{PPh}_3)_2\text{C}(\text{AuCl})_2$  **41**.

In 2009, Frenking investigated the theoretical properties and expected stabilities of different substituted carbones<sup>[105]</sup> and in an analog study, printed later the same year, he highlighted silylones.<sup>[100]</sup> In this work he used quantum chemical DFT methods to describe their bonding situation and electronic structure as follows: Silylones are strongly bent divalent  $\text{Si}(0)$  compounds with two donor-acceptor bonds and Si-located lone pairs of electrons in  $\pi$ - and  $\sigma$ -symmetry (Figure 20, right). The energetic level of the lone pairs was predicted calculating first and second proton affinities and revealed the better accessibility of the  $\pi$ -lone pair (first  $\text{PA} \approx 230 - 290 \text{ kcal mol}^{-1}$ ) and subsequent protonation of the  $\sigma$ -lone pair (second  $\text{PA} \approx 70 - 150 \text{ kcal mol}^{-1}$ ). The interaction of the ligands (in the singlet state) and the silicon atom (also in the singlet state) is described as sigma-donation into the vacant and orthogonal  $p$ -type orbitals. This description explains vividly why silylones are not linear but should be found with  $\text{L-Si-L}$  angles of near to  $90^\circ$ . If, on the other hand, the covalent bond shares – *i.e.* a silaallene with classical double bonds – are to be emphasized, the ligands as well as the central atom would technically need to reside in the triplet state. However, in main group chemistry the formation of multiple bond character using donor-acceptor interactions and  $\pi$ -back donation of  $\text{ER}_2$ -fragments ( $\text{E} = \text{p-block element}$ ) in the singlet state is a today well-known concept.

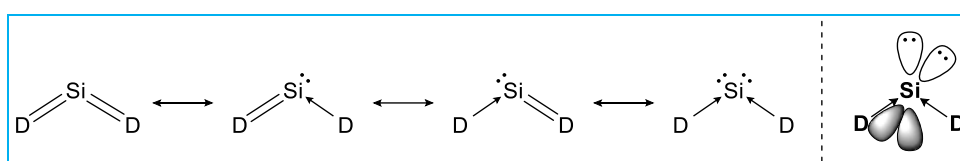


Figure 20. Mesomeric structures of silylones  $\text{SiD}_2$  (left) and approximated frontier orbitals (right). ( $\text{D} = \text{Donor}$ )

However, compounds of the type  $\text{R}_2\text{E}'=\text{E}=\text{E}'\text{R}_2$  ( $\text{E} = \text{Si, Ge, Sn}$ ,  $\text{E}' = \text{Si, Ge, Sn}$ ) – so called tritetrelallenes – were isolated much earlier with the first example of a tristanaallene in 1999.<sup>[107]</sup> Other than expected for standard carbon-like allenes these species do show a bending angle, which is  $156.0^\circ$  for the Wiberg tristanaallene. That found angle points out the existing share of a tetrylone character in tritetrelallenes, but the bond order and  $\text{E-E}$  distances indicate clear multiple bond character, as feature of allene-type bonding.

The discussion of silylone- vs. allene-character is a key aspect in understanding the nature of  $\text{L}_2\text{Si}^{(0)}$  compounds.<sup>[84,108,109]</sup> Whereas until today no ‘true’ ditetrelsilaallene or silylone could be

observed, the compounds isolated need to be discussed carefully using structural, experimental, and theoretical parameters (Figure 20, left):

#### Structural and spectroscopic properties

First and obvious parameters can be determined using structural-analytical characteristics of the compound in question. As a rule of thumb, the silylone character increases with the L–Si–L angle getting nearer to 90° and decreases as the angle approaches 180°. Of course, the ligands properties, such as steric demand, denticity, etc. influence the bonding angle, and therefore influence the nature of the compound to a certain extent. Turning to the <sup>29</sup>Si-NMR of silylones and related Si(0) species, the signals follow the trend of highfield shifting and therefore (de)shielding of the central Si-nucleus with increasing silylone character and range from roughly  $\delta(^{29}\text{Si}) = 220$  ppm to –100 ppm.

#### Experimental behavior

Experimentally, the compound can be tested for its coordination behavior to proof the existence of two stereo chemically active lone pairs, using small and Lewis acidic synthons such as ZnCl<sub>2</sub>, Fe(CO)<sub>4</sub>, GaCl<sub>3</sub>, or BCl<sub>3</sub>. This test can be thwarted by the candidate's unique chemical properties and possible instabilities, so that it should be seen as one puzzle piece of understanding.

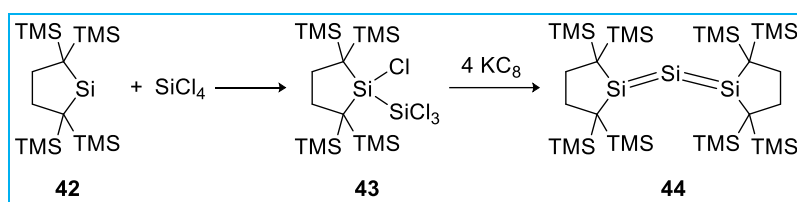
#### Computations

Performing detailed theoretical investigations, the properties of a silylone can be expressed by the frontier orbitals and bonding analysis, as well as calculation of proton affinities (1st and 2nd) that were determined between 1<sup>st</sup> 272.2 – 281.7 kcal mol<sup>-1</sup> / 2<sup>nd</sup> 186.7 – 213.1 kcal mol<sup>-1</sup> for today's known silylone compounds. It should be noted that these values were determined using different levels of theory and basis sets, limiting the comparability of the values.

For the reasons described, silylones should always be carefully characterized. For the sake of clarity, however, the representatives of this structure class in this thesis are consistently named silylones and described in terms of this structural feature, although the silylone character is never pure and other mesomeric structures may sometimes have a higher share.

#### History and Synthesis – State of the Art

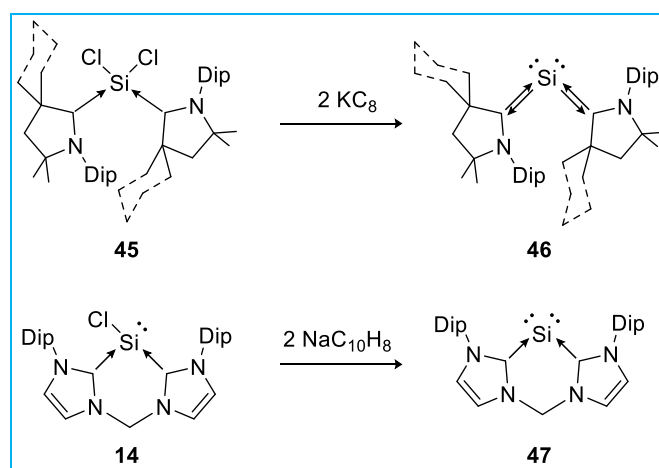
The seminal isolation of trisilaallene **44** by Kira in 2003 marks the first milestone in silylone chemistry.<sup>[110]</sup> It was synthesized from the SiCl<sub>4</sub> addition product **43** of cyclic silylene (**42**), by reductive dehalogenation using four equivalents of KC<sub>8</sub> over a reaction time of one day (Scheme 12).



Scheme 12. Synthesis of first trisilaallene **44**, starting from cyclo-alkyl silylene **42**, via oxidative addition product **43** and subsequent reduction using  $\text{KC}_8$ .

It is noteworthy that the compound was not discussed at that time because of its silylone character but for its unusual structure, since the idea of stable silylones was not yet widespread. Concluding, the authors indicated the structure to consist of two trans-bent  $\text{Si}=\text{Si}$  double bonds with a shared Si central atom.

Ten years later, the groups of Roesky and Driess reported independently on the compounds **46**<sup>[111]</sup> ( $\text{cAAC}_2\text{Si}$ ) and **47**<sup>[29]</sup> (bis-NHCSi) within few months (Scheme 13). Both silylones stem from reductive dehalogenation of suitable Si(II) precursors – a straight forward and until today the most often used synthetic procedure. In contrast, Roesky started with neutral silylene **45**, whereas Driess used silyliumylidene **14** as starting material.



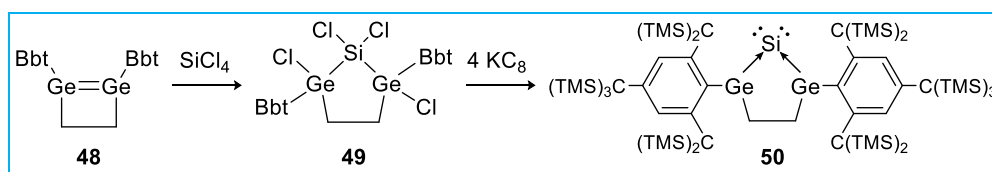
Scheme 13. Preparation of silylones **46** and **47**. Both compounds are formed by reductive dehalogenation of suitable Si(II) precursors (**45**, **14**).

**46** is isolated as deep blue powder and described as having a biradicaloid character, although no EPR signal could be found. Detailed theoretical study revealed the biradicaloid character being inherited from the precursor silylene, that forms a silylene carrying two radical substituents, in which the two unpaired electrons give the  $\pi$ -HOMO.<sup>[112]</sup> However, the computations suggest the silylone character to be dominating, since NBO analysis displayed a  $\sigma$ -lone pair and a slightly Si centered three-center C–Si–C  $\pi$ -orbital. In line with that finding, the calculated proton affinities of  $\text{PA}(1) = 272.2 \text{ kcal mol}^{-1}$  and quite high  $\text{PA}(2) = 186.7 \text{ kcal mol}^{-1}$  point towards two distinct lone-pairs of electrons. In summary the bonding situation of **46** was displayed as a silylone, stabilized by  $\sigma$ -donor cAAC ligands and accompanying  $\text{Si}\rightarrow\text{C}$

$\pi$ -back bonding. Analytical measurements of **46** showed the  $^{29}\text{Si}$  NMR signal to appear at  $\delta = 66.7$  ppm and in SC-XRD study the C–Si–C angle displays with  $117.7^\circ$ . Those values are in good agreement with a high degree of  $\pi$ -back bonding from the silylone center.

Cyclic silylone **47** is furnished as a deep red solid *via* reduction using a sodium naphthalenide solution. Computational investigations found the Si  $\pi$ -type electron lone pair in HOMO and the  $\sigma$ -type lone pair in HOMO–1. Admixture of the silicon  $\pi$ -bonding orbital with the Si–C bonds, indicate occurring  $\pi$ -back donation into the NHC ligands that, in fact, leads to shortened Si–C bonds. The calculated proton affinities are high with  $\text{PA}(1) = 281.7$  kcal mol $^{-1}$  and  $\text{PA}(2) = 189.4$  kcal mol $^{-1}$ , thus indicating a considerable silylone character. SC-XRD and NMR measurement provide further evidence by displaying C–Si–C angle of  $89.1^\circ$  and  $^{29}\text{Si}$  shift of  $\delta = -83.8$  ppm. The severe highfield shift of **47** compared to **46**, stems from the more effective shielding in **47**, rationalized by the stronger  $\sigma$ -donor and weaker  $\pi$ -acceptor ability of the NHC ligand framework.

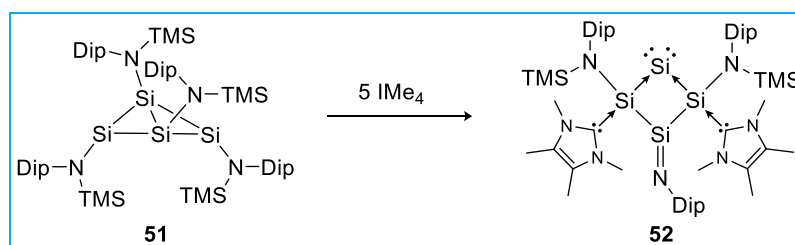
Since 2017 also bis-tetrylene stabilized silylones are accessible as in the case of 1,3-digerma-2-silylone **50**, ring compound **52**, and bis-NHSi-stabilized **54** and **56**.<sup>[91,113–115]</sup> Utilization of the ethylene [2+2] cycloaddition product of BbtGe $\equiv$ GeBbt **48**, affords a chlorinated Si(II) precursor (**49**), that features a five-membered SiGe $_2$ C $_2$ -ring. Reduction with KC $_8$  gives rise to orange **50** in 57% isolated yield (Scheme 14).<sup>[115]</sup> Structural investigations suggest a not negligible silylone character considering the acute Ge–Si–Ge angle of  $80.1^\circ$  and Ge–Si bond lengths of 2.2900 and 2.2681 Å that are in between typical single ( $\sim 2.4$  Å) and double bonds ( $\sim 2.26$  Å). Moreover, the – compared to the starting material – noticeable upfield shifted  $^{29}\text{Si}$  NMR signal at  $\delta = -16.5$  ppm, could be explained by the acute Ge–Si–Ge angle and the  $\sigma$ -donating ability of the bis-germylene ligand. This finding was further substantiated by DFT calculation that represents the frontier orbitals of a simplified model compound as follows: The HOMO could be found as a  $\pi$ -orbital, delocalized over the Ge–Si–Ge atoms, whereas the HOMO–1 and HOMO–2 represent the  $\sigma$ -Ge–Si interactions. One Si-located lone-pair of electrons (3s) can be found in the HOMO–5 additionally.



Scheme 14. Isolation of bis-germylene stabilized silylone **50**, starting from cycloaddition product **48** of respective digermyne. Addition of SiCl $_4$  (**49**) and subsequent reduction affords the silylone (Bbt = 2,6-bis[CH(SiMe $_3$ ) $_2$ ]-4-[C(SiMe $_3$ ) $_3$ ]-C $_6$ H $_2$ ).

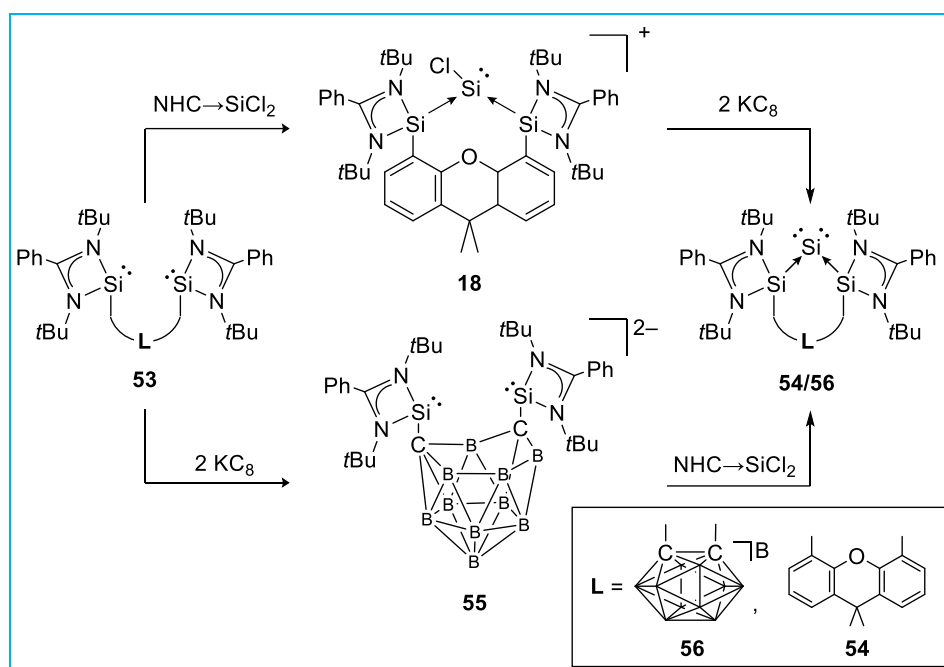
Both, theory and experimental findings concede **50** a silylone character, which, however, needs to be put into perspective by the double bond character present, that is in contrast to the description as a silylone.

The until today latest known ligand system, that has been employed successfully into the stabilization of silylones, are bis-silylenes. In 2019 the group of Lips could show the isolation of a cyclic Si<sub>4</sub>-ring based silylone **52**, yielded *via* conversion of the precursor Si<sub>4</sub>{N(SiMe<sub>3</sub>)Dip}<sub>2</sub>{IMe<sub>4</sub>}<sub>2</sub>{NDip} (**51**) with five equivalents IMe<sub>4</sub> (Scheme 15).<sup>[114]</sup> The compound formed shows one two-coordinate Si-atom, that is surrounded by two '(NHC)(NR<sub>2</sub>)Si:' silylenes that are part of the Si<sub>3</sub>-ligand's ring scaffolding. The (NHC)(NR<sub>2</sub>)Si–Si<sup>0</sup> bond lengths (2.318, 2.301 Å) are between single (2.4 Å) and double bonds (2.138 – 2.289 Å) and the (NHC)(NR<sub>2</sub>)Si–Si<sup>0</sup>–Si(NHC)(NR<sub>2</sub>) angle is found to be 93.43°, pronouncing the silylone character. The <sup>29</sup>Si NMR shows a signal at δ = 55.6 ppm for the central silylone Si nucleus. The calculated molecular orbitals show two lone pairs of electrons: one in the HOMO (π-type), which is partly delocalized over the R<sub>2</sub>Si–Si<sup>0</sup>–SiR<sub>2</sub> ring moiety, and another in the HOMO–1 and HOMO–2 (σ-type). Calculation of the proton affinities affords PA(1) = 278.2 kcal mol<sup>-1</sup> and PA(2) = 213.1 kcal mol<sup>-1</sup>, which is in the same range than **43** and **44**, although the PA(2) is slightly enlarged in comparison.



Scheme 15. Isolation of bis-silylene stabilized silylone **52**, through reaction of bicyclic silicon ring compound **51** with IMe<sub>4</sub>.

The latest examples were reported in 2019 and 2020 by Driess, using amidinate type bis-NHSi's, bridged *via* a xanthene backbone in **54**<sup>[91]</sup> and an *ortho*-carborane in **56**<sup>[113]</sup>. While compound **54** was synthesized according to the standard procedure by treating the respective silyliumylidene (**18**) with KC<sub>8</sub> (Scheme 16, top), the synthetic procedure of **56** uses a variation. In this case, the isolated ligand (NHSi)<sub>2</sub>-carbo (**53**) is reduced firstly to yield the nido-carborane dianionic form **55**. Subsequently, this is reacted with NHC→SiCl<sub>2</sub> to furnish the silylone **56** (Scheme 16, bottom). Interestingly, reversing the synthetic order is the key to the formation of this silylone, as all attempts to follow the 'standard' procedure resulted in unidentified mixtures without product formation.



Scheme 16. Syntheses of bis-silylene stabilized silylones **54** and **56**. The synthesis strategy involves complexation of a  $\text{SiCl}_2$  synthon and reductive dehalogenation using  $\text{KC}_8$  in both cases and is tailored to the corresponding bridging.

Following the procedure, **54** and **56** can be isolated as dark purple or red solids in moderate to high yields (78%, 61%), respectively. Structural analysis reveals the silylone  $^{29}\text{Si}$  NMR signals at  $\delta = -187.5$  ppm (**54**) and  $-263.8$  ppm (**56**). The exceptional highfield shifted resonances indicate a strong shielding of the  $\text{Si}^0$  nucleus provided by the applied ligands that is comparable with bare Si-atoms within siliconoid clusters. It is of note, that the compounds **54** and **56** are direct descendants to Kira's silylone **44**, and therefore imply clearly lower  $\pi$ -acceptor abilities of **53**, compared to the cyclic alkyl silylene **42**. The Si–Si–Si angles of **54** and **56** amount to  $104.4^\circ$  and  $82.7^\circ$ , respectively. The widened angle in **54** is obviously driven by the exceptional steric demand of the  $\text{Si}_3\text{C}_2\text{OC}_2$ -8-membered ring, however, it influences the electronic environment towards more allenic features. Theoretical calculations were performed to gain further information about the electronic environments in **54** and **56**. Whereas both calculated WBI (**54**: 1.40, **56**: 1.44) and Si–Si bond lengths (**54**: 2.2526, 2.2586 Å; **56**: 2.2272, 2.2225 Å) imply similar double bond contributions, NBO analysis manifests differences in the bonding nature. In **54** the  $\sigma$ -lone pair is found located within the LP1-orbital, while the  $\pi$ -type electrons are presenting delocalized over the Si–Si–Si moiety. In contrast, the lone pairs of electrons in **56** are found localized in HOMO ( $\pi$ -type lone pair) and HOMO–1 ( $\sigma$ -type lone pair).

Understandably, interest in ordering silylones by their silylone character is high; it would allow verification of the premise after a higher share of a silylone character entails higher reactivity. However, concluding from the given state of facts, it is not reasonable to strictly rank the

known compounds, since the data are not always comparable and conclusive. For example, an L–Si–L angle close to 90° should induce a very high silylone character, however, the angles are strongly influenced by the coordination and structural fashion of the ligand. So that in the case of **54**, it is quite high with 104°, although the theoretical description and reactivity imply a rather high silylone character.

An approximate idea of the relative silylone character of compounds **44–56** can best be made by comparing the <sup>29</sup>Si NMR shifts, according to which Figure 21 is plotted. The trend in <sup>29</sup>Si NMR shifts shows the increasing shielding of the Si<sup>0</sup> nucleus, with increasing donor ability and/or decreasing acceptor ability of the ligands, corresponding to the electron richness of the Si<sup>0</sup> center.

Within the line of isolated silylones, it is easy to understand that the stability of those complexes goes in hand with the degree of π-back donation that reduces the electron density at the Si(0) center. In a trade of, the enhanced stability comes at the cost of decreasing reactivity and a reduced silylone character. The quest for a ‘real’ silylone that shows no allene character is therefore both – academic eager and a pursuit for novel reactivities. Whether as a preparative building block, Si(0) transfer agent, or in small molecule activation and catalysis, silylones are considered to be promising candidates.

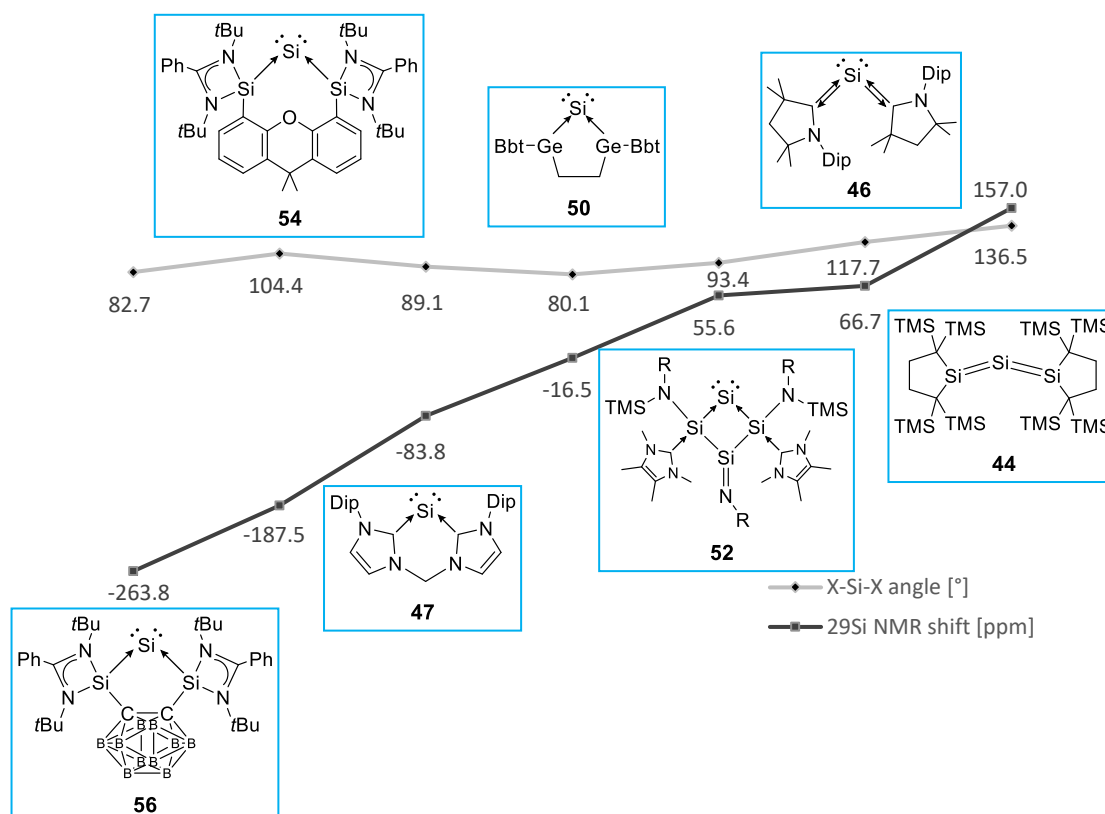
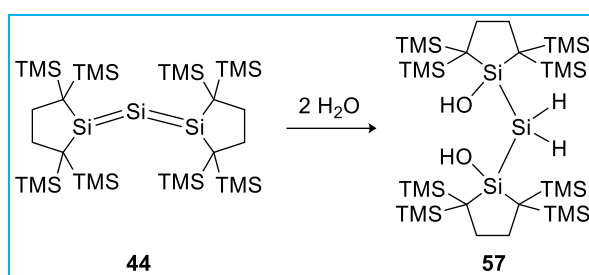


Figure 21. Graphic representation of isolated silylones **44** to **56** according to their L–Si–L angle [°] and <sup>29</sup>Si-NMR shift δ [ppm].

Reactivity (recent advances)

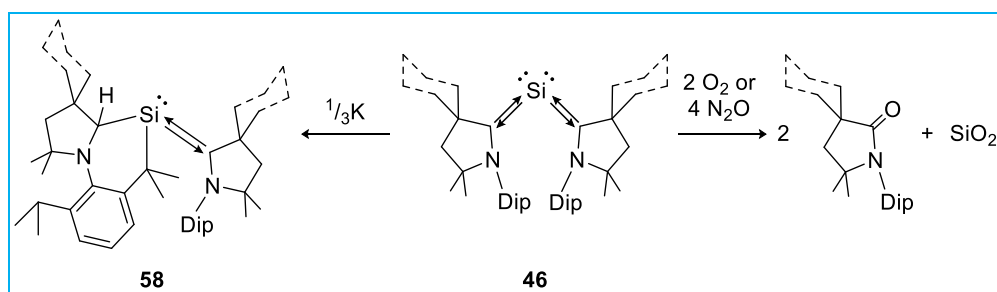
Since the formation and reactivity of transition metal complexes of silylones are to be emphasized in an extra subchapter (see 2.3.3), these are skipped here. Rather, this chapter will focus on conversion of silylones and their reactivity towards small molecules.

Together with the seminal report on the trisilaallene in 2003, Kira investigated the conversion of compound **44** with  $\text{H}_2\text{O}$ , which lead to addition product **57** pointing out the cooperativity within the  $\text{Si}_3$ -skeleton (Scheme 17).<sup>[110]</sup> The addition of water is conceivable for both mesomeric structures. However, the authors contribute the reactivity to anti-addition to the allene double bonds.



Scheme 17. Reaction of trisilaallene **44** with  $\text{H}_2\text{O}$  yielding addition product **57**.

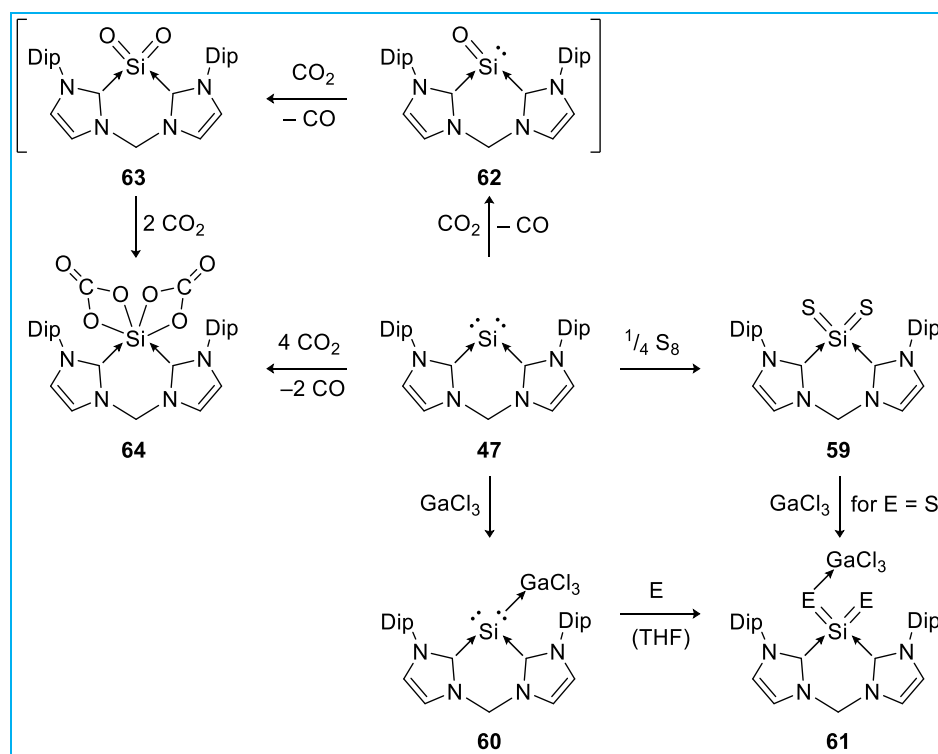
In 2014, Roesky could show an unusual intramolecular bond activation reaction of silylone  $(\text{cAAC})_2\text{Si}$  (**46**).<sup>[116]</sup> By treating **46** with substoichiometric amounts of elemental potassium the  $\text{Si}-\text{C}(\text{cAAC})$  bond was inserted in a  $\text{H}-\text{CMe}_2$  bond of one Dip-ligand resulting in three-coordinated silylene **58** (Scheme 18, left). The reaction mechanism was theoretically as well as spectroscopically shown to proceed *via* the formation of a radical anion localized at one cAAC-carbon center. This reactive intermediate abstracts one  $\text{H}-\text{CMe}_2$  radical resulting in  $\cdot\text{CMe}_2$  that is stabilized by reduction of a further silylone molecule and formation of the silylene **58**. Oxidation with molecular oxygen or  $\text{N}_2\text{O}$ , in contrast, results in defined decomposition of the silylone into  $\text{cAAC}=\text{O}$  and  $\text{SiO}_2$  (Scheme 18, right).



Scheme 18. Reduction (left) and oxidation (right) of silylone **46**, yielding compound **58** and free  $\text{SiO}_2$ , respectively.

Silylone bis-NHCSi (**47**) was investigated for its reactivity towards heavier elemental chalcogens (S, Se, and Te) as well as the small molecule  $\text{CO}_2$ .<sup>[109,117]</sup> With heavier chalcogens,

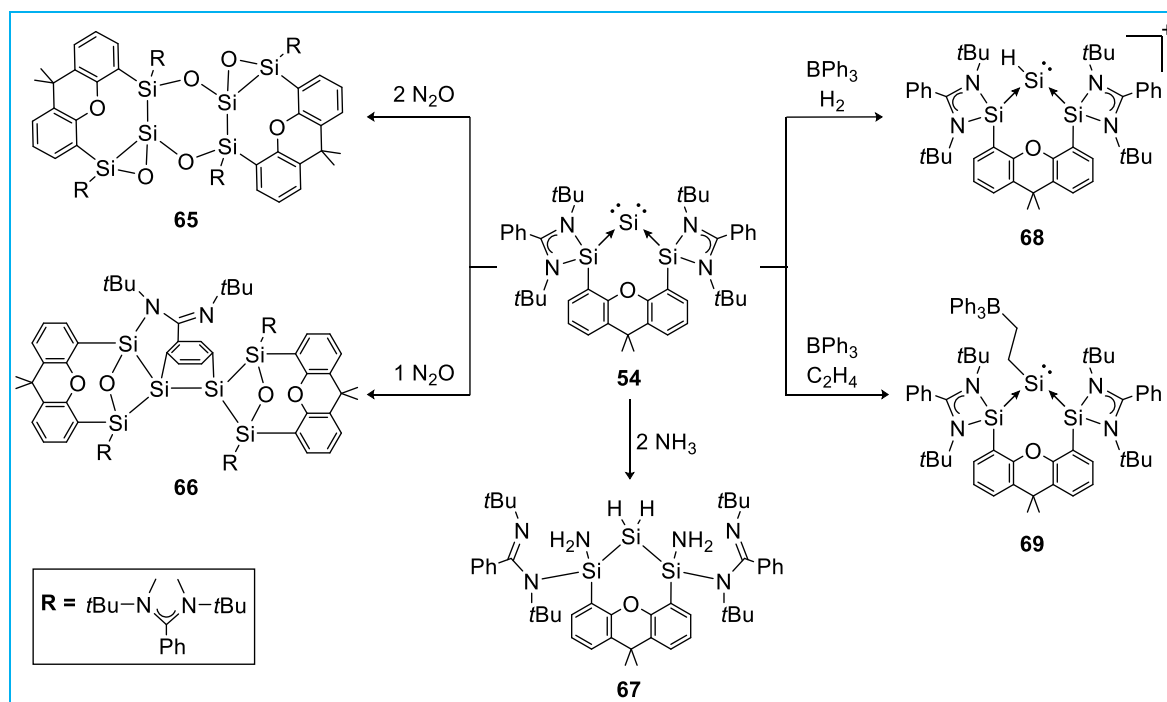
**47** shows oxidation of the silicon *via* one or both lone pairs of electrons (**59**, **61**), which could be accompanied by coordination of the Lewis acid GaCl<sub>3</sub> in **60** and **61** (Scheme 19, bottom right). The addition of CO<sub>2</sub> gives a silicon dicarbonate (**64**), that originates from intermediate formation of stabilized ‘Si=O’ **62** and ‘O=Si=O’ **63** (Scheme 19, top left). The reaction is accompanied by release of CO, which could be detected in <sup>13</sup>C NMR monitoring. With that the so-called ‘molecular sand’ (stabilized molecular SiO<sub>2</sub>) remains elusive but could be rationalized as an intermediate (**63**) in this reaction.



Scheme 19. Selected reactivity of silylone **47** with different chalcogen sources forming direct addition product **59** and Lewis acid adducts **60** and **61** (E = S, Se, Te (*via* TeP(*n*Bu)<sub>3</sub>)). Direct addition product of CO<sub>2</sub> (**62**) could not be isolated and reacted *via* **63** to stable **64**.

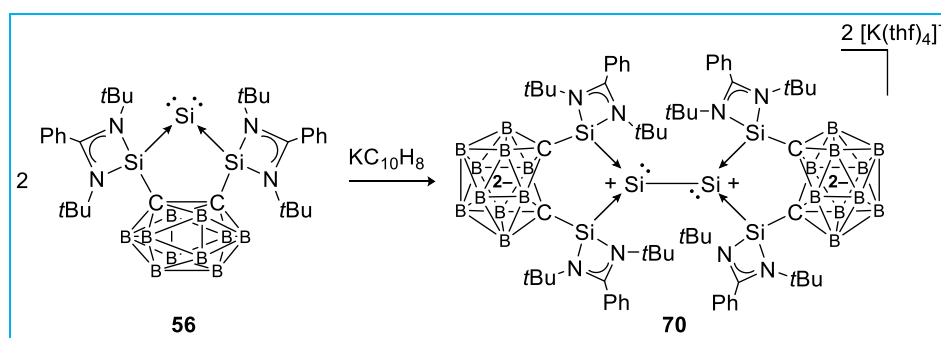
Bissilylene supported silylone **54** was tested towards a range of gaseous small molecules.<sup>[91]</sup> In this study the compound showed high reactivity toward N<sub>2</sub>O, NH<sub>3</sub>, H<sub>2</sub>, and C<sub>2</sub>H<sub>4</sub> (Scheme 20). In accordance with the oxophilic nature of silicon, the compound shows conversion with oxygen transfer agents CO<sub>2</sub>, O<sub>2</sub> and N<sub>2</sub>O; out of which only N<sub>2</sub>O produces selective products. Depending on the stoichiometry of the reaction, the dimerization products **65** and **66** were isolated. In both cases, no formation of ‘Si=O’ or ‘SiO<sub>2</sub>’ could be observed, instead, cooperativity between the silylene ligands and the Si<sup>0</sup> center determines the reactivity. Exposure of XantSi to NH<sub>3</sub> results in N–H activation of two ammonia molecules to form **67**. Similar to the conversion of **44** with water, the NH<sub>2</sub>-fragments are transferred to the silylene moieties. Furthermore, two hydride atoms are connected to the former Si<sup>0</sup> center. Whereas the silylone **54** does not react with nonpolar H<sub>2</sub> and C<sub>2</sub>H<sub>4</sub>, the reaction could be triggered by

addition of the sterically demanding Lewis acid  $\text{BPh}_3$ . As the authors state, an interaction of the silylone and  $\text{BPh}_3$  could be identified in spectroscopic analysis ( $^1\text{H}$  NMR) and a slight color change of the reaction mixture. In computations two minima were found corresponding to the perpendicular directions of the silylone's lone pairs. Using the FLP concept, the heteroleptic cleavage of  $\text{H}_2$  (**68**) and the addition of ethylene (**69**) could be observed.



Scheme 20. Selected reactivity of silylone **54** towards small and gaseous molecules  $\text{N}_2\text{O}$  (**65**, **66**; left),  $\text{H}_2$  (**68**) and  $\text{C}_2\text{H}_4$  (**69**; right) and  $\text{NH}_3$  (**67**; bottom).

In 2020, Driess reported on a substoichiometrical reduction of **56** using potassium naphthalenide (Scheme 21).<sup>[113]</sup> In contrast to **46**, no intramolecular bond activation was observed. Rather, the carborane bridge in **56** acts a redox non-innocent ligand, allowing electron uptake upon rearrangement to *nido*-carborane. Stabilization is achieved *via* homocoupling to zwitterionic compound **70**.



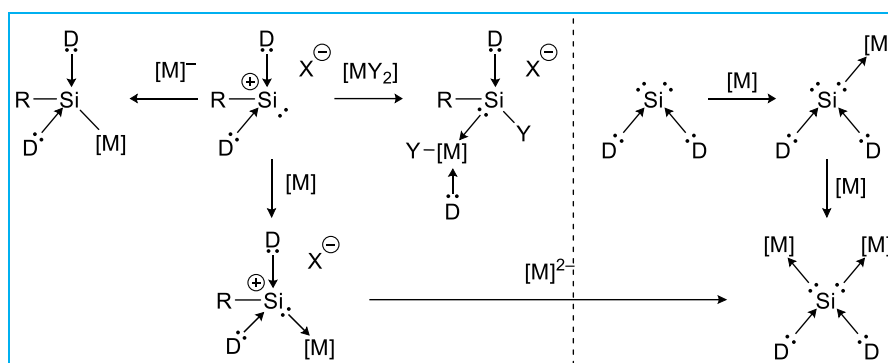
Scheme 21. Substoichiometrical reduction of silylone **56** using K Naph forming dimer **70**.

## 2.3.3 Silyliumylidene and Silylone Metal Complexes

Even though a major goal of main group chemistry is to mimic transition metals and thus provide a cost-effective and more environmentally friendly alternative, it would be a mistake to exclude the capability of low-valent silicon compounds as ligands for transition metal complexes out of false conceit. NHCs are the perfect example that teaches the overwhelming effect of a powerful ligand system. They do show catalytic activity as standalones, however, this clearly takes a back seat to their importance in organometallic complexes. Currently, silylenes are highlighted for their potential as auxiliary ligands in catalysis. Their influence on transition metal catalyst can be compared with those of phosphines and even NHCs, as demonstrated in several show cases. However, additional to 'standard' ligand properties – *i.e.*  $\sigma$ -donation and  $\pi$ -back donation – silylenes and related species enable Si–M cooperativity. Synergistic effects between these metal centers could further lower activation barriers and improve selectivity. Silyliumylidenes and silylones are gaining increasing attention currently, however, their coordination chemistry is still in its early stages.

Bonding and Electronic nature

Whereas, both species have accessible lone pairs of electrons for direct coordination, silyliumylidenes offer two more potential reactive sites for transition metals: (i) Their cationic nature should allow for salt metathesis reactions with metallates and metal hydrides, and (ii) commonly used stabilizing Lewis bases could undergo ligand exchange reactions and rearrangements, unblocking reactivity towards metal precursors. Halosilyliumylidene metal complexes, moreover, do have the potential to be converted into bimetallic silylone complexes *via* reductive dehalogenation using metallate precursors. Scheme 22 displays conceivable reaction pathways forming double donor-stabilized silyliumylidene- and silylone metal complexes.



Scheme 22. Selected reaction pathways towards silyliumylidene- (left) and silylone- (right) transition metal (M) complexes.

Although most silyliumylidene and silylone complexes are formed with late transition metals, especially group 6 metals are also popular.

Like commonly used phosphine or NHC ligands, silyliumylidenes and silylones are tunable in their steric demand. However, synthetic approaches are less handy and their electronic features are more in focus of recent investigations. Isolated examples reveal that silyliumylidenes combine  $\sigma$ -donor properties with pronounced electrophilicity to form novel Si(II)–M complexes (Figure 22, left). Thus, their cationic nature holds a contrary property to the more common silylene ligands. Silylones on the other hand are expected to show even stronger  $\sigma$ -donor properties, due to the exceptional electron-rich Si<sup>0</sup> center, while providing an additional lone pair of electrons at the same time (Figure 22, right).

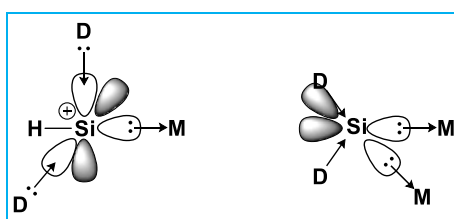
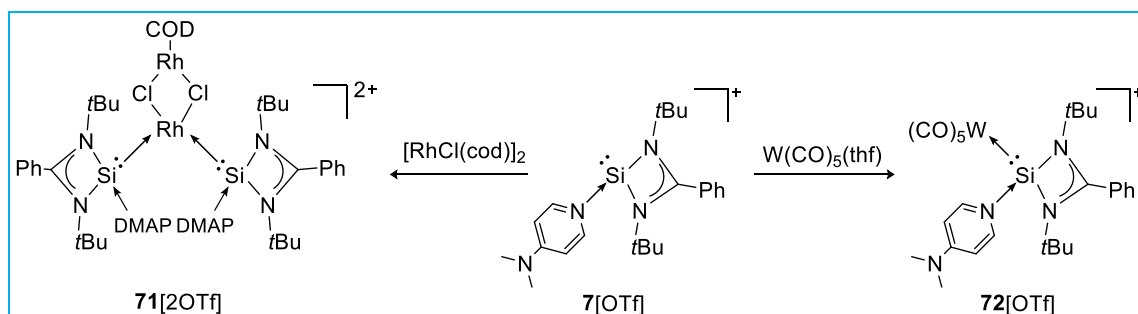


Figure 22. General depiction with approximated frontier orbitals of silyliumylidene- (left) and silylone- (right) transition metal (M) complexes.

## History and Synthesis – State of the Art

### Silyliumylidene

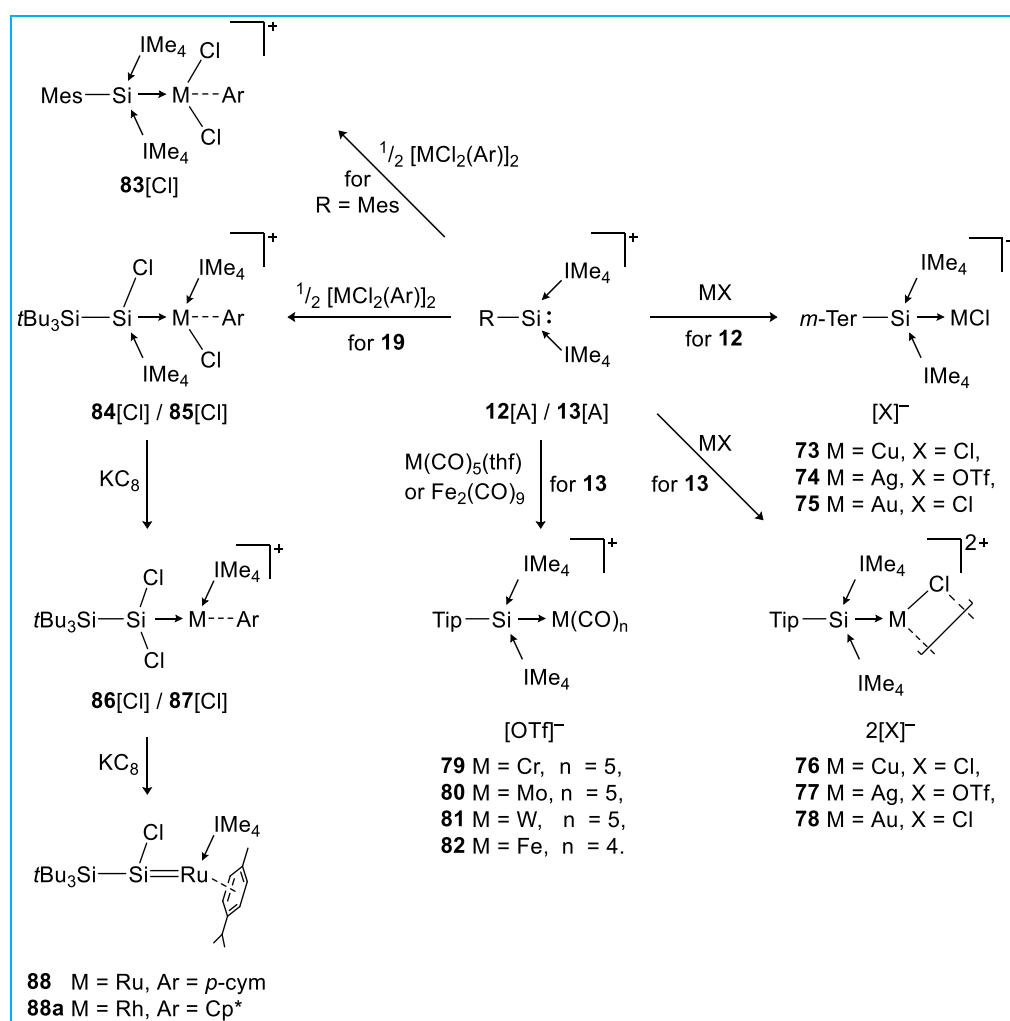
Two silyliumylidene transition metal complexes were reported by So from DMAP-stabilized silyliumylidene **7**.<sup>[118]</sup> In this case, **72** was isolated from reaction of the OTf- salt with W(CO)<sub>5</sub>(thf) complex, however, upon reaction with [RhCl(cod)]<sub>2</sub> the dimeric complex **71** is formed under release of one cod (Scheme 23). In **71** two silyliumylidene ligands are connected to one Rh center. In <sup>29</sup>Si NMR an expected downfield shift can be observed for dication **71** ( $\delta(^{29}\text{Si}) = 40.5$  ppm) and W(CO)<sub>5</sub> complex **72** ( $\delta(^{29}\text{Si}) = 51.6$  ppm) for deshielding of the Si-nuclei.



Scheme 23. Reactions of silyliumylidene **7** with [RhCl(cod)]<sub>2</sub> (left) and W(CO)<sub>5</sub>(thf) (right) to yield the respective complexes **71** and **72**.

Starting from R(IMe)<sub>2</sub>SiCl (R = *m*Ter (**12**), Tip (**13**), *t*Bu<sub>3</sub>Si (**19**), *t*Bu<sub>2</sub>MeSi), our group has reported a list of defined silyliumylidene metal complexes.<sup>[119,120]</sup> Using group 11 coinage

metals, it was shown that the complex structure (monomer vs. dimer) depends on the steric demand of the covalent substituent (Scheme 24, right). While **73-75** could be isolated in their monomeric form (in the solid state), the Tipp substituent allowed dimerization for **76-78**, as shown by SC-XRD analysis. In further coordination chemistry the smaller Tipp substituted silyliumylidene was used to form transition metal carbonyl complexes of group 6 (**79-81**) and 8 (**82**) (Scheme 24, middle). All of these complexes were furnished *via* direct coordination of the neutral metal fragments to the silyliumylidene's lone pair. In a slightly different approach, dimeric, halo-bridged Ru and Rh precursors revealed a further size dependency within the coordination chemistry of  $R(\text{NHC})_2\text{Si}^+\text{:}$ . Upon addition of a monomeric precursor moiety, one former Si bound NHC and one former metal bound chlorine, migrate *vice versa*. Complexes  $\text{NHC}(\text{Cl})\text{RSi} \rightarrow \text{MR}(\text{Cl})\text{NHC}$  were isolated for aryl substituent Tip and electropositive silyl (**84-85**) ligands. If the steric demand of aryl substituent is decreased further to Mes, the direct addition products  $R(\text{NHC})_2\text{Si} \rightarrow \text{MCl}_2\text{R}$  (**83**) were obtained. In all complexes an upfield shift in  $^{29}\text{Si}$  NMR signals, that range from  $\delta = -48.8$  to  $6.3$  ppm was observed.



Scheme 24. Selected reactivities of silyliumylidene **12** (R = *mTer*) / **13** (R = Tip) towards transition metal precursors of group 8, 9 (left), group 6, 8 (middle) and group 11 (right).

Finally, complexes **84–85** could be reduced using  $\text{KC}_8$  to the silyl-substituted metal complexes **86–87** and, in case of Ru, even to silylidene-type complex **88** (Scheme 24, left).

Besides it should be mentioned, that silyliumylidene metal complexes can also be furnished from alternative (non-silyliumylidene) starting materials. Our group reported in 2013 on a base stabilized silyliumylidene-phosphide **89**, derived from a zwitterionic phosphasilene (Figure 23).<sup>[121]</sup> Computations suggest the dinuclear platinum species to feature a  $\sigma$ -type silicon centered lone pair, overlapping in side-on fashion with  $\text{Pt}^0\text{--Pt}^0$  empty  $d$ -orbitals (HOMO). The silyliumylidene's vacant  $p$ -orbitals receive  $\pi$ -electrons from  $p$ -type lone pair of the phosphide (HOMO–1). With this compound **89** exhibits dominant silyliumylidene character as represented by resonance structures in Figure 23.

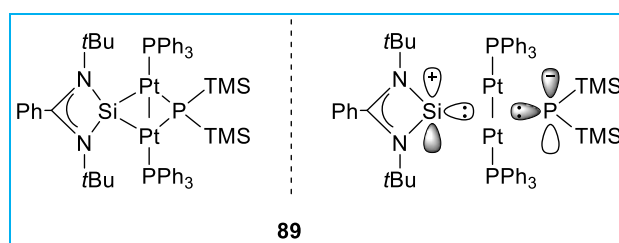


Figure 23. Dinuclear silyliumylidene platinum complex **89** in neutral depiction (left) and zwitterionic form with approximated frontier orbitals (right).

### Silylone

The coordination chemistry of silylones remains comparatively unexplored, with only few examples known today. Literature research affords the first coordination complex of a formal silylone (**90**) to be reported in 1988 by Zybill (Figure 24, left).<sup>[122]</sup> The  $\text{Si}^0$  center is covered by two hexamethylphosphoramide (HMPA) ligands and  $\text{Fe}(\text{CO})_4$  fragments. Within a two-step procedure,  $\text{SiCl}_4$  is reacted with two equivalents of  $\text{Na}_2\text{Fe}(\text{CO})_4$  in the highly coordinative solvent HMPA. The diiron silylone is poorly soluble in organic solvents and decomposes upon exposure to air. In a modified procedure, our group could furnish the NHC analog  $(\text{IME}_4)_2\text{Si}(\text{Fe}(\text{CO})_4)_2$  (**91**), using the Kuhn  $\text{NHC} \rightarrow \text{SiCl}_4$  adduct<sup>[123]</sup> as starting material (Figure 24, right).<sup>[124]</sup>

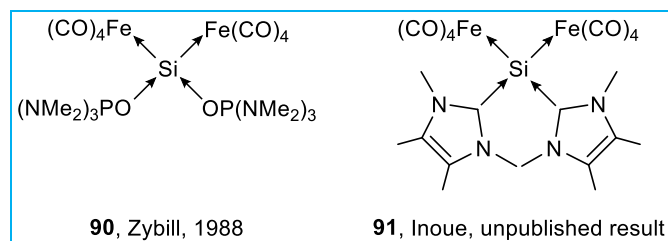
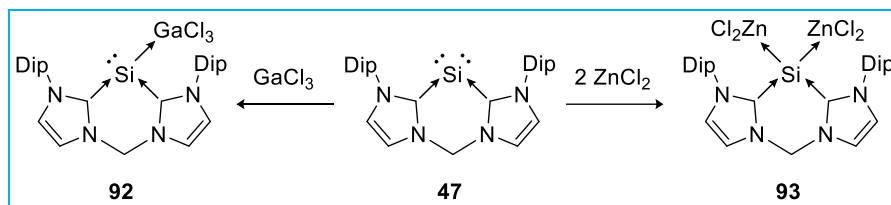


Figure 24. Silylone diiron complexes **90** and **91** derived from stepwise introduction of  $\text{Fe}(\text{CO})_4$  groups using Collman's reagent.

In the course of characterization, **47** was treated with  $\text{ZnCl}_2$  and  $\text{GaCl}_3$  as an experimental proof of the lone pair's reactivity towards Lewis acids. In both cases the corresponding complexes **92** and **93** could be yielded, however, only few characterizations were given (Scheme 25).<sup>[108]</sup>



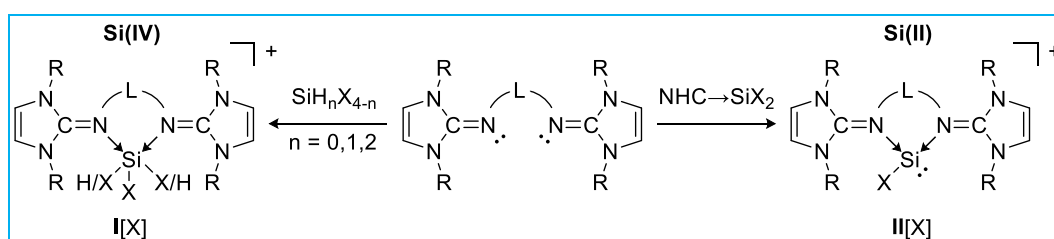
Scheme 25. Reaction of silylone **47** with Lewis acids  $\text{GaCl}_3$  and  $\text{ZnCl}_2$  yielding complexes **92** and **93**, respectively.

### 3 Scope of this Work

Whereas the chemistry of low valent silicon is a fast-growing scientific field, there are still voids that have not been investigated so far. The recent example of an industry-suitable application of a silyliumylidene ion as transition metal free catalyst in hydrosilylation,<sup>[10,11]</sup> shows that fundamental research in this field has great potential and is still worth a deeper look. Silyliumylidenes, as pointed out in the introduction, do also have a great potential to serve as starting material for electron enriched silylones, as well as a ligand support on transition metal complexes to tease novel and unexpected reactivities. Since the advances in those fields were quite scarce at the starting point of this thesis, it was aimed for a more detailed understanding of the reactivity and novel bonding motifs of silyliumylidene ions and related species. Accordingly, the aim of this PhD project is the synthesis, isolation, and characterization of novel bis-NHI-stabilized and therefore acceptor-free and electron-enriched halosilanes and silyliumylidenes, which should be subsequently tested for their coordination and reduction chemistry towards respective silylone complexes.

#### Ligand design and preparation of starting complexes

The bis-NHI ligand system is chosen to provide stabilization for these rather electron deficient species *via* its exceptional strong electron donating properties, and bidentate coordination fashion. The steric demand and electronic nature of bis-NHIs can be finely tuned by variation of the bridging moiety and the NHC's substituents 'R'. To achieve narrow N–Si–N angles and a well-sized coordination pocket, the number of bridging atoms is chosen to create 5-membered and 6-membered rings upon complexation of a silicon precursor. Steric protection is pursued by aryl and/or bulky substituents 'R'.



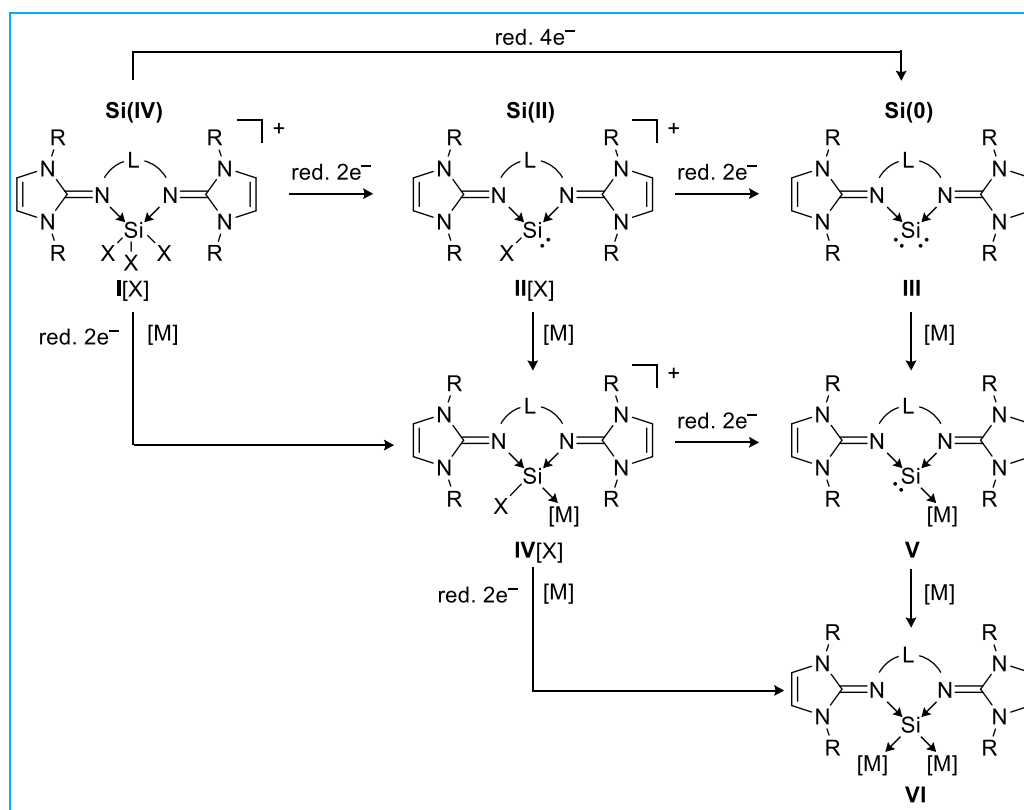
Scheme 26. Synthetic strategy to afford **I[X]** Si(IV) (left) and **II[X]** Si(II) (right) cationic bis-NHI complexes. R = aryl or alkyl wingtip substituents; L = aryl or alkyl bridging group; X = Cl, Br, I.

In a first step different novel as well as literature-known<sup>[44,45]</sup> bis-NHIs should be synthesized and tested for their ability to coordinate and stabilize Si(IV) as well as Si(II) synthons (Scheme 26). The readily available chlorosilanes are ideal candidates to form bis-NHI $\rightarrow$ SiCl<sub>4-n</sub>H<sub>n</sub> (n = 0, 1, 2) complexes (Scheme 26, left). Furthermore, NHC $\rightarrow$ SiX<sub>2</sub> (X = Cl, Br, I) can be

prepared following straight forward procedures,<sup>[26–28]</sup> in order to generate silyliumylidenes through direct conversion with neutral bis-NHI ligands (Scheme 26, right).

### Reductive Dehalogenation and Coordination Chemistry

In further investigations novel electron-rich low-valent species are targeted, such as transition metal mono-, and bimetallic silyliumylidene and silylone complexes. These investigations focus on two main reactivities: (i) Reduction of bis-NHI silicon complexes, either in defined 2-electron reducing steps or as single step reduction, and (ii) coordination of Lewis acidic transition metals. Naturally, to accomplish the synthetic goals, these reactivities were not only seen delineated from each other, but rather in all their combinations and variations (Scheme 27). One additional synthetic option is halide exchange to either weakly coordinating anions or alternating functional groups to enhance and modify properties and reactivities of the regarding compounds.



Scheme 27. Synthetic strategy to afford targeted free silylone III, silyliumylidene transition metal complex IV, and silylone transition metal complexes V and VI. R = aryl or alkyl wingtip substituents; L = aryl or alkyl bridging group; X = Cl, Br, I; red. = reduction agent; [M] = transition metal synthon.

---

(i) Reduction

Depending on the starting material and silicon precursor different reductive pathways are conceivable regarding either reductive dehalogenation (using *e.g.*  $\text{KC}_8$ ,  $\text{NaNaph}$ ,  $\text{CoCp}_2$  etc.) or HX-salt abstraction (using *e.g.*  $\text{K}^+\text{OtBu}^-$ ,  $n\text{-BuLi}$ , NHC, etc). The reductive agents need to be chosen carefully, to avoid over-reduction that could result in decomposition.

(ii) Coordination of Lewis acidic Transition Metals

Readily available Lewis acidic transition metal species like metal halides,  $\text{MX} / \text{MX}_2$ , metal carbonyls  $\text{M}(\text{CO})_x$  and ligand-stabilized derivatives of those are in the focus of the coordination chemistry. Dianionic metallates, such as the Collman's reagent ( $\text{Na}_2\text{Fe}(\text{CO})_4$ ) and derivatives thereof are especially handy, since they combine two-electron reduction and an iron carbonyl fragment for coordination. Considering the highly reactive nature of electron enriched silyliumylidenes and silylones, direct stabilization by Lewis acids could be essential for successful reduction chemistry.

All aforementioned species are potential candidates for application in small molecule activation, catalytic conversions, and as preparative building blocks. All obtained and isolated target compounds are to be tested for their ability to activate small molecules of enthalpically strong bonds, such as  $\text{CO}$ ,  $\text{CO}_2$ ,  $\text{NH}_3$ ,  $\text{H}_2$ ,  $\text{CH}_4$ , and  $\text{N}_2$  and catalytic applications, such as olefin hydrogenation and hydrosilylation. Whereas metal free species should show silylene-related chemistry *via* their accessible lone pair, transition metal complexes could (additionally) benefit from cooperative effects between the low valent silicon center and the respective metal in the fashion of  $[\text{M}-\text{Si}]$ ,  $[\text{M}-\text{Si}-\text{M}]$ , or  $[\text{M}\cdots\text{M}]$ .

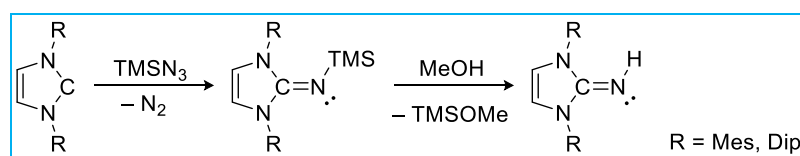
## 4 Results and Discussion

### 4.1 Ligand Synthesis

To generate a reasonable variety of neutral NHI ligands with well-sized coordinative pockets and steric protection, the selection was narrowed down to two criteria for bridged bis-NHI. Well-stabilized five- and six-membered rings are likely favored for the stabilization of resulting silicon complexes. Accordingly, 2C- (1,2-ethylene, 1,2-phenylene) and 3C- (1,3-propylene) bridges were chosen. Furthermore, different level of steric protection is provided through variation of the NHI wing-tip substituents. We selected mesityl- (Mes) and diisopropylphenyl- (Dip) as starting points with reasonable steric demand. In addition, two novel monodentate, but neutral, NHIs were synthesized and tested for their coordination ability to silicon precursors. The synthetic procedure was adapted from Tamm<sup>[40]</sup> and modified as needed.

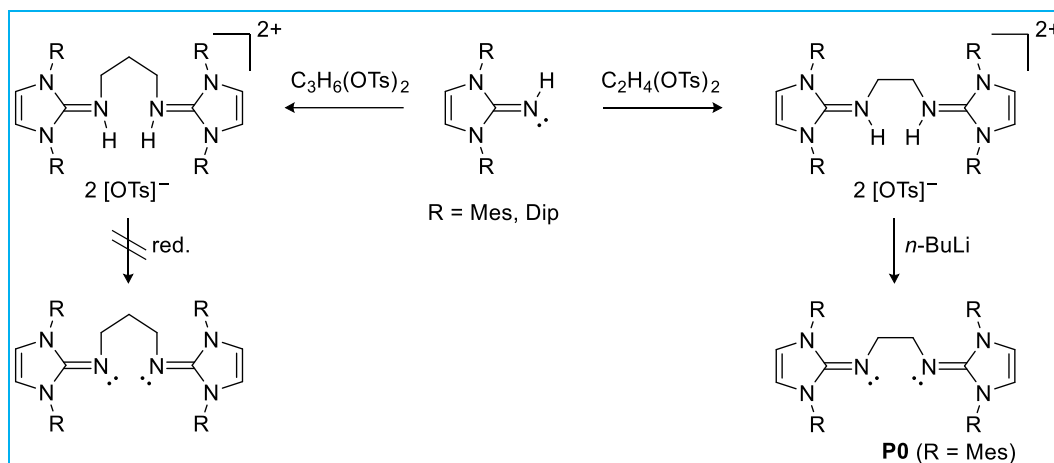
#### Synthetic Route A

Following well documented procedures, neutral monodentate NHI-H could be synthesized in moderate to high yields and sufficient purity. After a Staudinger-type reaction starting from the respective free NHC and trimethylsilylazide (TMSN<sub>3</sub>), the NHI-TMS is furnished as slightly air sensitive compound that could already be used for coordination chemistry. Hydrolysis with methanol (MeOH) releases NHI-H as air-stable and bottleable solids (Scheme 28).<sup>[43]</sup>



Scheme 28. Synthesis of R-substituted *N*-heterocyclic imines starting from corresponding free NHC using TMSN<sub>3</sub> in Staudinger-type reaction.

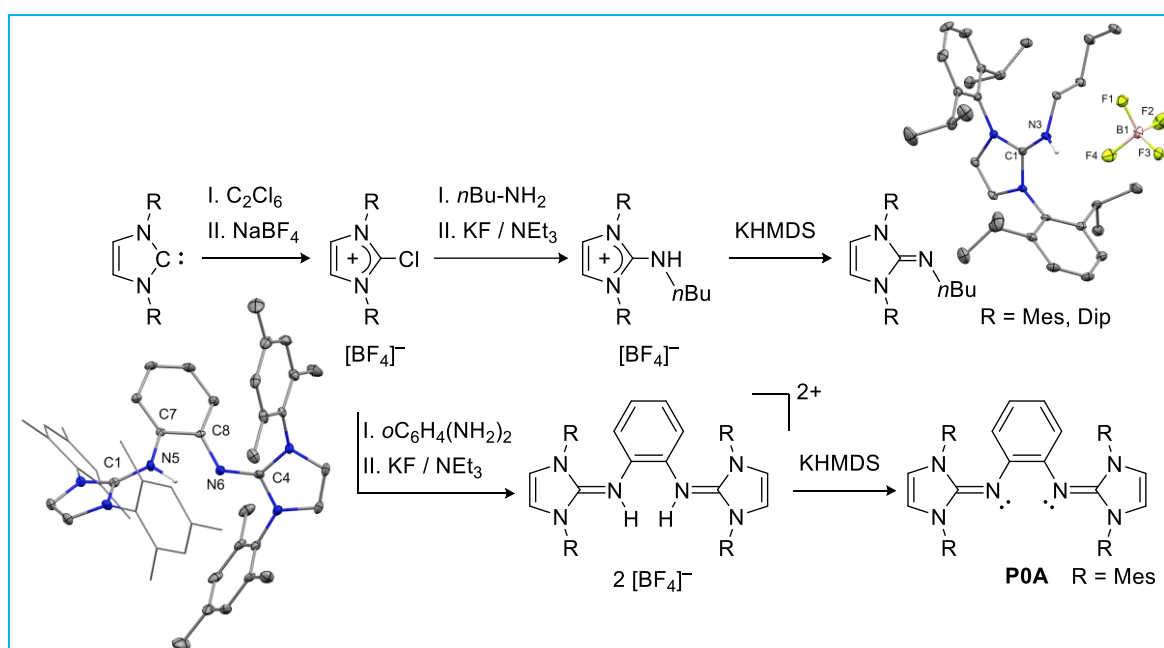
With NHI-H in hands bridging reactions with 1,2-bis(tosyloxy)ethane and 1,3-bis(tosyloxy)propane were pursued, following literature reported procedures for bis-NHI<sup>Mes</sup> (Scheme 29).<sup>[44,45]</sup> In case of bis-NHI<sup>Dip</sup> the procedure was modified towards higher temperature and reaction time to achieve full conversion. The resulting bridged NHI dications were deprotonated using *n*-BuLi to free neutral bis-NHI ligands bis<sup>Et</sup>-NHI<sup>Dip</sup> and bis<sup>Et</sup>-NHI<sup>Mes</sup>. Whereas the ethylene-bridged bis-NHI could be deprotonated successfully, all attempts to isolate neutral propylene-bridged bis-NHI failed, with degradation of the propylene bridge. It was assumed that the acidity of the middle CH<sub>2</sub>-group lead to undesired side-reactions.



Scheme 29. Attempted synthesis of propylene-bridged bis<sup>Pr</sup>-NHI<sup>R</sup> and successful synthesis of ethylene-bridged bis-<sup>Et</sup>-NHI<sup>R</sup> (R = Mes, Dip) via tosylate bridging and subsequent deprotonation.

### Synthetic Route B

In an alternative synthetic route, altering substituents and bridges can be introduced. Starting from the respective [NHC-Cl][BF<sub>4</sub>]<sup>-</sup> salt and primary amine the NHI can be yielded in a convenient one-pot reaction.<sup>[41]</sup> However, the exact reaction conditions and molarities need to be adjusted for different starting materials, thus some conversions presented unexpectedly challenging. Following this route, 1,2-phenyl-bridged bis<sup>Ph</sup>-NHI<sup>Mes</sup> (**P0A**) and *n*-Bu substituted <sup>n</sup>BuNHI<sup>Mes</sup> and <sup>n</sup>BuNHI<sup>Dip</sup> could be isolated in moderate yields and sufficient purity. All attempts to isolate less sterically demanding bis<sup>Ph</sup>-NHI<sup>iPr</sup>, as well as more sterically demanding bis<sup>Ph</sup>-NHI<sup>Dip</sup> failed upon intended bridging reaction (Scheme 30).



Scheme 30. Synthesis of mono *n*-butyl substituted <sup>n</sup>BuNHI<sup>R</sup> and phenylene-bridged bis<sup>Ph</sup>-NHI<sup>Mes</sup> via amination and subsequent deprotonation. Solid state structure of [<sup>n</sup>BuNHI<sup>Dip</sup>H][BF<sub>4</sub>]<sup>-</sup> (top) and [bis<sup>Ph</sup>-NHI<sup>Mes</sup>H][BF<sub>4</sub>]<sup>-</sup> (bottom) presented at the 50% probability level.

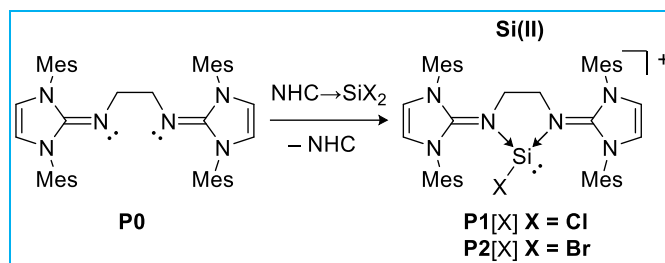
## 4.2 Synthesis and Characterization of bis-NHI-stabilized Silyliumylidenes and Halosilane Complexes

According to the synthetic strategy mentioned in the scope of this thesis, the prepared ligands were tested for complexation of several silicon precursors. Chlorosilanes and NHC-stabilized halosilylenes were rendered suitable and readily available candidates to be used as silicon synthons. Especially  $\text{NHC} \rightarrow \text{SiX}_2$  ( $\text{X} = \text{Cl}, \text{Br}, \text{I}$ ) are well established and handy, for their convenient preparation and direct transfer ability of the Si(II) synthon.<sup>[26–28]</sup>

$\text{Bis}^{\text{Et}}\text{-NHI}^{\text{Dip/Mes}}$

It is hypothesized that a sterically well-protected silicon central atom would provide a major advantage for subsequent reduction chemistry. Therefore, priority was given to the chelating  $\text{bis}^{\text{Et}}\text{-NHI}^{\text{Dip}}$  and  $\text{bis}^{\text{Et}}\text{-NHI}^{\text{Mes}}$  ligands.

Whereas no reaction could be observed upon mixing of  $\text{NHC} \rightarrow \text{SiCl}_2$  with  $\text{bis}^{\text{Et}}\text{-NHI}^{\text{Dip}}$  for several solvents and temperatures,  $\text{bis}^{\text{Et}}\text{-NHI}^{\text{Mes}}$  delivered the desired silyliumylidene complex  $\text{bis}^{\text{Et}}\text{-NHI}^{\text{Mes}}\text{SiCl}_2$  (**P1**) in a straightforward procedure (Scheme 31). The starting materials were mixed in a 1:1 molar ratio and treated with toluene at room temperature. Within 30 minutes precipitate formation is visible indicating successful conversion. After 16 hours of reaction time, the silyliumylidene could be isolated in 76% yield as a pearly solid.



Scheme 31. Synthesis of  $[\text{bis}^{\text{Et}}\text{-NHI}^{\text{Mes}}\text{SiX}][\text{X}]$  ( $\text{X} = \text{Cl}$  **P1**,  $\text{Br}$  **P2**) starting from free ligand  $\text{bis}^{\text{Et}}\text{-NHI}^{\text{Mes}}$  (**P0**) and base stabilized  $\text{NHC} \rightarrow \text{SiX}_2$ . The synthesis is carried out in toluene as solvent at room temperature over 16 hours.

The compound is stable under inert conditions at room temperature and is soluble in acetonitrile (MeCN), pyridine (pyr), and 1,2-difluorobenzene (DFB). Multinuclear NMR spectroscopy revealed the connection of the silicon moiety to the ligand in a symmetric fashion, indicating bidentate coordination. The proton NMR (Figure 25, big) displays the general ligand's pattern with two singlets at  $\delta(^1\text{H}) = 2.01$  and  $2.33$  ppm for the mesityl's *ortho*-, and *para*-methyl groups respectively. The bridging ethylene group causes two broad signals at  $\delta = 2.61$  and  $2.93$  ppm, while the imidazoline backbone and mesityl's aromatic protons were found at  $\delta = 6.80$  and  $6.97$  ppm respectively. Compared to the free  $\text{bis}^{\text{Et}}\text{-NHI}^{\text{Mes}}$  (**P0**) the

system loses flexibility, resulting in chemically non-equivalence of the mesityl-methyl- $CH_3$  and the bridge  $C_2H_4$ -protons, as expected.

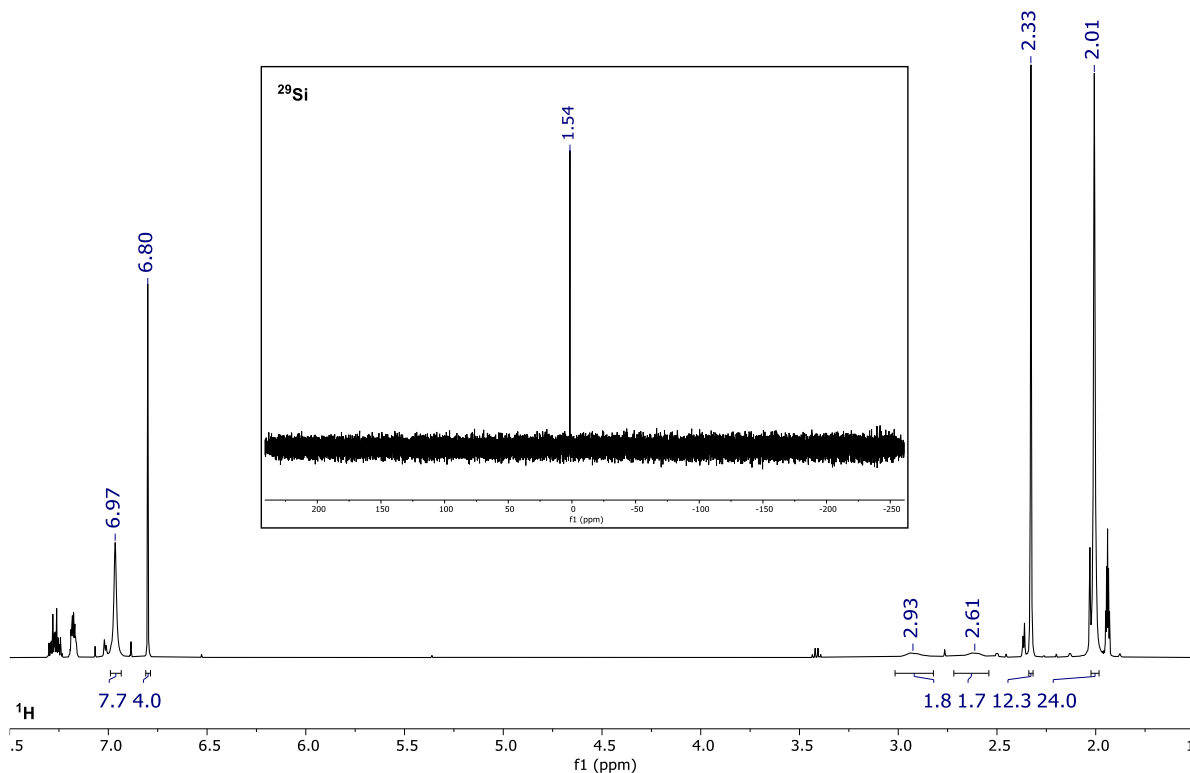


Figure 25.  $^1H$ -NMR (big) and  $^{29}Si$ -NMR (small) spectrum of  $[bis^{Et}NHI^{Mes}SiCl][Cl]$  **P1** recorded at 25°C in  $MeCN-d_3$ .

The  $^{29}Si$  NMR signal was found at  $\delta = 1.5$  ppm (Figure 25, small), which is slightly upfield shifted regarding the starting material  $NHC \rightarrow SiCl_2$ <sup>[28]</sup> ( $\delta(^{29}Si) = 19.1$  ppm) and in good agreement with bis-imino-stabilized silyliumylidene (**17**)<sup>[90]</sup> ( $\delta(^{29}Si) = -3.3$  ppm), thus indicating comparable electronic structure and coordination environment. However, reported NHC-stabilized silyliumylidenes, such as **9**,<sup>[30]</sup> **12**,<sup>[87]</sup> or **14**<sup>[29]</sup> resonate at considerably higher fields ( $\delta(^{29}Si) = -51$  to  $-91$  ppm).<sup>[85,86,88]</sup>

Single crystals suitable for SC-XRD analysis are grown in DFB solution under slow diffusion of diethylether ( $Et_2O$ ). The solid-state structure (Figure 26) confirms the assumed connectivity by showing a 5-membered  $C_2N_2Si$ -ring, from which the coordinated chlorine atom protrudes with almost  $90^\circ$ . The Si-atom is found in trigonal pyramidal geometry and the sum of bond angles around Si being  $273.9(2)^\circ$ , thus indicating the presence of a  $\sigma$ -type lone-pair of electrons, according to standard VSEPR-theory.

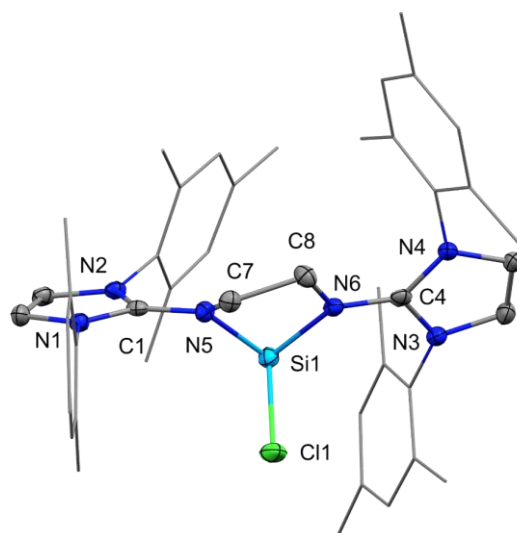


Figure 26. Solid-state plot of the molecular structure of  $[\text{bis}^{\text{Et}}\text{-NHI}^{\text{Mes}}\text{SiCl}][\text{Cl}]$  **P1**. Ellipsoids are set to the 50% probability level. Hydrogen atoms, the counter anion and solvent molecules are omitted for clarity; mesityl-substituents are depicted as wireframe for simplicity. Selected bond lengths [Å] and angles [°]: Si1–Cl1 2.2374(8), Si1–N5 1.8290(18), Si1–N6 1.8617(18), C1–N5 1.337(3), C4–N6 1.336(3), Cl1–Si1–N5 95.07(6), N5–Si1–N6 84.00(8), Cl1–Si1–N6 94.91(6).

Deploying  $\text{NHC} \rightarrow \text{SiBr}_2$  as starting material in an otherwise analogue experimental setup (Scheme 31) gave access to corresponding  $\text{bis}^{\text{Et}}\text{-NHI}^{\text{Mes}}\text{SiBr}_2$  in 53% isolated yield (corrected, due to high  $\text{NHC}^{\text{Dip}} \cdot \text{HCl}$  contamination of the  $\text{NHC} \rightarrow \text{SiBr}_2$  starting material). Although no single crystal could be grown, the structural conformity of  $\text{bis}^{\text{Et}}\text{-NHI}^{\text{Mes}}\text{SiBr}_2$  (**P2**) and **P1** is substantiated through multinuclear NMR spectroscopy, that reveals a slightly shifted pattern in  $^1\text{H}$  NMR experiment (Figure 27, big) and one single resonance at  $\delta = -7.7$  ppm in  $^{29}\text{Si}$  NMR (Figure 27, small). The upfield shift of the silicon resonance compared with **P1** ( $\delta(^{29}\text{Si}) = 1.5$  ppm) is in line with the less electronegative bromine substituent. However, with  $\text{NHC} \rightarrow \text{SiI}_2$  no complex formation was observed even at elevated temperatures and altered synthetic strategies.

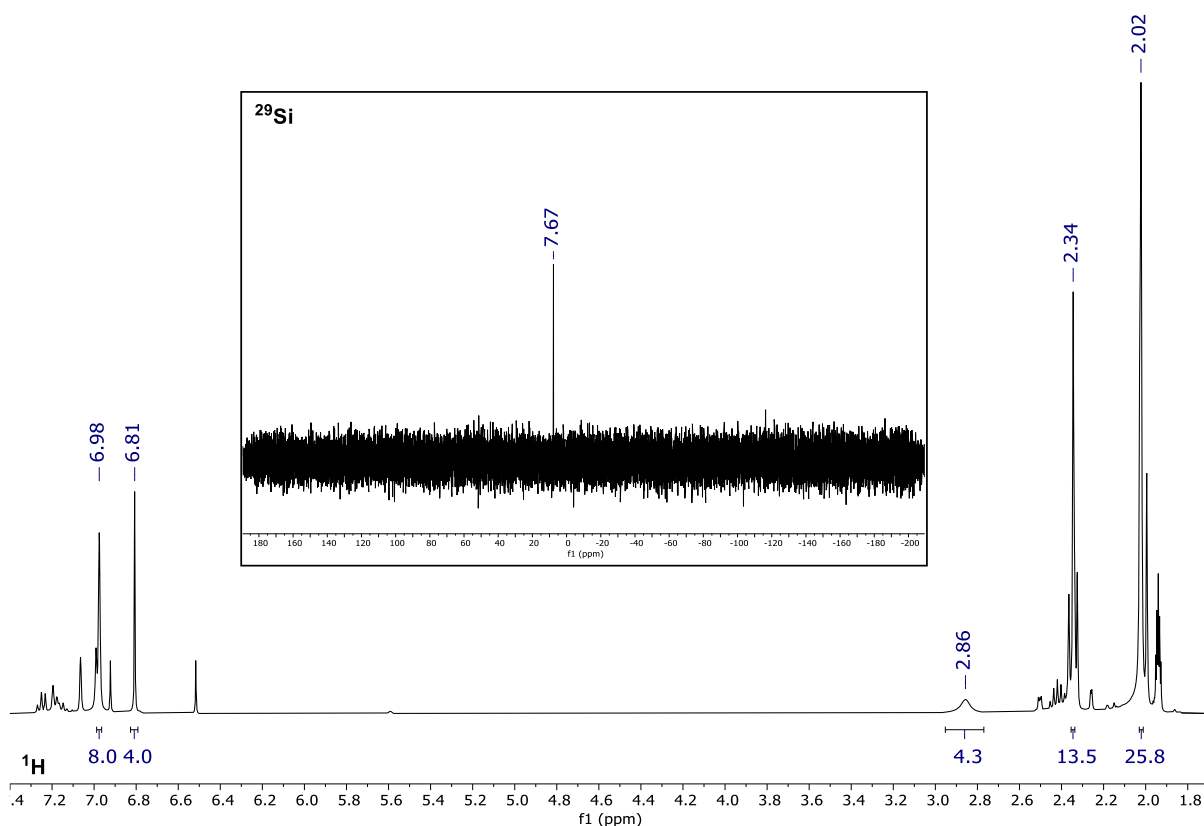
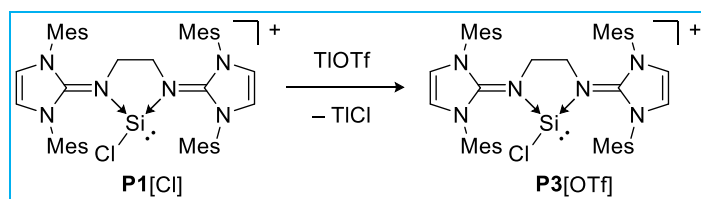


Figure 27.  $^1\text{H}$ -NMR (big) and  $^{29}\text{Si}$ -NMR (small) spectrum of  $[\text{bis}^{\text{Et}}\text{-NHI}^{\text{Mes}}\text{SiBr}][\text{Br}]$  (**P2**) recorded at  $25^\circ\text{C}$  in  $\text{MeCN-d}_3$ . Considerable amounts of  $\text{NHC}^{\text{Dip}}\cdot\text{HBr}$  are contained.

Although the  $\text{NHC}\rightarrow\text{SiX}_2$  ( $\text{X} = \text{Cl}, \text{Br}$ ) silylenes have proven to be suitable precursors to form bis-NHI-Si(II) complexes, the synthesis often suffers from accompanying  $\text{NHC}^{\text{Dip}}\cdot\text{HCl}$  salt impurities. The imidazolium salt originated either from incomplete reduction of  $\text{NHC}^{\text{Dip}}\cdot\text{SiH}_n\text{X}_{4-n}$  during synthesis or partly decomposition of  $\text{NHC}^{\text{Dip}}\rightarrow\text{SiX}_2$ , that is mostly kinetically stabilized by the sterically demanding  $\text{NHC}^{\text{Dip}}$ . Due to the similar solubility properties and behavior of  $\text{NHC}^{\text{Dip}}\cdot\text{HX}$  and **P1** ( $\text{X} = \text{Cl}$ ) / **P2** ( $\text{X} = \text{Br}$ ), a sufficient purification of contaminated batches remains challenging.

While halogen anions can in some cases support the driving force of desired conversions, in other cases they tend to provoke side reactions. Therefore, defined anion exchange reactions were conducted, in order to equip the silyliumylidene with rather chemically inert and weakly coordinating anions.



Scheme 32 Synthesis of anion exchange product  $[\text{bis}^{\text{Et}}\text{-NHI}^{\text{Mes}}\text{SiCl}][\text{OTf}]$  (**P3**) from **[Cl]** (**P1**) using  $\text{TlOTf}$ . The synthesis is carried out in THF as solvent at room temperature.

Due to complex formation (see chapter 4.4.3 and 4.4.4) and unselective reactivity, the choice of the anion transfer agent was crucial to obtain a defined exchange product in satisfactory yield. The best results were obtained using TlOTf as a halogen capturing, triflate transfer agent. The reaction was conducted in THF to simplify the separation of the soluble product [bis<sup>Et</sup>-NHI<sup>Mes</sup>SiCl][OTf] **P3** from insoluble **P1** (Scheme 32). When **P1** and a slight excess (1.3 equiv.) of TlOTf were mixed in THF at room temperature, an isolated yield of 80% **P3** was achievable after 48 hours. The characteristic ligand's pattern in <sup>1</sup>H NMR (Figure 28, big) is nearly identical compared to **P1**, as expected. However, minor changes in signal appearance are visible. The *ortho*-methyl groups at  $\delta(^1\text{H}) = 1.99$  and 2.02 ppm and the aromatic-C3,5 proton signals at  $\delta = 6.99$  and 6.95 ppm split into two closely lying singlets. Moreover, the broad bridge resonances at  $\delta = 2.93$  and 2.60 ppm appear as distinct multiplets. Further evidence for the successful anion exchange is provided by the sole <sup>19</sup>F NMR signal found at  $\delta = -79.3$  ppm in combination with unshifted <sup>29</sup>Si NMR at  $\delta = 1.55$  ppm (Figure 28, small). In contrast to **P1**, **P3** is well soluble in THF, opening the door for additional experiment designs.

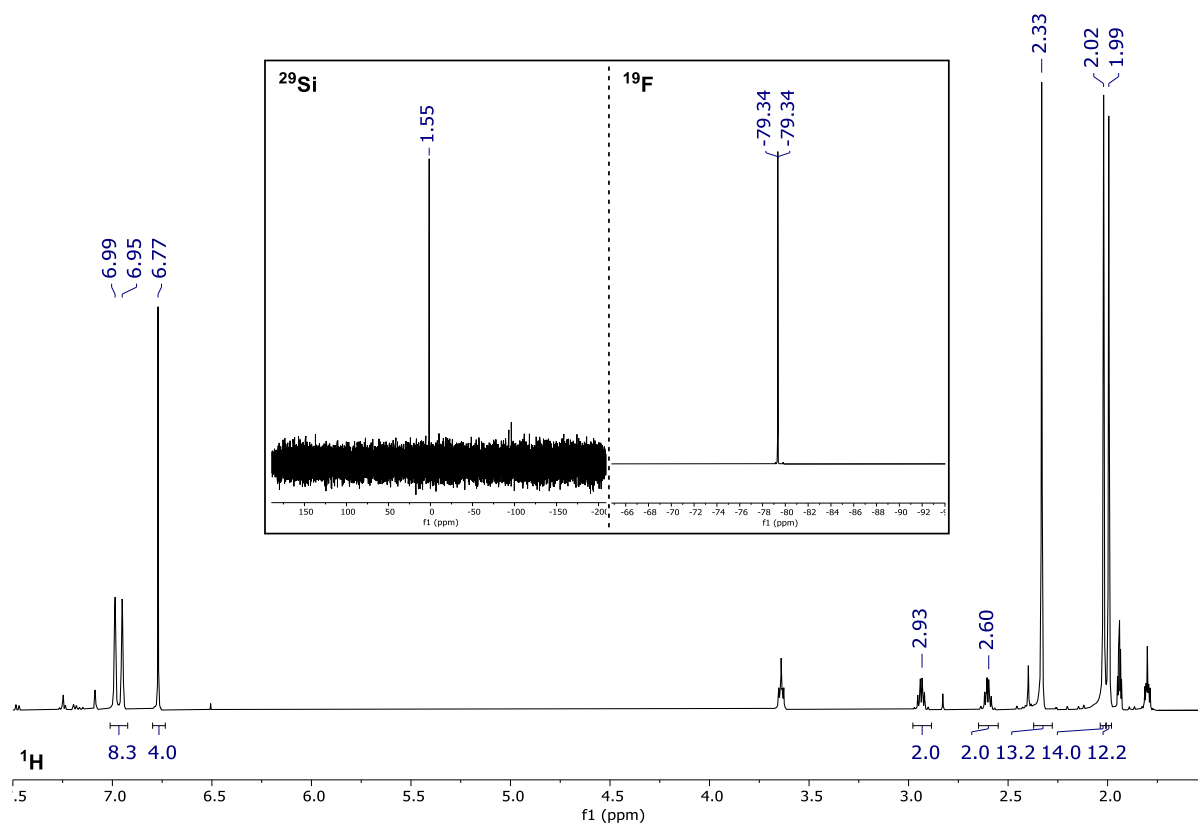
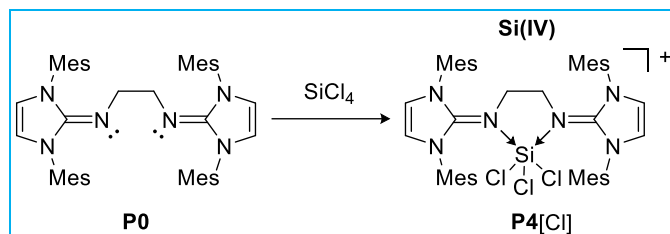


Figure 28. <sup>1</sup>H-NMR (big), <sup>29</sup>Si-NMR (small left), and <sup>19</sup>F-NMR (small right) spectrum of [bis<sup>Et</sup>-NHI<sup>Mes</sup>SiCl][OTf] (**P3**) recorded at 25 °C in MeCN-d<sub>3</sub>.

Complexations of base free halosilanes such as SiCl<sub>4</sub>, HSiCl<sub>3</sub> and H<sub>2</sub>SiCl<sub>2</sub>, were executed to provide further bis-NHI silicon(IV) complexes. Whereas the complexation of NHC → SiCl<sub>2</sub>

occurs rather slowly within several hours, base free silicon halides react immediately. Following the same reaction setup (Scheme 33 and Scheme 34), an equimolar amount of free bis<sup>Et</sup>-NHI<sup>Mes</sup> (**P0**) was treated dropwise with halosilanes in toluene, with rapid precipitation of the respective ionic Si(IV) complexes.



Scheme 33. Synthesis of  $[\text{bis}^{\text{Et}}\text{-NHI}^{\text{Mes}}\text{SiCl}_3][\text{Cl}]$  (**P4**) from free  $\text{bis}^{\text{Et}}\text{-NHI}^{\text{Mes}}$  (**P0**) and  $\text{SiCl}_4$ . The reaction is carried out in toluene as solvent at room temperature over 2 hours.

$\text{Bis}^{\text{Et}}\text{-NHI}^{\text{Mes}}\text{SiCl}_4$  (**P4**, Scheme 33) was isolated as a colorless powder in 93% yield directly without additional purification steps. Multinuclear NMR spectroscopy (Figure 29) in conjunction with 2D  $^1\text{H}^{29}\text{Si}$ -HMBC experiment identified the complex unambiguously and revealed the  $^{29}\text{Si}$  NMR resonance at  $\delta = -112.4$  ppm, despite the minor signal intensity in 1D  $^{29}\text{Si}$ -IG NMR experiment (Figure 29, small).

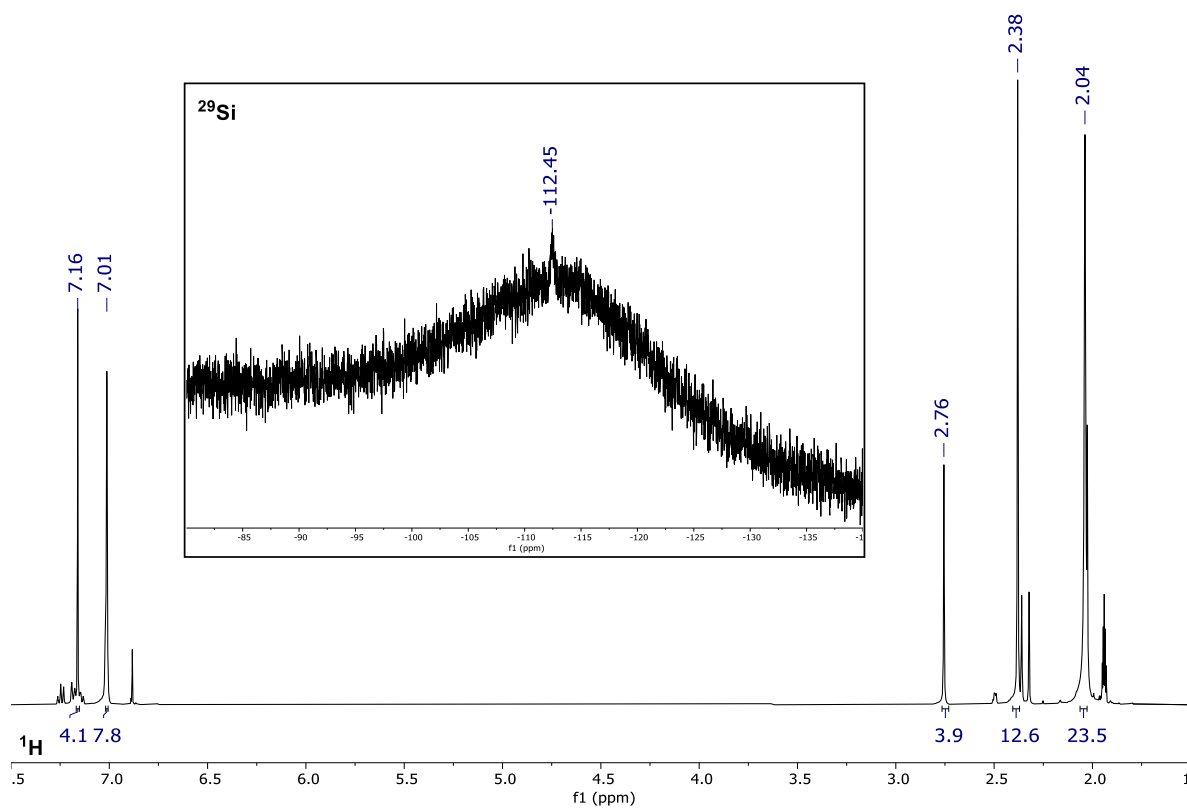


Figure 29.  $^1\text{H}$ -NMR (big) and  $^{29}\text{Si}$ -NMR (small) spectrum of  $[\text{bis}^{\text{Et}}\text{-NHI}^{\text{Mes}}\text{SiCl}_3][\text{Cl}]$  (**P4**) recorded at 25°C in  $\text{MeCN-d}_3$ .

The shift is in good agreement with a 5-coordinated silicon species, and thus is indicative for ionic  $[\text{bis}^{\text{Et}}\text{-NHI}^{\text{Mes}}\text{SiCl}_3][\text{Cl}]$  (**P4**). The structural motif was substantiated by SC-XRD analysis on crystals grown from a saturated MeCN / THF mixture.

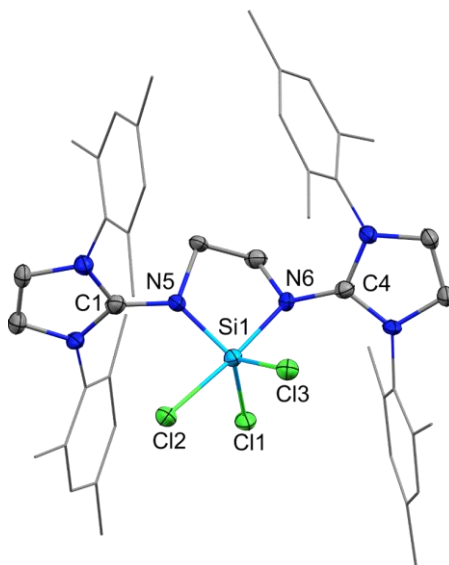
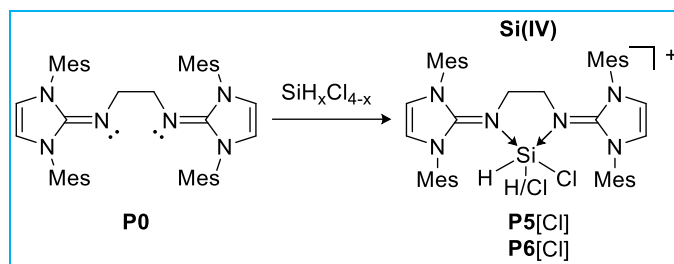


Figure 30. Solid-state plot of the molecular structure of  $[\text{bis}^{\text{Et}}\text{-NHI}^{\text{Mes}}\text{SiCl}_3][\text{Cl}]$  (**P4**). Ellipsoids are set to the 50% probability level. Hydrogen atoms, the counter anion and solvent molecules are omitted for clarity; mesityl-substituents are depicted as wireframe for simplicity. Selected bond lengths [Å] and angles [°]: Si1–Cl1 2.0822(19), Si1–Cl2 2.2117(19), Si1–Cl3 2.113(2), Si1–N5 1.771(4), Si1–N6 1.839(4), C1–N5 1.365(7), C4–N6 1.341(7), N5–Si1–N6 85.33(19), Cl2–Si1–N6 172.58(15), Cl1–Si1–Cl2 91.43(7), Cl1–Si1–Cl3 115.73(8).

The complex crystallizes in the monoclinic space group P2(1)/n with the silicon atom being in a trigonal bipyramidal coordination environment and the N6–Si1–Cl2 angle being 172.6° (Figure 30). Therefore, Cl2 holds an elongated Si–Cl bond length with 2.21 Å, compared to Cl1 (2.08 Å) and Cl3 (2.11 Å).

Using  $\text{HSiCl}_3$  and  $\text{H}_2\text{SiCl}_2$  as silicon sources, furnished the analog complexes  $\text{bis}^{\text{Et}}\text{-NHI}^{\text{Mes}}\text{HSiCl}_3$  (**P5**) and  $\text{bis}^{\text{Et}}\text{-NHI}^{\text{Mes}}\text{H}_2\text{SiCl}_2$  (**P6**), respectively (Scheme 34). While silicochloroform could be used in the same manner as  $\text{SiCl}_4$ , the (at room temperature) gaseous dichlorosilane first had to be condensed in toluene to be usable as a 37 wt% solution. Reactions with  $\text{H}_2\text{SiCl}_2$  should be performed at low temperature to avoid degassing of the volatile reactant. Therefore, the ligand solution was cooled to  $-30^\circ\text{C}$  prior to addition of the dichlorosilane. After warming of the reaction mixture to room temperature, the isolation of the complex proceeds as in the previous cases *via* filtration of the insoluble product  $\text{bis}^{\text{Et}}\text{-NHI}^{\text{Mes}}\text{H}_2\text{SiCl}_2$  (**P6**).



Scheme 34. Synthesis of  $[\text{bis}^{\text{Et-NHI}}\text{MesSiH}_x\text{Cl}_{3-x}][\text{Cl}]$  from free bis-NHI and  $\text{H}_x\text{SiCl}_{4-x}$  ( $x = 1$  **P5**,  $2$  **P6**) The reaction is carried out in toluene as solvent at room temperature ( $\text{HSiCl}_3$ ) or  $-30^\circ\text{C}$  ( $\text{H}_2\text{SiCl}_2$ ) over 2 hours ( $\text{R} = \text{Mesityl} = 2,4,6\text{-trimethylphenyl}$ ).

Both compounds can be isolated in high yields (86% for **P5**; 91% for **P6**) and in sufficient to excellent purity. Likewise to **P4**, **P5** and **P6** are furnished as colorless and, under exclusion of air, stable solids. The  $^{29}\text{Si}$  NMR signals appear slightly downfield shifted at  $\delta = -101.5$  (Figure S 12) and  $-104.9$  ppm (Figure 31, small), respectively. Additionally, characteristic Si–H signals in  $^1\text{H}$  NMR emerge at  $\delta = 5.3$  ppm (Si–H satellites  $^1J_{\text{SiH}} = 187.6$  Hz, Figure S 12) and 4.3 ppm (Si–H satellites  $^1J_{\text{SiH}} = 160.6$  Hz; Figure 31, small), thus verifying successful complex formation.

For this, the full range of bis-NHI $^{\text{Mes}}\text{SiH}_x\text{Cl}_{4-x}$  ( $x = 0$  **P4**,  $1$  **P5**,  $2$  **P6**) is accessible for the bidentate mesityl-substituted ligand with no greater effort by simple mixture of ligand and silicon precursor.

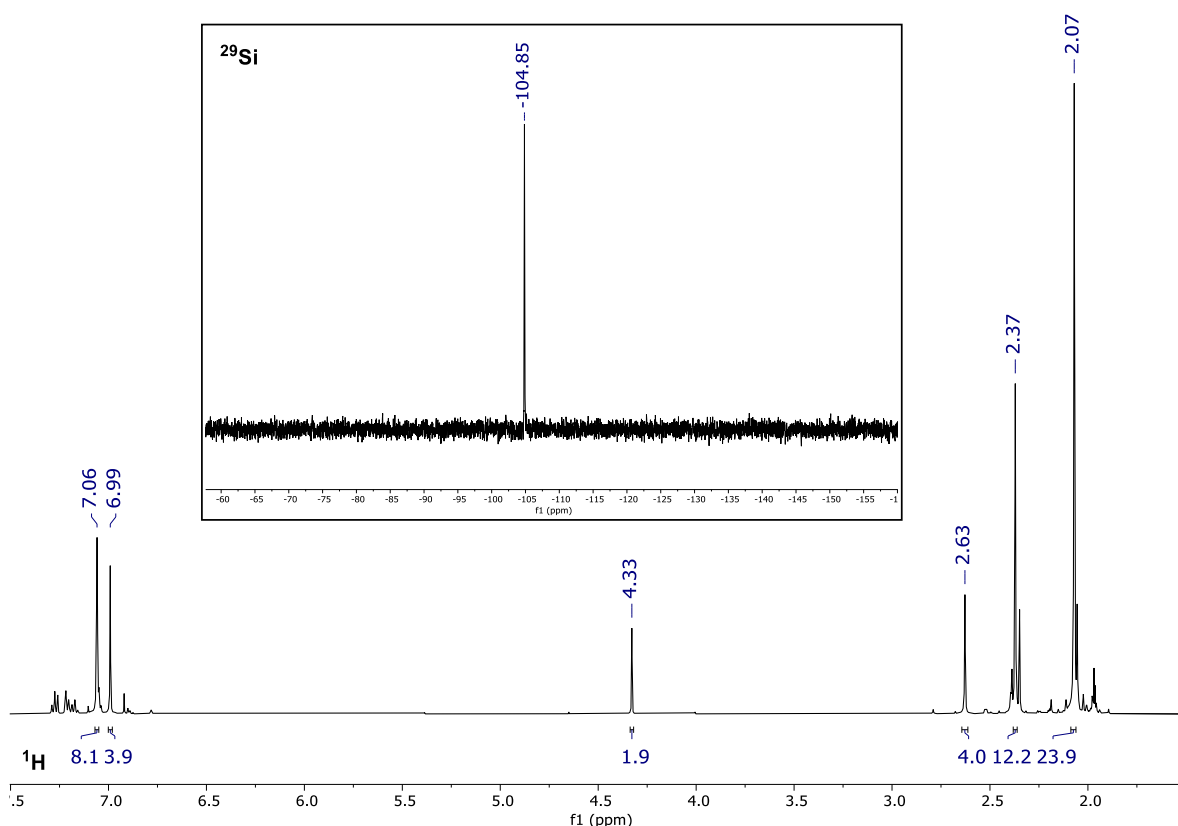
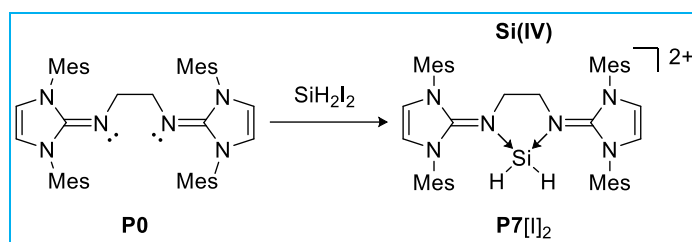


Figure 31.  $^1\text{H}$ -NMR (big) and  $^{29}\text{Si}$ -NMR (small) spectrum of  $[\text{bis}^{\text{Et-NHI}}\text{MesSiH}_2\text{Cl}][\text{Cl}]$  (**P6**) recorded at  $25^\circ\text{C}$  in  $\text{MeCN-d}_3$ . Toluene remaining from synthesis is contained.

Penta-coordination is a well-known bonding motif for Lewis base – silicon(IV) adducts. However, if monodentate NHCs are used, the adduct remains over-all neutral. In case of the bidentate bis-NHI, one halogen is cleaved off to produce 5-coordinated bis-NHISiX<sub>3</sub> cations. In addition, the bis-NHI enables stabilization of up to two positive charges within the aromatic imidazoline-rings (see mesomeric structures, bottom Scheme 1), which further favors the formation of cations.

The preference is particularly evident, when reacting bis<sup>Et</sup>-NHI<sup>Mes</sup> (**P0**) with H<sub>2</sub>SiI<sub>2</sub> (Scheme 35). When dropping equimolar amounts of an H<sub>2</sub>SiI<sub>2</sub> toluene solution into a solution of the free ligand, immediate product formation could be observed.



Scheme 35. Synthesis of [bis<sup>Et</sup>-NHI<sup>Mes</sup>SiH<sub>2</sub>][I]<sub>2</sub> (**P7**) from free bis<sup>Et</sup>-NHI<sup>Mes</sup> (**P0**) and H<sub>2</sub>SiI<sub>2</sub>. The reaction is carried out in toluene as solvent at room temperature.

The colorless bis<sup>Et</sup>-NHI<sup>Mes</sup>H<sub>2</sub>SiI<sub>2</sub> (**P7**) was isolated in 86% yield by filtration, and analyzed *via* multinuclear NMR spectroscopy. In addition to highly symmetric ligand framework signals, <sup>1</sup>H experiment revealed a direct Si–H resonance at δ(<sup>1</sup>H) = 3.0 ppm (Si–H satellites <sup>1</sup>J<sub>SiH</sub> = 282.3 Hz) that integrates as two hydrides (Figure 32, big). While the majority of known Si–H signals emerge between δ = 4.5 and 6.5 ppm, the observed resonance is notably highfield shifted but still within the known range (δ(<sup>1</sup>H) = 2.97 ppm to 6.20 ppm).<sup>[125]</sup>

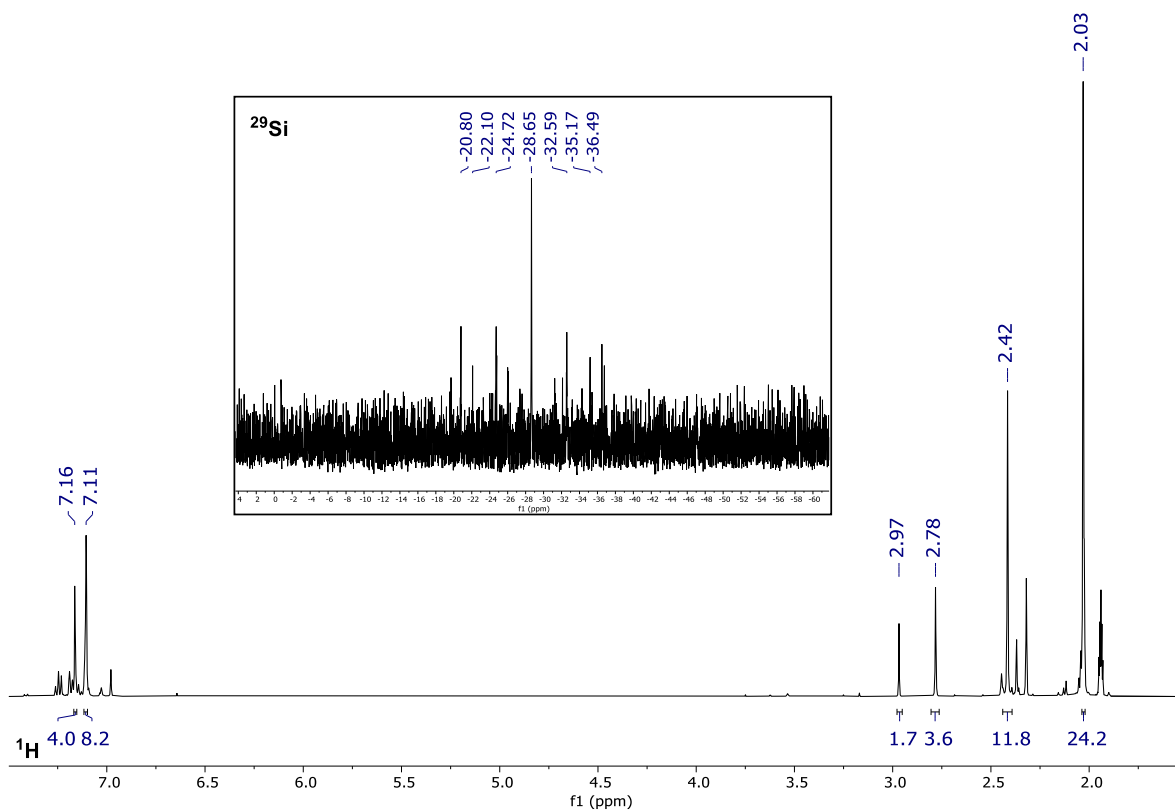


Figure 32.  $^1\text{H}$ -NMR (big) and  $^{29}\text{Si}$ -NMR (small) spectrum of  $[\text{bisEt-NHI}^{\text{Mes}}\text{SiH}_2][\text{I}]_2$  (**P7**) recorded at 25°C in  $\text{MeCN-d}_3$ .

Four-coordinate  $\text{SiH}_2$  dications are scarce in literature but neutral ferrocene-based *N*-heterocyclic- $\text{SiH}_2$  ( $[\text{Fe}\{(\eta^5\text{-C}_5\text{H}_4\text{NR})_2\text{SiH}_2\}]^{126}$ ) and bis(phosphine) diamine- $\text{SiH}_2$  ( $(\text{tBuP}^{\text{N}}\text{Si})\text{H}_2$ )<sup>127</sup> display corresponding  $\text{SiH}_2$  signals at  $\delta(^1\text{H}) = 5.25$  ppm and 6.60 ppm, respectively. In the  $^{29}\text{Si}$  NMR spectrum the assigned signal appears at  $\delta(^{29}\text{Si}) = -28.7$  ppm (Figure 32, small), which is significantly downfield shifted compared to the chlorine analog **P6** ( $\text{bisEt-NHI}^{\text{Mes}}\text{H}_2\text{SiCl}_2$ ). In  $^{29}\text{Si}_{\text{inept}}$  experiment H-Si-H coupling is observed as depicted in Figure 32. SC-XRD analysis, carried out on crystals grown from saturated  $\text{MeCN} / \text{Et}_2\text{O}$  solution, shows  $[\text{bisEt-NHI}^{\text{Mes}}\text{SiH}_2]^{2+} 2\text{I}^-$  (**P7**) in dicationic form with both iodine anions more than 3.0 Å separated from the cation (Figure 33). The silicon center occurs in distorted tetrahedral coordination environment with the N5-Si1-N6 angle being 91.9(5)°. The silicon bound hydrides H01 and H02 were found in the difference Fourier maps, but needed to be fixed in ideal positions for successful refinement. Admixture of metalimide character, throughout partial stabilization of the positive charge within the imidazoline rings, results in a slight elongation of the  $\text{C}_{\text{carb}}\text{-N}_{\text{imine}}$  bond lengths to 1.37 Å (C1-N5 1.367(10), C4-N6 1.370(9) Å) compared to **P1** ( $\text{C}_{\text{carb}}\text{-N}_{\text{imine}}$  1.33 / 1.33 Å) and  $\text{bisEt-NHI}^{\text{Mes}}\text{SiCl}_4$  (**P4**) ( $\text{C}_{\text{carb}}\text{-N}_{\text{imine}}$  1.36 / 1.34 Å). Likewise, the Si-N bond lengths are contracted upon strengthening of the iminato-character to  $\text{N}_{\text{imine}}\text{-Si}$  1.75 Å (Si1-N5 1.750(11), Si1-N6 1.748(9) Å) in comparison to **P1** (Si-N 1.82 / 1.86 Å) and **P4** (Si-N 1.77 / 1.84 Å).

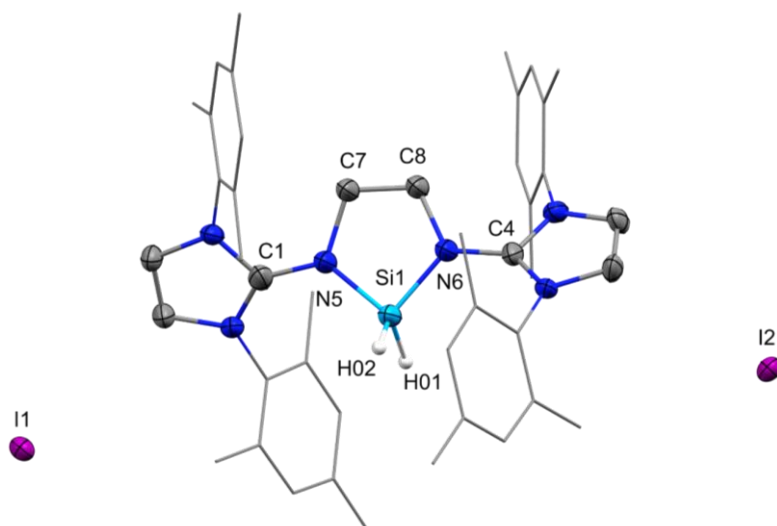
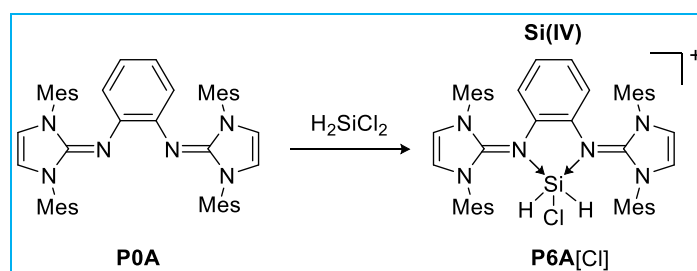


Figure 33. Solid-state plot of the molecular structure of  $[\text{bis}^{\text{Et}}\text{-NHI}^{\text{Mes}}\text{SiH}_2][\text{I}]_2$  (**P7**). Ellipsoids are set to the 50% probability level. Hydrogen atoms (except for H01 and H02), and solvent molecules are omitted for clarity; mesityl-substituents are depicted as wireframe for simplicity. Selected bond lengths [Å] and angles [°]: Si1–N5 1.750(11), Si1–N6 1.748(9), C1–N5 1.367(10), C4–N6 1.370(9), N5–Si1–N6 91.9(5).

The performed ligand complexation experiments show, that  $\text{bis}^{\text{Et}}\text{-NHI}^{\text{Mes}}$  complexes **P1** to **P7** could be prepared with a wide range of silicon starting materials with reasonable effort. In contrast,  $\text{bis}^{\text{Et}}\text{-NHI}^{\text{Dip}}$  was isolated in consistently lower yields and could not be directly converted to the corresponding silyliumylidene complex. In addition, reaction with base free halosilanes result invariably in the formation of imidazolium salt  $\text{NHC}^{\text{Dip}}\cdot\text{HX}$  ( $\text{X} = \text{Cl}, \text{I}$ ). Since, it was found that the mesityl wingtips do already form a pocket surrounding the silicon atom, which is expected to provide reasonable steric protection, the  $\text{bis}^{\text{Et}}\text{-NHI}^{\text{Mes}}$  ligand **P0** was chosen as the workhorse for further studies.

#### $\text{Bis}^{\text{Ph}}\text{-NHI}^{\text{Mes}}$

Testing the coordination ability of  $\text{bis}^{\text{Ph}}\text{-NHI}^{\text{Mes}}$  (**P0A**), reactions with Si-precursors  $\text{NHC}\rightarrow\text{SiX}_2$  and base-free halosilanes were pursued, analogous to the previous  $\text{bis}^{\text{Et}}\text{-NHI}$  system. As suggested from the protonated ligands' structure the  $\text{bis}^{\text{Ph}}\text{-NHI}$  ligand is more rigid and less accessible for coordination of Si-synthons. This lack of flexibility could explain, that out of the four tested Si precursors, only the smallest  $\text{H}_2\text{SiCl}_2$  could accomplish complex formation.



Scheme 36. Synthesis of  $[\text{bis}^{\text{Ph}}\text{-NHI}^{\text{Mes}}\text{SiClH}_2][\text{Cl}]$  (**P6A**) from free  $\text{bis}^{\text{Ph}}\text{-NHI}^{\text{Mes}}$  (**P0A**) and  $\text{H}_2\text{SiCl}_2$ . The reaction is carried out in toluene as solvent at room temperature over 48 hours.

Upon mixing of equimolar amounts of the free ligand **P0A** and  $\text{H}_2\text{SiCl}_2$  the formation of the product complex  $\text{bis}^{\text{Ph}}\text{-NHI}^{\text{Mes}}\text{H}_2\text{SiCl}_2$  was indicated by precipitation of colorless solid from the yellowish solution (Scheme 36). It is of note that full conversion takes significantly longer than in the  $\text{bis}^{\text{Et}}\text{-NHI}^{\text{Mes}}$  case (complex **P6**) according to  $^1\text{H}$  NMR monitoring. After 48 hours of reaction time the product could be isolated in 43% yield. The multinuclear NMR analysis gives a sound picture that is indicative for  $[\text{bis}^{\text{Ph}}\text{-NHI}^{\text{Mes}}\text{SiH}_2\text{Cl}][\text{Cl}]$  (**P6A**, Figure 34). However, the reaction proceeds in an unclear fashion, in which  $\text{NHC}^{\text{Mes}}\cdot\text{HCl}$  and at least one more not identified Si-H containing species was formed. Purification of **P6A** could not be accomplished, due to similar solubility and crystallization properties of the complex product mixture.

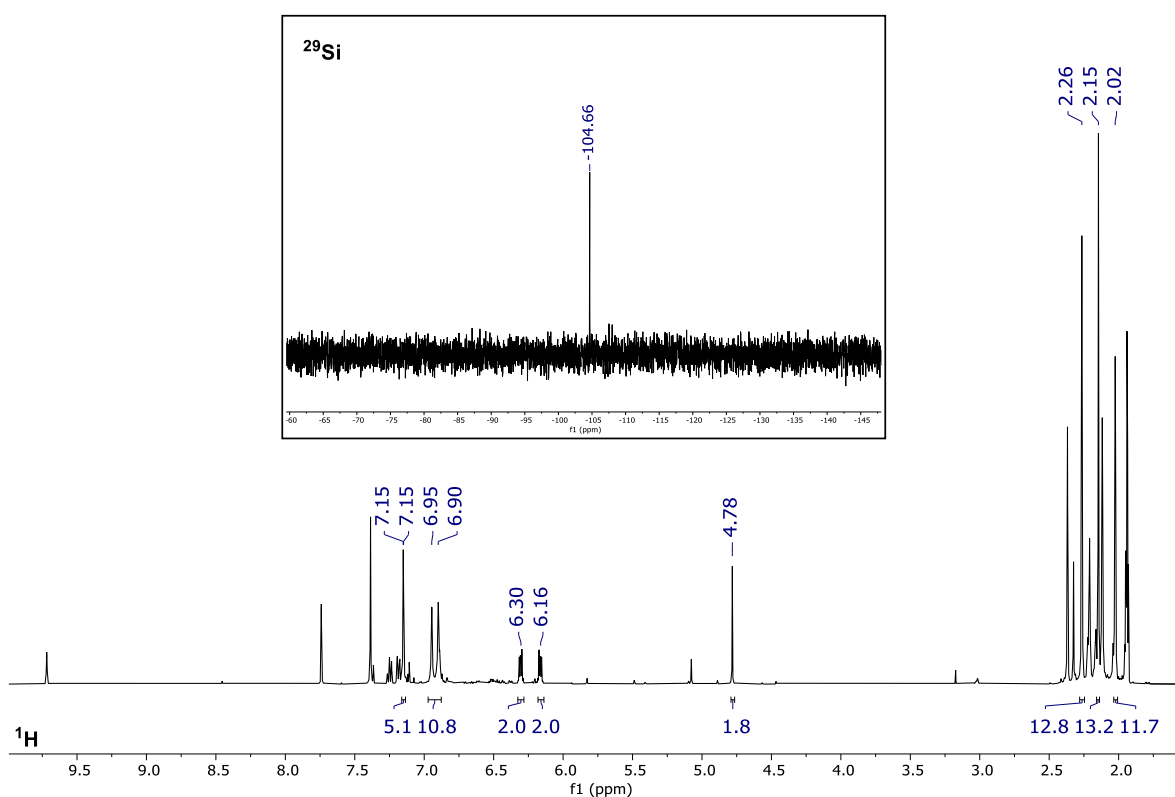


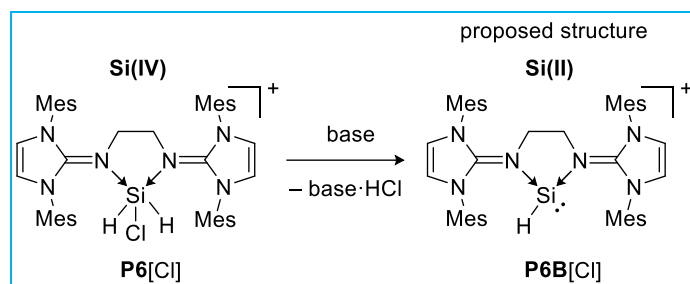
Figure 34.  $^1\text{H}$ -NMR (big) and  $^{29}\text{Si}$ -NMR (small) spectrum of  $[\text{bis}^{\text{Ph}}\text{-NHI}^{\text{Mes}}\text{SiH}_2\text{Cl}][\text{Cl}]$  (**P6A**) recorded at  $25^\circ\text{C}$  in  $\text{MeCN-d}_3$ . Product signals are picked, considerable amounts of  $\text{NHC}^{\text{Mes}}\cdot\text{HCl}$  and a minor Si-H containing species are contained.

$n\text{BuNHI}^{\text{Mes}} / n\text{BuNHI}^{\text{Dip}}$

Unfortunately, all attempts to afford mono-substituted  $n\text{BuNHI-Si}$  complexes from neutral  $n\text{BuNHI}$  and Si precursors failed, and no complex formation could be observed. However, reactions using the protonated ligand  $[n\text{BuNHI-H}][\text{BF}_4]$  and various Si synthons under reductive conditions were not tested and remain one reasonable synthetic option.

4.3 Chemistry of bis<sup>Et</sup>-NHI<sup>Mes</sup>SiH<sub>2</sub>X<sub>2</sub> (P6 X = Cl, P7 X = I)

HCl abstraction has proven to be a powerful synthetic concept in the isolation of low valent silicon species such as the silyl-substituted silyliumylidene **19** (Scheme 8), to name just one. To gain access to novel bis-NHI substituted silylones and silyliumylidene hydrides, the reactivity of bis<sup>Et</sup>-NHI<sup>Mes</sup>SiH<sub>2</sub>X<sub>2</sub> (X = Cl **P6**, X = I **P7**) towards different bases was tested. However, using KO<sup>t</sup>Bu, KHMDS, IMe<sub>4</sub>, DABCO, Na-Si<sup>t</sup>Bu<sub>3</sub>, *n*-BuLi, and pyridine no selective conversions could be obtained at different reaction conditions and temperatures.



Scheme 37. Intended reaction of [bis<sup>Et</sup>-NHI<sup>Mes</sup>SiCH<sub>2</sub>][Cl] (**P6**) with different bases to achieve HCl abstraction to silyliumylidene hydride species **P6B**.

It is noted, that an experiment using **P6** and one equivalent of potassium *tert*-butoxide as a base (Scheme 37) yielded promising shifts in multinuclear NMR analysis, which could not be reproduced, despite several attempts.

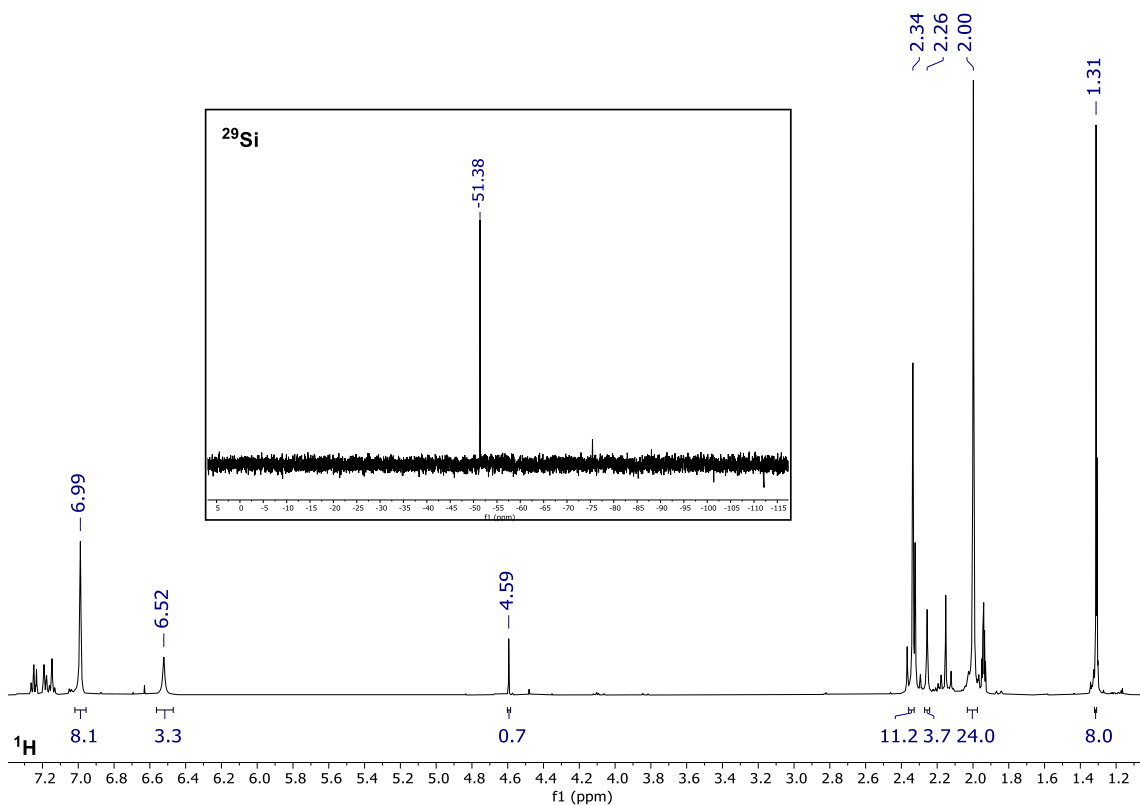
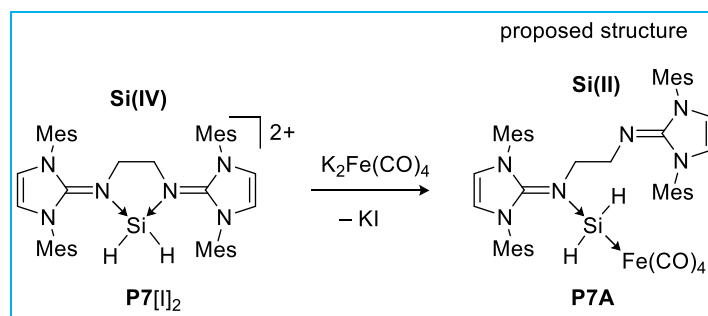


Figure 35. <sup>1</sup>H-NMR (big) and <sup>29</sup>Si-NMR (small) spectrum of reaction mixture of **P6** with KO<sup>t</sup>Bu to proposed structure **P6B** recorded at 25°C in MeCN-*d*<sub>3</sub>. Toluene remaining from synthesis is contained.

In a selective manner the Si–H signal of **P6A** shifts to  $\delta(^1\text{H}) = 4.59$  ppm (Si–H satellites  $^1J_{\text{SiH}} = 120.7$  Hz) in the  $^1\text{H}$  NMR and integrates as one hydride (Figure 35, big). The other signals of the bis-NHI ligand are shifted but remain in a symmetric pattern. More evident, the  $^{29}\text{Si}$  NMR resonance experienced a significant downfield shift to  $\delta(^{29}\text{Si}) = -51.4$  ppm (Figure 35, small), matching with the loss of the electronegative chlorine substituent within HCl-abstraction.



Scheme 38. Intended reaction of  $[\text{bis}^{\text{Et}}\text{-NHI}^{\text{Mes}}\text{SiH}_2][\text{I}]_2$  (**P7**) with  $\text{K}_2\text{Fe}(\text{CO})_4$  to achieve reductive dehalogenation to proposed reaction product **P7A**.

Attempts to reduce  $[\text{bis}^{\text{Et}}\text{-NHI}^{\text{Mes}}\text{SiH}_2]^{2+} 2\text{I}^-$  (**P7**) using  $\text{K}_2\text{Fe}(\text{CO})_4$  at room temperature (Scheme 38) resulted in one main species that was analyzed *via* multinuclear NMR spectroscopy. Upon addition of the ferrate reagent, the formerly clear and colorless solution of **P7** in acetonitrile- $\text{d}_3$  turned cloudy orange.

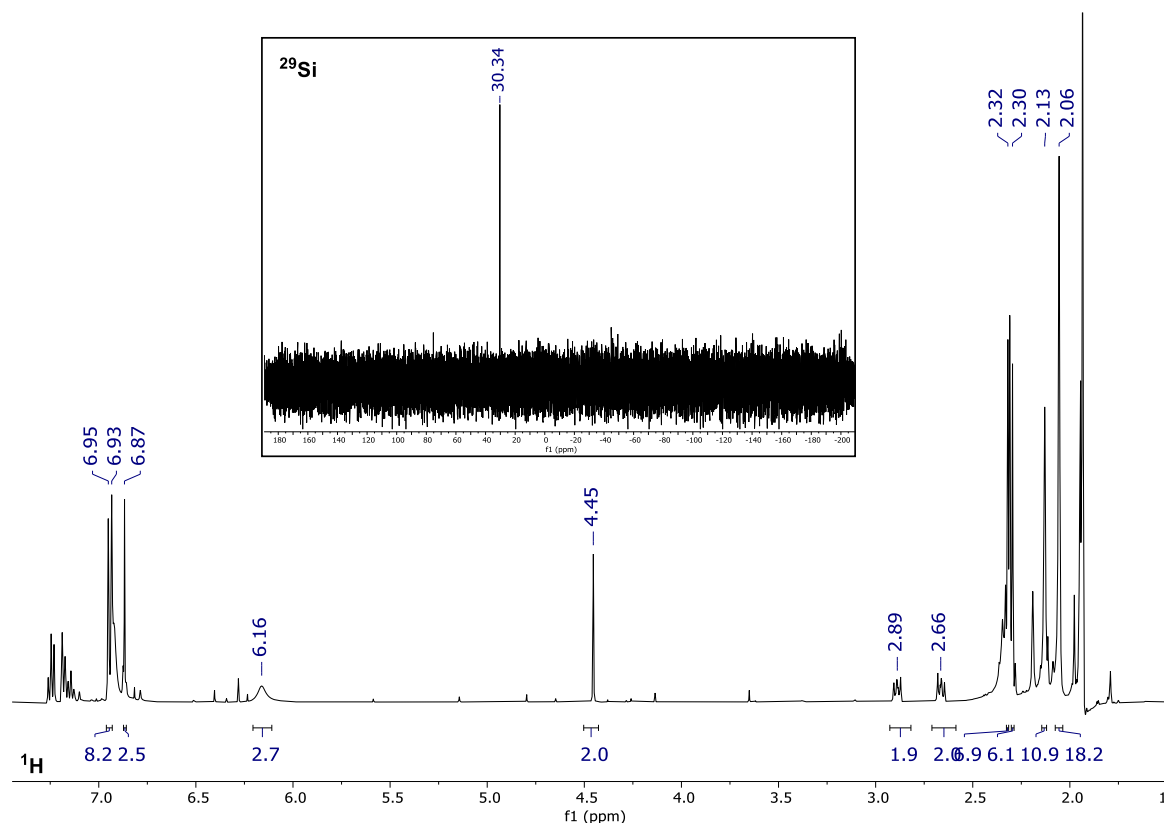


Figure 36.  $^1\text{H}$ -NMR (big) and  $^{29}\text{Si}$ -NMR (small) spectrum of reaction mixture of **P7** with  $\text{K}_2\text{Fe}(\text{CO})_4$  to proposed structure **P7A** recorded at  $25^\circ\text{C}$  in  $\text{MeCN-d}_3$ . Toluene remaining from synthesis is contained.

The precipitate was filtered off and the resulting clear orange solution was analyzed. Full conversion of the starting material can be confirmed in <sup>1</sup>H NMR with all signals being shifted compared to **P7**. A loss of molecular symmetry is indicated by the split of several signals (Figure 36, big). However, one distinct singlet at  $\delta(^1\text{H}) = 4.5$  ppm (Si–H satellites  $^1J_{\text{SiH}} = 195.0$  Hz) evidences the presence of two hydrides. The <sup>29</sup>Si NMR resonance appears at  $\delta = 30.3$  ppm (Figure 36, small) and thus suggesting a deshielding of the silicon center that is likely to be caused by coordination of the iron synthon, that is further evidenced *via* <sup>13</sup>C NMR experiment, in which the characteristic carbonyl signals can be found at  $\delta(^{13}\text{C}) = 225.0, 221.9$  and 217.5 ppm (Figure S 16).

For both complexes **P6** and **P7**, HX (X = Cl, I) abstraction presented challenging and could not clearly be evidenced. However, test reactions with KOtBu and K<sub>2</sub>Fe(CO)<sub>4</sub> gave promising preliminary results, that warrant further investigations on this reaction pathway.

#### 4.4 Chemistry of bis<sup>Et</sup>-NHI<sup>Mes</sup>SiCl<sub>2</sub> (**P1**)

With the first bis-NHI stabilized silyliumylidene in hand, this working horse complex was tested for its reactivity. The following chapter describes the oxidation using heavier chalcogens and coordination of transition metals of the groups 6, 8 and 11.

##### 4.4.1 Chalcogens

This chapter has been published in part within ref<sup>[128]</sup>

Recent studies reveal NHC- and phosphine-selenides to serve as model compounds to determine the  $\sigma$ -donor and  $\pi$ -acceptor strength of respective ligand by assessment of the <sup>77</sup>Se NMR shift (Chart 1).<sup>[129-131]</sup> Determination of the <sup>77</sup>Se NMR shift of NHC=Se complexes reflects the  $\pi$ -acidity ranking that is also found for NHCs using DFT calculations. By electron back donation the selenium nucleus experiences deshielding resulting in a downfield shift of the <sup>77</sup>Se NMR signal.

In addition, a correlation was found for the <sup>1</sup>J<sub>CSe</sub> coupling constant with the  $\sigma$ -donor strength of those carbenes. Originating from the Fermi contact between nuclear magnetic moments and electron spins, the coupling between neighboring atoms provides information on the basicity of Se bound NHC. Low coupling constants arise from strong  $\sigma$ -donation ability, as the s-character of the respective bonding orbital decreases. While those coupling constants can be challenging to observe, the <sup>77</sup>Se shift is a straightforward method to assess the relative  $\pi$ -acidity. Thus, an analog strategy might also be sound for [Si]=Se compounds.

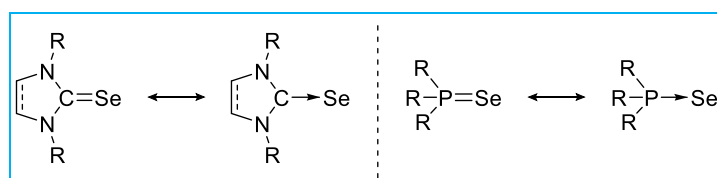
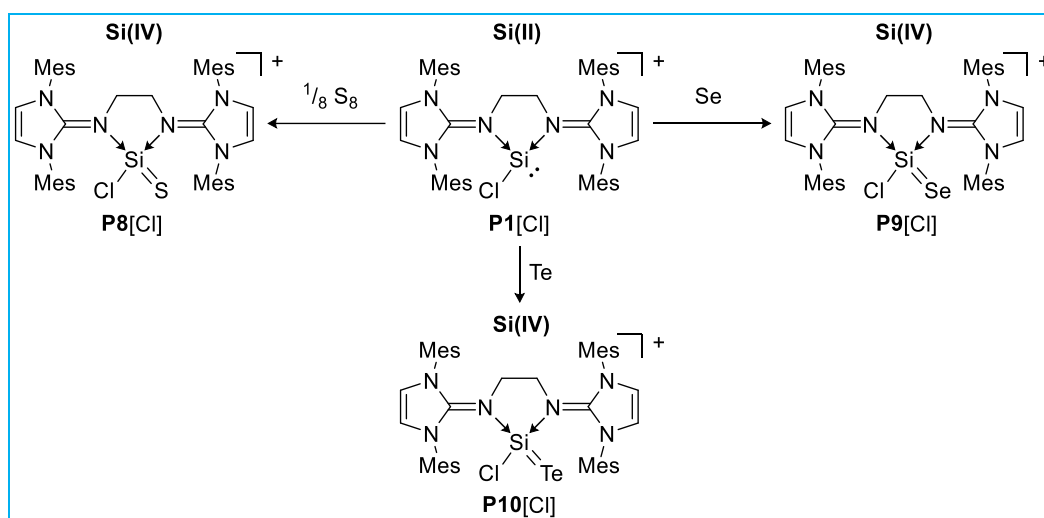


Chart 1. Depiction of donor-selenides NHC=Se and R<sub>3</sub>P=Se in two mesomeric structures (R = aryl and alkyl substituents).

As pointed out within the state-of-the-art part, the activation of heavier chalcogens is a well-known concept reactivity for Lewis base lone pairs of low-valent main group compounds. The addition of heavier chalcogens (S, Se, Te) results in higher oxidized and higher coordinate and therefore commonly more stable silicon complexes, favoring conversion and highlighting the lone pair reactivity. Indeed, elemental sulfur, selenium, and tellurium could be activated by reaction with **P1** in equimolar ratio in acetonitrile at room temperature, furnishing the heavier silaacylium ions **P8** to **P10** (Scheme 39).



Scheme 39. Synthesis of [bis<sup>ET</sup>-NHIMe<sup>S</sup>SiClE][Cl] (E = S **P8**, Se **P9**, Te **P10**) from **P1** and the respective chalcogen. The reaction is carried out in acetonitrile as solvent at room temperature over 30 minutes (**P8**) up to 48 hours (**P10**).

While sulfur reacted readily within 30 minutes to give **P8** (Scheme 39, left), the reaction took 48 hours in case of tellurium for complete conversion to **P10** (Scheme 39, right). To sustain full conversion and reduce the reaction time to the necessary minimum, the reaction can be executed with two equivalents of the respective chalcogen, without the formation of byproducts. The surplus reaction agent was filtered off and the product stripped from solvent to afford the silaacylium ions in nearly quantitative yields.

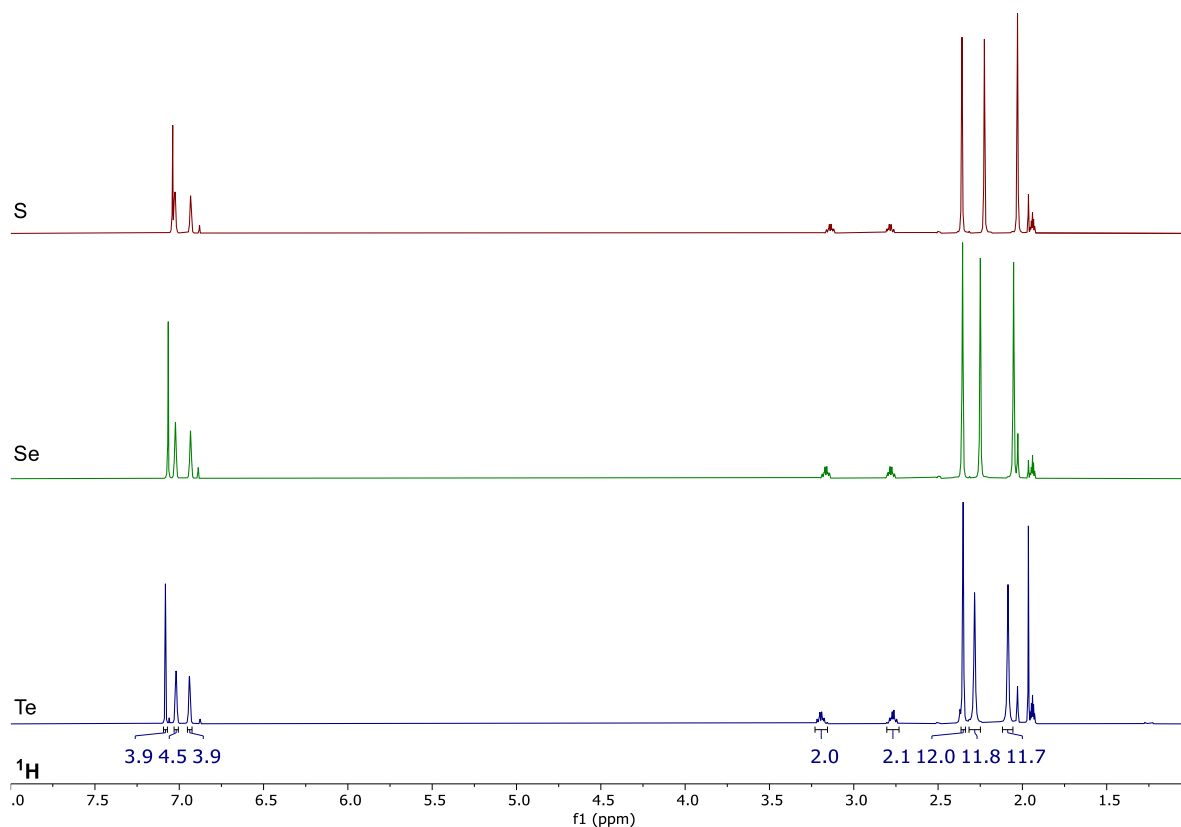


Figure 37. Stacked <sup>1</sup>H-NMR spectra of [bis<sup>ET</sup>-NHIMe<sup>S</sup>SiClE][Cl] (E = S **P8**, Se **P9**, Te **P10**) recorded at 25°C in MeCN-d<sub>3</sub>.

Successful formation of heavier silylium ions is verified *via* multinuclear NMR analysis (Figure 37 and Figure 38). The  $^{29}\text{Si}$  NMR spectroscopic analysis revealed the expected trend of upfield shift from **P8** to **P10** with  $\delta(^{29}\text{Si}) = -26.7$  ppm (**P8**),  $-31.0$  ppm (**P9**),  $-59.1$  ppm (**P10**), that was also observed for the heavier silylium ions of **12** (compound **32**, **33**).<sup>[96]</sup> For bis(iminophosphorane) stabilized **17<sup>S</sup>**,<sup>[90]</sup> a sharp singlet at  $\delta(^{29}\text{Si}) = -26.7$  ppm was observed, that matches the findings in **P8**, pointing out the structural and electronic similarity between the compounds.

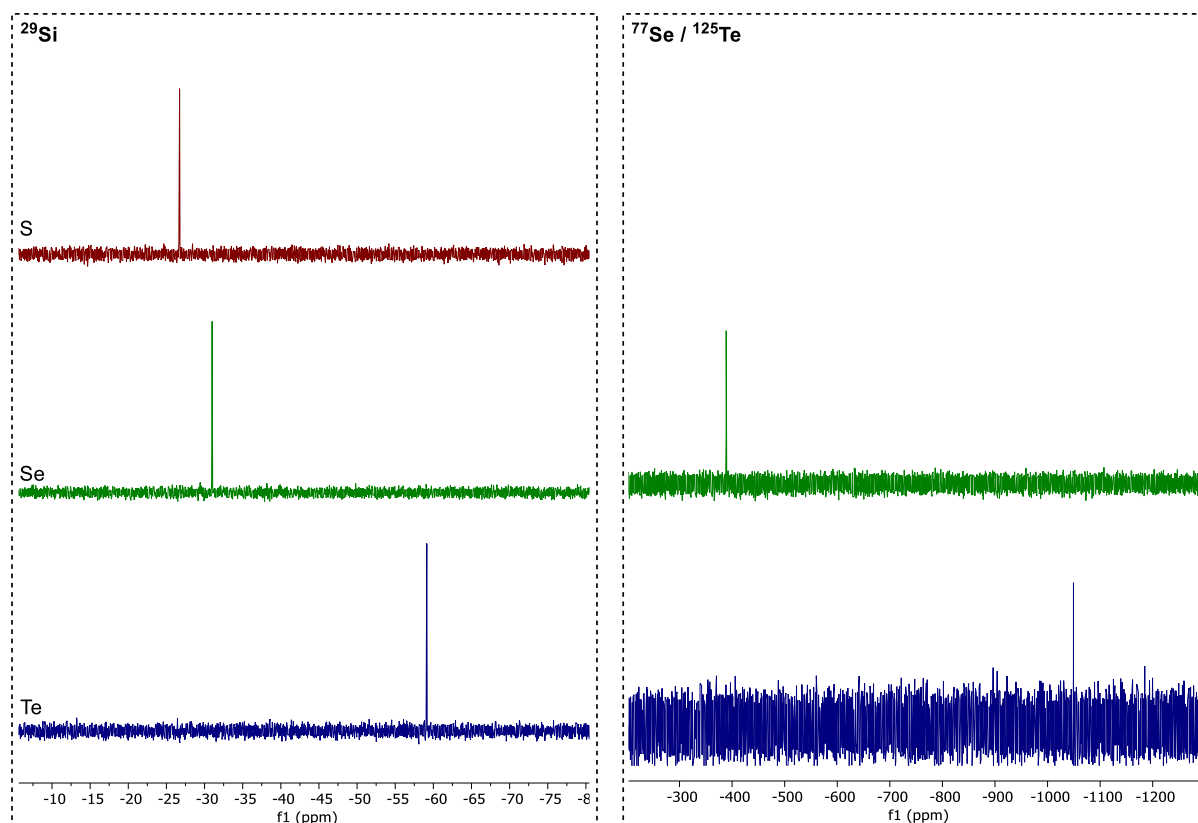


Figure 38. Stacked  $^{29}\text{Si}$ -NMR (left) and  $^{77}\text{Se}/^{125}\text{Te}$ -NMR (right) spectra of  $[\text{bis}^{\text{Et}}\text{-NHI}^{\text{Mes}}\text{SiClE}][\text{Cl}]$  (E = S **P8**, Se **P9**, Te **P10**) recorded at 25°C in  $\text{MeCN-d}_3$ .

For **P9**, the shift of  $\delta(^{77}\text{Se}) = -388.8$  ppm (Figure 38, right) is indicative for a reasonable but comparably low  $\pi$ -acidity of silyliumylidene **P1**, as being the selenide's ligand. Whereas NHC (NHC=Se) and phosphine ( $\text{R}_3\text{P}=\text{Se}$ ) complexes ranges roughly from 860 to  $-22$  ppm<sup>[129]</sup> and  $-30$  to  $-350$  ppm<sup>[132]</sup> respectively, known Si=Se compounds resonate between  $-244$  to  $-655$  ppm in  $^{77}\text{Se}$  NMR.<sup>[131,133–136]</sup> As anticipated, due to the electronegative chlorine substituent, **P9** seems a stronger  $\pi$ -acceptor than *m*Ter substituted selenium adduct **12<sup>Se</sup>** ( $\delta(^{77}\text{Se}) = -423.8$  ppm), and also three-coordinate Si=Se with anionic *N,N*-chelating ligands and additional donors tend to resonate at higher field. However, compared to chlorine substituted NHSi  $[\text{Ph}_2\text{P}(\text{NtBu})_2]\text{ClSi}=\text{Se}$  ( $\delta(^{77}\text{Se}) = -267.9$  ppm) **P9** shows an upfield shift, suggesting lower  $\pi$ -acidity.

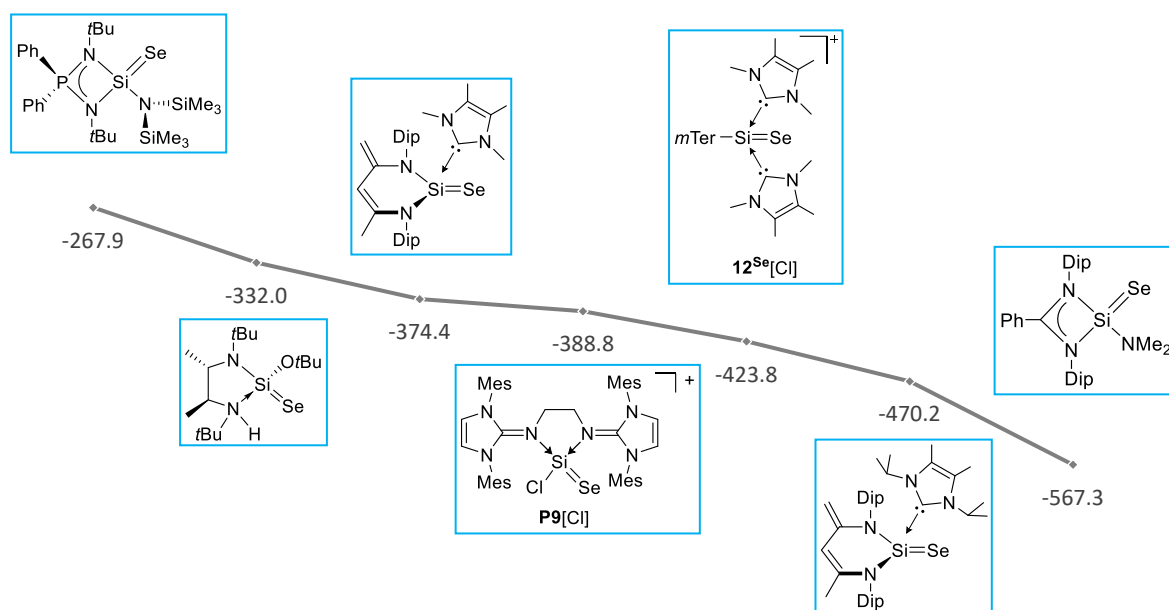


Chart 2. Selected examples of ligand-stabilized silicon-selenide complexes plotted according to their  $^{77}\text{Se}$ -NMR shift  $\delta(\text{ppm})$ .<sup>[133–136]</sup>

SC-XRD analysis of compound **P8** was carried out on colorless crystals grown from a MeCN / DME mixture (Figure 39). Upon addition of sulfur, the silicon atom adopts a tetrahedral coordination. The Si=S bond length (1.9740(6) Å) is in good agreement with other donor stabilized Si=S double bonds (1.96 – 2.08 Å)<sup>[96,137]</sup> reported before and matches the Si=S bond in **17<sup>s</sup>** (1.984(2) Å). The molecular structure of **P8** serves as a representative for the heavier homologues by replacing S for Se or Te.

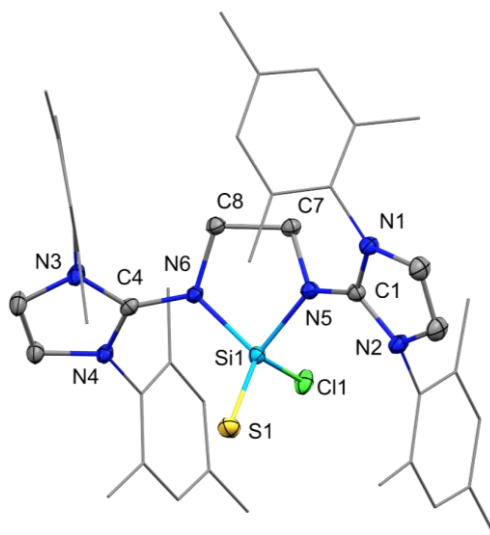


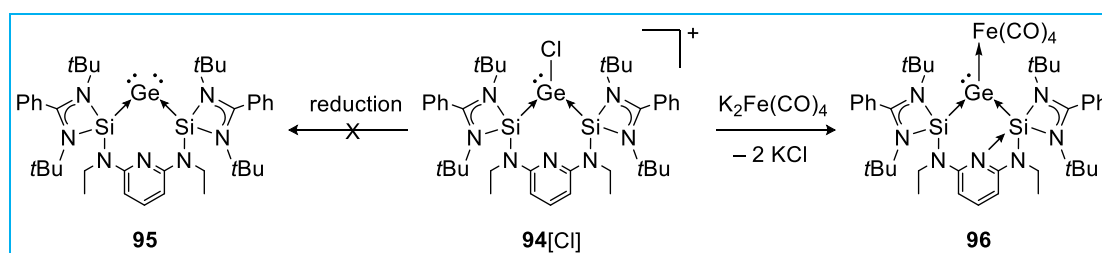
Figure 39. Solid-state plot of the molecular structure of  $[\text{bis}^{\text{Et}}\text{-NHI}^{\text{Mes}}\text{SiClS}][\text{Cl}]$  (**P8**). Ellipsoids are set to the 50% probability level. Hydrogen atoms, the counter anion and solvent molecules are omitted for clarity; mesityl-substituents are depicted as wireframe for simplicity. Selected bond lengths [Å] and angles [°]: Si1–S1 1.9740(6), Si1–Cl1 2.0678(6), Si1–N5 1.7839(12), Si1–N6 1.7972(14), C1–N5 1.3446(19), N6–C4 1.356(2), N5–Si1–N6 89.89(6), N5–Si1–S1 120.22(5), S1–Si1–Cl1 117.05(3), N5–Si1–Cl1 101.96(5).

Compounds **P9** and **P10** were characterized by multinuclear NMR techniques including <sup>77</sup>Se (**P9**  $\delta(^{77}\text{Se}) = -388.8$  ppm) and <sup>125</sup>Te (**P10**  $\delta(^{125}\text{Te}) = -1049.4$  ppm) as well as mass spectroscopy (ESI). The data are found to be consistent in all structural means and strongly suggest that **P9** and **P10** are structural analogues of **P8**.

The oxidation of silyliumylidene **P1** using oxygen sources, would not only complete the series of chalcogens, but provide the possibility of stabilizing the monomeric ‘Si=O’ or ‘O=Si=O’ unit. Despite several today known silaacylium-ions, the neutral and monomeric ‘SiO<sub>2</sub>’ – so-called ‘molecular sand’ – remains an elusive dream compound. As described in the state-of-the-art, reaction of silylone **47** with CO<sub>2</sub> afforded the carbonate derivative **64**, indicating ‘Si=O’ and ‘O=Si=O’ as non-isolable intermediates. However, treatment of **P1** with 1 bar of CO<sub>2</sub>, O<sub>2</sub>, or N<sub>2</sub>O unselectively resulted in unidentified mixtures of products even at low temperature.

#### 4.4.2 Transition metals of Group 12, 10, and 8

According to the scope of this thesis, the coordination of transition metals was expected to introduce on the one hand a potent second active center and on the other hand a Lewis acidic fragment into bis-NHI silyliumylidene chemistry to provide surplus synthetic options. Studies on a pyridine-pincer bridged bis-silylene germanium complex demonstrated the stabilizing effect of the Lewis acidic metal fragment Fe(CO)<sub>4</sub> (Scheme 40). The corresponding iron-germylone could be isolated as L<sub>2</sub>Ge→Fe(CO)<sub>4</sub> **96** upon direct reduction of the chlorogermlyliumylidene precursor **94** using K<sub>2</sub>Fe(CO)<sub>4</sub>, however the free germlylone **95** remained elusive with this specific ligand backbone.<sup>[138]</sup>

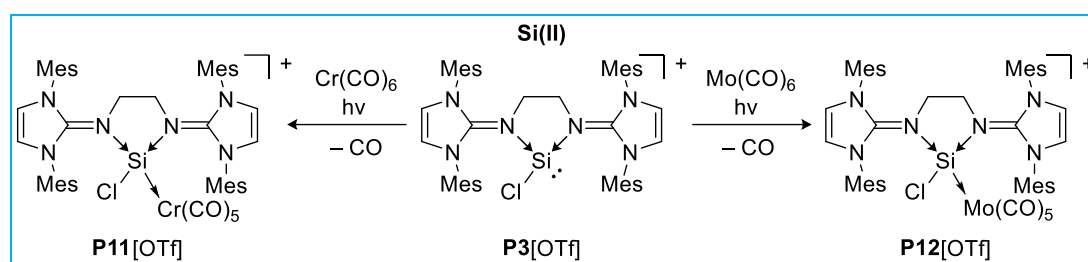


Scheme 40. Unsuccessful reduction of bis-silylene-stabilized germlyliumylidene **94** to free germlylone **95** and isolable germlylone-iron complex **96** via K<sub>2</sub>Fe(CO)<sub>4</sub> reduction of **94**.

Several test reactions were conducted to achieve conversion to transition metal silyliumylidene complexes. The substrates were chosen from early to late transition metals and tested for direct coordination to the silyliumylidene’s lone pair of electrons. Selective conversion with ZnCl<sub>2</sub>, Ni(cod)<sub>2</sub>, Ni(PPh<sub>3</sub>)<sub>2</sub>(CO)<sub>2</sub>, Pd(PPh<sub>3</sub>)<sub>4</sub>, Fe(CO)<sub>5</sub>, and Fe<sub>2</sub>(CO)<sub>9</sub> remained unsuccessful despite several attempts at different reaction conditions. Whether sterically demanding auxiliary ligands or unfavored ligand exchange inhibited the formation of the corresponding silyliumylidene complexes could not be conclusively elucidated.

## 4.4.3 Transition metals of Group 6

Reaction of **P1** with  $\text{Cr}(\text{CO})_5$  in acetonitrile expectably resulted in the formation of anion exchange product. Whereas the color of the reaction mixture changed to yellow and  $\text{Cr}(\text{CO})_5$  got dissolved upon applying radiation with 340 nm, only very small variation of the shifts in  $^1\text{H}$  NMR were detectable.  $^{13}\text{C}$  NMR spectroscopy confirmed the formation of  $\text{Cr}(\text{CO})_5\text{Cl}$ . To achieve successful and selective coordination, the reaction was repeated using **P3**.



Scheme 41. Synthesis of  $[\text{bis}^{\text{Et}}\text{-NH}^{\text{Mes}}\text{SiCIM}][\text{OTf}]$  ( $\text{M} = \text{Cr}(\text{CO})_5$  **P11**,  $\text{Mo}(\text{CO})_5$  **P12**) from **P3** and the respective carbonyl complex. The reaction is carried out in THF as solvent at room temperature under radiation with 360nm.

When equimolar amounts of **P3** and  $\text{Cr}(\text{CO})_6$  or  $\text{Mo}(\text{CO})_6$  were mixed in THF at room temperature, no reaction was observed until the  $\text{M}(\text{CO})_5\text{THF}$  ( $\text{M} = \text{Cr}, \text{Mo}$ ) complexes were allowed to form under radiation at 340 nm (Scheme 41). The reaction mixture turned yellow and within 72 hours formation of the desired complexes could be detected *via* NMR monitoring.

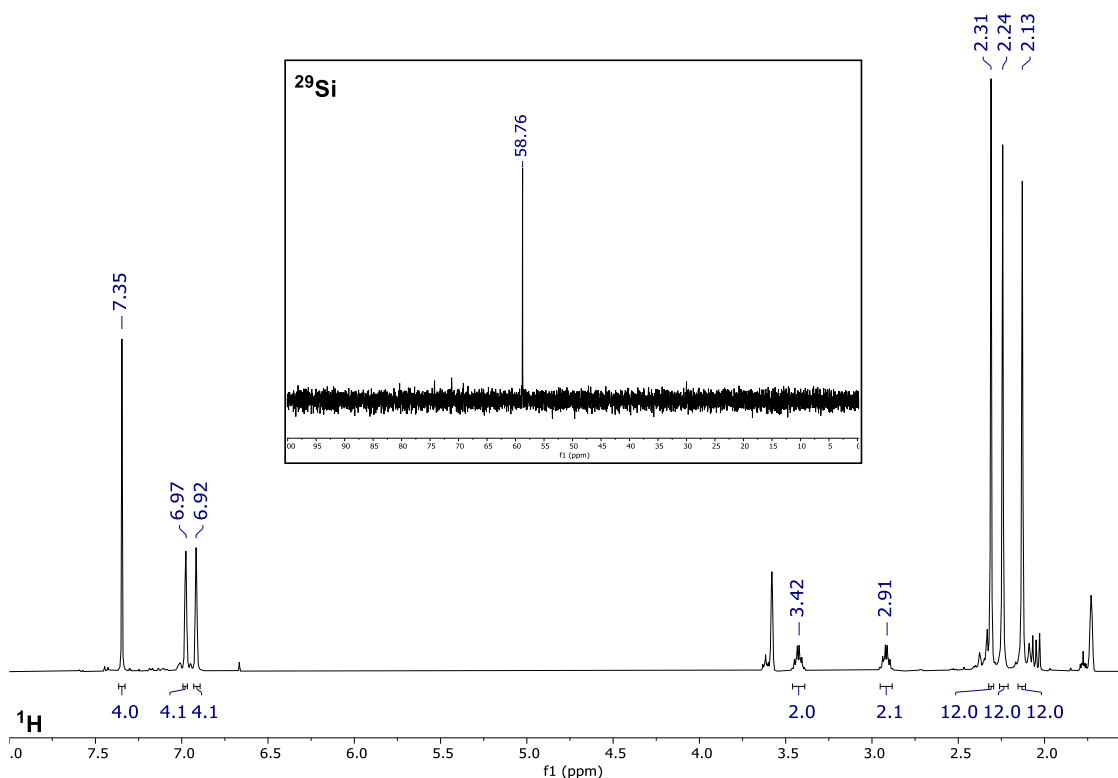


Figure 40.  $^1\text{H}$ -NMR (big) and  $^{29}\text{Si}$ -NMR (small) spectrum of  $[\text{bis}^{\text{Et}}\text{-NH}^{\text{Mes}}\text{SiClCr}(\text{CO})_5][\text{OTf}]$  (**P11**) recorded at 25°C in  $\text{THF-d}_8$ .

While the reaction forming  $[\text{bis}^{\text{Et}}\text{-NHI}^{\text{Mes}}\text{SiClCr}(\text{CO})_5][\text{OTf}]$  (**P11**, Figure 40) reached full conversion at room temperature, reaction forming  $[\text{bis}^{\text{Et}}\text{-NHI}^{\text{Mes}}\text{SiClMo}(\text{CO})_5][\text{OTf}]$  (**P12**, Figure 41) remained at approximately 70% starting material even after 14 days. The  $^1\text{H}$  NMR of the complexes **P11** and **P12** display the full ligand's pattern, with one respective signal per NHI component (Figure 40 and Figure 41, big).

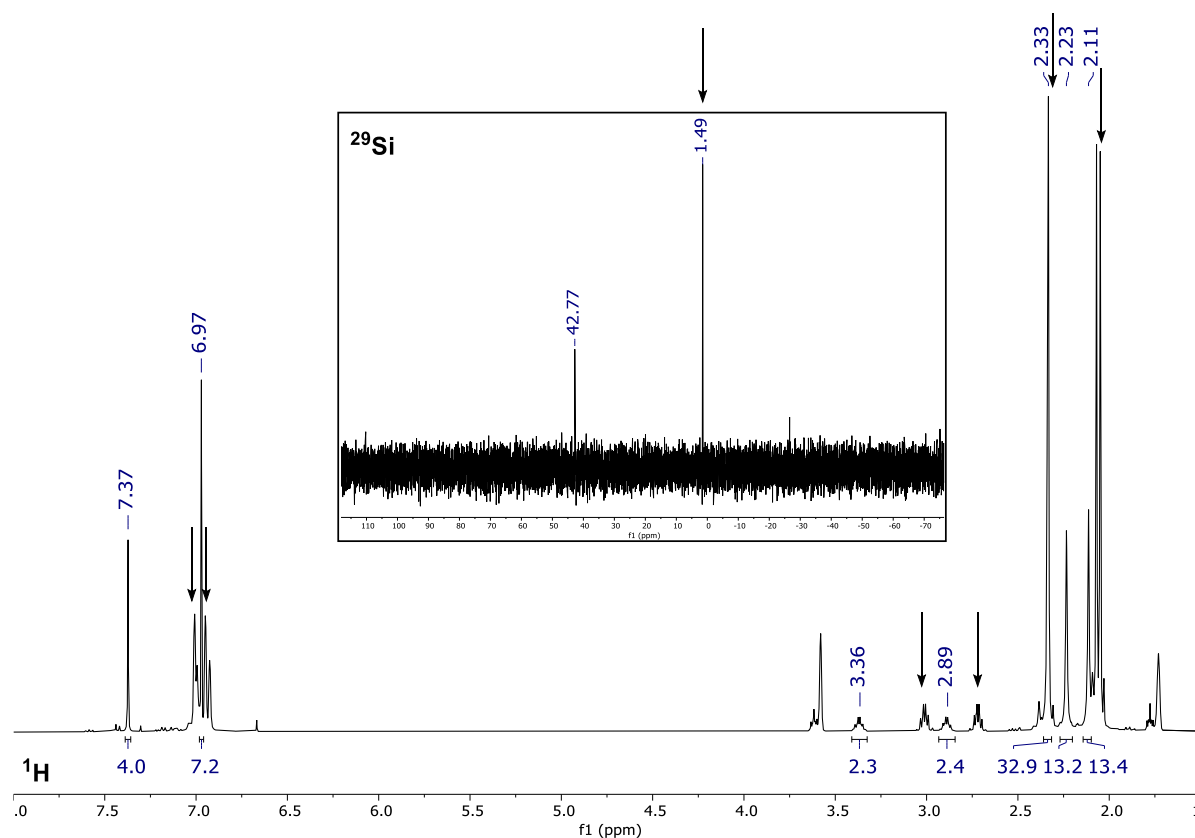


Figure 41.  $^1\text{H}$ -NMR (big) and  $^{29}\text{Si}$ -NMR (small) spectrum of  $[\text{bis}^{\text{Et}}\text{-NHI}^{\text{Mes}}\text{SiClMo}(\text{CO})_5][\text{OTf}]$  (**P12**) recorded at 25°C in THF- $d_8$ . Unreacted starting material **P3** is marked with arrows.

This is indicative for a similar symmetry and thus a complex geometry comparable to chalcogen addition products. Moreover, characteristic carbonyl signals in  $^{13}\text{C}$  NMR were found at  $\delta(^{13}\text{C}) = 212.9, 221.5,$  and  $224.7$  ppm for **P11** (Figure S 20) and at  $\delta(^{13}\text{C}) = 202.3, 210.0,$  and  $211.7$  ppm for **P12** (Figure S 21), verifying the coordination of the  $\text{M}(\text{CO})_5$  synthons. The  $^{29}\text{Si}$  NMR resonance were found at  $\delta(^{29}\text{Si}) = 58.8$  ppm in case of **P11** and  $\delta(^{29}\text{Si}) = 42.8$  ppm in case of **P12** (Figure 40 and Figure 41, small). Compared to the starting material **P3**, the Si centers experience a noticeable downfield shift of almost 60 ppm, indicating the intended deshielding of the Si nucleus caused by reduced electron density. The same trend with also comparable shifting of the  $^{29}\text{Si}$  NMR signals is apparent in  $\text{Tip-Si}(\text{IMe})_2\text{M}(\text{CO})_5$  ( $\text{M}$  [ $\delta^{29}\text{Si}$ ] = / [−69.5 ppm] **13**, Cr [6.3 ppm] **79**, Mo [−17.3 ppm] **80**, W [−30.5 ppm] **81**) complexes, published in 2019 by our group.<sup>[120]</sup> In 2012, Roesky, Stalke, and Ghadwal published neutral chloro-silylene metal complexes that feature a similar coordination environment to **P11** and



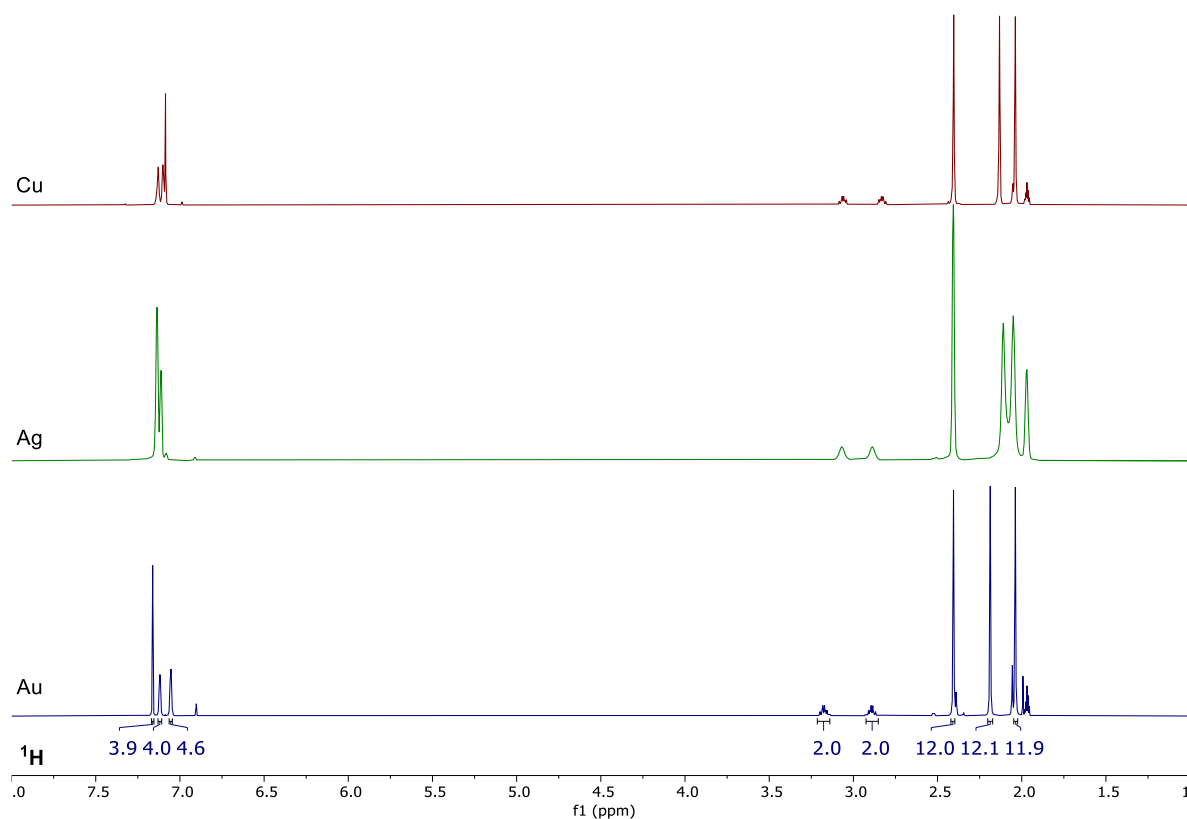


Figure 42. Stacked  $^1\text{H}$ -NMR spectra of  $[\text{bis}^{\text{Et}}\text{-NHIMeSSiClM}][\text{Cl}]$  ( $M = \text{Cu}$  **P13**,  $\text{Ag}$  **P14**,  $\text{Au}$  **P15**) recorded at  $25^\circ\text{C}$  in  $\text{MeCN-d}_3$ .

Complexes **P13** to **P15** could be identified *via* 1D and 2D -  $^1\text{H}$ ,  $^{13}\text{C}$ , and  $^{29}\text{Si}$  NMR techniques (Figure 42 and Figure 43) and mass spectrometry (ESI).

Coordination of the corresponding transition metal causes an expected downfield shift in  $^{29}\text{Si}$  NMR for  $\delta(^{29}\text{Si}) = 13.8$  ppm (**P13**), 20.2 ppm (**P14**,  $^1J_{\text{Si}^{109}\text{Ag}} = 592.8$  Hz,  $^1J_{\text{Si}^{107}\text{Ag}} = 514.3$  Hz), and 18.2 ppm (**P15**, Figure 43). Notably, compound **P14** features the up to now highest observed Si–Ag coupling constant with 592.8 Hz for the  $^{109}\text{Ag}$  nucleus. As opposed to compounds **P8**–**P10**, the trend for downfield shifting in **P13**–**P15** does not reflect the trends going down the group from Cu to Au. Relativistic effects in case of the gold complex **P15** arguably cause the observed behavior.

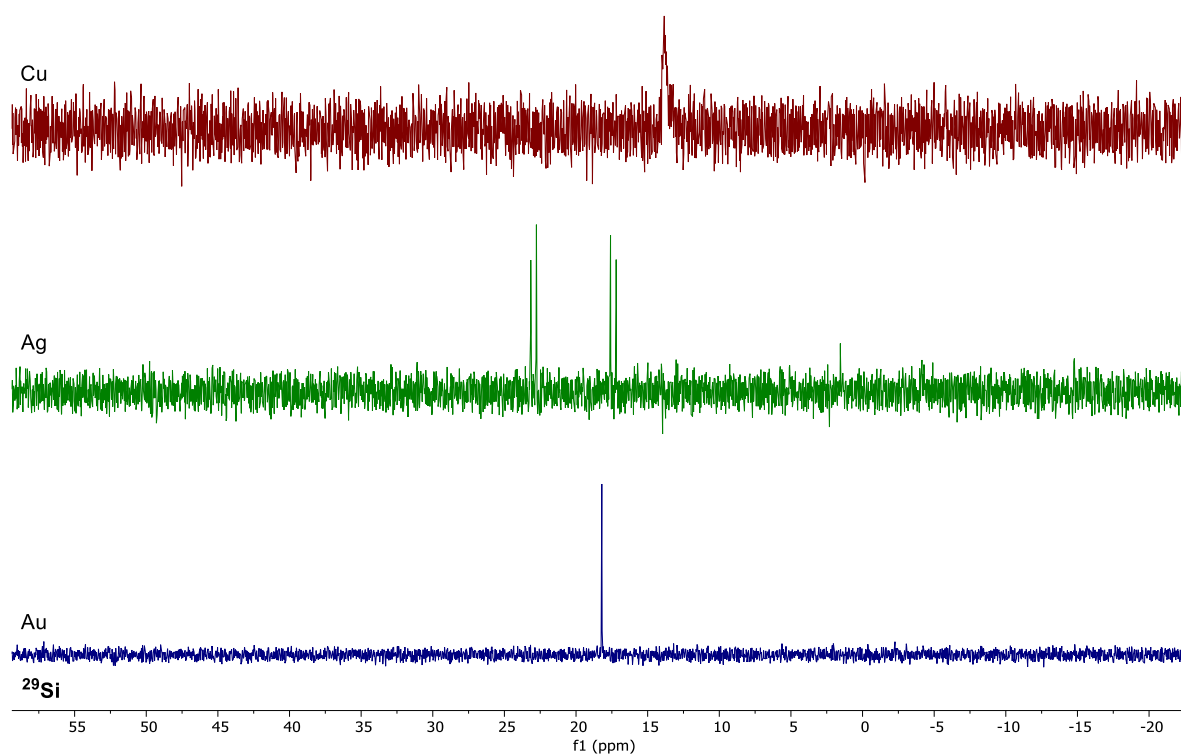
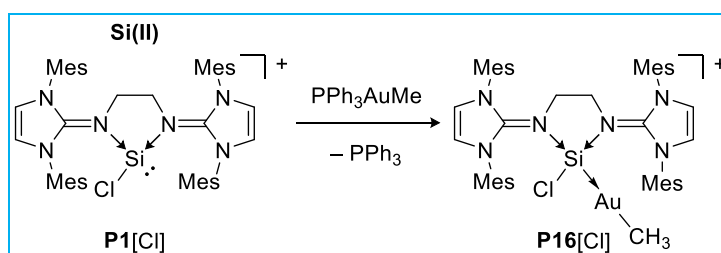


Figure 43. Stacked  $^{29}\text{Si}$ -NMR spectra of  $[\text{bis}^{\text{Et}}\text{-NHI}^{\text{Mes}}\text{SiClMCl}][\text{Cl}]$  ( $\text{M} = \text{Cu}$  **P13**,  $\text{Ag}$  **P14**,  $\text{Au}$  **P15**) recorded at  $25^\circ\text{C}$  in  $\text{MeCN-d}_3$ .

It is noted, that reaction of **P3** with two equivalents of  $\text{AgOTf}$  results in selective conversion, forming a similar complex to **P14** with slight shifts in  $^1\text{H}$  and  $^{29}\text{Si}$  NMR ( $\delta = 21.1$  ppm;  $^1\text{J}_{\text{Si}^{109}\text{Ag}} = 674.6$  Hz,  $^1\text{J}_{\text{Si}^{107}\text{Ag}} = 583.7$  Hz) and even higher Si–Ag coupling. However, preliminary SC-XRD results indicated the formation of a Si–Ag–MeCN motif, the full elucidation of which failed due to strong disorder and partial occupancies in the examined crystals. Reaction of either **P1** or **P3** with one equivalent of  $\text{AgOTf}$  resulted in unclear conversions.

To circumvent possible halogen driven side reaction,  $\text{PPh}_3\text{AuMe}$  was tested in a similar reaction setup than  $\text{Me}_2\text{SAuCl}$  (Scheme 43). Within 30 minutes the corresponding  $[\text{bis}^{\text{Et}}\text{-NHI}^{\text{Mes}}\text{ClSiAuMe}][\text{Cl}]$  complex **P16** formed readily with only minor amounts of residual starting material.



Scheme 43. Synthesis of  $[\text{bis}^{\text{Et}}\text{-NHI}^{\text{Mes}}\text{ClSiAuMe}][\text{Cl}]$  (**P16**) from **P1** and  $\text{PPh}_3\text{AuMe}$ . The reaction is carried out in acetonitrile as solvent at room temperature over 2 hours.

All bis-NHI signals were found within the expected regions in  $^1\text{H}$  NMR and an additional  $\text{AuCH}_3$  resonance appears highfield shifted at  $\delta(^1\text{H}) = -0.2$  ppm (Figure 44, big), verifying successful coordination of the AuMe synthon. The  $^{29}\text{Si}$  signal shifts to  $\delta(^{29}\text{Si}) = 76.2$  ppm, due to the altered methyl substituent (Figure 44, small). While the 17 ppm downfield shifting from **P1** to **P15** appears rather moderate, this shift is more significant ( $\Delta\delta(^{29}\text{Si}) = 75$  ppm). The higher Lewis acidity of the AuMe synthon in conjunction with the lower chlorine load, renders **P16** another promising candidate for follow up reduction chemistry.

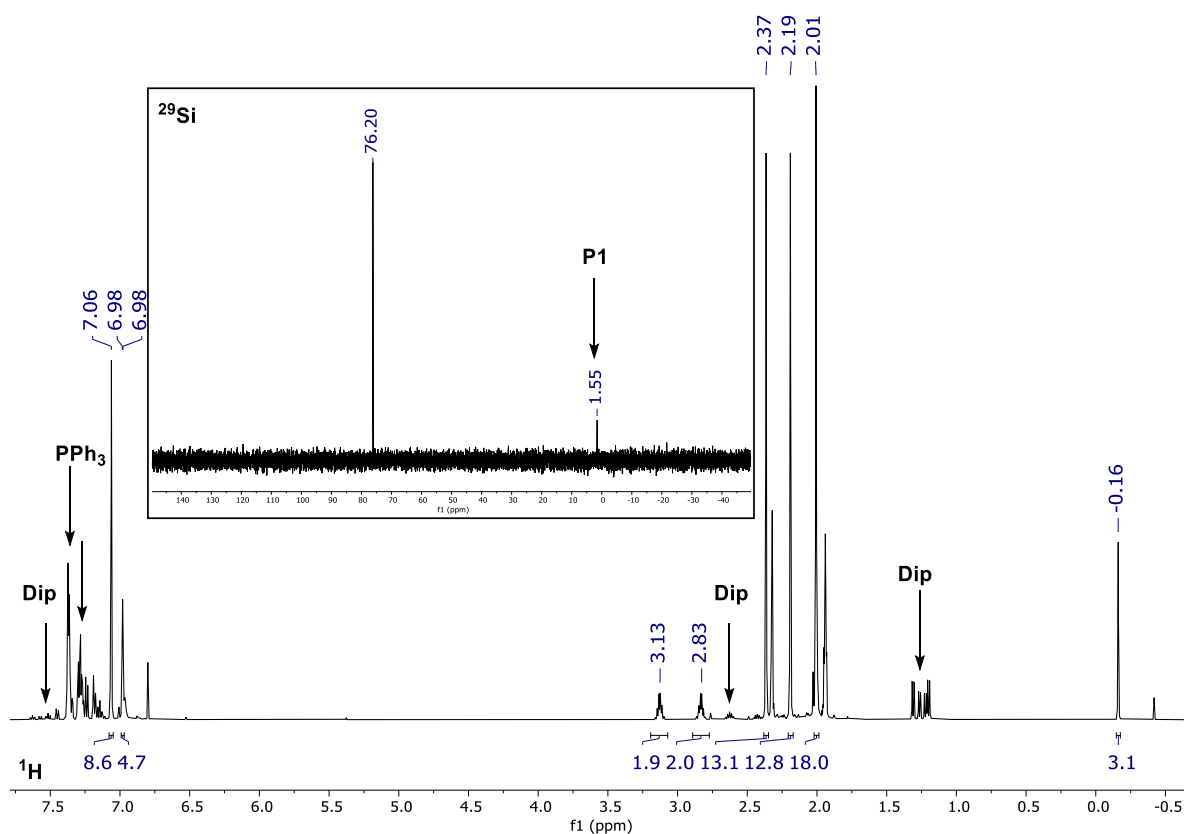


Figure 44.  $^1\text{H}$ -NMR (big) and  $^{29}\text{Si}$ -NMR (small) spectrum of  $[\text{bis}^{\text{Et}}\text{-NHIMe}_s\text{SiClAuMe}][\text{Cl}]$  (**P16**) recorded at 25°C in  $\text{MeCN-d}_3$ . Small amounts of unreacted starting material **P1** and impurities of  $\text{NHC}^{\text{Dip}}\cdot\text{HCl}$  and  $\text{PPh}_3$  marked. Toluene remaining from synthesis is contained.

4.4.5 Heterobimetallic Silyliumylidene complex bis<sup>Et</sup>-NHI<sup>Mes</sup>CiSiAuFe(CO)<sub>4</sub> (**P17**)

This chapter has been published in part within ref<sup>[128]</sup>, with collaborating scientists:  
DFT: Prof. Dr. D. Munz | Mößbauer spectroscopy: Prof. Dr. K. Meyer, Dr. J. Sutter

Heterobimetallic complexes arguably represent monomeric subunits of alloy clusters that could help us to understand the fundamental reaction mechanisms in cooperativity driven reactions. Such reactions occur e.g. in catalytic conversions using gold-iron mixed metal clusters and nanoparticles. Whereas gold and iron already show catalytic activity, the alloy clusters have attracted attention for their application in electrocatalytic oxygen evolution reactions (OER), for example.<sup>[140]</sup> The cooperativity between two well-defined reactive sites is believed to endeavor these additional reactivity, still heterobimetallic complexes such as **97-101** or defined small clusters are rare, especially for the metallophilic Au-Fe unit (Chart 3).<sup>[141]</sup> These metals engage in strong interactions leading to favorable aggregation and cluster growth.

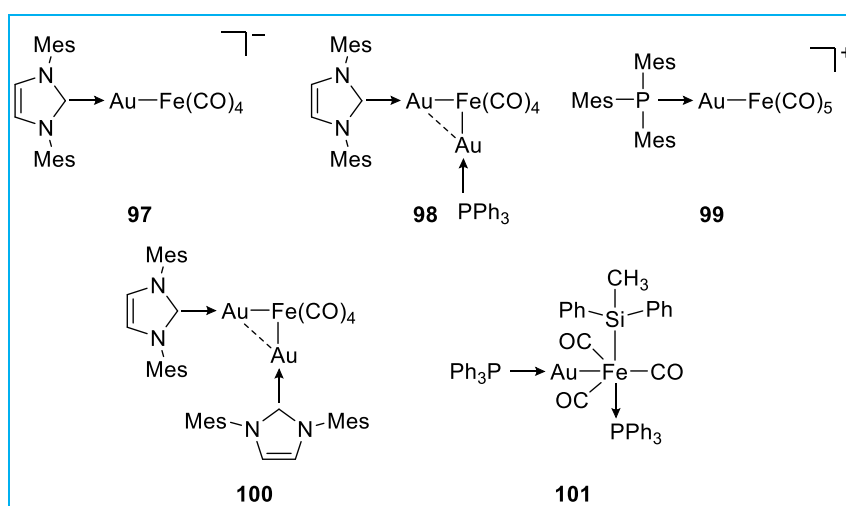
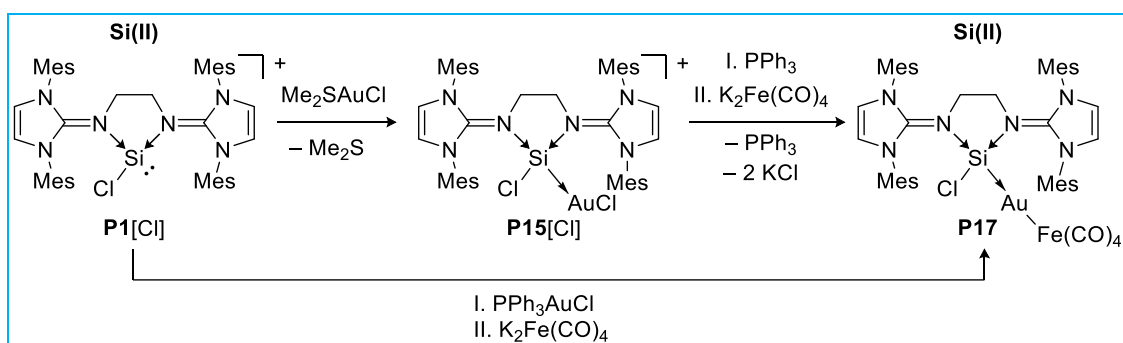


Chart 3. Selected examples for ligand stabilized monomeric (**97**, **99**, **101**) and dimeric (**98**, **100**) heterobimetallic Au-Fe complexes.

To assess the silyliumylidene's ability to serve as stabilizing ligand for the Au-Fe unit, halogen abstraction reactions using  $K_2Fe(CO)_4$  were pursued. For the bigger picture the lighter congener complexes were examined as well for their reactivity towards heterobimetallic Si-M-Fe complexes (M = Cu, Ag, Au). However, reaction with **P13** showed no conversion even after 16 hours at 60 °C, after which formation of a copper mirror indicated decomposition of the starting complex **P13** into an ill-defined mixture detected *via* NMR inspection. **P14** in contrast, reacted readily at room temperature under regeneration of **P1** as evidenced in <sup>1</sup>H and <sup>29</sup>Si NMR analysis. The formation of Ag-Fe(CO)<sub>4</sub> containing small clusters is a conceivable explanation, but was not evidenced in this case.



Scheme 44. Synthesis of bis<sup>Et</sup>-NHI<sup>Mes</sup>CiSiAuFe(CO)<sub>4</sub> (**P17**) from **P1** in one-pot procedure (bottom reaction way) or intermediate isolation of **P15** using  $\text{K}_2\text{Fe}(\text{CO})_4$ . The reaction is carried out in acetonitrile as solvent at  $-30^\circ\text{C}$  to room temperature.

When **P15** was mixed with  $\text{K}_2\text{Fe}(\text{CO})_4$  at low temperature, a mixture of various products was formed that could neither be isolated nor identified. We hypothesized that the addition of an auxiliary donor molecule might stabilize the unsupported vacant coordination site after chloride abstraction. Indeed, admixture of  $\text{PPh}_3$  to **P15** before addition of  $\text{K}_2\text{Fe}(\text{CO})_4$  resulted in the formation of bis<sup>Et</sup>-NHI<sup>Mes</sup>CiSiAuFe(CO)<sub>4</sub> (**P17**), that was isolated as bright yellow crystals (Scheme 44, upper reaction pathway). Interestingly, using deviant donors, such as  $\text{Ime}_4$ ,  $\text{SMe}_2$ , DMAP, or pyridine did not provide access to compound **P17**. Notably, **P17** is also accessible through one-pot reaction of **P1** with the metal precursor  $\text{PPh}_3\text{AuCl}$  and subsequent addition of  $\text{K}_2\text{Fe}(\text{CO})_4$  (Scheme 44, bottom reaction pathway) in higher purity and 54% yield.

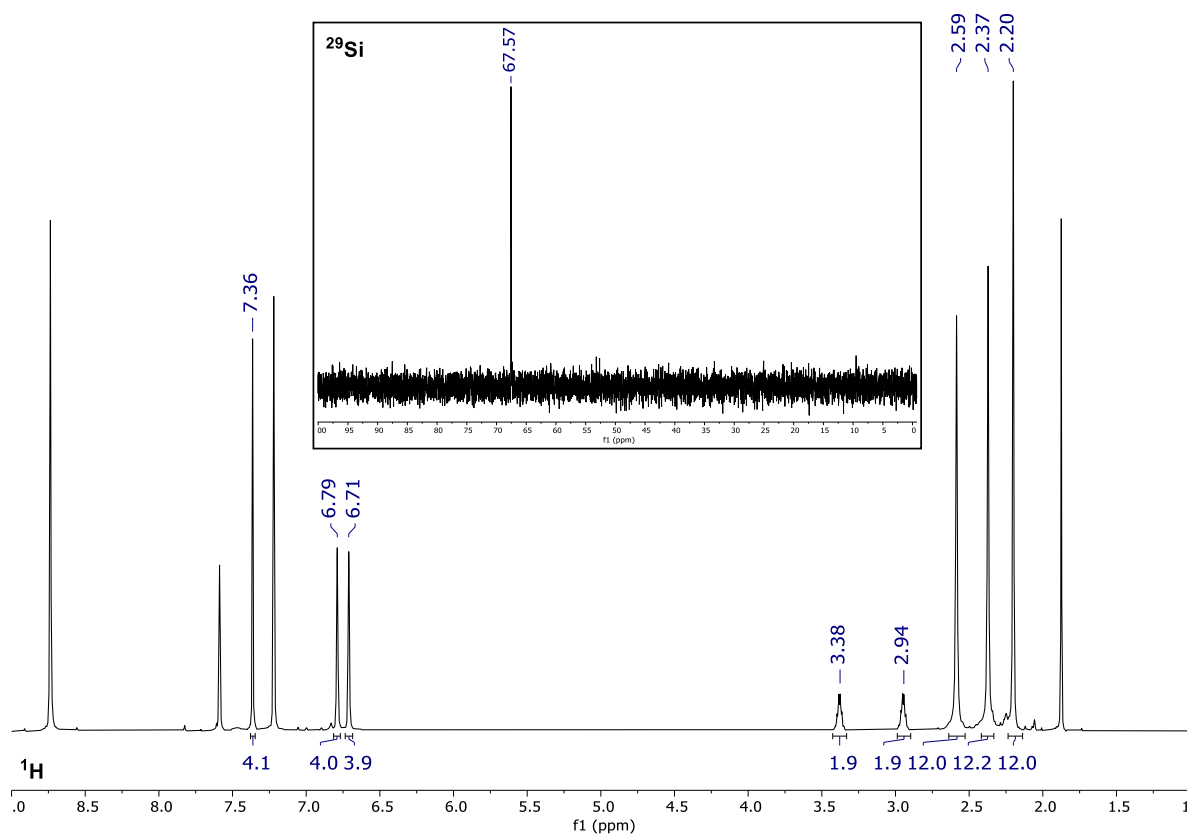


Figure 45.  $^1\text{H}$ -NMR (big) and  $^{29}\text{Si}$ -NMR (small) spectrum of bis<sup>Et</sup>-NHI<sup>Mes</sup>CiSiAuFe(CO)<sub>4</sub> (**P17**) recorded at  $25^\circ\text{C}$  in pyridine- $d_5$ . Remaining acetonitrile from synthesis is contained.

Overall neutral **P17** is insoluble in benzene, fluorobenzene and THF, sparingly soluble in acetonitrile and dissolves readily in pyridine. It is stable in pyridine solution up to 80 °C according to <sup>1</sup>H NMR monitoring (Figure 45 and Figure 46). After 48 hours at 80°C, decomposition sets in with slow discoloring of the yellow solution to brown. The <sup>29</sup>Si NMR spectrum displays a single resonance at  $\delta(^{29}\text{Si}) = 67.6$  ppm (Figure 45, small). This is further downfield shifted compared to starting material **P1** ( $\delta(^{29}\text{Si}) = 1.24$  ppm) and precursor compound **P15** ( $\delta(^{29}\text{Si}) = 18.2$  ppm). A single signal at  $\delta(^{13}\text{C}) = 229.0$  ppm in carbon NMR (Figure S 26) represents the coordinated Fe(CO)<sub>4</sub> moiety.

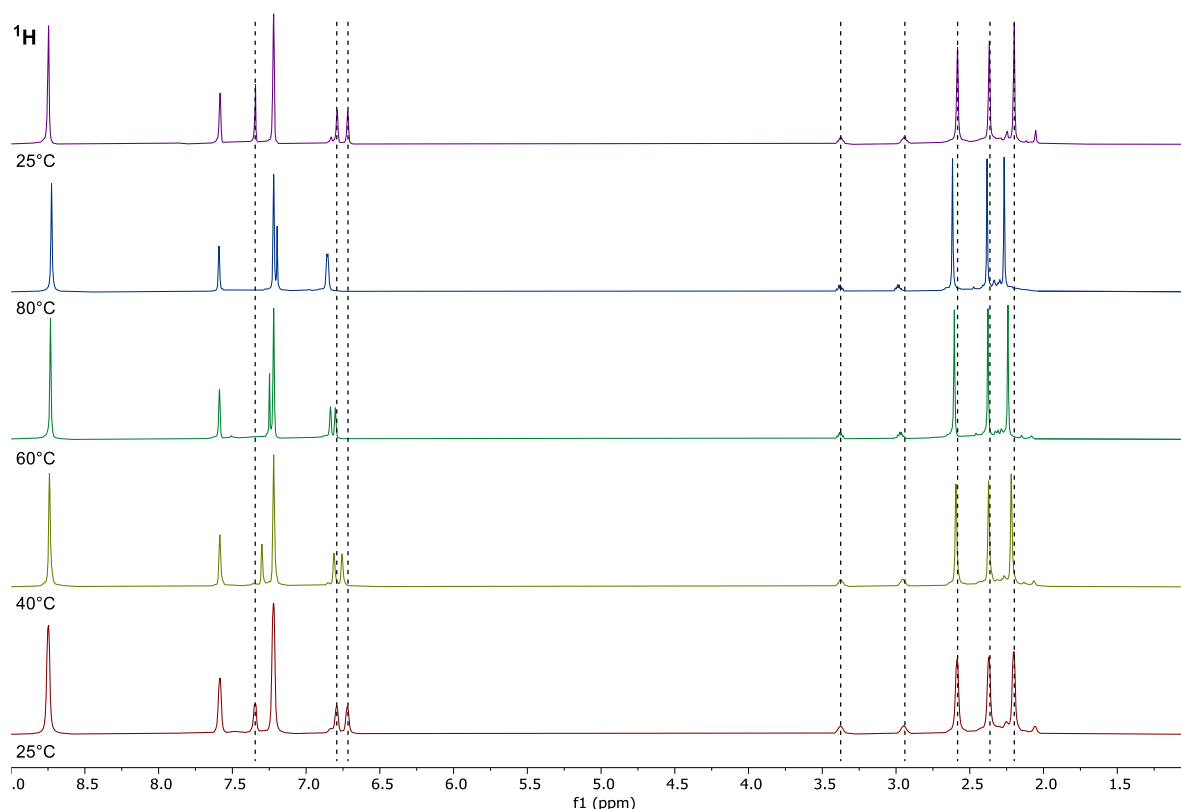


Figure 46. Stacked <sup>1</sup>H-VT-NMR spectra of bisEt-NHIMe<sup>s</sup>ClSiAuFe(CO)<sub>4</sub> (**P17**) recorded at 25°C→80°C→25°C in pyridine-d<sub>5</sub>.

SC-XRD analysis confirmed the heterobimetallic structure of **P17**. The silicon atom remains in a distorted tetrahedral coordination environment with the N–Si–N angle being strained to 87.80(13)° as shown in Figure 47. As common for Au(I) complexes the gold atom is nearly linear coordinated with a Si–Au–Fe angle of 173.65(3)°. The Si–Au bond length (2.2676(9) Å) is comparable short for a Si(II) gold complex, which range from 2.246 – 2.363 Å. The Au–Fe distance of 2.5305(6) Å matches related compound **97** (2.5168 Å) and is in good agreement with the range of Fe–Au single bond lengths in small molecular gold-iron cluster (**97-101**: 2.516 – 2.567 Å). Moreover, comparatively short C–H⋯Au distances can be detected for the mesityl's *ortho*-methyl groups pointing towards the gold atom, indicating rare anagostic

interactions. The shortest contact is detected for CH42...Au with 2.70(3) Å, while two more are slightly elongated (CH17...Au 2.87(6), CH33...Au 2.97(5) Å) but still shorter than  $\Sigma\text{vdW}(\text{H,Au}) = 3.3 \text{ \AA}$ .<sup>[142]</sup> Also computationally, an anagostic interaction is found between the gold ion and a methyl group of the mesityl ligand (BP: 2.361 Å; PBE0: 2.445 Å; Figure 49).

Although agostic interactions of Au(III) complexes have been recently evidenced, C–H...Au interactions remain extremely rare.<sup>[143]</sup> In contrast to agostic interactions, the weaker anagostic interactions are formed *via* the filled *d*-orbitals of transition metals and C–H bonds.<sup>[144]</sup> Therefore, M(I) (M = Cu, Ag, Au) complexes, that exclusively feature filled *d*-orbitals, are candidates to observe those contacts. Thus, the concept of anagostic C–H...Au interactions is a topic of current interest.

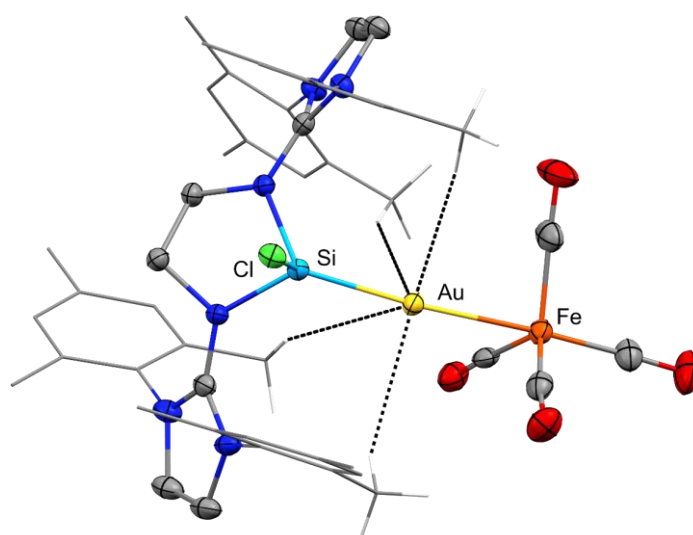


Figure 47. Solid-state plot of the molecular structure of bis<sup>Et</sup>-NHIM<sup>es</sup>ClSiAuFe(CO)<sub>4</sub> (**P17**). Ellipsoids are set to the 50% probability level. Hydrogen atoms and solvent molecules are omitted for clarity; mesityl-substituents are depicted as wireframe for simplicity. Selected bond lengths [Å] and angles [°]: Au1–Si1 2.2676(9), Au1–Fe1 2.5305(6), Si1–N5 1.793(3), Si1–N6 1.819(2), Si1–Cl1 2.1076(11), C1–N5 1.352(5), C4–N6 1.355(4), CH42...Au1 2.70(3), CH17...Au1 2.87(6), CH33...Au1 2.97(5), CH26...Au1 3.58(4), Si1–Au1–Fe1 173.65(3), Cl1–Si1–Au1 119.02(5), N5–Si1–N6 87.80(13).

Infrared (IR) spectroscopic measurements reveal the carbonyl stretching frequencies of **P17** to occur at 1924, 1835, 1811, and 1796 cm<sup>-1</sup> (Table 1). The position of these bands, which is reproduced by calculations at the ZORA-BP86-D3/def2-SVP level of theory, is indicative for the donor properties, *i.e.* combined  $\sigma$ -donor/ $\pi$ -acceptor abilities of the ‘ligand’ **P15**, which coordinates anionic Fe(CO)<sub>4</sub> in **P17**. These bands are bathochromically shifted in case of zwitterionic **P17** compared to related compounds such as **97**, **82**, IMes–Fe(CO)<sub>4</sub>, Na<sub>2</sub>Fe(CO)<sub>4</sub>.

Table 1. Experimental (AT-IR) and computed (ZORA-BP86-D3BJ/def2-SVP) CO stretching frequencies of **P17** and relevant (gold-)iron carbonyl compounds. [a] solid state, neat AT-IR [b] solid state, neat nujol-IR.

Compound	Experimental	Calculated
<b>P17</b> <sup>[a]</sup>	1924, 1835, 1811, 1796	1954, 1872, 1833, 1825
<b>97</b> <sup>[b]</sup>	1975, 1927, 1830, 1790	1926, 1866, 1843, 1818
<b>82</b> <sup>[a]</sup>	2021, 1943, 1903, 1887	2027, 1958, 1915, 1895
IMes-Fe(CO) <sub>4</sub> <sup>[b]</sup>	2035, 1949, 1915	2022, 1959, 1934, 1920
Na <sub>2</sub> Fe(CO) <sub>4</sub> <sup>[a]</sup>	1762	1787

Prompted by its unexpected polar solubility properties and CO stretching IR bands, we aimed for further understanding of the bonding situation of **P17**. Whereas structural data is consistent with gold in the formal oxidation state of +I, the iron center presents itself comparatively electron-rich. Zero-field <sup>57</sup>Fe Mößbauer spectroscopy was performed in order to assess the complex's electronic structure (Figure 48). For comparison, the starting material K<sub>2</sub>Fe(CO)<sub>4</sub>, which is commonly assigned a formal oxidation state of -II, was analyzed as well.

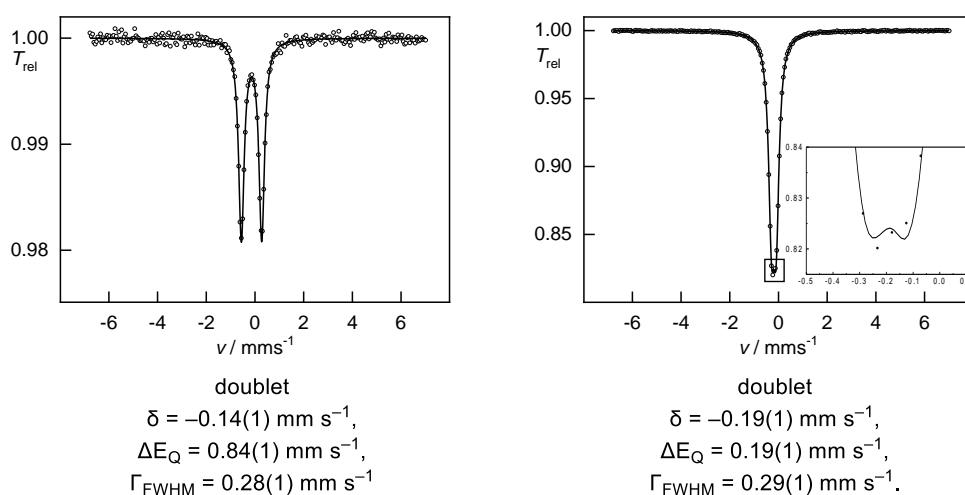


Figure 48. Zero-field <sup>57</sup>Fe Mößbauer spectrum of a solid sample of bis<sup>Et</sup>-NHI<sup>Mes</sup>ClSiAuFe(CO)<sub>4</sub> (**P17**, left) and K<sub>2</sub>Fe(CO)<sub>4</sub> (right) at 77 K.

Electronic structure analysis of **P17** revealed the formal dative interaction between the silicon's  $\sigma$ -type lone pair of electrons (Si: 0.70) and the gold atom (Au: 0.30) that further supports the compound to be well described as a silyliumylidene complex. IBO (Intrinsic Bond Orbitals) analysis give insights into the  $d$ -orbital populations of gold and iron (Figure 49), showing formally  $d^{10}$ -configured Au(+I). Furthermore, all  $d$ -orbitals of iron appear to be fully occupied, thus suggesting iron to be in the formal oxidation state of Fe(-II). The Fe  $d(z^2)$ -orbital engages in the Fe-Au bond, that features dative bond character with considerable covalency (contribution Fe: 0.58, Au: 0.26). Turing the spotlight from the direct Si-Au-Fe bonds, a

hyperconjugative interaction between the non-bonding Au  $d(z^2)$ -orbital that shows admixture of the 6s-orbital, and  $d(xz)$  and  $d(yz)$  in observed that donates  $\pi$ -electron density back towards the silyliumylidene ligand. Also Löwdin bond order of 1.56 indicates the described hyperconjugative interaction. As expected by the results of  $^{57}\text{Fe}$  Mössbauer spectroscopy, the irons  $d$ -orbitals ( $d(xy)$ ,  $d(xz)$ ,  $d(yz)$ ) are stripped from electron density by the four CO ligands (contribution Fe: 0.75). Both, the Hirshfeld as well as Löwdin (Figure S 3) population analysis indicate accumulation of negative partial charge at the iron atom, whereas the positive partial charge is delocalized across the silyliumylidene, the gold ion, and the NHI moieties. Over all, electronics suggest compound **P17** to be well described as zwitterionic bis-NHISi(II) $^+ \rightarrow \text{Au(I)}^+ \leftarrow \text{Fe(II)}^{2-}(\text{CO})_4$ , with considerably covalent Au–Si and, especially, Au–Fe bonds.

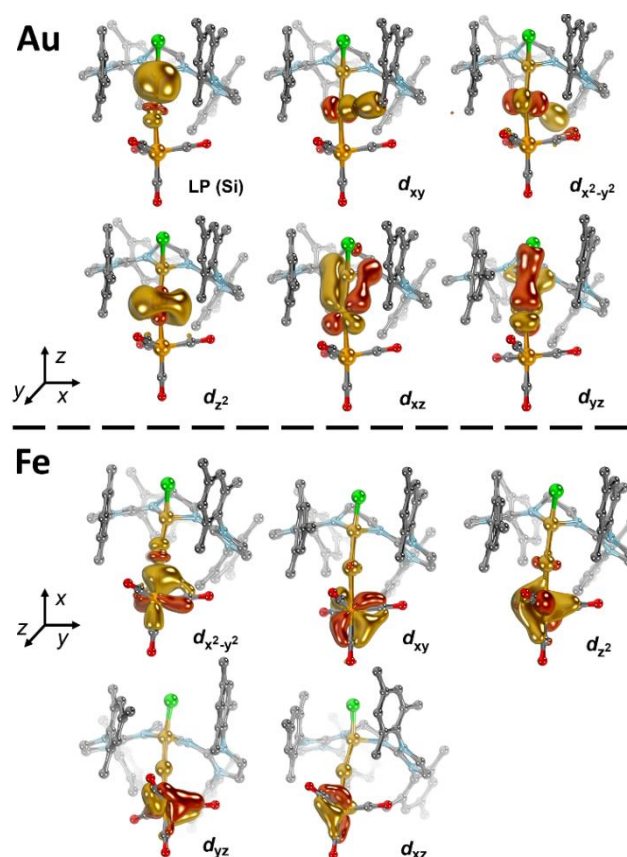


Figure 49. IBOs (PBE0-D3/def2-TZVPP//PBE0-D3BJ/def2-SVP) of bis<sup>Et</sup>-NHI<sup>Me</sup>SiAuFe(CO)<sub>4</sub> (**P17**) with strong valence  $d$ -orbital admixture.

#### 4.4.5.1 Reactivity of Heterobimetallic Silyliumylidene Complex

Being the first example of a silyliumylidene serving as ligand for a heterobimetallic Au–Fe fragment, its reactivity was tested to evaluate the complex' ability to show cooperative behavior of silicon, gold and iron, beyond others. Especially the rather strong charge separation of Si<sup>(+)</sup>–Au<sup>(+)</sup>–Fe<sup>(2-)</sup> was hypothesized to reveal unusual reactivities. In initial small molecule and bond activation reactions compound **P17** was treated with gaseous CO, CO<sub>2</sub>,

$\text{N}_2\text{O}$ ,  $\text{H}_2$ , ethylene ( $\text{C}_2\text{H}_4$ ), and phenylacetylene ( $\text{PhCCH}$ ), however, no reaction was detectable, to our surprise.

### Oxidative Addition

Upon further reflection of the heterobimetallic complex moiety, it is notable that the charge separation between the terminal  $\text{Fe}(\text{CO})_4^{2-}$  group and the linearly coordinated  $\text{Au}^+$  atom in combination with the relatively facile accessibility in **P17**, is promising to show  $\text{Au}(\text{I}) / \text{Au}(\text{III})$  catalytic activity. Gold complexes are well known to show diverse catalytic capability with cross coupling and functionalization of multiple bonds being two examples. Nowadays, homogeneous gold catalysis is mostly done using simple  $\text{Cl-Au}(\text{I})\text{-L}$  ( $\text{L}$  = ligand =  $\text{PPh}_3$ ,  $\text{SMe}_2$ , etc.) precatalysts.<sup>[145]</sup>

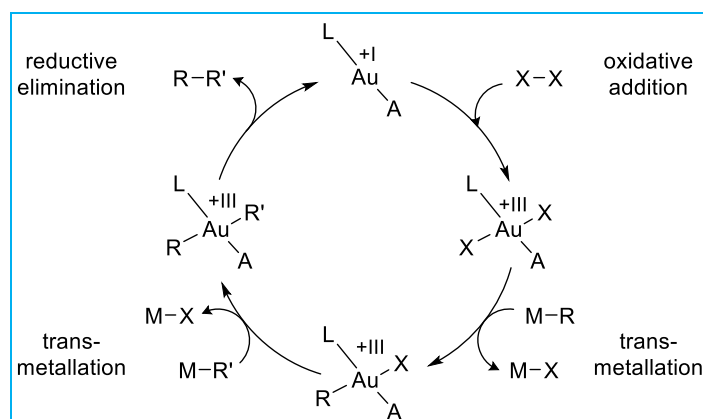
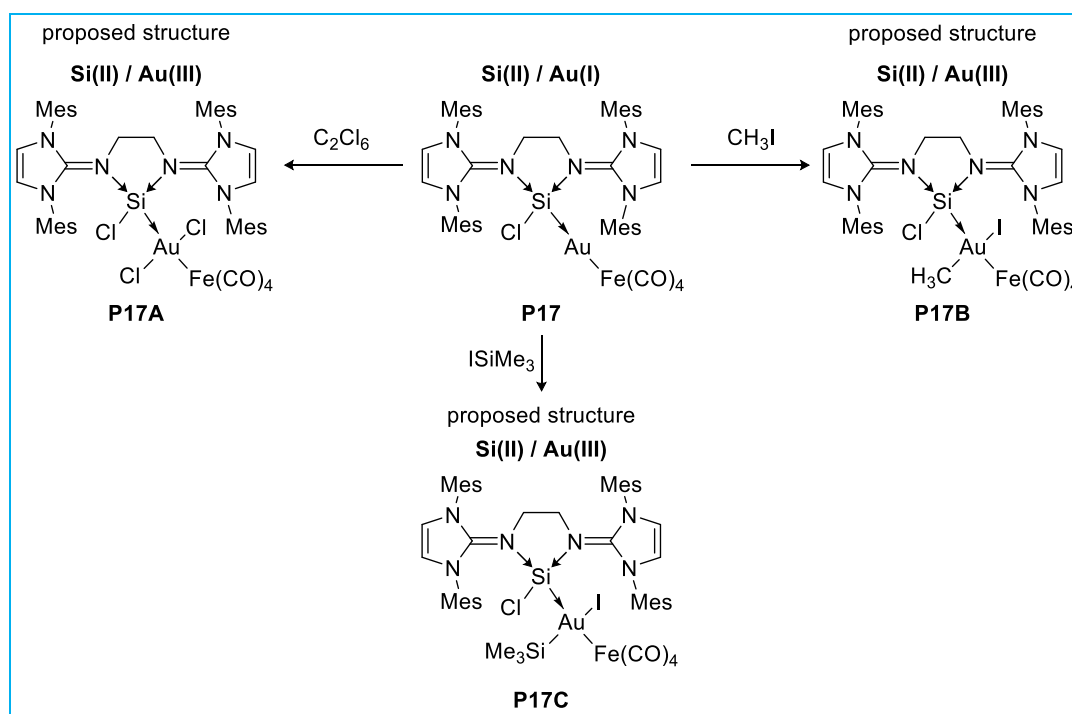


Chart 4. General depiction of an  $\text{Au}(\text{I})/\text{Au}(\text{III})$  redox catalytic cycle for C–C cross coupling reaction ( $\text{L}$  = ligand,  $\text{A}$  = anion,  $\text{X}$  = leaving group e.g. halogen,  $\text{M}$  = transmetalation reagent,  $\text{R}^{(\prime)}$  = organic alkyl-, aryl substituents).

The active species are considered to be free or only weakly coordinated  $\text{A}^- \text{L-Au}^+$  cations ( $\text{A}$  = weakly coordinating anion =  $\text{OTf}$ ,  $\text{SbF}_6^-$ , etc.), generated *via* chlorine exchange reactions (Chart 4). Considering the bonding situation in **P17**, catalytic pre-studies were performed to reveal its potential in the first key step, oxidative addition. Characteristic substrates with polarized C–X bonds, such as  $\text{CH}_3\text{I}$ ,  $\text{TMSI}$  and the strong chlorinating reagent  $\text{C}_2\text{Cl}_6$  were chosen.



Scheme 45. Attempted oxidative addition of C<sub>2</sub>Cl<sub>6</sub> (**P17A**), CH<sub>3</sub>I (**P17B**), and TMSI (**P17C**) on **P17**. The reactions were carried out in the NMR scale with each one equivalent of the reagent at room temperature in acetonitrile-d<sub>3</sub> as a solvent.

The reaction of **P17** with one equivalent of C<sub>2</sub>Cl<sub>6</sub> resulted in fast conversion, giving rise to two species obtained in <sup>1</sup>H and <sup>29</sup>Si NMR analysis (Scheme 45, left). The solid starting materials were mixed and treated with CD<sub>3</sub>CN at room temperature. Whereas compound **P17** is not soluble in acetonitrile, the reaction mixture dissolved completely after 30 minutes. Examination of the spectra reveals two full sets of the ligand's pattern in a roughly 1:2 ratio. 2D NMR experiment (<sup>1</sup>H<sup>29</sup>Si-HMBC) confirmed the main species to contain a silicon center resonating at δ(<sup>29</sup>Si) = 18.3 ppm (Figure 51). Comparison to the **P15** precursor complex shows only very slight differences in <sup>1</sup>H, <sup>13</sup>C, and <sup>29</sup>Si NMR shifts (Figure S 27), suggesting a similar structure. Thus, the Fe(CO)<sub>4</sub>-moiety is hypothesized to be cleaved from the complex resisting either as non-coordinating anion, or forming non-identified complex(es) with C<sub>2</sub>Cl<sub>6</sub> remains, such as (C<sub>2</sub>Cl<sub>4</sub>)Fe(CO)<sub>4</sub> olefin-, or dechlorination complexes.

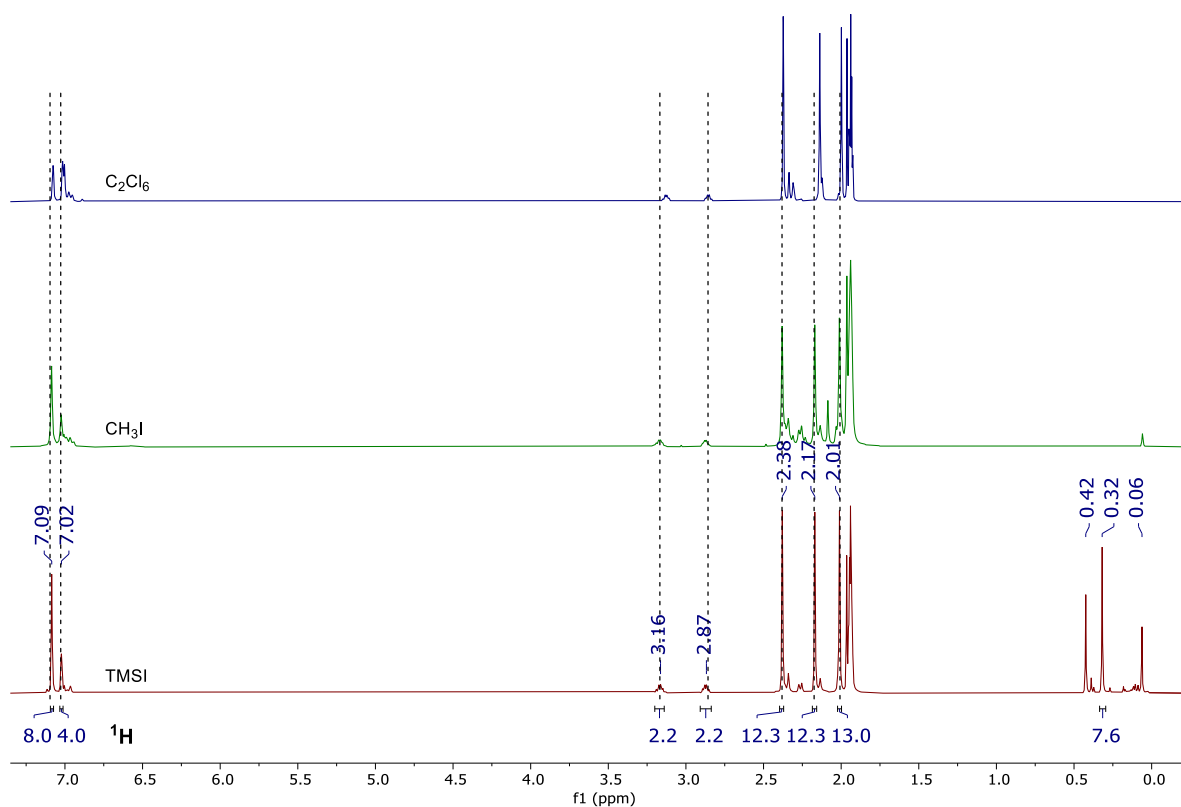


Figure 50. Stacked  $^1\text{H}$ -NMR spectra of  $\text{bis}^{\text{Et}}\text{-NHIMe}^{\text{SSi}}\text{ClSiAuFe}(\text{CO})_4 + \text{C}_2\text{Cl}_6$  (**P17A**, top) /  $\text{CH}_3\text{I}$  (**P17B**, middle) /  $\text{TMSI}$  (**P17C**, bottom) recorded at  $25^\circ\text{C}$  in  $\text{MeCN-d}_3$ . Spotted lines highlight the similar positions of the ligand's framework signals.

The minor species, however, shows a silicon signal at  $\delta(^{29}\text{Si}) = 45.0$  ppm (Figure 51, small), which is indicative for a more electron rich silicon center. The desired addition of  $\pi$ -donating chloride substituents could explain an upfield shift, as it is observed in this case. To avoid side-reactions that stem from over-chlorination, the reaction was repeated with trimethylsilyl iodide and methyl iodide.

Upon addition of one equivalent of  $\text{TMSI}$  or  $\text{CH}_3\text{I}$  to a suspension of **P17** in  $\text{CD}_3\text{CN}$  (Scheme 45, bottom and right), the solid dissolves into a dark yellow solution. After two hours no solid was left in the reaction mixture and multinuclear NMR analysis evidenced the formation of a single species similar to **P15** (Figure 50). After several hours the second species with a  $^{29}\text{Si}$  NMR shift of  $\delta = 45$  ppm grown in, suggesting the second species to originate from a consecutive reaction. Preliminary testing of transmetalation using  $\text{CH}_3\text{I}$  and  $\text{ZnPh}_2$  did not yield toluene as the desired cross-coupling product, but benzene that is believed to be formed from unselective protonation of diphenylzinc.

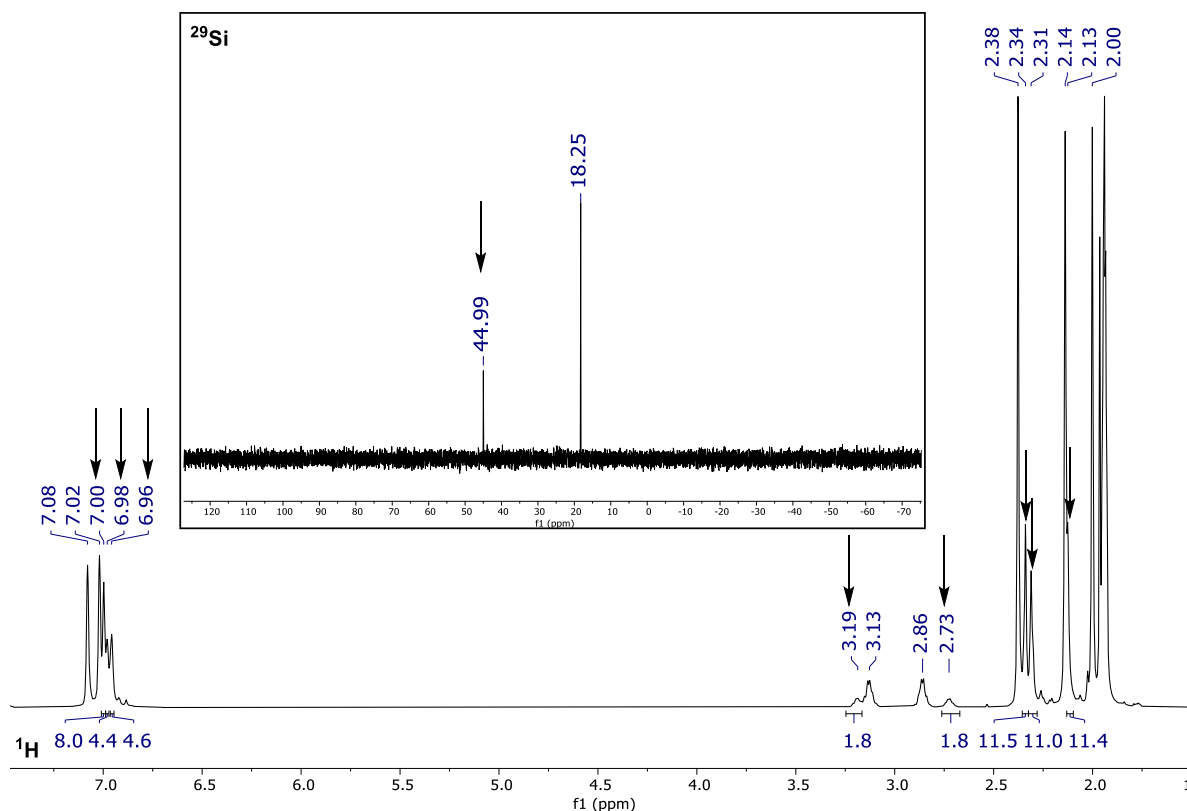


Figure 51.  $^1\text{H}$ -NMR (big) and  $^{29}\text{Si}$ -NMR (small) spectrum of **P17** after 5 hours of mixing with  $\text{C}_2\text{Cl}_6$  (**P17A**) recorded at  $25^\circ\text{C}$  in  $\text{MeCN-d}_3$ . Arrows mark the signals of a subsequently forming species in  $^1\text{H}$  and  $^{29}\text{Si}$  NMR.

## Functionalization

To address a further reactive site, complex **P17** was tested for functionalization at the remained coordinated chloride. Exchanging the chloride substituent to less electronegative and/or less  $\pi$ -donating nitrogen-, silicon- or aryl-based substituents should result in altered electronic environment at the Si–Au–Fe synthon that might lead to enhanced reactivity.

In an unexpected side reaction several single crystals revealed the general ability of nucleophilic chloride exchange. When **P17** was treated with a slight excess of  $\text{LiMo}(\text{CO})_2(\text{PMe}_3)\text{Cp}$  in  $\text{THF-d}_8$  no reaction was observed within 72 hours at  $60^\circ\text{C}$ . The reaction mixture was treated with several drops of pyridine and kept at  $60^\circ\text{C}$  for 16 more hours, to enhance solubility of starting material **P17**. Although no reaction was observed in NMR monitoring, a couple of single crystals could be collected from the reaction vessel, subsequently. Surprisingly, SC-XRD analysis revealed the formation of bipyridine-functionalized **P17** ( $[\text{bis}^{\text{Et}}\text{-NHI}^{\text{Mes}}\text{SiAuFe}]_2\text{-4,4'-bipyridine}$  / **P18**).

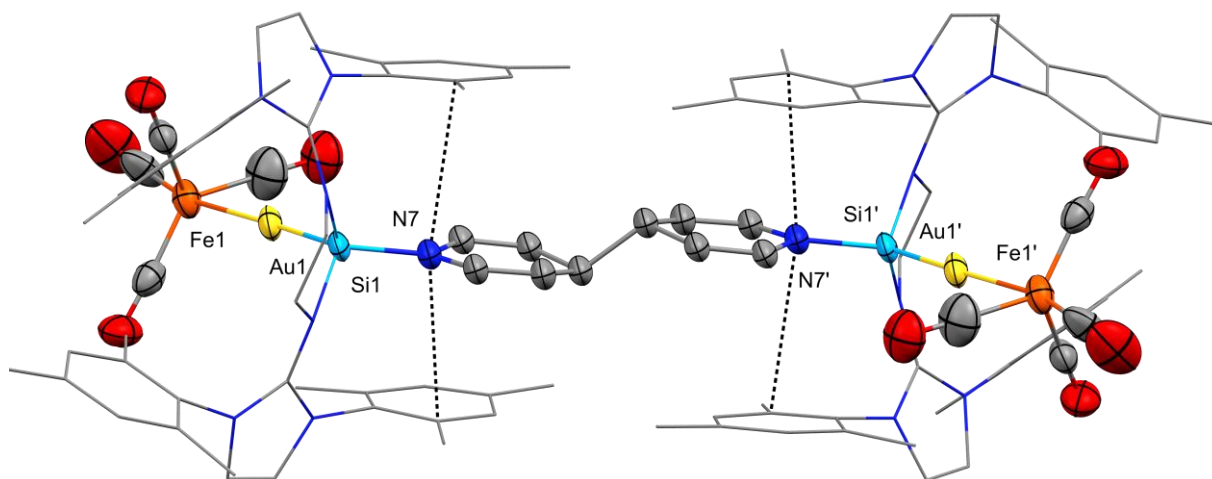
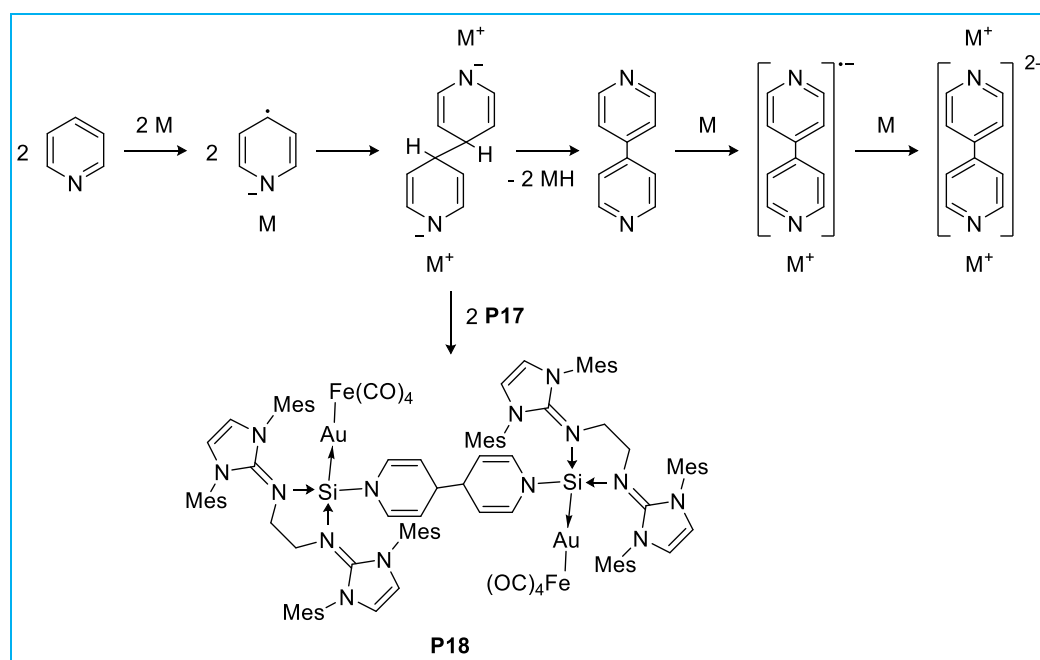


Figure 52. Solid-state plot of the molecular structure of  $[\text{bis}^{\text{Et}}\text{-NHI}^{\text{Mes}}\text{SiAuFe}(\text{CO})_4]_2\text{-4,4'-bipyr}$  (**P18**). Ellipsoids are set to the 50% probability level. Hydrogen atoms and solvent molecules are omitted for clarity; bis-NHIs are depicted as wireframe for simplicity. Selected bond lengths [ $\text{\AA}$ ] and angles [ $^\circ$ ]: Si1–Au1 2.273(2), Si1–N7 1.776(11), Si1–N5 1.826(7), Si1–N6 1.831(8), Au1–Fe1 2.5508(15), N5–C1 1.352(11), N6–C4 1.349(12), Si1–Au1–Fe1 176.45(7), N5–Si1–N6 87.7(4), N7–Si1–Au1 121.1(4).

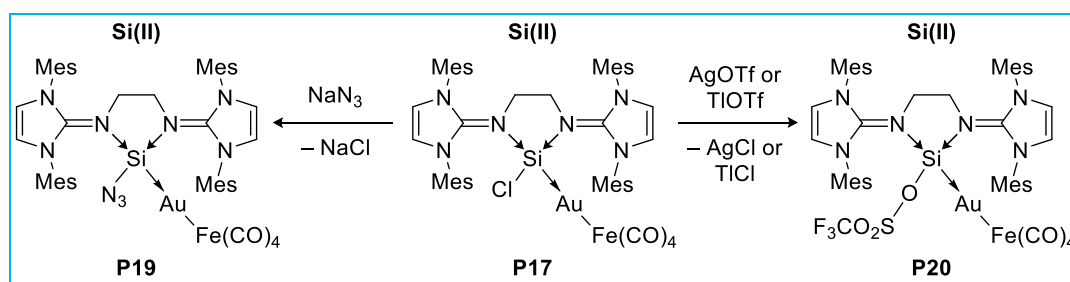
The solid state structure of **P18** shows the Si centers Si1 and Si1' in similar coordination environment to **P17** (Figure 52). However, the bis-NHI ligands are bended to establish  $\pi$ -ring stacking between each, two bis-NHI's mesityls and the pyridyl ring with Mes...pyr distance of 3.29 and 3.47  $\text{\AA}$ , respectively. The newly formed Si1–N7 bond (1.776(11)  $\text{\AA}$ ) is shorter than the bis-NHI ligand's coordinative N–Si–N bonds (1.826(7) / 1.831(8)  $\text{\AA}$ ), indicating a noticeably covalency as expected.



Scheme 46. Synthesis of  $[\text{bis}^{\text{Et}}\text{-NHI}^{\text{Mes}}\text{SiAuFe}(\text{CO})_4]_2\text{-4,4'-bipyr}$  (**P18**) from **P17** via unpredicted reduction of pyridine and trapping of dimerized radical anion. The reaction is carried out in THF- $d_8$  as solvent over 72 hours at 80 $^\circ\text{C}$ .

The reaction can be rationalized by a here unexpected reduction of pyridine molecules that is known to happen between alkali metals and pyridine since 1870.<sup>[146]</sup> Intriguingly, the reaction does not proceed completely but is trapped at the dimerized pyridine radical anion stage, which shows activity towards chlorine exchange (Scheme 46). In previous studies, this dimer was shown to be stable for seconds to minutes in pyridine solution, but was isolable from and persistent in THF suspensions. Despite of several attempts, aimed preparation of the 4,4'-bipyridyl radical anion dimer, to cleanly furnish **P18** remained unsuccessful.

Different reagents were utilized in order to cleanly introduce novel substituents. Whereas alkali salts of sterically demanding substituents such as  $\text{Si}^t\text{Bu}_2\text{Me}$ ,  $\text{N}(i\text{Pr})_2$ , and  $\text{CH}_2\text{Ph}$  presented themselves inert towards chlorine exchange with **P17**, the small pseudo halogen salt  $\text{NaN}_3$  (Scheme 47, left) and strongly chlorine abstracting agent  $\text{AgOTf}$  (as well as  $\text{TiOTf}$ ) showed selective reactivity with full conversions (Scheme 47, right).



Scheme 47. Synthesis of bis<sup>Et</sup>-NHIMe<sup>s</sup>XSiAuFe(CO)<sub>4</sub> (X = N<sub>3</sub> (**P19**, left), OTf (**P20**, right)) from **P17** via halogen exchange. The reaction is carried out in acetonitrile as solvent over 48 hours at -60°C ( $\text{NaN}_3$ , left), or over 2 hours at room temperature in pyridine ( $\text{AgOTf}$ , right).

Reaction of **P17** and 1.5 equivalents of  $\text{NaN}_3$  in acetonitrile results in a suspension that clears upon product formation. After 72 hours at 60°C a clear yellow solution indicates full conversion. Isolation of the product as a yellow powder and multinuclear NMR analysis proves the selective formation of a new  $\text{N}_3$  species (**P19**). In <sup>1</sup>H NMR the ligand's full pattern is displayed, suggesting preserved bidentate coordination of the bis-NHI ligand (Figure 53, big). One characteristic singlet at  $\delta(^{13}\text{C}) = 228.2$  ppm in carbon NMR denotes the presence of the iron carbonyl moiety (Figure S 28). It is of note, that no <sup>1</sup>H NMR highfield signal in the -8 ppm region was observed, which would indicate  $\text{HFe(CO)}_4$  anion formation. Exchange from Cl to N<sub>3</sub> results in a highfield shift in silicon NMR of ca. 20 ppm to a singlet signal at  $\delta(^{29}\text{Si}) = 46.6$  ppm (Figure 53, small). The less electronegative and strongly  $\pi$ -donating nitrogen substituent causes less effective shielding of the silicon nucleus that could consequently indicate a higher electron density. The formed complex is stable towards radiation and heating with no change in the NMR, nor gas formation, was detected after exposure to 24 hours at 60°C or radiation with 340 nm.

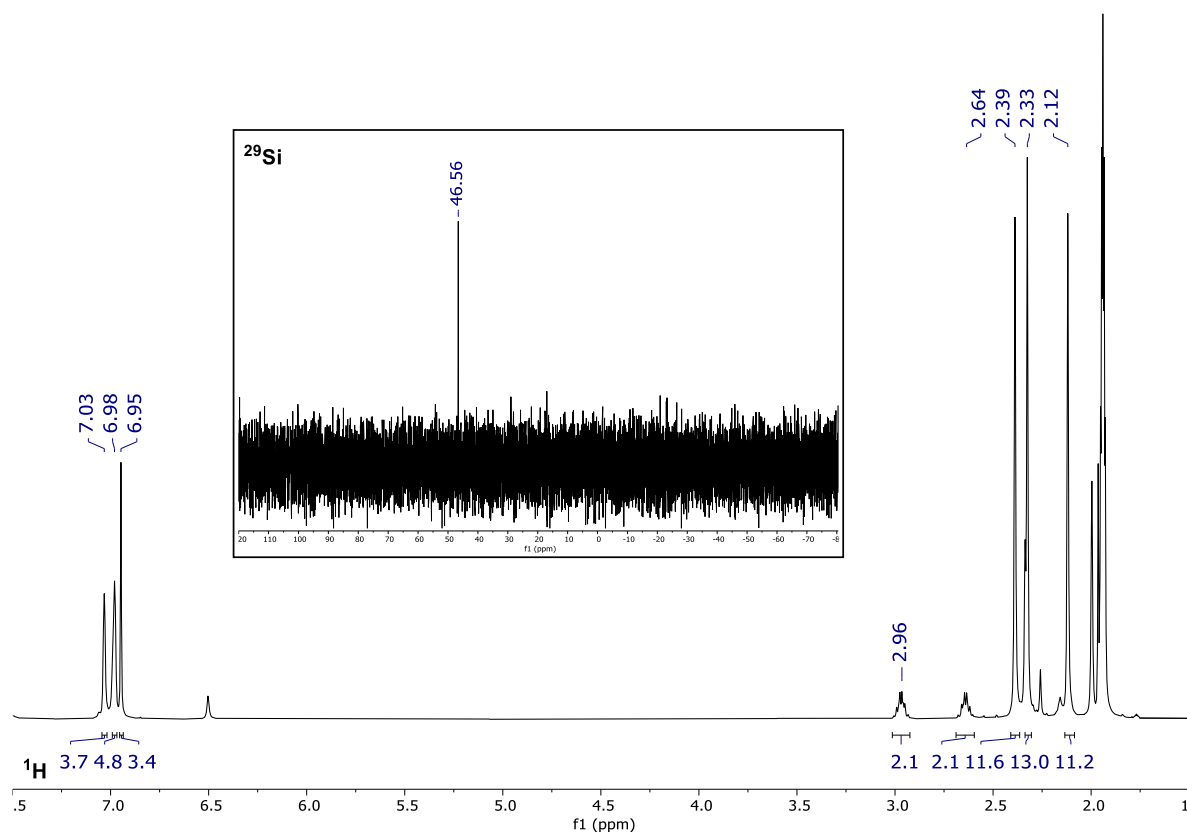


Figure 53.  $^1\text{H}$ -NMR (big) and  $^{29}\text{Si}$ -NMR (small) spectrum of  $\text{bis}^{\text{Et}}\text{-NHIMesN}_3\text{SiAuFe(CO)}_4$  (**P19**) recorded at 25°C in  $\text{MeCN-d}_3$ .

Further functionalization could be achieved by treating **P17** with equimolar amounts of  $\text{AgOTf}$  or  $\text{TiOTf}$ , respectively. By performing the reaction in pyridine- $\text{d}_5$  the reaction was monitored via  $^1\text{H}$  NMR. Within 6 hours full conversion to  $\text{bis}^{\text{Et}}\text{-NHIMesOTfSiAuFe(CO)}_4$  (**P20**) can be achieved at room temperature (Scheme 47, right). Alternatively the reagents can also be mixed in acetonitrile, however, the reaction time is elongated compared to the pyridine case. This is attributed to the superior solubility of **P17** in pyridine that results in faster conversion. It should also be noted, that the use of  $\text{AgOTf}$  accelerates the reaction, but it proceeds in a less clean fashion than with  $\text{TiOTf}$ , due to the light sensitivity of silver reagents.

Apart from a full bis-NHI ligand's pattern (Figure 54, big), the complex shows one singlet in the silicon NMR, and characteristic signals in the  $^{13}\text{C}$  NMR at  $\delta(^{13}\text{C}) = 221.5$  (CO) and 129.51 ( $\text{CF}_3$ ) ppm (Figure S 29) that further suggest the sustainment of the  $\text{Fe(CO)}_4$  synthon and the coordination of OTf. The silicon shift appears at  $\delta(^{29}\text{Si}) = 47.2$  ppm (Figure 54, small), which is almost identical to **P19** ( $\delta(^{29}\text{Si}) = 46.6$  ppm).

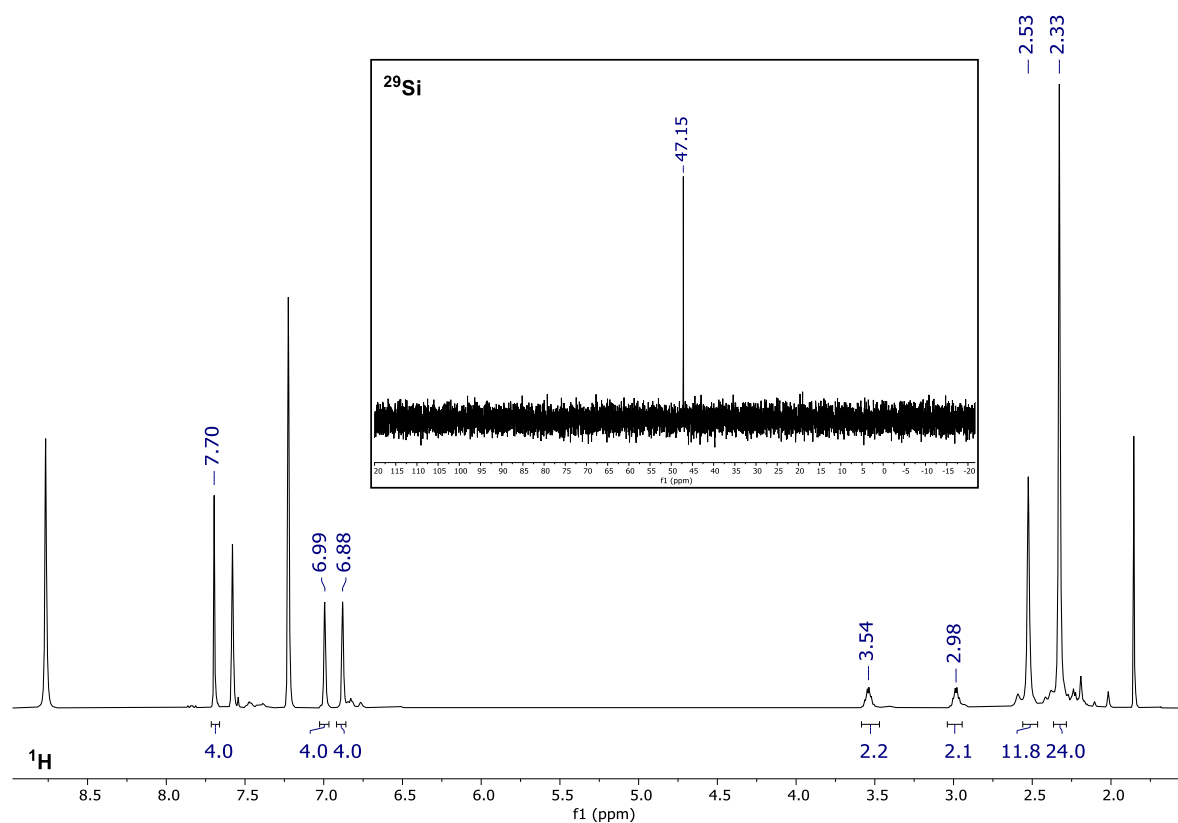


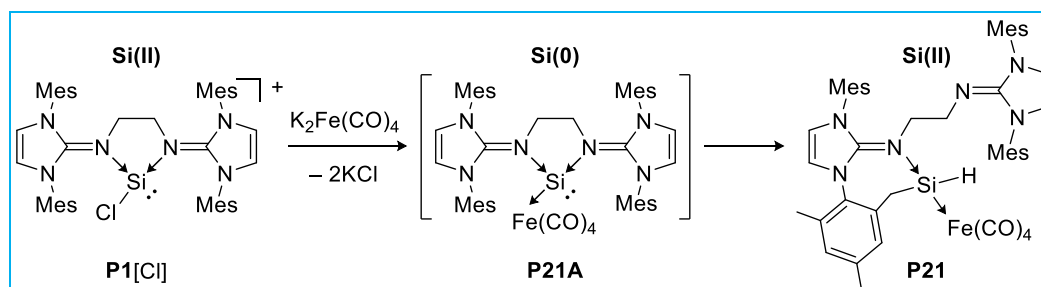
Figure 54.  $^1\text{H}$ -NMR (big) and  $^{29}\text{Si}$ -NMR (small) spectrum of  $\text{bis}^{\text{Et}}\text{-NH}^{\text{Mes}}\text{OTfSiAuFe}(\text{CO})_4$  (**P20**) recorded at 25°C in pyridine- $d_5$ . Acetonitrile remaining from synthesis is contained.

Thus the spectroscopic data are consistent and suggest that using OTf and  $\text{N}_3$  salts result in a similar fashion of halogen exchange to electronically similar complexes **P19** and **P20**. Unfortunately, both complexes decompose during mass spectrometric examination (ESI and LIFDI) to free ligand **P0**.

#### 4.4.6 Silylone metal complexes

Following the standard procedure for the reductive dehalogenation of Si(II) precursors, **P1** was reacted in different settings and reaction conditions with reductive agents, such as  $\text{KC}_8$ ,  $\text{NaC}_{10}\text{H}_8$ , and the milder  $[\text{NacnacMg}]_2$ . The reactions didn't yield free silylone  $\text{bis}^{\text{Et}}\text{-NH}^{\text{Mes}}\text{Si}(0)$  but ended in ill-defined mixtures. Within several attempts, the results varied between decomplexation into free ligand and unidentified precipitate, and ligand degradation resulting in free  $^{\text{Mes}}\text{NHC}$ , beyond others. As the ligand framework provides exceptional strong donor contributions, the missing formation of  $\text{bis}^{\text{Et}}\text{-NH}^{\text{Mes}}\text{Si}(0)$  could be attributed to a too electron rich silicon center. With that in mind, the strategy was changed. Lewis acidic  $\text{Fe}(\text{CO})_4$ -fragment, was introduced to achieve stabilization by reducing the electron density around the Si center without introducing  $\pi$ -acceptor ability to the ligand. The starting material **P1**,

therefore was reacted with one equivalent of the two-electron reducing agent  $\text{K}_2\text{Fe}(\text{CO})_4$  (Scheme 48). Interestingly, when carrying out the reaction in THF, benzene or acetonitrile even at low temperatures, only inseparable mixtures of up to six species were obtained. In contrast, reaction in dimethoxyethane (DME) gives a bright yellow mixture that fades within several minutes to uncover colorless crystals of **P21** in 50% isolated yield.



Scheme 48. Synthesis of bis<sup>Et</sup>-NHIMeHSiFe(CO)<sub>4</sub> (**P21**) from **P1** via intermediate iron silylone (**P21A**) formation. The reaction is carried out in dimethoxy ethane as solvent at  $-30^\circ\text{C}$  to room temperature.

It is supposed that first the iron silylone complex **P21A** forms, which is still exceptional electron-rich and is stabilized by release of one imino-nitrogen and insertion of the silicon into the C–H bond of one mesityl's *ortho*-methyl group (**P21**).

Intramolecular stabilization rearrangements are a known concept for low-valent silicon compounds, as seen for example in the case of the acyclic silylene **U**.<sup>[39]</sup> However the systems use different stabilization mechanisms: The corresponding acyclic silylene gets inserted into one Dip-C6 ring to form silepin **U**, from which it can be recovered by well-steerable temperature management. Intriguingly, in case of **P21** no silepin formation was observed. In total, ring insertions seem to be more likely with Dip-substituents, than they are with mesityl-substituents.

Upon C–H activation the molecule loses symmetry and displays additional sets of signals in proton NMR accordingly (Figure 55, big). The compound is poorly soluble in benzene- $d_6$  and well soluble in thf- $d_8$ , however, sufficient analytical spectra could be obtained in both solvents. Using Si–H 2D NMR methods in  $\text{C}_6\text{D}_6$  the Si–H can be identified as a singlet at  $\delta(^1\text{H}) = 6.53$  ppm with a Si–H coupling constant of 181 Hz (Figure 55, small). In  $^{29}\text{Si}$  NMR the four-coordinate Si was found at  $\delta(^{29}\text{Si}) = 68.2$  ppm. Donor-stabilized hydridosilylene iron complexes resonate in a broad range from  $\delta(^{29}\text{Si}) = -48.3$  ppm ( $^1J_{\text{SiH}} = 157$  Hz) to  $+105.2$  ppm ( $^1J_{\text{SiH}} = 180$  Hz).<sup>[125]</sup>

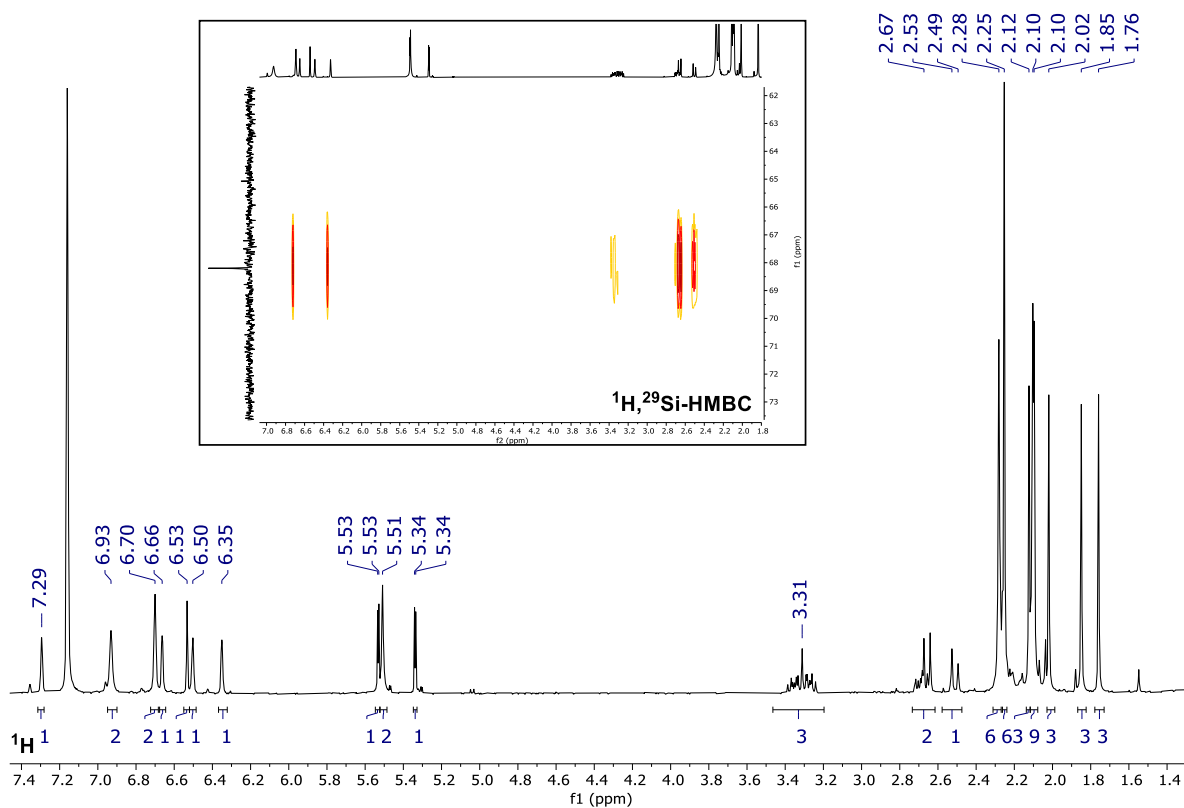


Figure 55.  $^1\text{H}$ -NMR (big) and  $^1\text{H}$ - $^{29}\text{Si}$ -HMBC-NMR (small) spectrum of  $\text{bis}^{\text{Et}}\text{-NHIMesSiHFe}(\text{CO})_4$  (**P21**) recorded at  $25^\circ\text{C}$  in benzene- $d_6$ .

Crystals for SC-XRD analysis formed upon cooling of a saturated DME solution of **P21** (Figure 56). An intramolecular CH-activation is evident with silicon insertion into one *ortho*-methyl group of a mesityl wingtip. The silicon Si1 is embedded within a newly formed 7-membered ring in boat conformation, whilst retaining a distorted tetrahedral coordination environment.

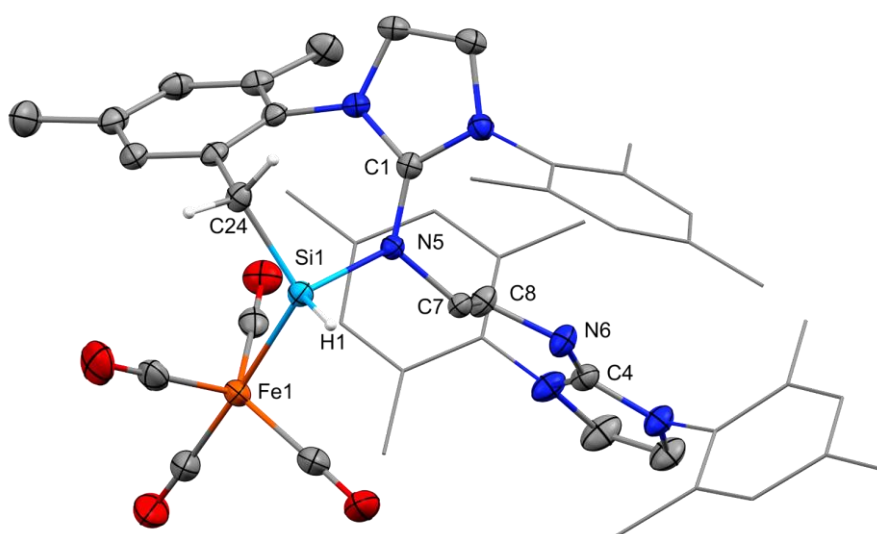
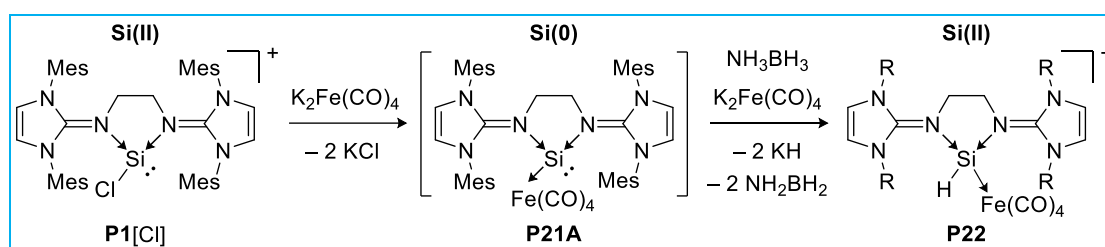


Figure 56. Solid-state plot of the molecular structure of  $\text{bis}^{\text{Et}}\text{-NHIMesSiHFe}(\text{CO})_4$  (**P21**). Ellipsoids are set to the 50% probability level. Hydrogen atoms (except for H1) and solvent molecules are omitted for clarity; mesityl-substituents are partly depicted as wireframe for simplicity. Selected bond lengths [Å] and angles [°]: Si1–Fe1 2.2881(6), Si1–H1 1.39(3), Si1–N5 1.8146(17), Si1–C24 1.907(2), N5–Si1–C24 100.20(8), C24–Si1–Fe1 117.92(7), Fe1–Si1–H1 112.5(10), H1–Si1–N5 101.8(10).

The former Si1–N6 bond is cleaved and the therefore free NHI-arm rotates by nearly 180° compared to the precursor **P1**. By inserting into the C–H bond, the Si1–H1 hydride bond is formed. H1 could be found within the difference Fourier maps and was allowed to refine freely. The Si1–H1 bond length amounts to 1.39(3) Å, which matches those of transition metal substituted triangular (IMe<sub>4</sub>)<sub>2</sub>Ni(Si(H)Si<sub>t</sub>Bu<sub>3</sub>)<sub>2</sub> (Si–H: 1.38 / 1.39 Å) almost perfectly. The Si1–Fe1 bond length of 2.2881(6) Å reflects an elongated single bond.

Since the intramolecular reaction of **P21A** occurs within a short time, it eluded isolation or spectroscopic observation despite multiple attempts. However, its presence could be evidenced *via* a trapping reaction using ammonia-borane complex NH<sub>3</sub>BH<sub>3</sub> as ready H<sub>2</sub> source (Scheme 49). Whereas H<sub>2</sub> itself, HSiEt<sub>3</sub>, HCCPh, and ethylene could not be activated before the intramolecular C–H activation occurred, reaction with NH<sub>3</sub>BH<sub>3</sub> yielded iron-silyliumylidene hydride complex **P22** in initially poor purity and yield. The reaction was repeated with adjusted stoichiometric ratio of 1:2:2 (1 : NH<sub>3</sub>BH<sub>3</sub> : K<sub>2</sub>Fe(CO)<sub>4</sub>), which lead to pure **P22** in good yield (67 %). It is worth noting that NH<sub>3</sub>BH<sub>3</sub> was tested for initial reactivity towards **P1** and K<sub>2</sub>Fe(CO)<sub>4</sub> without any detectable conversion. Upon addition of K<sub>2</sub>Fe(CO)<sub>4</sub> to a mixture of **P1** and NH<sub>3</sub>BH<sub>3</sub> in DME the mixture turned yellow for approximately 30 seconds indicating the formation of **P21A** and subsequently faded to a pale beige.



Scheme 49. Synthesis of [bis<sup>Et</sup>-NHIMe<sup>s</sup>HSiFe(CO)<sub>4</sub>][HFe(CO)<sub>4</sub>] (**P22**) from **P1** *via* trapping of the elusive iron silylone complex **P21A** using NH<sub>3</sub>BH<sub>3</sub> and additional K<sub>2</sub>Fe(CO)<sub>4</sub>. The reaction is carried out in dimethoxy ethane as solvent at –30°C to room temperature.

The now preserved symmetry of **P22** is demonstrated by the single set of ligand signals in <sup>1</sup>H-NMR, where Si–H could be found as a singlet at δ(<sup>1</sup>H) = 4.7 ppm (Figure 57, big). In addition, an upfield signal at δ = –8.95 ppm pinpoints the formation of an iron hydride species, that could be identified as HFe(CO)<sub>4</sub><sup>–</sup>. Two signals in the carbonyl range of <sup>13</sup>C-NMR at δ = 221.7 ppm for HFe(CO)<sub>4</sub><sup>–</sup> and δ = 216.9 ppm for silicon coordinated Fe(CO)<sub>4</sub> support the structure containing one coordinated iron carbonyl and one non-coordinated iron anion (Figure S 31). The central silicon nucleus resonates at δ(<sup>29</sup>Si) = 54.4 ppm (Figure 57, small left), which is upfield shifted compared to **P21**, probably caused by the second donating imino-nitrogen replacing the alkyl-CH<sub>2</sub> coordination leading to enhanced shielding of the silicon center in **P22**.

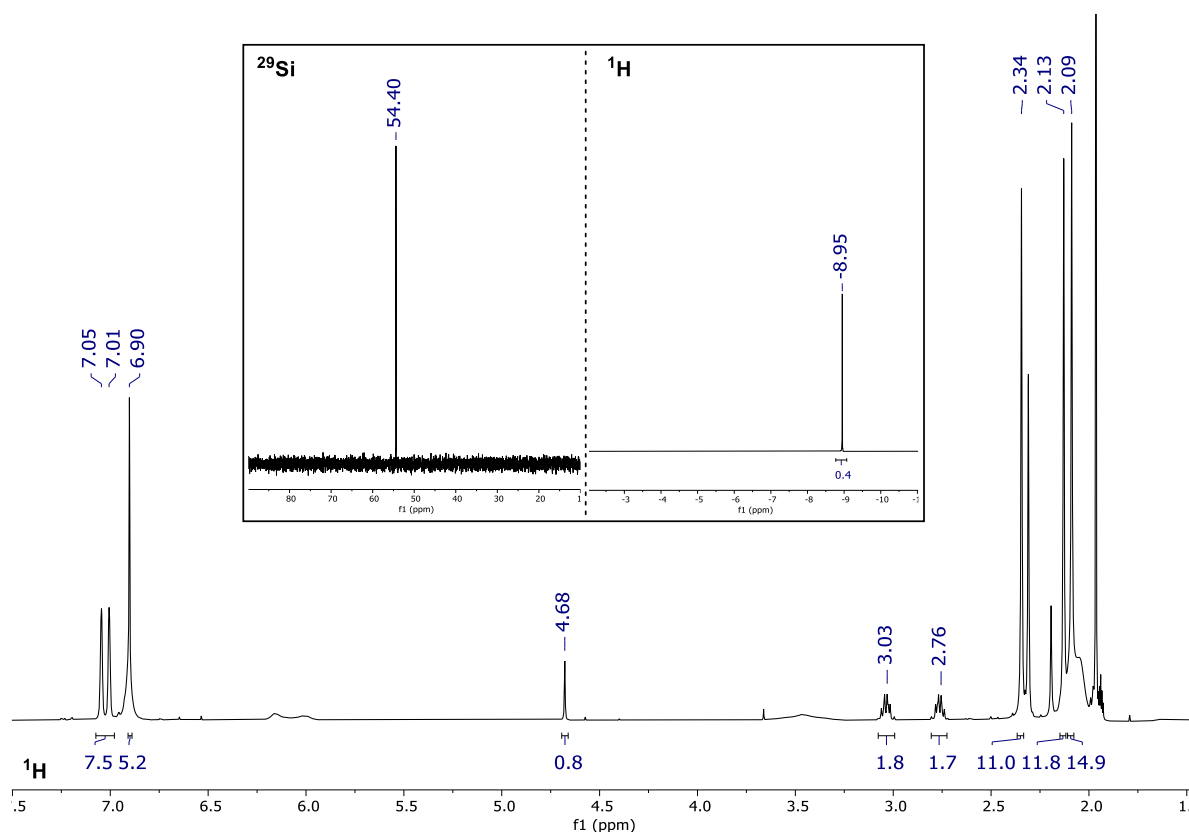


Figure 57.  $^1\text{H}$ -NMR (big and highfield region small right) and  $^{29}\text{Si}$ -NMR (small, left) spectrum of  $[\text{bis}^{\text{Et}}\text{-NHI}^{\text{Mes}}\text{SiHFe}(\text{CO})_4][\text{HFe}(\text{CO})_4]$  (**P22**) recorded at 25°C in acetonitrile- $d_3$ .

Crystals suitable for SC-XRD analysis were grown from a MeCN / THF solution (Figure 58). The bidentate coordination fashion of the bis-NHI ligand is substantiated also in the solid state structure with the N5–Si1–N6 angle being strained to 87.6°. The central silicon Si1 is further connected to H1 and Fe1, which features a trigonal bipyramidal coordination environment. H1 and H2 could be found in the difference Fourier maps and were allowed to refine freely. The Si1–H1 bond length (1.39(4) Å) is similar to that found in **P21**. The Si1–Fe1 distance of 2.2695(10) Å is within the range known for silylene iron complexes (2.154 to 2.363 Å). The shortest O···H distance within the asymmetric unit is found between the  $\text{HFe}(\text{CO})_4$  anion's carbonyl and the ligands backbone H at 2.680 Å.

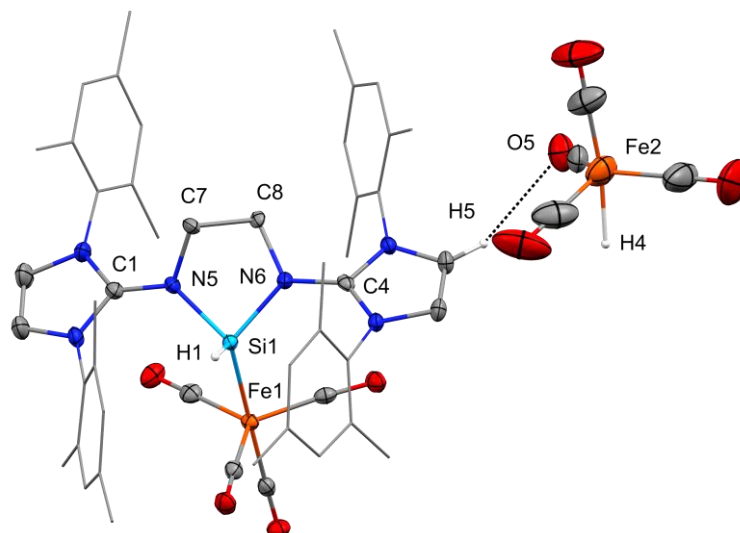
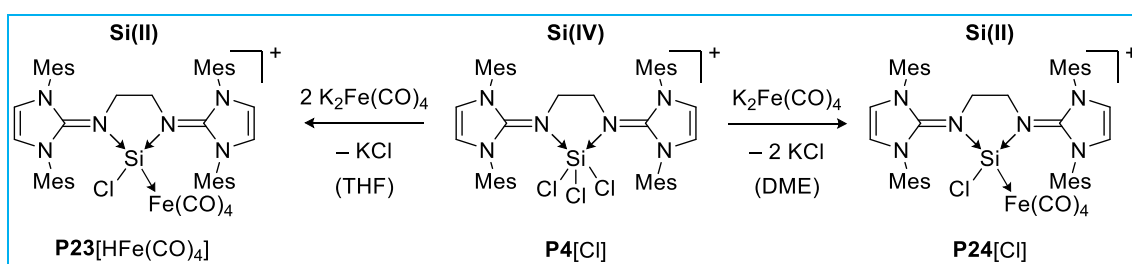


Figure 58. Solid-state plot of the molecular structure of [bis<sup>Et</sup>-NHIMesSiHFe(CO)<sub>4</sub>][HFe(CO)<sub>4</sub>] (**P22**). Ellipsoids are set to the 50% probability level. Hydrogen atoms (except for H1 and H4) and solvent molecules are omitted for clarity; mesityl-substituents are depicted as wireframe for simplicity. Selected bond lengths [Å] and angles [°]: Si1–H1 1.39(4), Si1–Fe1 2.2695(10), Si1–N5 1.833(3), Si1–N6 1.817(3), N5–C1 1.346(5), N6–C4 1.352(5), H5···O5 2.680, H1–Si1–Fe1 116.4(14), N5–Si1–N6 87.59(14).

4.5 Chemistry of bis<sup>Et</sup>-NHIMesSiCl<sub>4</sub> (**P4**)

Starting from the tetrachloro silane adduct bis-NHIMes-SiCl<sub>4</sub> **P4** coordination chemistry in conjunction with reduction chemistry was tested. Examination of the silyliumylidene showed no successful coordination of more than one transition metal synthon to the silicon center. The bigger coordination sphere at the higher coordinated silicon center, however, was hypothesized to vary the reactivity towards reductive transition metals *via* pre-orientation of the reactive cavity.

As mentioned, using silyliumylidene **P1** and neutral iron carbonyls such as Fe(CO)<sub>5</sub> and Fe<sub>2</sub>(CO)<sub>9</sub> no conversion to iron complexes could be observed. To obtain iron silyliumylidene (bis-NHIMesSiClFe(CO)<sub>4</sub><sup>+</sup>) and/or silylone (bis-NHIMesSi(Fe(CO)<sub>4</sub>)<sub>2</sub>) complexes, bis<sup>Et</sup>-NHIMesSiCl<sub>4</sub> (**P4**) was reacted with two equivalents of K<sub>2</sub>Fe(CO)<sub>4</sub> (Scheme 50, left). The mixed solid starting materials were cooled to -80°C and treated with pre-cooled THF. The suspension was allowed to warm to room temperature overnight and the product was extracted with benzene from the dried mixture. Using this procedure, compound [bis<sup>Et</sup>-NHIMesSiClFe(CO)<sub>4</sub>][HFe(CO)<sub>4</sub>] (**P23**) was isolated in 48% yield as a slight orange powder.



Scheme 50. Synthesis of [bis<sup>Et</sup>-NHIMesSiClFe(CO)<sub>4</sub>][X] (X = HFe(CO)<sub>4</sub> **P23**, Cl **P24**) from SiCl<sub>4</sub> complex **P4**. The reaction is carried out in either THF or DME resulting in complex **P23** and **P24**, respectively.

The compound features a high solubility in non-polar solvents, due to the HFe(CO)<sub>4</sub><sup>-</sup> anion, and is stable under inert conditions at room temperature. It is of note, that experiments using one equivalent of K<sub>2</sub>Fe(CO)<sub>4</sub> resulted in the same product **P23** in lower yield mixed with remaining starting material **P4**. Crystals, suitable for SC-XRD analysis, were grown from a THF / Et<sub>2</sub>O solvent diffusion setup (Figure 59).

The solid state structure reveals a distorted tetrahedral and therefore similar coordination environment of the silicon center compared to **P22** with the silicon atom Si1 being connected to the ligand's N5 and N6, the remaining chloride Cl1, and the Fe(CO)<sub>4</sub> synthon. All bond lengths are in similar regions compared to **P22** and four-coordinate **P24** and **P17**, respectively. Detection of the [bis<sup>Et</sup>-NHIMesSiClFe(CO)<sub>4</sub>]<sup>+</sup> cation in mass spectrometry (ESI) evidences the separated cation-anion-pair to be persistent also in solution.

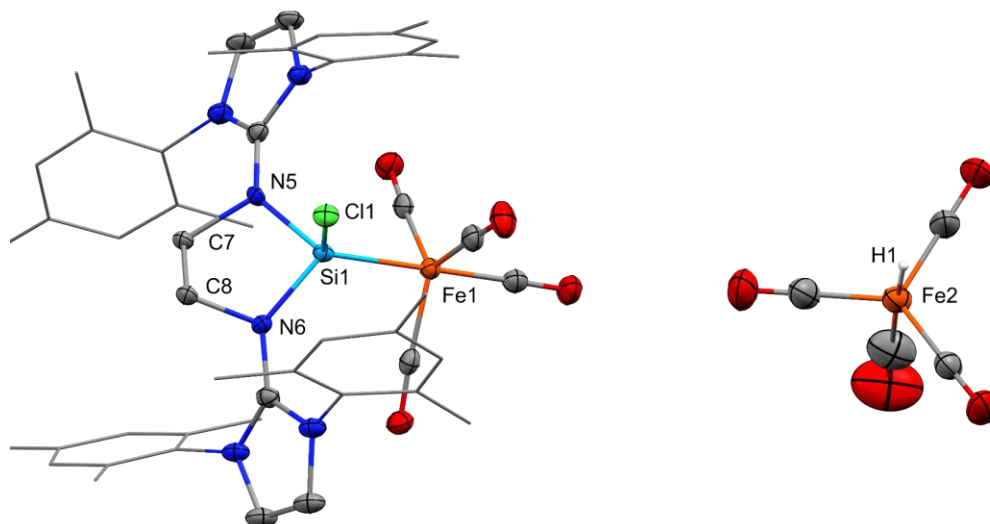


Figure 59. Solid-state plot of the molecular structure of  $[\text{bis}^{\text{Et}}\text{-NHIMesSiClFe}(\text{CO})_4][\text{HFe}(\text{CO})_4]$  (**P23**). Ellipsoids are set to the 50% probability level. Hydrogen atoms (except for H1) and solvent molecules are omitted for clarity; mesityl-substituents are depicted as wireframe for simplicity. Selected bond lengths [Å] and angles [°]: Si1–Fe1 2.2591(7), Si1–Cl1 2.0968(9), Si1–N5 1.77(3), Si1–N6 1.75(3), Cl1–Si1–Fe1 116.64(4), N5–Si1–N6 91.1(12), N5–Si1–Fe1 122.1(10).

Multinuclear NMR analysis in  $\text{D}_6\text{C}_6$  shows the bis-NHI ligand's pattern with the pseudo aromatic NHC-backbone signals comparably high-field shifted at  $\delta = 5.6$  ppm in  $^1\text{H}$  NMR experiment (Figure 60, big).

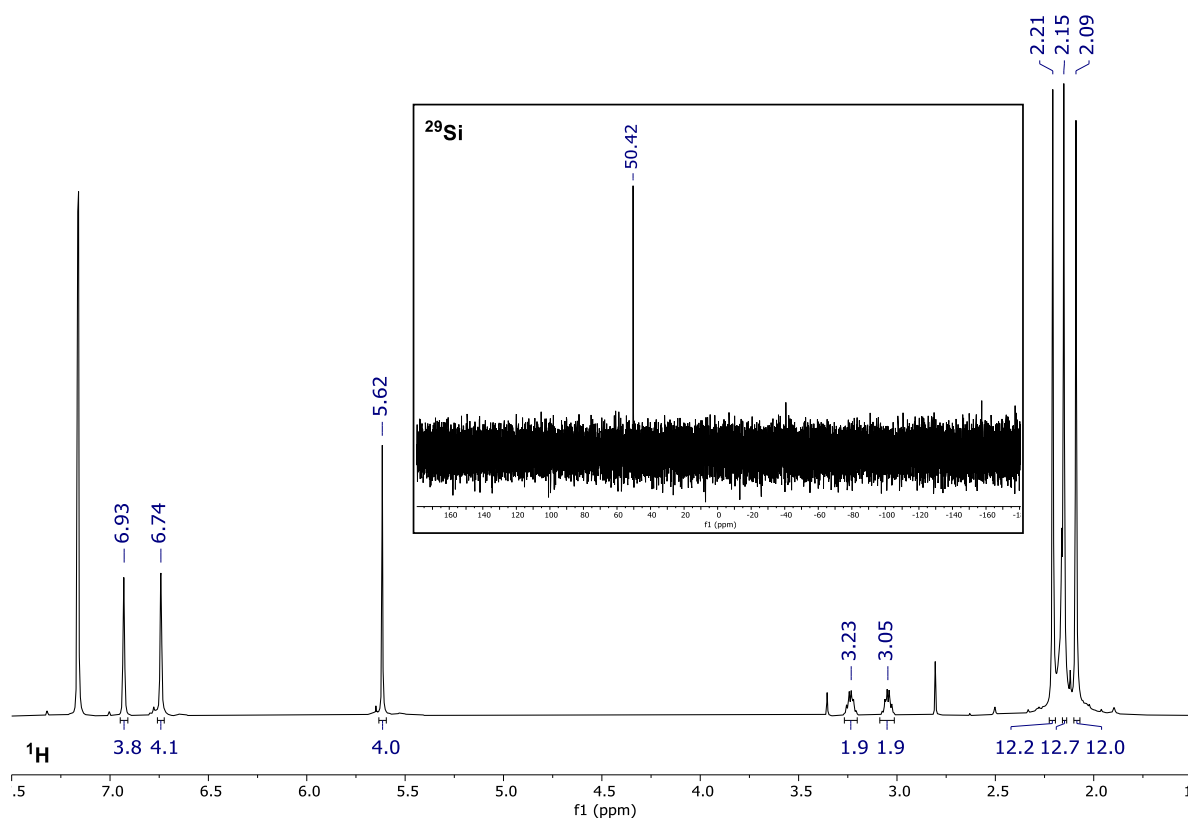


Figure 60.  $^1\text{H}$ -NMR (big) and  $^{29}\text{Si}$ -NMR (small) spectrum of  $[\text{bis}^{\text{Et}}\text{-NHIMesSiClFe}(\text{CO})_4][\text{HFe}(\text{CO})_4]$  (**P23**) recorded at 25°C in benzene- $\text{d}_6$ .

The characteristic  $^{13}\text{C}$  NMR carbonyl signals at  $\delta = 216.3$  and  $222.7$  ppm represent the iron carbonyl (Figure S 32). The silicon center resonates with one distinct singlet in  $^{29}\text{Si}$  NMR at  $\delta = 50.4$  ppm, respectively (Figure 60, small). Compared to  $[\text{bis}^{\text{Et}}\text{-NHI}^{\text{Mes}}\text{SiHFe}(\text{CO})_4][\text{HFe}(\text{CO})_4]$  (**P22**), the silicon center presents itself a bit more shielded which can be attributed to the  $\pi$ -donor halogen substituent. Whereas the synthesis of  $[\text{bis}^{\text{Et}}\text{-NHI}^{\text{Mes}}\text{SiClFe}(\text{CO})_4][\text{HFe}(\text{CO})_4]$  (**P23**) requires careful temperature management to obtain the pure product in acceptable yields (approx. 50%), upon solvent exchange in favor of dimethoxyethane (DME) the reaction proceeds in a heterogeneous fashion at room temperature. The mixture of equimolar amounts of bis-NHISiCl<sub>4</sub> and K<sub>2</sub>Fe(CO)<sub>4</sub> results in 46% isolable yield of  $[\text{bis}^{\text{Et}}\text{-NHI}^{\text{Mes}}\text{SiClFe}(\text{CO})_4][\text{Cl}]$  (**P24**), as direct product without verifiable anion exchange (Scheme 50, right). The now colorless solid is insoluble in non-polar solvents and resonates with only minor changes in multinuclear NMR analysis (Figure 61). The silicon  $^{29}\text{Si}$  NMR signal remains at  $\delta = 50.2$  ppm, as expected. The  $^1\text{H}$  NMR of **P24** lack the characteristic resonance of  $\text{HFe}(\text{CO})_4^-$  at  $\delta(^1\text{H}) = -9$  ppm, further substantiating the eluding anion exchange.

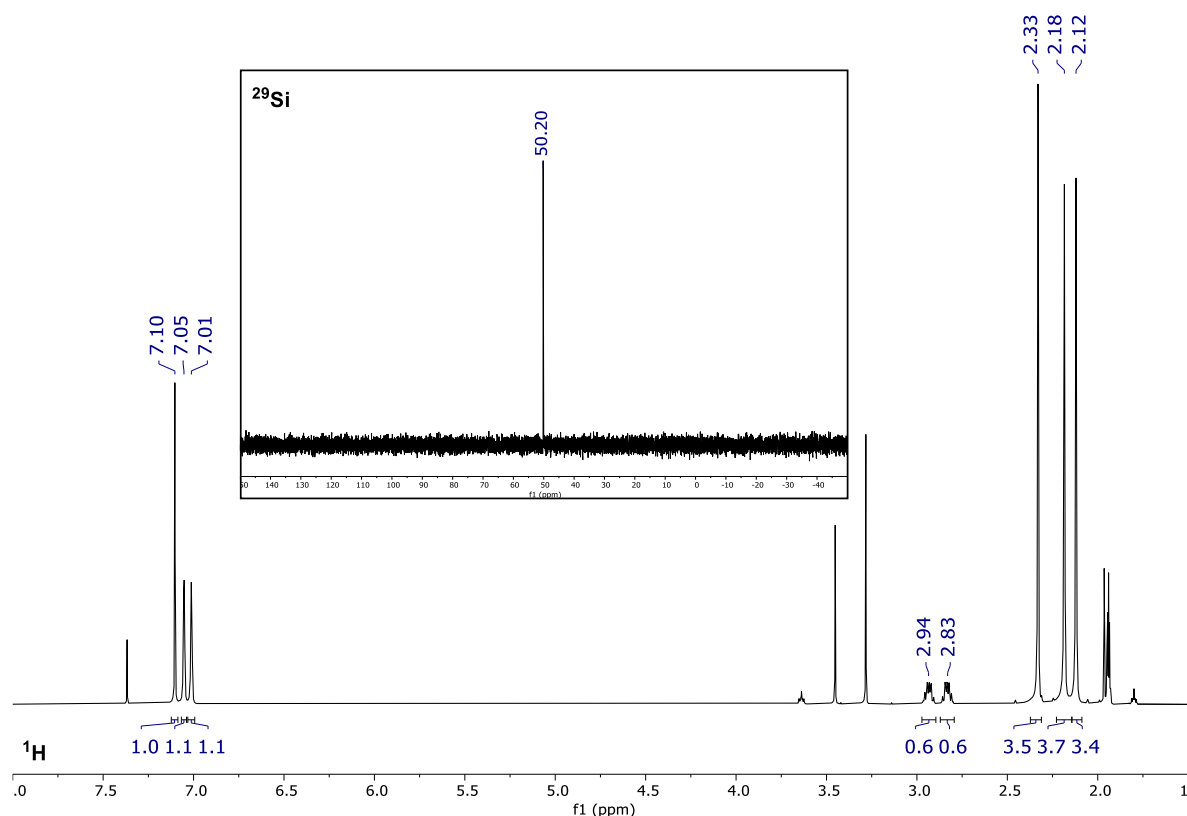
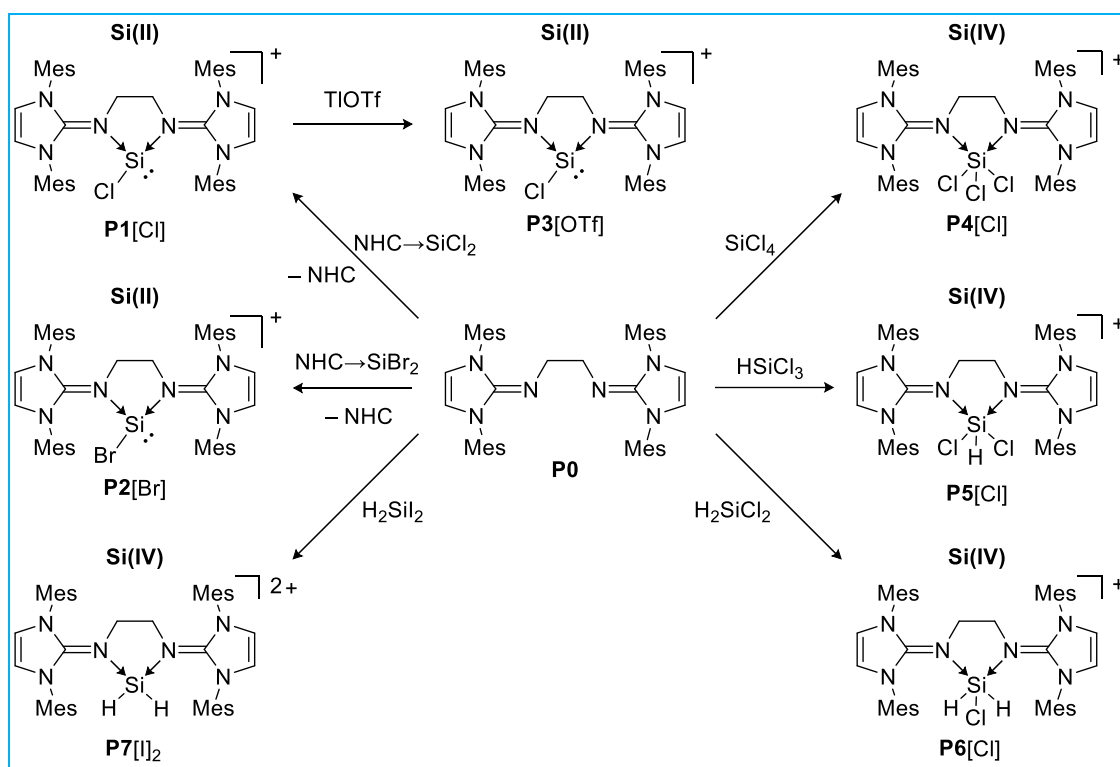


Figure 61.  $^1\text{H}$ -NMR (big) and  $^{29}\text{Si}$ -NMR (small) spectrum of  $[\text{bis}^{\text{Et}}\text{-NHI}^{\text{Mes}}\text{SiClFe}(\text{CO})_4][\text{Cl}]$  (**P24**) recorded at 25°C in  $\text{MeCN-d}_3$ .

Conducted HCl-abstracting experiments using bases such as  $\text{IMe}_4$ , DABCO, KHMDs, and pyridine did show either no conversion even at elevated temperatures or resulted in  $(\text{CO})_4\text{Fe}-\text{Fe}(\text{CO})_4^{2-}$  dianion formation, as found in preliminary SC-XRD analysis.

## 5 Conclusion

The presented work addresses the synthesis and characterization of novel bis-NHI-stabilized and low-valent silicon species and their coordination chemistry. In the first part several bis-NHI complexes of halosilanes (**P4-P7**) and halosilylenes (**P1-P3**) were obtained. The complexes can conveniently be isolated from reaction mixtures of the free ligand bis<sup>Et</sup>-NHI<sup>Mes</sup> and the respective silicon source (NHC→SiCl<sub>2</sub> (**P1**), NHC→SiBr<sub>2</sub> (**P2**), SiCl<sub>4</sub> (**P4**), HSiCl<sub>3</sub> (**P5**), H<sub>2</sub>SiCl<sub>2</sub> (**P6**), H<sub>2</sub>SiI<sub>2</sub> (**P7**)) at room temperature (Scheme 51). For anion exchange, **P1** was treated with TlOTf to obtain **P3** in moderate yields. Reactivity studies were conducted to evaluate the highly  $\sigma$ - and  $\pi$ -donating bis-NHI ligand system for its ability to stabilize novel silyliumylidene-, and desired electron-enriched silylone-complexes.



Scheme 51. Compilation of silicon complexes syntheses, furnished *via* coordination of different Si-synthons on **P0**.

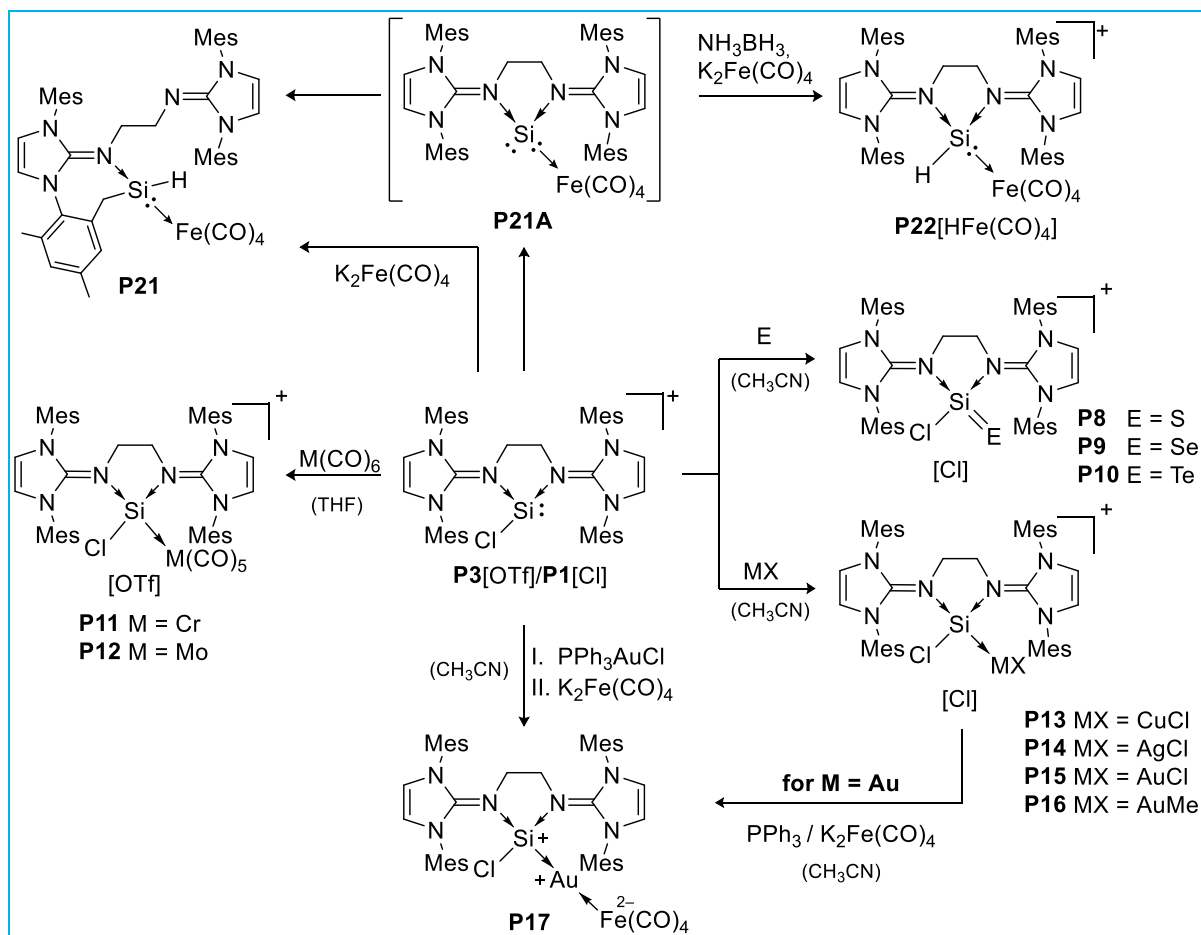
The furnished silyliumylidenes **P1-P3** feature two main reactive sites: (i) Coordination of Lewis acids onto the electron lone-pair, and (ii) reduction towards reactive silicon complexes in lower oxidation states *via* reductive dehalogenation or respective HX (X = halogen) extraction. Both reaction strategies were combined to observe several transition metal complexes as well as heavier silacylium ions (Scheme 52). In addition, halosilanes **P4-P7** were tested for their reducibility under comparable conditions (Scheme 53).

Direct reaction of **P1** and heavier chalcogens (S, Se, Te) gave rise to the heavier silacylium ions **P8-P10** in good to excellent yields and provided the possibility to assess the silyliumylidenes ligand properties (*i.e.*  $\pi$ -acceptor strength) *via* the  $^{77}\text{Se}$  NMR shift of selenide complex **P9**.

Using OTf-salt **P3** and the carbonyls  $\text{Cr}(\text{CO})_6$  and  $\text{Mo}(\text{CO})_6$ , the respective group 6 silyliumylidene complexes **P11** and **P12** could be obtained *via* NMR monitoring of radiated THF solutions.

Sterically less demanding coinage metals, such as  $\text{CuCl}$ ,  $\text{AgCl}$ , and stabilized gold precursors  $\text{ClAuSMe}_2$ ,  $\text{ClAuPPh}_3$ , as well as  $\text{MeAuPPh}_3$  gave the direct coordination products **P13-P16**. Varying  $\text{AuCl}$  (**P15**) towards  $\text{AuCH}_3$  (**P16**) results in a similar complex coordination environment, as concluded from heteronuclear NMR analysis. However, the silicon center experiences a remarkable down-field shift in  $^{29}\text{Si}$  NMR of  $\delta = 58.0$  ppm.

Whereas direct reductions of bis-NHI-stabilized silicon complexes **P1-P16** using several reductive reagents remained unsuccessful, the reducing and Lewis acidic iron providing Collman's reagent ( $\text{Na}_2\text{Fe}(\text{CO})_4$  and its derivative  $\text{K}_2\text{Fe}(\text{CO})_4$ ) allowed the isolation of several iron-containing complexes. Upon treatment of gold complex **P15** with one equivalent  $\text{PPh}_3$  and subsequent  $\text{K}_2\text{Fe}(\text{CO})_4$ , the first heterobimetallic and zwitterionic silyliumylidene complex **P17** could be isolated. The compound features a rather high thermal stability and is fully characterized including theoretical computations and Mössbauer spectroscopy. All considerations suggest **P17** to be best described as  $\text{bis}^{\text{Et}}\text{-NHI}^{\text{Mes}}\text{CISi}^+\text{-}\rightarrow\text{Au}^+\leftarrow\text{Fe}^{2-}(\text{CO})_4$ .

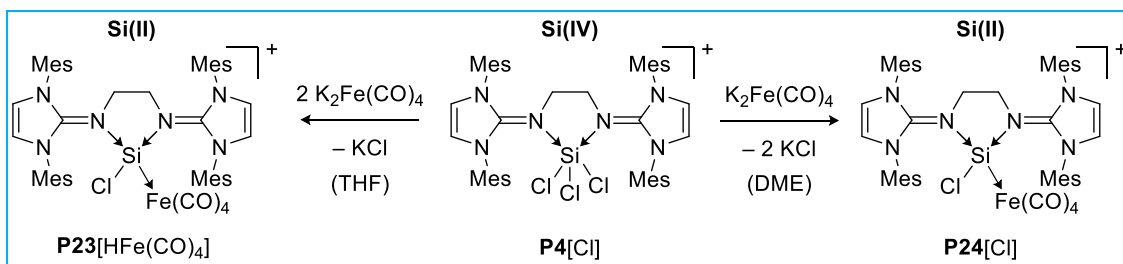


Scheme 52. Compilation of silyliumylidene complex (**P1**, **P3**) reactivity towards heavier chalcogens and transition metal synthons of group 6,8, and 11.

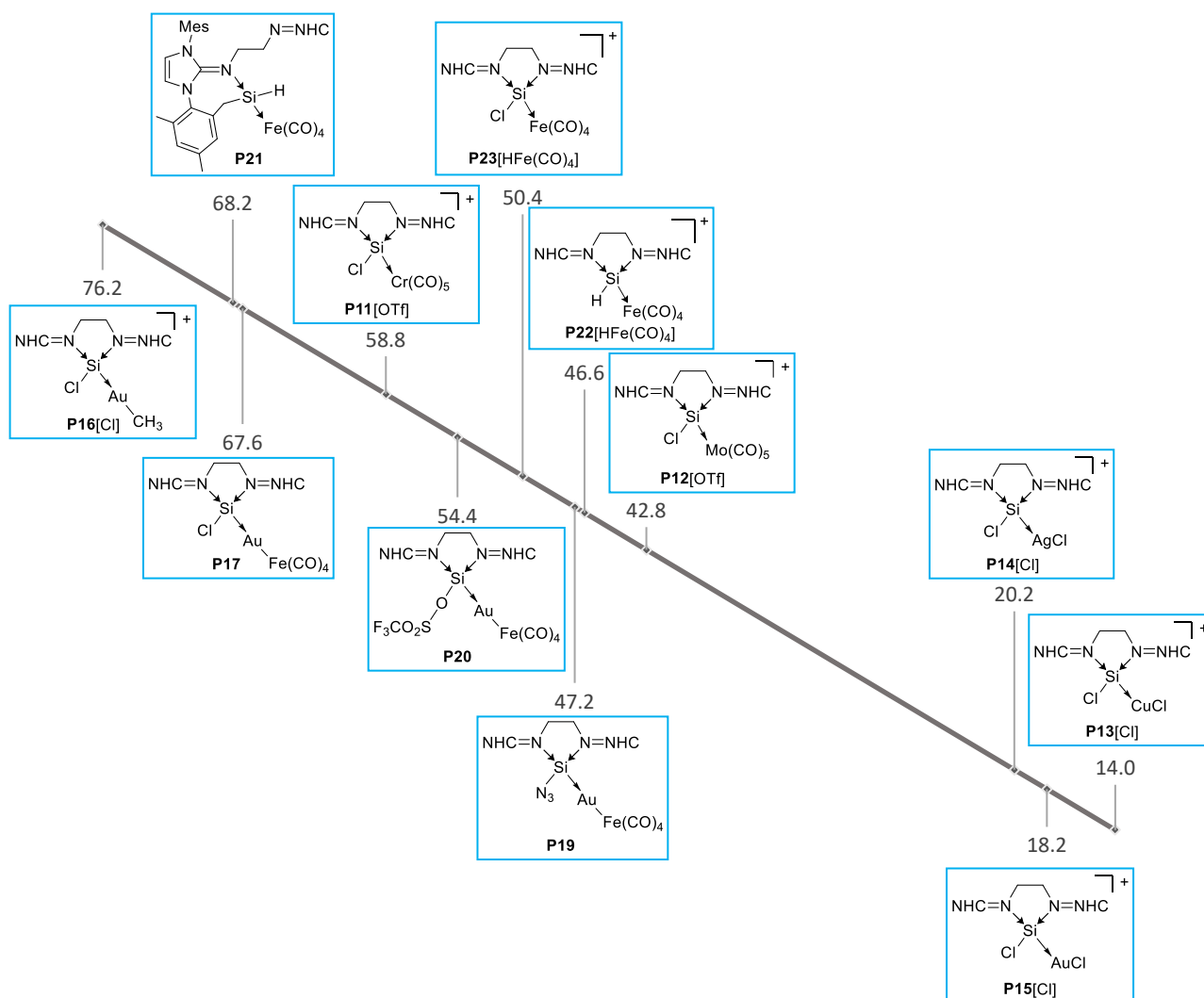
Initial reactivity studies of **P17** reveal possible functionalization *via* chloride exchange with 4,4'-bipyr<sup>2-</sup> (**P18**), NaN<sub>3</sub> (**P19**), and AgOTf (**P20**) as well as selective reactivity towards standard substrates for oxidative addition such as C<sub>2</sub>Cl<sub>6</sub> (**P17A**), CH<sub>3</sub>I (**P17B**), and TMSI (**P17C**).

Direct reduction of **P1** with K<sub>2</sub>Fe(CO)<sub>4</sub> in DME afforded the intramolecular C–H activation product **P21** that is suggested to form upon stabilization of the elusive three-coordinate iron silylone complex **P21A**. Carried out trapping reaction with NH<sub>3</sub>BH<sub>3</sub> and one additional equivalent of K<sub>2</sub>Fe(CO)<sub>4</sub> allowed the isolation of silyliumylidene hydride iron-complex **P22**. The findings further support the presents of **P21A**, however, it eluded spectroscopic observation.

Starting from halosilane complex **P4**, the reaction with K<sub>2</sub>Fe(CO)<sub>4</sub> gives rise to iron silyliumylidene complexes **P24** and **P23**, depending on the reaction conditions. Synthesis in thf requires careful temperature control and two equivalents of K<sub>2</sub>Fe(CO)<sub>4</sub> to form **P23** with <sup>-</sup>HFe(CO)<sub>4</sub> anion. In contrast, when DME was used as solvent, the conversion was allowed to proceed at room temperature and results in **P24** with preserved <sup>-</sup>Cl anion.

Scheme 53. Compilation of halosilane complex reactivity (**P4**) towards  $\text{K}_2\text{Fe}(\text{CO})_4$ .

In this thesis it could be shown, that the bis-NHI system is capable to stabilize various silicon synthons with reasonable effort. Using this complexes as starting materials for reduction and coordination chemistry revealed a diverse chemistry that lead to unique bonding motifs with silicon centers in variable shielding situations that resonate from  $\delta(^{29}\text{Si}) = 76$  ppm to  $-112$  ppm (Chart 5 and Chart 6) and promising transition metal complexes for further research.

Chart 5. Graphic presentation of the thesis' product complexes plotted according to their  $^{29}\text{Si}$ -NMR shift  $\delta = 77$  to  $14$  ppm.

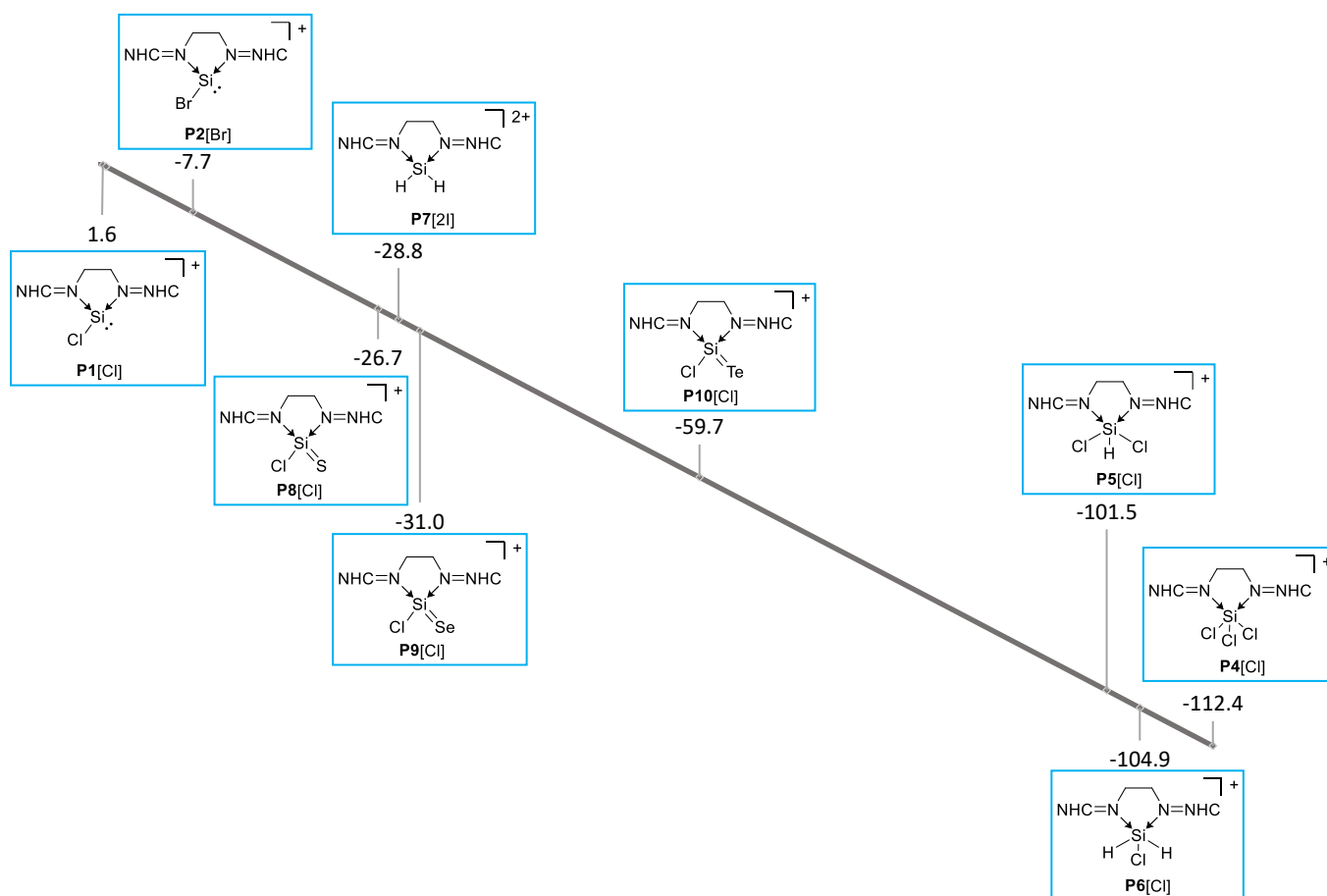


Chart 6. Graphic presentation of the thesis' product complexes plotted according to their  $^{29}\text{Si}$ -NMR shift  $\delta = 2$  to  $-113$  ppm.

Whereas all complexes are of interest for reactivity studies, of particular note is the potential of heterobimetallic complex **P17**, as well as silyliumylidene-hydride iron-complex **P22** and **P7A**, for application in small molecule activation and catalysis, such as the potential hydration of olefins and cross-coupling reactions.

## 6 Experimental

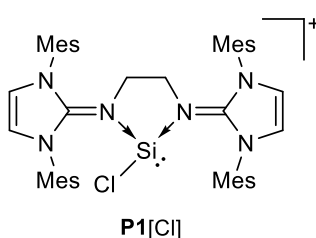
**General considerations:** All experiments and manipulations were carried out under dry oxygen-free argon using standard Schlenk techniques and glassware or in a MBraun glovebox workstation containing an atmosphere of purified argon if not stated otherwise. Solvents were dried by standard methods (e.g. withdrawal from MBraun Solvent Purification System, storage over molecular sieves (3 & 4 Å), degassing *via* freeze-pump-thaw cycling, distillation from sodium/ketylradical or CaH<sub>2</sub>). <sup>1</sup>H-, <sup>29</sup>Si-, <sup>77</sup>Se-, <sup>125</sup>Te-, <sup>19</sup>F-, and <sup>13</sup>C{<sup>1</sup>H} NMR spectra were recorded on Bruker Avance 300 MHz, 400 MHz, or 500 MHz spectrometers and referenced to residual solvent signals as internal standards (<sup>1</sup>H and <sup>13</sup>C). δ(<sup>29</sup>Si) was referenced to the signal of SiMe<sub>4</sub> (TMS) (δ = 0 ppm) as external standard. Values for the chemical shift (δ) are given in parts per million (ppm). Elemental analyses were carried out by the microanalytical laboratory of the Catalysis Research Center, Technische Universität München, using a HEKAtech EURO EA instrument equipped with a CHNS combustion analyze. Melting Points (M.P.) were determined in sealed glass capillaries under inert gas by a Büchi M-565 melting point apparatus. Liquid injection field desorption ionization mass spectrometry (LIFDI-MS) was measured directly from an inert atmosphere glovebox with a Thermo Fisher Scientific Exactive Plus Orbitrap equipped with an ion source from Linden CMS.<sup>[147]</sup> Electrospray ionization mass spectrometry (ESI-MS) analysis was conducted on a Bruker HCT Instrument with a dry gas temperature of 300 °C and an injection speed of 240 μLs<sup>-1</sup>. Samples were prepared in a glovebox and spectra were visualized using OriginPro 2018.

**Mössbauer spectroscopy (Dr. J. Sutter, Prof. Dr. K. Meyer):** Zero-field <sup>57</sup>Fe-Mössbauer spectra were recorded on a WissEl Mössbauer spectrometer (MRG-500) at 77 K in constant acceleration mode. <sup>57</sup>Co/Rh was used as the radiation source. Least-square fitting of the Lorentzian signals was carried out with the Mfir software, developed by Dr. Eckhard Bill (MPI Mülheim/Ruhr). The minimum experimental line widths were 0.21 mms<sup>-1</sup>. The temperature of the samples was controlled by an MBBC-HE0106 MÖSSBAUER He/N<sub>2</sub> cryostat within an accuracy of ±0.3 K. Isomer shifts were determined relative to α-iron at 298 K.

Reagents were purchased from commercial suppliers and processed as received if not stated otherwise. Precursors were synthesized according to literature procedures: K<sub>2</sub>Fe(CO)<sub>4</sub>, IDip→SiCl<sub>2</sub>,<sup>[28]</sup> IDip→SiBr<sub>2</sub>,<sup>[27]</sup> Li[MoCp(CO)<sub>2</sub>PMe<sub>3</sub>],<sup>[148]</sup> [IRCl][BF<sub>4</sub>]<sup>[41]</sup> (R = Mes, Dip), bis<sup>Et</sup>-NHI<sup>Mes</sup> (PO).<sup>[44,45]</sup>

Abbreviations: s = singlet, d = doublet, quint = quintet, t = triplet, sept = septet, br = broad, n.a. = not applicable/no answer, n.r. = not resolved, n.o. = not observed.

### Procedure for the isolation of [bis<sup>Et</sup>-NHI<sup>Mes</sup>SiCl]Cl (**P1**)



70 ml of toluene was added to a mixture of bis<sup>Et</sup>-NHI<sup>Mes</sup> (**P0**, 750 mg, 1.13 mmol) and NHC<sup>Dip</sup>→SiCl<sub>2</sub> (605 mg, 1.24 mmol, 1.1 eq.) in one portion at r.t.. After filtration of very little insoluble residue, the mixture was stirred for 16 h. The product was separated from the solution by filtration and consequently washed with 20 ml of toluene. The colorless, pearly solid was dried in fine vacuum to obtain 654 mg (76%) of **P1** as a colorless solid. X-ray quality crystals were obtained by gas phase diffusion of solvent between a solution of **P1** in *o*-DFB and a reservoir of Et<sub>2</sub>O over 2 days.

<sup>1</sup>H NMR (500.1 MHz, CD<sub>3</sub>CN): δ [ppm] = 6.97 (s, 8H, MesH-3,5), 6.80 (s, 4H, NCH), 2.93 (br, 2H C<sub>2</sub>H<sub>4</sub>), 2.61 (br, 2H, C<sub>2</sub>H<sub>4</sub>), 2.33 (s, 12H, Mes-*p*-CH<sub>3</sub>), 2.01 (s, 24H, Mes-*o*-CH<sub>3</sub>).

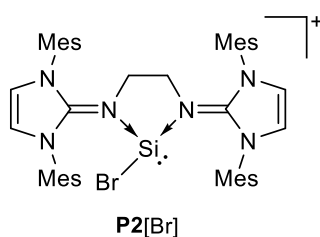
<sup>13</sup>C{<sup>1</sup>H} NMR (125.8 MHz, CD<sub>3</sub>CN): δ [ppm] = 147.90 (NCN), 141.61 (MesC-1), 137.16 (MesC-2,6), 132.61 (MesC-4), 130.19 (MesC-3,5), 119.83 (NCH), 47.26 (C<sub>2</sub>H<sub>4</sub>), 21.24 (*p*-MesCH<sub>3</sub>), 18.32 (*o*-MesCH<sub>3</sub>).

<sup>29</sup>Si NMR (99.4 MHz, CD<sub>3</sub>CN): δ [ppm] = 1.54.

**Elemental analysis:** [763.93] calcd: C 69.18, H 6.86, N 11.00; found: C 65.73, H 6.71, N 9.77. (Consistently low C values can be explained by the formation of silicon carbide.)

**M.P.:** 215.4 °C (decomposition, color change to dark red)

### Procedure for the isolation of [bis<sup>Et</sup>-NHI<sup>Mes</sup>-SiBr]Br (**P2**)



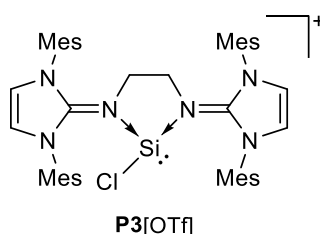
5 ml of toluene was added to a mixture of bis<sup>Et</sup>-NHI<sup>Mes</sup> (**P0**, 100 mg, 0.15 mmol) and NHC<sup>Dip</sup>→SiBr<sub>2</sub> (104 mg, 0.18 mmol, 1.2 eq.) at r.t.. The orange suspension was stirred for 16 h. The formed precipitate was separated from the solution by filtration and consequently washed with 2x10 ml of toluene. The off-white solid was dried in fine-vacuum to obtain 51 mg (40% corrected yield from crude product that contained 60% of NHC<sup>Dip</sup>HCl) of **P2**.

<sup>1</sup>H NMR (500.1 MHz, CD<sub>3</sub>CN): δ [ppm] = 6.98 (s, 8H, MesH-3,5) 6.81 (s, 4H, NCH), 2.86 (br, 4H C<sub>2</sub>H<sub>4</sub>), 2.34 (s, 12H, Mes-*p*-CH<sub>3</sub>), 2.02 (s, 24H, Mes-*o*-CH<sub>3</sub>).

<sup>13</sup>C{<sup>1</sup>H} NMR (125.8 MHz, CD<sub>3</sub>CN): δ [ppm] = 146.25 (NCN), 141.65 (MesC-1), 136.99 (MesC-2,6), 136.70 (MesC-2,6), 132.93 (MesC-4), 130.68 (MesC-3,5), 130.26 (MesC-3,5), 125.53 (NCH), 47.63 (C<sub>2</sub>H<sub>4</sub>), 29.80 (MesCH<sub>3</sub>), 24.57 (MesCH<sub>3</sub>), 23.67 (MesCH<sub>3</sub>).

<sup>29</sup>Si NMR (99.4 MHz, CD<sub>3</sub>CN): δ [ppm] = 7.67.

### Procedure for the isolation of [bis<sup>Et</sup>-NHI<sup>Mes</sup>-SiCl]OTf (**P3**)



TfOTf (315 mg, 0.89 mmol, 1.3 eq.) was dissolved in 10 ml of THF and added to **P1** (500 mg, 0.69 mmol) in one portion at r.t.. The suspension was stirred for 46 h, after what the mixture was stripped from all volatiles in fine vacuum. The product was extracted with 2x5 ml MeCN and subsequently dried to afford 480 mg (80%) of **P3** as colorless powdery solid.

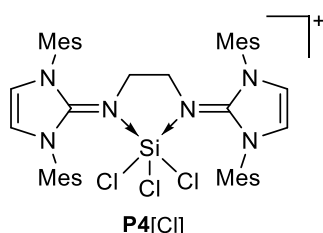
<sup>1</sup>H NMR (500.1 MHz, CD<sub>3</sub>CN): δ [ppm] = 6.99 (s, 4H, MesH-3,5), 6.95 (s, 4H, MesH-3,5) 6.77 (s, 4H, NCH), 2.93 (m, 2H C<sub>2</sub>H<sub>4</sub>), 2.60 (m, 2H, C<sub>2</sub>H<sub>4</sub>), 2.33 (s, 12H, Mes-*p*-CH<sub>3</sub>), 2.02 (s, 12H, Mes-*o*-CH<sub>3</sub>), 1.99 (s, 12H, Mes-*o*-CH<sub>3</sub>).

<sup>13</sup>C{<sup>1</sup>H} NMR (125.8 MHz, CD<sub>3</sub>CN): δ [ppm] = 147.88 (NCN), 141.59 (MesC-1), 137.14 (MesC-2,6), 137.10 (MesC-2,6) 132.57 (MesC-4), 130.20 (MesC-3,5), 130.11 (MesC-3,5), 119.76 (NCH), 47.22 (C<sub>2</sub>H<sub>4</sub>), 21.19 (*p*-MesCH<sub>3</sub>), 18.32 (*o*-MesCH<sub>3</sub>), 18.22 (*o*-MesCH<sub>3</sub>).

<sup>29</sup>Si NMR (99.4 MHz, CD<sub>3</sub>CN): δ [ppm] = 1.55.

<sup>19</sup>F NMR (470.8 MHz, CD<sub>3</sub>CN): δ [ppm] = 79.34.

### Procedure for the isolation of [bis<sup>Et</sup>-NHI<sup>Mes</sup>-SiCl<sub>3</sub>]Cl (**P4**)



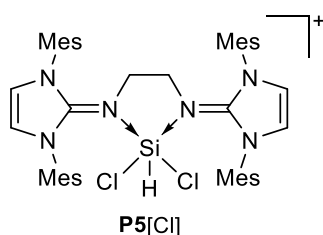
bis<sup>Et</sup>-NHI<sup>Mes</sup> (**P0**, 579 mg, 0.87 mmol) was dissolved in 20 ml of toluene and treated with neat SiCl<sub>4</sub> (148 mg, 0.1 ml, 0.87 mmol, 1 eq.). The rapidly formed colorless precipitate was stirred for 1 h and separated afterwards. The isolated solid was washed with 10 ml toluene and subsequently dried in fine vacuum to afford 697 mg (96%) **P4** as colorless solid. A single crystal suitable for SC-XRD analysis is grown from gas phase diffusion of solvent between a solution of **P4** in MeCN and a reservoir of THF over 4 weeks.

<sup>1</sup>H NMR (500.1 MHz, CD<sub>3</sub>CN): δ [ppm] = 7.16 (s, 4H, NCH), 7.01 (s, 8H, MesH-3,5), 2.76 (s, 4H C<sub>2</sub>H<sub>4</sub>), 2.38 (s, 12H, Mes-*p*-CH<sub>3</sub>), 2.04 (s, 24H, Mes-*p*-CH<sub>3</sub>).

<sup>13</sup>C{<sup>1</sup>H} NMR (125.8 MHz, CD<sub>3</sub>CN): δ [ppm] = 148.98 (NCN), 141.34 (MesC-1), 136.71 (MesC-2,6), 136.44 (MesC-2,6), 132.35 (MesC-4), 130.75 (MesC-3,5), 130.57 (MesC-3,5), 122.17 (NCH), 48.36 (C<sub>2</sub>H<sub>4</sub>), 21.11 (MesCH<sub>3</sub>), 19.06 (MesCH<sub>3</sub>), 17.90 (MesCH<sub>3</sub>).

<sup>29</sup>Si NMR (99.4 MHz, CD<sub>3</sub>CN): δ [ppm] = -112.45.

### Procedure for the isolation of [bis<sup>Et</sup>-NHI<sup>Mes</sup>-SiHCl<sub>2</sub>]Cl (**P5**)



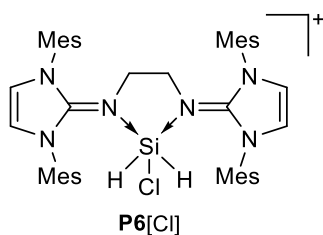
bis<sup>Et</sup>-NHI<sup>Mes</sup> (**P0**, 330 mg, 0.50 mmol) was dissolved in 15 ml of toluene and treated with neat HSiCl<sub>3</sub> (67 mg, 0.05 ml, 0.87 mmol, 1 eq.). The rapidly formed colorless precipitate was stirred for 1 h and separated afterwards. The isolated solid was washed with 8 ml toluene and subsequently dried in fine vacuum to afford 343 mg (86%) **P5** as colorless solid.

<sup>1</sup>H NMR (400 MHz, CD<sub>3</sub>CN): δ [ppm] = 7.08 (s, 2H, NCH), 7.02 (s, 4H, MesH-3,5), 7.01 (s, 4H, MesH-3,5), 6.90 (s, 2H, NCH), 5.35 (s, 1H, SiH), 2.76 (s, 2H, C<sub>2</sub>H<sub>4</sub>), 2.36 (s, 12H, MesCH<sub>3</sub>), 2.32 (s, 2H C<sub>2</sub>H<sub>4</sub>), 2.03 (s, 24H, MesCH<sub>3</sub>).

<sup>13</sup>C{<sup>1</sup>H} NMR (100 MHz, CD<sub>3</sub>CN): δ [ppm] = 145.02 (NCN), 141.78 (MesC-1), 136.70 (MesC-2,6), 136.42 (MesC-2,6), 132.60 (MesC-4), 130.66 (MesC-3,5), 130.56 (MesC-5,6), 121.64 (NCH), 119.45 (NCH), 47.22 (C<sub>2</sub>H<sub>4</sub>), 44.22 (C<sub>2</sub>H<sub>4</sub>), 21.22 (MesCH<sub>3</sub>), 18.74 (MesCH<sub>3</sub>), 17.90 (MesCH<sub>3</sub>).

<sup>29</sup>Si NMR (99.4 MHz, CD<sub>3</sub>CN): δ [ppm] = -101.52.

### Procedure for the isolation of [bis<sup>Et</sup>-NHI<sup>Mes</sup>-SiHCl<sub>2</sub>]<sup>+</sup>Cl<sup>-</sup> (**P6**)



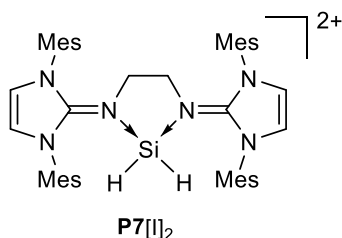
bis<sup>Et</sup>-NHI<sup>Mes</sup> (**P0**, 244 mg, 0.37 mmol) was dissolved in 10 ml of toluene and treated dropwise with a 37 wt% H<sub>2</sub>SiCl<sub>2</sub> in toluene (100 mg, 0.37 mmol, 1 eq.) solution at -30°C. The rapidly formed precipitate was stirred for 1 h at r.t. and separated afterwards. The isolated solid was washed with 5 ml toluene and subsequently dried in fine vacuum to afford 268 mg (91%) **P6** as colorless solid.

<sup>1</sup>H NMR (500.1 MHz, CD<sub>3</sub>CN): δ [ppm] = 7.06 (s, 8H, MesH-3,5), 6.99 (s, 4H, NCH), 4.33 (s, 2H, SiH), 2.63 (s, 4H C<sub>2</sub>H<sub>4</sub>), 2.37 (s, 12H, Mes-*p*-CH<sub>3</sub>), 2.07 (s, 24H, Mes-*o*-CH<sub>3</sub>).

<sup>13</sup>C{<sup>1</sup>H} NMR (125.8 MHz, CD<sub>3</sub>CN): δ [ppm] = 148.65 (NCN), 141.43 (MesC-1), 136.69 (MesC-2,6), 132.21 (MesC-4), 130.38 (MesC-3,5), 120.26 (NCH), 47.52 (C<sub>2</sub>H<sub>4</sub>), 21.09 (*p*-MesCH<sub>3</sub>), 18.63 (*o*-MesCH<sub>3</sub>).

<sup>29</sup>Si NMR (99.4 MHz, CD<sub>3</sub>CN): δ [ppm] = -104.85.

### Procedure for the isolation of [bis<sup>Et</sup>-NHI<sup>Mes</sup>-SiH<sub>2</sub>]<sup>2+</sup>[I<sub>2</sub>]<sup>-</sup> (**P7**)

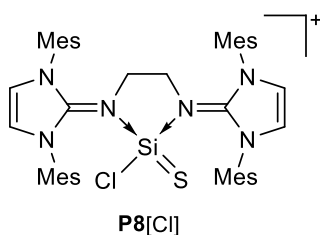


bis<sup>Et</sup>-NHI<sup>Mes</sup> (**P0**, 325 mg, 0.49 mmol) was dissolved in 15 ml of toluene and treated dropwise with a 0.24 M H<sub>2</sub>SiI<sub>2</sub> in toluene (139 mg, 2.00 ml, 0.49 mmol, 1 eq.) solution. The rapidly formed colorless precipitate was stirred for 30 min at r.t. and separated afterwards. The isolated solid was washed with 5 ml toluene and dried in fine vacuum to afford 398 mg (86%) **P7** as colorless solid. Crystals for SC-XRD analysis were grown from gas phase diffusion of solvent between a **P7** solution in MeCN and a reservoir of Et<sub>2</sub>O over 4 days.

<sup>1</sup>H NMR (500.1 MHz, CD<sub>3</sub>CN): δ [ppm] = 7.16 (s, 4H, NCH), 7.11 (s, 8H, MesH-3,5), 2.97 (s, 2H SiH), 2.78 (s, 4H, C<sub>2</sub>H<sub>4</sub>), 2.42 (s, 12H, Mes-*p*-CH<sub>3</sub>), 2.03 (s, 24H, Mes-*o*-CH<sub>3</sub>).

<sup>29</sup>Si NMR (99.4 MHz, CD<sub>3</sub>CN): δ [ppm] = -28.65.

### Procedure for the isolation of [bis<sup>Et</sup>-NHI<sup>Mes</sup>-SiClS]Cl (**P8**)



3 ml of MeCN was added to a mixture of **P1** (80.0 mg, 0.10 mmol) and S<sub>8</sub> (6.7 mg, 0.21 mmol, 2 eq.) in one portion at r.t. and the mixture was stirred for 45 min. Excess of sulfur was separated by filtration and the solution was evaporated under reduced pressure to yield the crude product as an off-white solid. The product was washed with 0.5 ml of toluene and dried in fine vacuum to obtain 80.0 mg (96%) of **P8** as a colorless solid. X-ray quality crystals were obtained by gas phase diffusion of solvent between a solution of **P8** in MeCN and a reservoir of THF over 3 weeks.

**<sup>1</sup>H NMR** (500.1 MHz, CD<sub>3</sub>CN):  $\delta$  [ppm] = 7.04 (s, 4H, NCH), 7.02 (s, 4H, MesH-3,5), 6.93 (s, 4H, MesH-3,5), 3.13 (m, 2H C<sub>2</sub>H<sub>4</sub>), 2.78 (m, 2H, C<sub>2</sub>H<sub>4</sub>), 2.36 (s, 12H, Mes-CH<sub>3</sub>), 2.23 (s, 12H, Mes-CH<sub>3</sub>), 2.03 (s, 12H, Mes-CH<sub>3</sub>).

**<sup>13</sup>C{<sup>1</sup>H} NMR** (125.8 MHz, CD<sub>3</sub>CN):  $\delta$  [ppm] = 146.70 (NCN), 141.68 (MesC-1), 136.62 (MesC-2,6), 136.41 (MesC-2,6), 132.32 (MesC-4), 130.89 (MesC-3,5), 130.55 (MesC-3,5), 122.14 (NCH), 47.59 (C<sub>2</sub>H<sub>4</sub>), 21.33 (p-MesCH<sub>3</sub>), 18.91 (o-MesCH<sub>3</sub>), 18.57 (o-MesCH<sub>3</sub>).

**<sup>29</sup>Si NMR** (99.4 MHz, CD<sub>3</sub>CN):  $\delta$  [ppm] = -26.73.

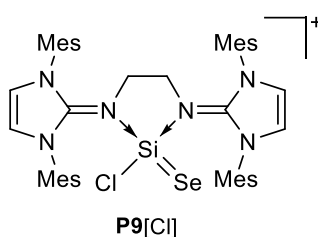
**MS** (ESI<sup>+</sup>)  $m/z$  calcd: 759.34;  $m/z$  found: 759.3

**Elemental analysis:** [794.31] calcd: C 66.39, H 6.59, N 10.56, S 4.03; found: C 63.78, H 6.45, N 10.36, S 3.35.

(Consistently low C values can be explained by the formation of silicon carbide.)

**M.P.:** 268.2 °C (decomposition, color change to black)

### Procedure for the isolation of [bis<sup>Et</sup>-NH]<sup>Mes</sup>-SiClSe]Cl (**P9**)



3 ml of MeCN was added to a mixture of **P1** (80.0 mg, 0.10 mmol) and Se (16.5 mg, 0.21 mmol, 2 eq.) in one portion at r.t. and the mixture was stirred for 6 h. Excess of selenium was separated by filtration and the solution was evaporated under reduced pressure to yield the crude product as a slightly yellow solid. The product was washed with 0.5 ml of toluene and dried in fine vacuum to obtain 82.0 mg (93%) of **P9** as a colorless solid.

**<sup>1</sup>H NMR** (500.1 MHz, CD<sub>3</sub>CN):  $\delta$  [ppm] = 7.07 (s, 4H, NCH), 7.02 (s, 4H, MesH-3,5), 6.93 (s, 4H, MesH-3,5), 3.16 (m, 2H C<sub>2</sub>H<sub>4</sub>), 2.77 (m, 2H, C<sub>2</sub>H<sub>4</sub>), 2.35 (s, 12H, Mes-CH<sub>3</sub>), 2.25 (s, 12H, Mes-CH<sub>3</sub>), 2.05 (s, 12H, Mes-CH<sub>3</sub>).

**<sup>13</sup>C{<sup>1</sup>H} NMR** (125.8 MHz, CD<sub>3</sub>CN):  $\delta$  [ppm] = 146.63 (NCN), 141.68 (MesC-1), 136.57 (MesC-2,6), 136.37 (MesC-2,6), 132.37 (MesC-4), 130.93 (MesC-3,5), 130.57 (MesC-3,5), 122.26 (NCH), 48.04 (C<sub>2</sub>H<sub>4</sub>), 21.34 (p-MesCH<sub>3</sub>), 19.24 (o-MesCH<sub>3</sub>), 18.93 (o-MesCH<sub>3</sub>).

**<sup>29</sup>Si NMR** (99.4 MHz, CD<sub>3</sub>CN):  $\delta$  [ppm] = -30.99.

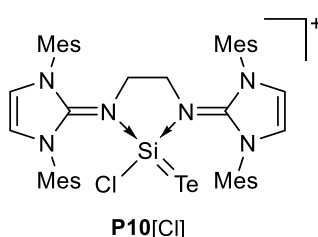
**<sup>77</sup>Se NMR** (76.3 MHz, CD<sub>3</sub>CN):  $\delta$  [ppm] = -388.78.

**MS** (ESI<sup>+</sup>)  $m/z$  calcd: 807.29;  $m/z$  found: 807.4

**Elemental analysis:** [842.26] calcd: C 62.70, H 6.22, N 9.97; found: C 61.41, H 6.05, N 9.47. (Consistently low C values can be explained by the formation of silicon carbide.)

**M.P.:** 254.5 °C (decomposition, color change to green-black)

### Procedure for the isolation of [bis<sup>Et</sup>-NHI<sup>Mes</sup>-SiClTe]Cl (P10)



3 ml of MeCN was added to a mixture of **P1** (80,0 mg, 0.10 mmol) and Te (26.7 mg, 0.21 mmol, 2 eq.) in one portion at r.t. and the mixture was stirred for 72 h. Excess of tellurium was separated by filtration and the solution was evaporated under reduced pressure to yield the crude product as a slightly yellow solid. The product was washed with 0.5 ml of toluene and dried in fine vacuum to obtain 86.0 mg (92%) of **P10** as a colorless solid.

<sup>1</sup>H NMR (500.1 MHz, CD<sub>3</sub>CN): δ [ppm] = 7.11 (s, 4H, NCH), 7.05 (s, 4H, MesH-3,5), 6.97 (s, 4H, MesH-3,5), 3.22 (m, 2H C<sub>2</sub>H<sub>4</sub>), 2.79 (m, 2H, C<sub>2</sub>H<sub>4</sub>), 2.38 (s, 12H, Mes-CH<sub>3</sub>), 2.31 (s, 12H, Mes-CH<sub>3</sub>), 2.11 (s, 12H, Mes-CH<sub>3</sub>).

<sup>13</sup>C{<sup>1</sup>H} NMR (125.8 MHz, CD<sub>3</sub>CN): δ [ppm] = 146.60 (NCN), 141.74 (MesC-1), 136.47 (MesC-2,6), 136.28 (MesC-2,6), 132.45 (MesC-4), 131.02 (MesC-3,5), 130.61 (MesC-3,5), 122.45 (NCH), 48.81 (C<sub>2</sub>H<sub>4</sub>), 21.34 (p-MesCH<sub>3</sub>), 20.00 (o-MesCH<sub>3</sub>), 19.74 (o-MesCH<sub>3</sub>).

<sup>29</sup>Si NMR (99.4 MHz, CD<sub>3</sub>CN): δ [ppm] = -59.14.

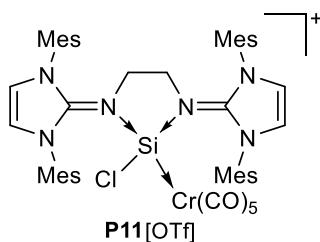
<sup>125</sup>Te NMR (126.24 MHz, CD<sub>3</sub>CN): δ [ppm] = -1049.36.

**MS** (ESI<sup>+</sup>) *m/z* calcd: 857.28; *m/z* found: 857.4

**Elemental analysis:** [892.25] calcd: C 59.28, H 5.88, N 9.43; found: C 60.11, H 6.19, N 9.28.

**M.P.:** 271.8 °C (decomposition, color change to black)

### Procedure for the isolation of [bis<sup>Et</sup>-NHI<sup>Mes</sup>-SiCl(Cr(CO)<sub>5</sub>)]OTf (**P11**)



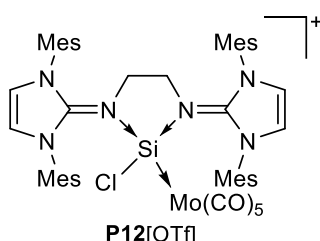
0.4 ml of THF-d<sub>8</sub> was added to a mixture of **P3** (15.0 mg, 0.17 mmol) and Cr(CO)<sub>6</sub> (3.8 mg, 0.17 mmol, 1 eq.) in one portion at r.t. and the mixture was irradiated with 340 nm. After the starting Cr(CO)<sub>6</sub> dissolved completely into a yellow solution, the reaction was irradiated for additional 72 h. NMR monitoring showed full conversion to **P11** as a still yellow solution.

**<sup>1</sup>H NMR** (500.1 MHz, THF-d<sub>8</sub>): δ [ppm] = 7.35 (s, 4H, NCH), 6.98 (s, 4H, MesH-3,5), 6.92 (s, 4H, MesH-3,5), 3.43 (br, 2H C<sub>2</sub>H<sub>4</sub>), 2.92 (br, 2H, C<sub>2</sub>H<sub>4</sub>), 2.31 (s, 12H, Mes-CH<sub>3</sub>), 2.24 (s, 12H, Mes-CH<sub>3</sub>), 2.13 (s, 12H, Mes-CH<sub>3</sub>).

**<sup>13</sup>C{<sup>1</sup>H} NMR** (125.8 MHz, THF-d<sub>8</sub>): δ [ppm] = 224.67 (CO), 221.47 (CO), 212.94 (CO), 149.27 (NCN), 141.08 (MesC-1), 136.73 (MesC-2,6), 136.20 (MesC-2,6), 133.97 (MesC-4), 131.13 (MesC-3,5), 130.63 (MesC-3,5), 123.32 (NCH), 51.90 (C<sub>2</sub>H<sub>4</sub>), 21.17 (MesCH<sub>3</sub>), 19.66 (MesCH<sub>3</sub>), 19.27 (MesCH<sub>3</sub>).

**<sup>29</sup>Si NMR** (99.4 MHz, THF-d<sub>8</sub>): δ [ppm] = 58.76.

### Procedure for the isolation of [bis<sup>Et</sup>-NHI<sup>Mes</sup>-SiCl(Mo(CO)<sub>5</sub>)]Cl (**P12**)



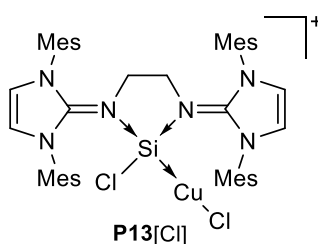
0.4 ml of THF-d<sub>8</sub> was added to a mixture of **P3** (15.0 mg, 0.17 mmol) and Mo(CO)<sub>6</sub> (4.5 mg, 0.17 mmol, 1 eq.) in one portion at r.t. and the mixture was irradiated with 340 nm. After the starting Mo(CO)<sub>6</sub> dissolved completely into a yellow solution, the reaction was irradiated for additional 72 h. NMR monitoring showed 30% conversion to **P12** (70% starting material) as a still yellow solution.

**<sup>1</sup>H NMR** (500.1 MHz, THF-d<sub>8</sub>): δ [ppm] = 7.38 (s, 4H, NCH), 6.99 (s, 4H, MesH-3,5), 6.92 (s, 4H, MesH-3,5), 3.37 (br, 2H C<sub>2</sub>H<sub>4</sub>), 2.89 (br, 2H, C<sub>2</sub>H<sub>4</sub>), 2.33 (s, 12H, Mes-CH<sub>3</sub>), 2.23 (s, 12H, Mes-CH<sub>3</sub>), 2.11 (s, 12H, Mes-CH<sub>3</sub>).

**<sup>13</sup>C{<sup>1</sup>H} NMR** (125.8 MHz, THF-d<sub>8</sub>): δ [ppm] = 211.67 (CO), 209.99 (CO), 202.31 (CO), 149.37 (NCN), 141.00 (MesC-1), 136.42 (MesC-2,6), 136.03 (MesC-2,6), 133.78 (MesC-4), 131.23 (MesC-3,5), 130.73 (MesC-3,5), 123.30 (NCH), 52.05 (C<sub>2</sub>H<sub>4</sub>), 21.22 (MesCH<sub>3</sub>), 19.85 (MesCH<sub>3</sub>), 19.44 (MesCH<sub>3</sub>).

**<sup>29</sup>Si NMR** (99.4 MHz, THF-d<sub>8</sub>): δ [ppm] = 42.77.

### Procedure for the isolation of [bis<sup>Et</sup>-NHI<sup>Mes</sup>-SiCl(CuCl)]Cl (**P13**)



3 ml of MeCN was added to a mixture of **P1** (80 mg, 0.10 mmol) and CuCl (10.4 mg, 0.10 mmol, 1 eq.) in one portion at r.t. and the mixture was stirred for 6 h. Minor amount of insoluble residue was separated by filtration and the solution was evaporated under reduced pressure to yield the crude product as a slightly yellow solid. The product was washed with 0.5 ml of toluene and dried in fine vacuum to obtain 89.0 mg (94%) of **P13** as a colorless solid.

<sup>1</sup>H NMR (500.1 MHz, CD<sub>3</sub>CN): δ [ppm] = 7.10 (s, 4H, MesH-3,5), 7.07 (s, 4H, MesH-3,5), 7.06 (s, 4H, NCH), 3.03 (m, 2H C<sub>2</sub>H<sub>4</sub>), 2.80 (m, 2H, C<sub>2</sub>H<sub>4</sub>), 2.38 (s, 12H, Mes-CH<sub>3</sub>), 2.10 (s, 12H, Mes-CH<sub>3</sub>), 2.01 (s, 12H, Mes-CH<sub>3</sub>).

<sup>13</sup>C{<sup>1</sup>H} NMR (125.8 MHz, CD<sub>3</sub>CN): δ [ppm] = 147.01 (NCN), 142.11 (MesC-1), 136.14 (MesC-2,6), 136.05 (MesC-2,6), 131.86 (MesC-4), 131.35 (MesC-3,5), 131.00 (MesC-3,5), 121.80 (NCH), 48.48 (C<sub>2</sub>H<sub>4</sub>), 21.30 (p-MesCH<sub>3</sub>), 18.97 (o-MesCH<sub>3</sub>).

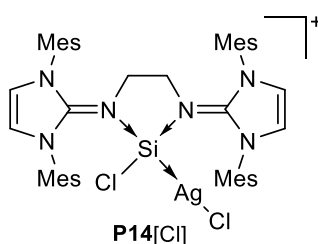
<sup>29</sup>Si NMR (99.4 MHz, CD<sub>3</sub>CN): δ [ppm] = 13.84.

**MS** (ESI<sup>+</sup>) *m/z* calcd: 827.47; *m/z* found: 827.4

**Elemental analysis:** [860.24] calcd: C 61.24, H 6.07, N 9.74; found: C 54.36, H 5.43, N 8.27. (Consistently low C values can be explained by the formation of silicon carbide.)

**M.P.:** 168.9 °C (decomposition, color change to black)

### Procedure for the isolation of [bis<sup>Et</sup>-NHI<sup>Mes</sup>-SiCl(AgCl)]Cl (**P14**)



3 ml of MeCN was added to a mixture of **P1** (80 mg, 0.10 mmol) and AgCl (30.0 mg, 0.21 mmol, 2 eq.) in one portion at r.t. and the mixture was stirred for 16 h. Excess of silver chloride was separated by filtration and the solution was evaporated under reduced pressure to yield the crude product as a beige solid. The product was washed with 0.5 ml of toluene and dried in fine vacuum to obtain 72.0 mg (76%) of **P14** as a colorless solid.

**<sup>1</sup>H NMR** (500.1 MHz, CD<sub>3</sub>CN):  $\delta$  [ppm] = 7.11 (s, 8H, MesH-3,5), 7.08 (s, 4H, NCH), 3.04 (br, 2H C<sub>2</sub>H<sub>4</sub>), 2.86 (br, 2H, C<sub>2</sub>H<sub>4</sub>), 2.38 (s, 12H, Mes-CH<sub>3</sub>), 2.08 (s, 12H, Mes-CH<sub>3</sub>), 2.02 (s, 12H, Mes-CH<sub>3</sub>).

**<sup>13</sup>C{<sup>1</sup>H} NMR** (125.8 MHz, CD<sub>3</sub>CN):  $\delta$  [ppm] = 146.79 (NCN), 142.35 (MesC-1), 136.16 (MesC-2,6), 131.77 (MesC-4), 131.37 (MesC-3,5), 131.04 (MesC-3,5), 121.92 (NCH), 48.46 (C<sub>2</sub>H<sub>4</sub>), 21.31 (p-MesCH<sub>3</sub>), 18.96 (o-MesCH<sub>3</sub>).

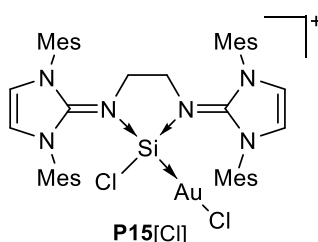
**<sup>29</sup>Si NMR** (99.4 MHz, CD<sub>3</sub>CN):  $\delta$  [ppm] = 20.18 (d,  $^1J_{\text{Si}^{109}\text{Ag}} = 592.8$  Hz), 20.18 (d,  $^1J_{\text{Si}^{107}\text{Ag}} = 514.3$  Hz).

**MS** (ESI<sup>+</sup>)  $m/z$  calcd: 871.80;  $m/z$  found: 871.4

**Elemental analysis:** Sufficient elemental analysis could not be obtained due to high light sensitivity.

**M.P.:** 254.6 °C (decomposition)

### Procedure for the isolation of $[\text{bis}^{\text{Et}}\text{-NHI}^{\text{Mes}}\text{-SiCl(AuCl)]\text{Cl}$ (**P15**)



3 ml of MeCN was added to a mixture of **P1** (80 mg, 0.10 mmol) and  $\text{Me}_2\text{SAuCl}$  (30.9 mg, 0.10 mmol, 1 eq.) in one portion at r.t. and the mixture was stirred for 1 h. Minor amount of insoluble residue was separated by filtration and the solution was evaporated under reduced pressure to yield the crude product as a slightly violet solid. The product was washed with 0.5 ml of toluene and dried in fine vacuum to obtain 92.0 mg (88%) of **P15** as a colorless solid.

**$^1\text{H}$  NMR** (500.1 MHz,  $\text{CD}_3\text{CN}$ ):  $\delta$  [ppm] = 7.13 (s, 4H, NCH), 7.09 (s, 4H, MesH-3,5), 7.02 (s, 4H, MesH-3,5), 3.14 (m, 2H  $\text{C}_2\text{H}_4$ ), 2.86 (m, 2H,  $\text{C}_2\text{H}_4$ ), 2.38 (s, 12H, Mes- $\text{CH}_3$ ), 2.16 (s, 12H, Mes- $\text{CH}_3$ ), 2.01 (s, 12H, Mes- $\text{CH}_3$ ).

**$^{13}\text{C}\{^1\text{H}\}$  NMR** (125.8 MHz,  $\text{CD}_3\text{CN}$ ):  $\delta$  [ppm] = 146.29 (NCN), 142.13 (MesC-1), 136.27 (MesC-2,6), 136.16 (MesC-2,6), 131.75 (MesC-4), 131.14 (MesC-3,5), 130.95 (MesC-3,5), 122.32 (NCH), 48.44 ( $\text{C}_2\text{H}_4$ ), 21.31 (p-Mes $\text{CH}_3$ ), 19.21 (o-Mes $\text{CH}_3$ ), 18.95 (o-Mes $\text{CH}_3$ ).

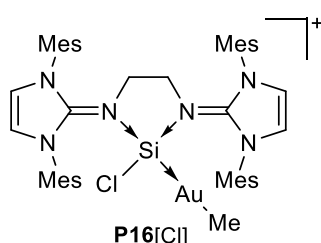
**$^{29}\text{Si}$  NMR** (99.4 MHz,  $\text{CD}_3\text{CN}$ ):  $\delta$  [ppm] = 18.20.

**MS** (ESI<sup>+</sup>)  $m/z$  calcd: 959.31;  $m/z$  found: 959.2

**Elemental analysis:** [994.28] calcd: C 53.04, H 5.26, N 8.44; found: C 50.75, H 5.11, N 8.06. (Consistently low C values can be explained by the formation of silicon carbide.)

**M.P.:** 172.6 °C (decomposition)

### Procedure for the isolation of [bis<sup>Et</sup>-NHI<sup>Mes</sup>-SiCl(AuMe)]Cl (**P16**)



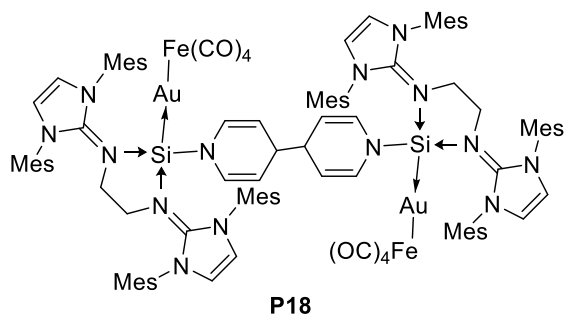
3 ml of MeCN was added to a mixture of **P1** (100 mg, 0.13 mmol) and PPh<sub>3</sub>AuMe (62.1 mg, 0.13 mmol, 1 eq.) at r.t. and the mixture was stirred for 3 h. The solution was evaporated under reduced to yield the crude product as an off-white solid. The product was washed with 2x1 ml of toluene to remove PPh<sub>3</sub> and dried in fine vacuum to obtain 94.7 mg (74%) of **P16** as a colorless solid.

**<sup>1</sup>H NMR** (500.1 MHz, CD<sub>3</sub>CN): δ [ppm] = 7.07 (s, 4H, Mes<sub>H</sub>-3,5), 7.06 (s, 4H, NCH), 6.98 (s, 4H, Mes<sub>H</sub>-3,5), 3.13 (m, 2H C<sub>2</sub>H<sub>4</sub>), 2.83 (m, 2H, C<sub>2</sub>H<sub>4</sub>), 2.37 (s, 12H, Mes-CH<sub>3</sub>), 2.19 (s, 12H, Mes-CH<sub>3</sub>), 2.01 (s, 12H, Mes-CH<sub>3</sub>), -0.16 (s, 3H, AuCH<sub>3</sub>).

**<sup>13</sup>C{<sup>1</sup>H} NMR** (125.8 MHz, CD<sub>3</sub>CN): δ [ppm] = 147.20 (NCN), 141.61 (MesC-1), 136.38 (MesC-2,6), 136.16 (MesC-2,6), 132.01 (MesC-4), 130.83 (MesC-3,5), 130.73 (MesC-3,5), 121.80 (NCH), 48.65 (C<sub>2</sub>H<sub>4</sub>), 21.24 (MesCH<sub>3</sub>), 19.03 (MesCH<sub>3</sub>), 18.78 (MesCH<sub>3</sub>), 15.57 (AuCH<sub>3</sub>).

**<sup>29</sup>Si NMR** (99.4 MHz, CD<sub>3</sub>CN): δ [ppm] = 76.19.

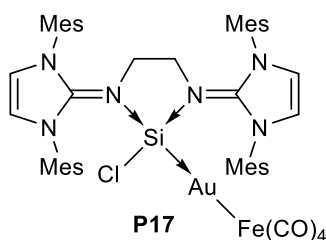
### Procedure for the isolation of [bis<sup>Et</sup>-NHI<sup>Mes</sup>SiAuFe]<sub>2</sub>-4,4'-bipyr (**P18**)



0.4 ml of THF-d<sub>8</sub> was added to a mixture of **P17** (15 mg, 0.014 mmol) and Li[MoCp(CO)<sub>2</sub>PMe<sub>3</sub>] (5.0 mg, 0.017 mmol, 1.2 eq.) at r.t. and the mixture was left at 60°C for 72 h. After addition of several drops of pyr-d<sub>5</sub> the redish-brown suspension was left at 60°C for 16 h. After cooling to r.t. several single crystals of **P18** were collected from the glass wall of the NMR tube.

**NMR:** No reaction could be detected from the solution in thf-d<sub>8</sub> that showed only starting material Li[MoCp(CO)<sub>2</sub>PMe<sub>3</sub>]. Upon alternating the NMR solvent to pyr-d<sub>5</sub> an ill-defined mixture was detected.

### Procedure for the isolation of bis<sup>Et</sup>-NHI<sup>Mes</sup>-SiClAuFe(CO)<sub>4</sub> (**P17**)



4 ml of MeCN was added to a mixture of **P1** (100 mg, 0.13 mmol) and PPh<sub>3</sub>AuCl (64.8 mg, 0.13 mmol, 1 eq.) in one portion at r.t. and the mixture was stirred for 30 min under the exclusion of light. The stirring solution is cooled to -30 °C and K<sub>2</sub>Fe(CO)<sub>4</sub> (32.2 mg, 0.13 mmol, 1 eq.) suspended in 2 ml MeCN is added expeditiously dropwise. The mixture was allowed to warm to r.t. and stirred for additional 10 min. Precipitated KCl was separated from the yellow solution by filtration. The filtrate was concentrated under reduced pressure to ca. 2 ml. The product solution was stored at +5 °C over 2 days to yield **P17** as yellow crystals. The Product was separated from the mother liquor and dried in fine vacuum to obtain 80 mg (56%) of **P17** as a yellow crystalline solid. X-ray quality crystals of **P17** were obtained from a concentrated MeCN solution after 2 days.

<sup>1</sup>H NMR (500.1 MHz, pyr-d<sub>5</sub>): δ [ppm] = 7.36 (s, 4H, NCH), 6.78 (s, 4H, MesH-3,5), 6.70 (s, 4H, MesH-3,5), 3.38 (m, 2H C<sub>2</sub>H<sub>4</sub>), 2.94 (m, 2H, C<sub>2</sub>H<sub>4</sub>), 2.58 (s, 12H, Mes-CH<sub>3</sub>), 2.36 (s, 12H, Mes-CH<sub>3</sub>), 2.19 (s, 12H, Mes-CH<sub>3</sub>).

<sup>13</sup>C{<sup>1</sup>H} NMR (125.8 MHz, pyr-d<sub>5</sub>): δ [ppm] = 228.95 (CO), 147.52 (NCN), 140.75 (MesC-1), 136.20 (MesC-2,6), 132.36 (MesC-4), 130.96 (MesC-3,5), 130.25 (MesC-3,5), 121.70 (NCH), 48.49 (C<sub>2</sub>H<sub>4</sub>), 21.54 (p-MesCH<sub>3</sub>), 19.36 (o-MesCH<sub>3</sub>), 19.26 (o-MesCH<sub>3</sub>).

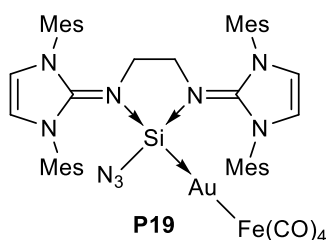
<sup>29</sup>Si NMR (99.4 MHz, pyr-d<sub>5</sub>): δ [ppm] = 67.56.

IR (ATR, neat) [cm<sup>-1</sup>]: ν(CO) = 1924, 1835, 1811, 1796.

**Elemental analysis:** [1092.25] calcd: C 52.73, H 4.79, N 7.69; found: C 51.37, H 5.06, N 7.71. (Consistently low C values can be explained by the formation of silicon carbide.)

**M.P.:** 155.8 °C (decomposition, color change to dark brown)

### Procedure for the isolation of bis<sup>Et</sup>-NHI<sup>Mes</sup>-SiN<sub>3</sub>AuFe(CO)<sub>4</sub> (**P19**)



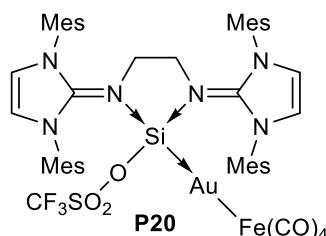
5 ml of MeCN was added to a mixture of **P17** (100 mg, 0.09 mmol) and NaN<sub>3</sub> (11.9 mg, 0.18 mmol, 2 eq.) in one portion at r.t. and the mixture was stirred at 60°C for 72 h. During this time the suspension turned into a dark yellow solution. Filtration of with precipitate (NaCl) and evaporation under reduced pressure afforded 74 mg (73%) of **P19** as a yellow powder.

<sup>1</sup>H NMR (500.1 MHz, CD<sub>3</sub>CN): δ [ppm] = 7.03 (s, 4H, MesH-3,5), 6.98 (s, 4H, MesH-3,5), 6.95 (s, 4H, NCH), 2.96 (m, 2H C<sub>2</sub>H<sub>4</sub>), 2.63 (m, 2H, C<sub>2</sub>H<sub>4</sub>), 2.39 (s, 12H, Mes-CH<sub>3</sub>), 2.33 (s, 12H, Mes-CH<sub>3</sub>), 2.12 (s, 12H, Mes-CH<sub>3</sub>).

<sup>13</sup>C{<sup>1</sup>H} NMR (125.8 MHz, CD<sub>3</sub>CN): δ [ppm] = 228.22 (CO), 147.68 (NCN), 141.52 (MesC-1), 136.52 (MesC-2,6), 136.26 (MesC-2,6), 132.10 (MesC-4), 131.17 (MesC-3,5), 130.33 (MesC-3,5), 121.53 (NCH), 48.84 (C<sub>2</sub>H<sub>4</sub>), 21.32 (MesCH<sub>3</sub>), 19.07 (MesCH<sub>3</sub>), 18.97 (MesCH<sub>3</sub>).

<sup>29</sup>Si NMR (99.4 MHz, CD<sub>3</sub>CN): δ [ppm] = 46.56.

### Procedure for the isolation of bis<sup>Et</sup>-NHI<sup>Mes</sup>-SiOTfAuFe(CO)<sub>4</sub> (**P20**)



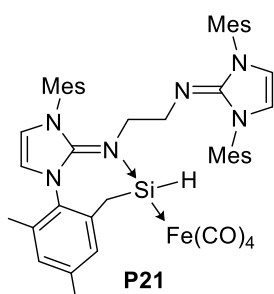
TfOTf (6.5 mg, 0.02 mmol, 1 eq.) or AgOTf (4.7 mg, 0.02 mmol, 1 eq.) was added to a solution of **P17** (20.0 mg, 0.02 mmol, 1 eq.) in 0.5 ml pyridine-d<sub>5</sub> at r.t.. The reaction mixture turn dark yellow with formation of precipitate. After separation of the (dark) precipitate, the NMR monitoring showed full conversion to **P20** as a dark yellow solution.

<sup>1</sup>H NMR (500.1 MHz, pyr-d<sub>5</sub>): δ [ppm] = 7.71 (s, 4H, NCH), 6.99 (s, 4H, MesH-3,5), 6.88 (s, 4H, MesH-3,5), 3.54 (m, 2H C<sub>2</sub>H<sub>4</sub>), 2.98 (m, 2H, C<sub>2</sub>H<sub>4</sub>), 2.53 (s, 12H, Mes-*p*-CH<sub>3</sub>), 2.33 (s, 24H, Mes-*o*-CH<sub>3</sub>).

<sup>13</sup>C{<sup>1</sup>H} NMR (125.8 MHz, pyr-d<sub>5</sub>): δ [ppm] = 221.48 (CO), 147.13 (NCN), 141.24 (MesC-1), 134.58 (MesC-2,6), 134.43 (MesC-2,6), 132.40 (MesC-4), 131.00 (MesC-3,5), 130.62 (MesC-3,5), 129.51 (CF<sub>3</sub>), 122.55 (NCH), 49.27 (C<sub>2</sub>H<sub>4</sub>), 21.70 (MesCH<sub>3</sub>), 19.57 (MesCH<sub>3</sub>), 19.21 (MesCH<sub>3</sub>).

<sup>29</sup>Si NMR (99.4 MHz, pyr-d<sub>5</sub>): δ [ppm] = 47.15

### Procedure for the isolation of bis<sup>Et</sup>-NHIMesHSiFe(CO)<sub>4</sub> (**P21**)



4 ml of DME was added to a mixture of **P1** (80 mg, 0.10 mmol) and K<sub>2</sub>Fe(CO)<sub>4</sub> (25.8 mg, 0.10 mmol, 1 eq.) in one portion at 0°C. The reaction mixture was kept at 0°C for 1 h and additionally stirred at r.t. for 72 h. Colorless precipitate was filtered off and the pale solution was concentrated to 0.7 ml under reduced pressure (start of product crystallization). Precipitation was completed after 5 h at -33°C, when the product was collected from the liquor, washed with 0.7 ml Et<sub>2</sub>O and dried in fine vacuum to obtain 49 mg (54%) of **P21** as colorless crystals.

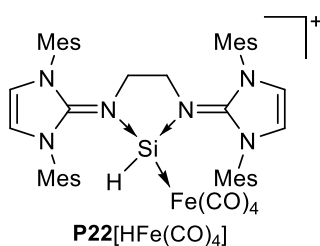
**<sup>1</sup>H NMR** (500.1 MHz, C<sub>6</sub>D<sub>6</sub>): δ [ppm] = 7.30 (s, 1H, MesH), 6.93 (s, 1H, MesH), 6.70 (s, 2H, MesH), 6.66 (s, 1H, MesH), 6.55 (s, 1H, SiH), 6.50 (s, 1H, MesH), 6.33 (s, 1H, MesH), 5.50 (d, 1H, NCH) 5.50 (s, 2H, NCH), 5.30 (d, 1H, NCH), 3.32 (m, 2H SiCH<sub>2</sub>), 2.68 (m, 2H, C<sub>2</sub>H<sub>4</sub>), 2.51 (d, 2H, C<sub>2</sub>H<sub>4</sub>), 2.28 (s, 6H, MesCH<sub>3</sub>), 2.25 (s, 6H, MesCH<sub>3</sub>), 2.12 (s, 3H, MesCH<sub>3</sub>), 2.11 (s, 3H, MesCH<sub>3</sub>), 2.09 (s, 3H, MesCH<sub>3</sub>), 2.02 (s, 3H, MesCH<sub>3</sub>), 1.84 (s, 3H, MesCH<sub>3</sub>), 1.75 (s, 3H, MesCH<sub>3</sub>).

**<sup>13</sup>C{<sup>1</sup>H} NMR** (125.8 MHz, C<sub>6</sub>D<sub>6</sub>): δ [ppm] = 217.89 (CO), 149.43 (NCN), 143.10 (NCN), 140.20 (MesC), 139.65 (MesC), 138.02 (MesC), 135.11 (MesC), 134.99 (MesC), 134.55 (MesC), 132.19 (MesC), 131.97 (MesC), 130.29 (MesC), 130.19 (MesC), 129.96 (MesC), 129.20 (MesC), 128.56 (MesC), 118.31 (NCH), 117.47 (NCH), 50.93 (C<sub>2</sub>H<sub>4</sub>), 46.68 (C<sub>2</sub>H<sub>4</sub>), 25.39 (SiCH<sub>2</sub>), 21.26 (MesCH<sub>3</sub>), 21.23 (MesCH<sub>3</sub>), 21.13 (MesCH<sub>3</sub>), 18.38 (MesCH<sub>3</sub>), 18.07 (MesCH<sub>3</sub>), 18.03 (MesCH<sub>3</sub>), 17.64 (MesCH<sub>3</sub>), 17.36 (MesCH<sub>3</sub>).

**<sup>29</sup>Si NMR** (99.4 MHz, C<sub>6</sub>D<sub>6</sub>): δ [ppm] = 68.20.

**MS** (LIFDI) *m/z* calcd: 861.32; *m/z* found: 861.32.

### Procedure for the isolation of [bis<sup>Et</sup>-NHI<sup>Mes</sup>-SiH(Fe(CO)<sub>4</sub>)]HFe(CO)<sub>4</sub> (**P22**)



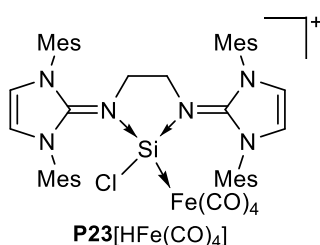
1.5 ml of MeCN was added to a mixture of **P1** (60 mg, 0.08 mmol) and NH<sub>3</sub>BH<sub>3</sub> (3.6 mg, 0.12 mmol, 1.5 eq.) and the mixture was stirred for 5 min. The solution was added to K<sub>2</sub>Fe(CO)<sub>4</sub> (19.3 mg, 0.08 mmol, 1 eq.) in one portion at r.t. and stirred for 45 min. All insoluble material was filtered off and the orange filtrate was evaporated under reduced pressure, to yield 43 mg (63%) of **P22** as a slight orange powder.

<sup>1</sup>H NMR (500.1 MHz, CD<sub>3</sub>CN): δ [ppm] = 7.05 (s, 4H, MesH-3,5), 7.01 (s, 4H, MesH-3,5), 6.90 (s, 4H, NCH), 4.68 (s, 1H, SiH), 3.04 (m, 2H C<sub>2</sub>H<sub>4</sub>), 2.77 (m, 2H, C<sub>2</sub>H<sub>4</sub>), 2.34 (s, 12H, Mes-CH<sub>3</sub>), 2.13 (s, 12H, Mes-CH<sub>3</sub>), 2.09 (s, 12H, Mes-CH<sub>3</sub>).

<sup>13</sup>C{<sup>1</sup>H} NMR (125.8 MHz, CD<sub>3</sub>CN): δ [ppm] = 221.99 (CO), 221.95 (CO), 217.79 (CO), 146.91 (NCN), 141.81 (MesC-1), 136.68 (MesC-2,6), 136.45 (MesC-2,6), 132.46 (MesC-4), 131.09 (MesC-3,5), 130.71 (MesC-3,5), 121.25 (NCH), 46.79 (C<sub>2</sub>H<sub>4</sub>), 21.22 (MesCH<sub>3</sub>), 18.77 (MesCH<sub>3</sub>), 18.64 (MesCH<sub>3</sub>).

<sup>29</sup>Si NMR (99.4 MHz, CD<sub>3</sub>CN): δ [ppm] = 54.40.

### Procedure for the isolation of [bis<sup>Et</sup>-NHI<sup>Mes</sup>-SiCl(Fe(CO)<sub>4</sub>)]HFe(CO)<sub>4</sub> (**P23**)



15 ml of THF was added to a mixture of **P4** (292 mg, 0.35 mmol) and K<sub>2</sub>Fe(CO)<sub>4</sub> (172 mg, 0.70 mmol, 2 eq.) in one portion at -78°C. The suspension was allowed to slowly warm to r.t. over 72 h. All volatiles were evaporated from the reaction mixture and the yellow product solution was extracted with 10 ml benzene. Freeze dry in fine vacuum afforded 195 mg (52%) of **P23** as a fine beige powder.

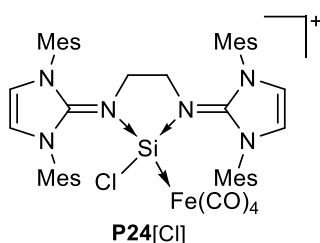
<sup>1</sup>H NMR (500.1 MHz, C<sub>6</sub>D<sub>6</sub>): δ [ppm] = 6.93 (s, 4H, MesH-3,5), 6.74 (s, 4H, MesH-3,5), 5.61 (s, 4H, NCH), 3.23 (m, 2H C<sub>2</sub>H<sub>4</sub>), 3.04 (m, 2H, C<sub>2</sub>H<sub>4</sub>), 2.20 (s, 12H, Mes-CH<sub>3</sub>), 2.15 (s, 12H, Mes-CH<sub>3</sub>), 2.09 (s, 12H, Mes-CH<sub>3</sub>), -7.92 (s, 1H, HFe).

<sup>13</sup>C{<sup>1</sup>H} NMR (125.8 MHz, C<sub>6</sub>D<sub>6</sub>): δ [ppm] = 222.68 (CO), 216.33 (CO), 147.52 (NCN), 141.41 (MesC-1), 135.47 (MesC-2,6), 135.26 (MesC-2,6), 132.33 (MesC-4), 131.30 (MesC-3,5), 130.69 (MesC-3,5), 120.68 (NCH), 48.27 (C<sub>2</sub>H<sub>4</sub>), 21.11 (MesCH<sub>3</sub>), 19.25 (MesCH<sub>3</sub>), 18.70 (MesCH<sub>3</sub>).

<sup>29</sup>Si NMR (99.4 MHz, C<sub>6</sub>D<sub>6</sub>): δ [ppm] = 52.42.

MS (ESI<sup>+</sup>) *m/z* calcd: 895.28; *m/z* found: 895.4.

### Procedure for the isolation of [bis<sup>Et</sup>-NHI<sup>Mes</sup>-SiCl(Fe(CO)<sub>4</sub>)]Cl (**P24**)

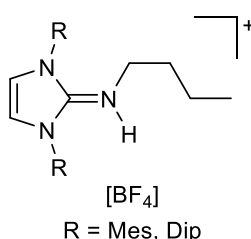


1 ml of DME was added to a mixture of **P4** (50 mg, 0.06 mmol) and K<sub>2</sub>Fe(CO)<sub>4</sub> (29.5 mg, 0.12 mmol, 2 eq.) at r.t.. The slurry suspension was stirred for 48 h upon the color changes to red-orange. 0.5 ml of toluene is added to complete precipitation of the orange product. The product is separated *via* filtration and dried in fine vacuum to obtain 38.0 mg (68%) of **P24** as an orange solid.

<sup>1</sup>H NMR (500.1 MHz, CD<sub>3</sub>CN): δ [ppm] = 7.10 (s, 4H, NCH), 7.05 (s, 4H, MesH-3,5), 7.01 (s, 4H, MesH-3,5), 2.93 (m, 2H C<sub>2</sub>H<sub>4</sub>), 2.83 (m, 2H, C<sub>2</sub>H<sub>4</sub>), 2.33 (s, 12H, Mes-CH<sub>3</sub>), 2.18 (s, 12H, Mes-CH<sub>3</sub>), 2.12 (s, 12H, Mes-CH<sub>3</sub>).

<sup>29</sup>Si NMR (99.4 MHz, CD<sub>3</sub>CN): δ [ppm] = 50.19.

### Procedure for the isolation of NHI<sup>nBu</sup>H BF<sub>4</sub><sup>[41]</sup>



8 ml MeCN were added to a mixture of [IRCl][BF<sub>4</sub>] (R = Mes; (2-chloro-1,3-dimesitylimidazolium tetrafluoroborate, 600 mg, 1.4 mmol, 1 eq. | R = Dip; (2-chloro-1,3-di(2,6-diisopropylphenyl)imidazolium tetrafluoroborate, 700 mg, 1.4 mmol, 1 eq.) and KF (478 mg, 8.2 mmol, 6 eq.). NEt<sub>3</sub> (0.6 ml, 4.1 mmol, 3 eq.) was added, followed by *n*-Butylamine (100 mg, 1.4 mmol, 1 eq.). The reaction mixture is stirred for 24 h at r.t., after that

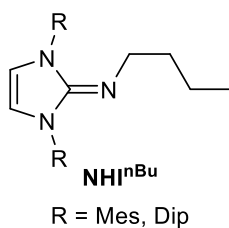
8 ml chloroform were added under air and insoluble remains were filtered off. The filtrate was washed with 8 ml 2M NaBF<sub>4</sub> (aq.). The organic layer was dried with Na<sub>2</sub>SO<sub>4</sub>, filtered and evaporated under reduced pressure, yielding NHI<sup>nBu</sup>H BF<sub>4</sub> (<sup>Mes</sup>NHI<sup>nBu</sup>H BF<sub>4</sub>: 393 mg (60%) | <sup>Dip</sup>NHI<sup>nBu</sup>H BF<sub>4</sub>: 560 mg (77%)) as colorless powder.

#### <sup>Mes</sup>NHI<sup>nBu</sup>H BF<sub>4</sub>

<sup>1</sup>H NMR (400.1 MHz, C<sub>6</sub>D<sub>6</sub>): δ [ppm] = 7.08 (s, 4H, MesH-3,5), 6.70 (s, 2H, NCH), 5.45 (s, 1H, NH), 2.61 (t, 2H, NCH<sub>2</sub>CH<sub>2</sub>CH<sub>2</sub>CH<sub>3</sub>), 2.34 (s, 6H, Mes-CH<sub>3</sub>), 2.17 (s, 12H, Mes-CH<sub>3</sub>), 1.08 (m, 2H, NCH<sub>2</sub>CH<sub>2</sub>CH<sub>2</sub>CH<sub>3</sub>), 0.93 (m, 2H, NCH<sub>2</sub>CH<sub>2</sub>CH<sub>2</sub>CH<sub>3</sub>), 0.64 (t, 3H, NCH<sub>2</sub>CH<sub>2</sub>CH<sub>2</sub>CH<sub>3</sub>).

#### <sup>Dip</sup>NHI<sup>nBu</sup>H BF<sub>4</sub>

<sup>1</sup>H NMR (400.1 MHz, C<sub>6</sub>D<sub>6</sub>): δ [ppm] = 7.64 (t, 2H, Dip-*p*-), 7.46 (d, 4H, Dip-*m*-H), 7.12 (s, 2H, NCH), 6.00 (br, 1H, NH), 3.14 (q, 2H NCH<sub>2</sub>CH<sub>2</sub>CH<sub>2</sub>CH<sub>3</sub>), 2.64 (sep, 4H, Dip-CH), 1.29 (d, 12H, Dip-C-CH<sub>3</sub>), 1.24 (d, 12H, Dip-C-CH<sub>3</sub>), 1.11 (m, 2H, NCH<sub>2</sub>CH<sub>2</sub>CH<sub>2</sub>CH<sub>3</sub>), 0.88 (m, 2H, NCH<sub>2</sub>CH<sub>2</sub>CH<sub>2</sub>CH<sub>3</sub>), 0.59 (t, 3H, NCH<sub>2</sub>CH<sub>2</sub>CH<sub>2</sub>CH<sub>3</sub>).

**Procedure for the isolation of  $\text{NHI}^{\text{nBu}}$ <sup>[41]</sup>**

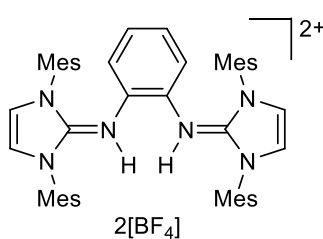
A solution of  $[\text{R}^{\text{nBu}}\text{NHI}][\text{BF}_4]$  (R = Mes, 419 mg, 0.9 mmol, 1 eq. | R = Dip, 500 mg, 0.9 mmol, 1 eq.) in 10 ml THF was treated dropwise with KOtBu (113 mg, 1.0 mmol, 1.1 eq.) in 3 ml THF at 0°C. The milky mixture was warmed to r.t. and stirred for 2 h. The insoluble material was filtered off and washed with 2 ml THF. Volatiles were removed under reduced pressure to afford  $\text{NHI}^{\text{nBu}}$  (Mes $\text{NHI}^{\text{nBu}}$ : 301 mg (80%) | Dip $\text{NHI}^{\text{nBu}}$ : 309 mg (74%) as beige powder.

**Mes $\text{NHI}^{\text{nBu}}$** 

$^1\text{H NMR}$  (400.1 MHz,  $\text{C}_6\text{D}_6$ ):  $\delta$  [ppm] = 6.73 (s, 4H, Mes $H$ -3,5), 6.42 (m, 2H, NCH), 2.71 (m, 2H,  $\text{NCH}_2\text{C}_3\text{H}_7$ ), 2.09 (s, 6H, Mes- $\text{CH}_3$ ), 2.01 (s, 12H, Mes- $\text{CH}_3$ ), 1.16 (m, 2H,  $\text{NCH}_2\text{CH}_2\text{C}_2\text{H}_5$ ), 0.81 (m, 2H,  $\text{NC}_2\text{H}_4\text{CH}_2\text{CH}_3$ ), 0.53 (m, 3H,  $\text{NC}_2\text{H}_6\text{CH}_3$ ).

**Dip $\text{NHI}^{\text{nBu}}$** 

$^1\text{H NMR}$  (400.1 MHz,  $\text{C}_6\text{D}_6$ ):  $\delta$  [ppm] = 7.20 (t, 2H, Dip), 7.10 (d, 4H, Dip $H$ -3,5), 5.81 (s, 2H, NCH), 3.35 (sep, 4H, Dip- $\text{CH}$ ), 2.88 (t, 2H,  $\text{NCH}_2\text{C}_3\text{H}_7$ ), 1.40 (d, 12H, Dip-C- $\text{CH}_3$ ), 1.32 (m, 2H,  $\text{NCH}_2\text{CH}_2\text{C}_2\text{H}_5$ ), 1.23 (d, 12H, Dip-C- $\text{CH}_3$ ), 1.19 (m, 2H,  $\text{NC}_2\text{H}_4\text{CH}_2\text{CH}_3$ ), 0.69 (t, 3H,  $\text{NC}_3\text{H}_6\text{CH}_3$ ).

**Procedure for the isolation of bis $^{\text{Ph}}\text{-NHI}^{\text{Mes}}\text{H}_2 \text{BF}_4$  ( $[\text{POAH}_2]_2[\text{BF}_4]$ )<sup>[41]</sup>**

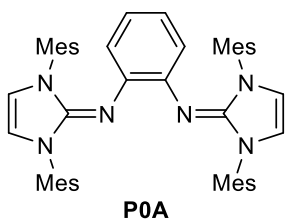
25 ml MeCN were added to a mixture of  $[\text{IMesCl}][\text{BF}_4]$  (2-chloro-1,3-dimesitylenimidazolium tetrafluoroborate, 1.5 g, 3.5 mmol, 2 eq.) and KF (613 mg, 10.6 mmol, 6 eq.).  $\text{NEt}_3$  (0.7 ml, 5.3 mmol, 3 eq.) were added, followed by 1,2-phenylenediamine (190 mg, 1.8 mmol, 1 eq.). The reaction mixture was stirred for 48 h, after that

25 ml chloroform were added under air and insoluble remains were filtered off. The filtrate was washed with 12 ml 5% NaOH (aq.) and 12 ml 2M  $\text{NaBF}_4$  (aq.). The organic layer was dried with  $\text{Na}_2\text{SO}_4$ , filtered and evaporated under reduced pressure. The brown residue was taken up in chloroform. Precipitation with  $\text{Et}_2\text{O}$ , yielded 375 mg (24%) of  $[\text{POAH}_2]_2[\text{BF}_4]$  as colorless crystals after isolation and drying.

$^1\text{H NMR}$  (400.1 MHz,  $\text{CDCl}_3$ ):  $\delta$  [ppm] = 6.78 (s, 4H, NCH), 6.77 (s, 8H, Mes $H$ -3,5), 5.98 (s, 4H,  $\text{C}_6\text{H}_4$ ), 2.22 (s, 12H, Mes- $\text{CH}_3$ ), 1.94 (s, 24H, Mes- $\text{CH}_3$ ).

$^{13}\text{C}\{^1\text{H}\}$  NMR (101 MHz,  $\text{CDCl}_3$ ):  $\delta$  [ppm] = 143.77 (NCN), 139.75 (MesC-1), 134.90 (MesC-2,6), 130.84 (MesC-4), 129.89 ( $\text{C}^{\text{Ar}}$ -1,2), 129.50 (MesC-3,5), 120.59 ( $\text{C}^{\text{Ar}}$ -3,6), 118.25 ( $\text{C}^{\text{Ar}}$ -4,5), 117.51 (NCH), 21.03 (Mes $\text{CH}_3$ ), 17.75 (Mes $\text{CH}_3$ ).

### Procedure for the isolation of bis<sup>Ph</sup>-NHI<sup>Mes</sup> (**P0A**)<sup>[41]</sup>

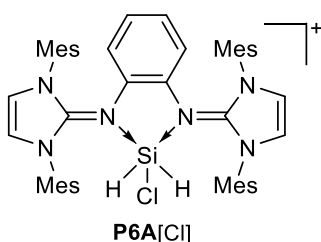


A solution of [P0AH<sub>2</sub>]<sub>2</sub>[BF<sub>4</sub>]<sub>2</sub> (1.5 g, 1.7 mmol, 1 eq.) in 15 ml *o*-DFB was treated dropwise with KHMDS (707 mg, 3.5 mmol, 2.1 eq.) in 15 ml *o*-DFB at 0°C. The dark mixture was warmed to r.t. and stirred for 2 h. Volatiles were removed under reduced pressure, and the product was extracted with 2x15 ml hexane. After solvent removal, 1.15 g (96%) of **P0A** as brownish foam was obtained.

<sup>1</sup>H NMR (400.1 MHz, C<sub>6</sub>D<sub>6</sub>): δ [ppm] = 6.68 (s, 8H, Mes*H*-3,5), 6.36 (m, 2H, C<sub>6</sub>H<sub>4</sub>), 6.22 (m, 2H, C<sub>6</sub>H<sub>4</sub>), 5.67 (s, 4H, NCH), 2.24 (s, 24H, Mes-CH<sub>3</sub>), 2.08 (s, 12H, Mes-CH<sub>3</sub>).

<sup>13</sup>C{<sup>1</sup>H} NMR (101 MHz, C<sub>6</sub>D<sub>6</sub>): δ [ppm] = 143.37 (NCN), 142.68 (MesC-1), 136.77 (MesC-2,6), 134.78 (C<sup>Ar</sup>-1,2), 129.15 (MesC-4), 128.79 (MesC-3,5), 121.33 (C<sup>Ar</sup>-3,6), 118.90 (C<sup>Ar</sup>-4,5), 113.61 (NCH), 21.03 (MesCH<sub>3</sub>), 18.66 (MesCH<sub>3</sub>).

### Procedure for the isolation of [bis<sup>Ph</sup>-NHI<sup>Mes</sup>SiH<sub>2</sub>Cl]<sup>+</sup>Cl<sup>-</sup> (**P6A**)

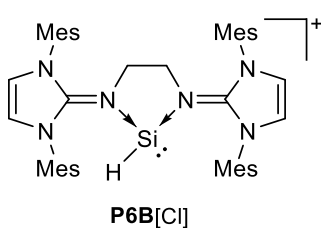


**P0A** (150 mg, 0.21 mmol) was dissolved in 3 ml of toluene and treated dropwise with a 37 wt% H<sub>2</sub>SiCl<sub>2</sub> in toluene (58 mg, 0.21 mmol, 1 eq.) solution at -30°C. The rapidly formed precipitate was stirred for 1 h at r.t. and separated afterwards. The isolated solid was washed with 1 ml toluene and subsequently dried in fine vacuum to afford 146 mg (89%) **P6A** as off-white solid.

<sup>1</sup>H NMR (400.1 MHz, CD<sub>3</sub>CN): δ [ppm] = 7.38 (s, 4H, NCH), 6.95 (s, 4H, Mes*H*-3,5), 6.90 (s, 4H, Mes*H*-3,5), 6.31 (m, 2H, C<sub>6</sub>H<sub>4</sub>), 6.17 (m, 2H, C<sub>6</sub>H<sub>4</sub>), 4.79 (s, 2H, SiH<sub>2</sub>Cl), 2.27 (s, 12H, Mes-CH<sub>3</sub>), 2.12 (s, 12H, Mes-CH<sub>3</sub>), 2.03 (s, 12H, Mes-CH<sub>3</sub>).

<sup>29</sup>Si NMR (99.4 MHz, CD<sub>3</sub>CN): δ [ppm] = -104.66.

### Procedure for the isolation of [bis<sup>Et</sup>-NHI<sup>Mes</sup>SiH]Cl (P6B)



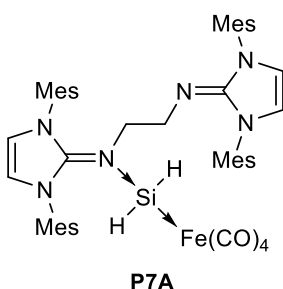
0.4 ml of pre-cooled CD<sub>3</sub>CN were added to a mixture of **P6** (20 mg, 0.03 mmol) and KO<sup>t</sup>Bu (2.9 mg, 0.03 mmol, 1 eq.). The yellow suspension was filtered after 30 min and the NMR monitoring showed selective formation of **P6B** and HO<sup>t</sup>Bu.

<sup>1</sup>H NMR (500.1 MHz, CD<sub>3</sub>CN): δ [ppm] = 6.99 (s, 8H, MesH-3,5), 6.52 (s, 4H, NCH), 4.59 (s, 1H, SiH), 2.34 (s, 12H, Mes-CH<sub>3</sub>), 2.26 (s, 4H C<sub>2</sub>H<sub>4</sub>), 2.00 (s, 24H, Mes-CH<sub>3</sub>).

<sup>13</sup>C{<sup>1</sup>H} NMR (125.8 MHz, CD<sub>3</sub>CN): δ [ppm] = 144.85 (NCN), 140.51 (MesC-1), 137.11 (MesC-2,6), 132.53 (MesC-4), 129.98 (MesC-3,5), 129.84 (MesC-3,5), 126.18 (NCH), 46.01 (C<sub>2</sub>H<sub>4</sub>), 31.57 (MesCH<sub>3</sub>), 21.16 (MesCH<sub>3</sub>).

<sup>29</sup>Si NMR (99.4 MHz, CD<sub>3</sub>CN): δ [ppm] = -51.38.

### Procedure for the isolation of bis<sup>Et</sup>-NHI<sup>Mes</sup>SiH<sub>2</sub>Fe(CO)<sub>4</sub> (P7A)



A solution of **P7** (20 mg, 0.02 mmol) in 0.4 ml of CD<sub>3</sub>CN was treated with K<sub>2</sub>Fe(CO)<sub>4</sub> (5 mg, 0.02 mmol, 1 eq.) at r.t.. After 2 h and separation of colorless precipitate the orange solution showed selective formation of **P7A** in NMR monitoring.

<sup>1</sup>H NMR (500.1 MHz, CD<sub>3</sub>CN): δ [ppm] = 6.95 (s, 4H, MesH-3,5), 6.93 (s, 4H, MesH-3,5), 6.87 (s, 2H, NCH), 6.16 (br, 2H, NCH), 4.45 (s, 2H, SiH<sub>2</sub>), 2.89 (m, 2H, C<sub>2</sub>H<sub>4</sub>), 2.66 (m, 2H, C<sub>2</sub>H<sub>4</sub>), 2.32 (s, 6H, Mes-CH<sub>3</sub>), 2.30 (s, 6H, Mes-CH<sub>3</sub>), 2.13 (s, 12H, Mes-CH<sub>3</sub>), 2.06 (s, 12H, Mes-CH<sub>3</sub>).

<sup>13</sup>C{<sup>1</sup>H} NMR (125.8 MHz, CD<sub>3</sub>CN): δ [ppm] = 224.95 (CO), 221.90 (CO), 217.49 (CO), 150.40 (NCN), 144.33 (NCN), 141.14 (MesC-1), 136.29 (MesC-2,6), 132.90 (MesC-4), 130.34 (MesC), 129.80 (MesC), 129.11 (MesC), 126.14 (NCH), 120.55 (NCH), 53.55 (C<sub>2</sub>H<sub>4</sub>), 48.89 (C<sub>2</sub>H<sub>4</sub>), 21.14 (MesCH<sub>3</sub>), 21.04 (MesCH<sub>3</sub>), 18.48 (MesCH<sub>3</sub>), 18.11 (MesCH<sub>3</sub>).

<sup>29</sup>Si NMR (99.4 MHz, CD<sub>3</sub>CN): δ [ppm] = 30.34.

**MS** (LIFDI) *m/z* calcd: 861.32; *m/z* found: 861.33

**Procedure for the Reaction of P17 with C<sub>2</sub>Cl<sub>6</sub> (P17A)**

A solution of **P17** (20 mg, 0.02 mmol) in 0.4 ml of CD<sub>3</sub>CN was treated with C<sub>2</sub>Cl<sub>6</sub> (4.3 mg, 0.02 mmol, 1 eq.) at r.t.. After 10 min the formerly colorless solution turned yellow upon dissolution of **P17**. <sup>1</sup>H and <sup>29</sup>Si NMR monitoring of the reaction was carried out over 72 hours.

**Procedure for the Reaction of P17 with CH<sub>3</sub>I (P17B)**

A solution of **P17** (20 mg, 0.02 mmol) in 0.4 ml of CD<sub>3</sub>CN was treated with CH<sub>3</sub>I (2.6 mg, 0.02 mmol, 1 eq.) at r.t.. After 10 min the formerly colorless solution turned yellow upon dissolution of **P17**. <sup>1</sup>H and <sup>29</sup>Si NMR monitoring of the reaction was carried out over 72 hours.

**Procedure for the Reaction of P17 with TMSI (P17C)**

A solution of **P17** (20 mg, 0.02 mmol) in 0.4 ml of CD<sub>3</sub>CN was treated with TMSI (3.7 mg, 0.02 mmol, 1 eq.) at r.t.. After 30 min the formerly colorless solution turned yellow upon dissolution of **P17**. <sup>1</sup>H and <sup>29</sup>Si NMR monitoring of the reaction was carried out over 72 hours.

## 7 References

- [1] R. West, M. K. Fink, J. Michl, *Science* **1981**, *214*, 1343.
- [2] M. Yoshifuji, I. Shima, N. Inamoto, K. Hirotsu, T. Higuchi, *J. Am. Chem. Soc.* **1981**, *103*, 4587.
- [3] A. G. Brook, F. Abdesaken, B. Gutekunst, G. Gutekunst, R. K. Kallury, *J. Chem. Soc., Chem. Commun.* **1981**, 191.
- [4] P. Jutzi, *Angew. Chem., Int. Ed. Engl.* **1975**, *14*, 232.
- [5] a) R. S. Mulliken, *J. Am. Chem. Soc.* **1955**, *77*, 884; b) R. S. Mulliken, *J. Am. Chem. Soc.* **1950**, *72*, 4493; c) K. S. Pitzer, *J. Am. Chem. Soc.* **1948**, *70*, 2140.
- [6] B. E. Hoogenboom, *J. Chem. Educ.* **1998**, *75*, 596.
- [7] R. J. Gilliard, C.-W. Chiu, *Organometallics* **2020**, *39*, 4123.
- [8] P. P. Power, *Nature* **2010**, *463*, 171.
- [9] a) T. Chu, G. I. Nikonov, *Chem. Rev.* **2018**, *118*, 3608; b) C. Weetman, S. Inoue, *ChemCatChem* **2018**, *10*, 4213; c) J. M. Lipshultz, G. Li, A. T. Radosevich, *J. Am. Chem. Soc.* **2021**, *143*, 1699.
- [10] E. Fritz-Langhals, *Org. Process Res. Dev.* **2019**, *23*, 2369.
- [11] E. Fritz-Langhals, R. Weidner, WO2019068357.
- [12] a) D. Bourissou, O. Guerret, F. P. Gabbaï, G. Bertrand, *Chem. Rev.* **2000**, *100*, 39; b) A. J. Arduengo, R. Krafczyk, *Chemie Unserer Zeit* **1998**, *32*, 6.
- [13] A. Nemirowski, P. R. Schreiner, *J. Org. Chem.* **2007**, *72*, 9533.
- [14] G. Rouschias, B. L. Shaw, *J. Chem. Soc., A* **1971**, 2097.
- [15] a) D. J. Cardin, B. Cetinkaya, M. F. Lappert, *Chem. Rev.* **1972**, *72*, 545; b) K. H. Dötz, J. Stendel, *Chem. Rev.* **2009**, *109*, 3227.
- [16] E. O. Fischer, A. Maasböl, *Angew. Chem., Int. Ed. Engl.* **1964**, *76*, 645.
- [17] R. R. Schrock, P. R. Sharp, *J. Am. Chem. Soc.* **1978**, *100*, 2389.
- [18] "The Nobel Prize in Chemistry 2005. Nobel Prize Outreach AB 2021", can be found under <https://www.nobelprize.org/prizes/chemistry/2005/summary/>, **2021**.
- [19] V. P. W. Böhm, W. A. Herrmann, *Angew. Chem., Int. Ed. Engl.* **2000**, *39*, 4036.
- [20] A. Igau, H. Grutzmacher, A. Baceiredo, G. Bertrand, *J. Am. Chem. Soc.* **1988**, *110*, 6463.
- [21] A. J. Arduengo, R. L. Harlow, M. Kline, *J. Am. Chem. Soc.* **1991**, *113*, 361.
- [22] T. Dröge, F. Glorius, *Angew. Chem., Int. Ed. Engl.* **2010**, *122*, 7094.
- [23] W. A. Herrmann, *Angew. Chem., Int. Ed. Engl.* **2002**, *114*, 1342.
- [24] V. Nesterov, D. Reiter, P. Bag, P. Frisch, R. Holzner, A. Porzelt, S. Inoue, *Chem. Rev.* **2018**, *118*, 9678.
- [25] Y. Wang, Y. Xie, P. Wei, R. B. King, H. F. Schaefer, P. von R. Schleyer, G. H. Robinson, *Science* **2008**, *321*, 1069.
- [26] A. C. Filippou, Y. N. Lebedev, O. Chernov, M. Straßmann, G. Schnakenburg, *Angew. Chem., Int. Ed. Engl.* **2013**, *52*, 6974.
- [27] A. C. Filippou, O. Chernov, G. Schnakenburg, *Angew. Chem., Int. Ed. Engl.* **2009**, *48*, 5687.
- [28] R. S. Ghadwal, H. W. Roesky, S. Merkel, J. Henn, D. Stalke, *Angew. Chem., Int. Ed. Engl.* **2009**, *48*, 5683.
- [29] Y. Xiong, S. Yao, S. Inoue, J. D. Epping, M. Driess, *Angew. Chem., Int. Ed. Engl.* **2013**, *52*, 7147.
- [30] Y. Li, Y.-C. Chan, B.-X. Leong, Y. Li, E. Richards, I. Purushothaman, S. De, P. Parameswaran, C.-W. So, *Angew. Chem., Int. Ed. Engl.* **2017**, *56*, 7573.
- [31] N. Kuhn, R. Fawzi, M. Steimann, J. Wiethoff, D. Bläser, R. Boese, *Z. Naturforsch. B* **1995**, *50*, 1779.
- [32] W. Kolitsch, K. Dehnicke, *Z. Naturforsch. B* **1970**, *25*, 1080.
- [33] K. Dehnicke, *Coord. Chem. Rev.* **1997**, *158*, 103.
- [34] M. Tamm, S. Randoll, T. Bannenberg, E. Herdtweck, *Chem. Commun.* **2004**, 876.
- [35] K. Dehnicke, *Z. anorg. allg. Chem.* **2003**, *629*, 729.

- [36] J. Volbeda, P. G. Jones, M. Tamm, *Inorg. Chim. Acta* **2014**, *422*, 158.
- [37] T. Ochiai, D. Franz, S. Inoue, *Chem. Soc. Rev.* **2016**.
- [38] a) M. W. Lui, C. Merten, M. J. Ferguson, R. McDonald, Y. Xu, E. Rivard, *Inorg. Chem.* **2015**, *54*, 2040; b) D. Franz, T. Szilvasi, E. Irran, S. Inoue, *Nat. Commun.* **2015**, *6*; c) D. Franz, E. Irran, S. Inoue, *Dalton Trans.* **2014**, *43*, 4451; d) D. Franz, S. Inoue, *Chem. Eur. J.* **2014**, *20*, 10645; e) S. Inoue, K. Leszczyńska, *Angew. Chem., Int. Ed. Engl.* **2012**, *51*, 8589; f) D. Wendel, D. Reiter, A. Porzelt, P. J. Altmann, S. Inoue, B. Rieger, *J. Am. Chem. Soc.* **2017**, *139*, 17193.
- [39] D. Wendel, A. Porzelt, F. A. D. Herz, D. Sarkar, C. Jandl, S. Inoue, B. Rieger, *J. Am. Chem. Soc.* **2017**, *139*, 8134.
- [40] X. Wu, M. Tamm, *Coord. Chem. Rev.* **2014**, *260*, 116.
- [41] R. A. Kunetskiy, S. M. Polyakova, J. Vavřík, I. Císařová, J. Saame, E. R. Nerut, I. Koppel, I. A. Koppel, A. Kütt, I. Leito et al., *Chem. Lett.* **2012**, *18*, 3621.
- [42] a) N. Kuhn, M. Grathwohl, M. Steimann, G. Henkel, *Z. Naturforsch. B* **1998**, *53*, 997; b) N. Kuhn, M. Grathwohl, C. Nachtigal, M. Steimann, *Z. Naturforsch. B* **2001**, *56*, 704.
- [43] D. Petrovic, T. Glöge, T. Bannenberg, C. G. Hrib, S. Randoll, P. G. Jones, M. Tamm, *Eur. J. Inorg. Chem.* **2007**, *2007*, 3472.
- [44] D. Franz, T. Szilvási, A. Pöthig, F. Deiser, S. Inoue, *Chem. Eur. J.* **2018**, *24*, 4283.
- [45] D. Franz, E. Irran, S. Inoue, *Angew. Chem., Int. Ed. Engl.* **2014**, *53*, 14264.
- [46] F. S. Tschernuth, F. Hanusch, T. Szilvási, S. Inoue, *Organometallics* **2020**, *39*, 4265.
- [47] W. M. Haynes (Ed.) *CRC handbook of chemistry and physics. A ready-reference book of chemical and physical data*. S. 12, CRC Press, Boca Raton, London, New York, **2017**.
- [48] V. Y. Lee, A. Sekiguchi, *Organometallic compounds of low-coordinate Si, Ge, Sn and Pb. From phantom species to stable compounds*, Wiley, Chichester, **2010**.
- [49] C. E. Housecroft, A. G. Sharpe, *Inorganic chemistry*, Pearson, Harlow, **2012**.
- [50] D. E. Goldberg, D. H. Harris, M. F. Lappert, K. M. Thomas, *J. Chem. Soc., Chem. Commun.* **1976**, 261.
- [51] R. West, M. J. Fink, J. Michl, *Science* **1981**, *214*, 1343.
- [52] D. Gau, T. Kato, N. Saffon-Merceron, A. De Cózar, F. P. Cossío, A. Baceiredo, *Angew. Chem., Int. Ed. Engl.* **2010**, *122*, 6735.
- [53] A. Sekiguchi, R. Kinjo, M. Ichinohe, *Science* **2004**, *305*, 1755.
- [54] A. J. Bridgeman, L. R. Ireland, *Polyhedron* **2001**, *20*, 2841.
- [55] F. Hanusch, L. Groll, S. Inoue, *Chem. Sci.* **2021**.
- [56] J. Belzner, *Angew. Chem., Int. Ed. Engl.* **1997**, *36*, 1277.
- [57] a) M. Arshadi, D. Johnels, U. Edlund, C.-H. Ottosson, D. Cremer, *J. Am. Chem. Soc.* **1996**, *118*, 5120; b) Y. Apeloig, A. Stanger, *J. Am. Chem. Soc.* **1987**, *109*, 272; c) J. B. Lambert, L. Kania, S. Zhang, *Chem. Rev.* **1995**, *95*, 1191.
- [58] K.-C. Kim, C. A. Reed, D. W. Elliott, L. J. Mueller, F. Tham, L. Lin, J. B. Lambert, *Science (New York, N.Y.)* **2002**, *297*, 825.
- [59] a) J. S. Siegel, *Nat. Rev. Chem.* **2020**, *4*, 4; b) J. C. L. Walker, H. F. T. Klare, M. Oestreich, *Nat. Rev. Chem.* **2020**, *4*, 54.
- [60] V. J. Scott, R. Celenligil-Cetin, O. V. Ozerov, *J. Am. Chem. Soc.* **2005**, *127*, 2852.
- [61] M. W. Stanford, A. Bismuto, M. J. Cowley, *Chem. Eur. J.* **2020**, *26*, 9855.
- [62] a) K. Tamao, A. Kawachi in *Advances in Organometallic Chemistry*, Elsevier, **1995**, pp. 1–58; b) C. Marschner in *Organosilicon Compounds* (Ed.: V. Y. Lee), Academic Press, **2017**, pp. 295–360.
- [63] C. Chatgililoglu, *Chem. Rev.* **1995**, *95*, 1229.
- [64] M. Kira, T. Obata, I. Kon, H. Hashimoto, M. Ichinohe, H. Sakurai, S. Kyushin, H. Matsumoto, *Chem. Lett.* **1998**, *27*, 1097.
- [65] A. Sekiguchi, T. Matsuno, M. Ichinohe, *J. Am. Chem. Soc.* **2001**, *123*, 12436.

- [66] M. Nakamoto, T. Fukawa, V. Y. Lee, A. Sekiguchi, *J. Am. Chem. Soc.* **2002**, *124*, 15160.
- [67] H. Maruyama, H. Nakano, M. Nakamoto, A. Sekiguchi, *Angew. Chem., Int. Ed. Engl.* **2014**, *126*, 1348.
- [68] G. Trinquier, *J. Am. Chem. Soc.* **1990**, *112*, 2130.
- [69] M. Denk, J. R. Lennon, R. Hayashi, R. West, A. V. Belyakov, H. P. Verne, A. Haaland, M. Wagner, N. Metzler, *J. Am. Chem. Soc.* **1994**, *116*, 2691.
- [70] a) M. J. Krahfuss, U. Radius, *Dalton Trans.* **2021**; b) Y. P. Zhou, M. Driess, *Angew. Chem., Int. Ed. Engl.* **2019**, *58*, 3715; c) S. Raoufmoghaddam, Y.-P. Zhou, Y. Wang, M. Driess, *J. Organomet. Chem.* **2017**, *829*, 2; d) B. Blom, D. Gallego, M. Matthias Driess, *Inorg. Chem. Front.* **2014**, *1*, 134; e) S. Inoue in *Discovering the Future of Molecular Sciences* (Ed.: B. Pignataro), **2014**, pp. 243–273; f) B. Burgert, S. Miriam, D. Matthias, *Chem. Lett.* **2013**, *19*, 40.
- [71] M. Kira, S. Ishida, T. Iwamoto, C. Kabuto, *J. Am. Chem. Soc.* **1999**, *121*, 9722.
- [72] a) S. Tsutsui, K. Sakamoto, M. Kira, *J. Am. Chem. Soc.* **1998**, *120*, 9955; b) G.-H. Lee, R. West, T. Müller, *J. Am. Chem. Soc.* **2003**, *125*, 8114.
- [73] a) M. Yoshida, N. Tamaoki, *Organometallics* **2002**, *21*, 2587; b) M. C. Holthausen, W. Koch, Y. Apeloig, *J. Am. Chem. Soc.* **1999**, *121*, 2623.
- [74] S. Fujimori, S. Inoue, *Eur. J. Inorg. Chem.* **2020**, *2020*, 3131.
- [75] A. Sekiguchi, T. Tanaka, M. Ichinohe, K. Akiyama, S. Tero-Kubota, *J. Am. Chem. Soc.* **2003**, *125*, 4962.
- [76] G. Bertrand, *Science* **2004**, *305*, 783.
- [77] T. Müller, *Organometallics* **2010**, *29*, 1277.
- [78] a) B. H. Boo, P. B. Armentrout, *J. Phys. Chem.* **1987**, *91*, 5777; b) A. E. Douglas, B. L. Lutz, *Can. J. Phys.* **1970**, *48*, 247; c) N. Grevesse, A. J. Sauval, *Astron. Astrophys.* **1970**, *9*, 232; d) A. B. Sannigrahi, R. J. Buenker, G. Hirsch, J. Gu, *Chem. Phys. Lett.* **1995**, *237*, 204; e) P. D. Singh, F. G. Vanlandingham, *Astron. Astrophys.* **1978**, *66*, 87.
- [79] P. Jutzi, A. Mix, B. Rummel, W. W. Schoeller, B. Neumann, H.-G. Stammler, *Science* **2004**, *305*, 849.
- [80] P. Jutzi, D. Kanne, C. Krüger, *Angew. Chem., Int. Ed. Engl.* **1986**, *25*, 164.
- [81] T. Kühler, P. Jutzi in *Advances in Organometallic Chemistry*, Elsevier, **2003**, pp. 1–34.
- [82] M. Driess, S. Yao, M. Brym, C. van Wüllen, *Angew. Chem., Int. Ed. Engl.* **2006**, *45*, 6730.
- [83] H.-X. Yeong, H.-W. Xi, Y. Li, K. H. Lim, C.-W. So, *Chem. Lett.* **2013**, *19*, 11786.
- [84] S. L. Powley, F. Hanusch, S. Inoue in *Catalysis with Earth-abundant Elements* (Eds.: U. Schneider, S. Thomas), The Royal Society of Chemistry, **2021**, pp. 284–308.
- [85] P. Frisch, S. Inoue, *Dalton Trans.* **2019**, *48*, 10403.
- [86] S. L. Powley, S. Inoue, *Chem. Rec.* **2019**, *19*, 1.
- [87] S. U. Ahmad, T. Szilvasi, S. Inoue, *Chem. Commun.* **2014**, *50*, 12619.
- [88] A. C. Filippou, Y. N. Lebedev, O. Chernov, M. Straßmann, G. Schnakenburg, *Angew. Chem., Int. Ed. Engl.* **2013**, *52*, 6974.
- [89] Y. Li, Y.-C. Chan, Y. Li, I. Purushothaman, S. De, P. Parameswaran, C.-W. So, *Inorg. Chem.* **2016**, *55*, 9091.
- [90] Y. Xiong, S. Yao, S. Inoue, E. Irran, M. Driess, *Angew. Chem., Int. Ed. Engl.* **2012**, *51*, 10074.
- [91] Y. Wang, M. Karni, S. Yao, A. Kaushansky, Y. Apeloig, M. Driess, *J. Am. Chem. Soc.* **2019**, *141*, 12916.
- [92] a) K. Leszczyńska, A. Mix, R. J. F. Berger, B. Rummel, B. Neumann, H.-G. Stammler, P. Jutzi, *Angew. Chem., Int. Ed. Engl.* **2011**, *50*, 6843; b) R. J. F. Berger, K. Leszczyńska, P. Jutzi, *Silicon* **2010**, *2*, 229.

- [93] a) S. Keess, A. Simonneau, M. Oestreich, *Organometallics* **2015**, *34*, 790; b) M. Oestreich, J. Hermeke, J. Mohr, *Chem Soc Rev* **2015**, *44*, 2202; c) M. Rubin, T. Schwier, V. Gevorgyan, *J. Org. Chem.* **2002**, *67*, 1936.
- [94] a) P. Jutzi, *Chem. Lett.* **2014**, *20*, 9192; b) P. Jutzi, K. Leszczyńska, A. Mix, B. Neumann, W. W. Schoeller, H.-G. Stammler, *Organometallics* **2009**, *28*, 1985; c) P. Jutzi, K. Leszczyńska, B. Neumann, W. W. Schoeller, H.-G. Stammler, *Angew. Chem., Int. Ed. Engl.* **2009**, *48*, 2596; d) P. Jutzi, A. Mix, B. Neumann, B. Rummel, W. W. Schoeller, H.-G. Stammler, A. B. Rozhenko, *J. Am. Chem. Soc.* **2009**, *131*, 12137.
- [95] S. U. Ahmad, T. Szilvási, E. Irran, S. Inoue, *J. Am. Chem. Soc.* **2015**, *137*, 5828.
- [96] D. Sarkar, D. Wendel, S. U. Ahmad, T. Szilvási, A. Pöthig, S. Inoue, *Dalton Trans.* **2017**, *46*, 16014.
- [97] A. Porzelt, J. Schweizer, R. Baierl, P. Altmann, M. Holthausen, S. Inoue, *Inorganics* **2018**, *6*.
- [98] D. Sarkar, V. Nesterov, T. Szilvási, P. J. Altmann, S. Inoue, *Chem. Eur. J.* **2019**, *25*, 1198.
- [99] K. C. Mondal, S. Roy, B. Dittrich, D. M. Andrada, G. Frenking, H. W. Roesky, *Angew. Chem., Int. Ed. Engl.* **2016**, *55*, 3158.
- [100] N. Takagi, T. Shimizu, G. Frenking, *Chem. Lett.* **2009**, *15*, 3448.
- [101] F. Ramirez, N. B. Desai, B. Hansen, N. McKelvie, *J. Am. Chem. Soc.* **1961**, *83*, 3539.
- [102] G. E. Hardy, J. I. Zink, W. C. Kaska, J. C. Baldwin, *J. Am. Chem. Soc.* **1978**, *100*, 8001.
- [103] R. Appel, F. Knoll, H. Schöler, H.-D. Wihler, *Angew. Chem., Int. Ed. Engl.* **1976**, *15*, 702.
- [104] G. Frenking, R. Tonner, *Wiley Interdiscip. Rev. Comput. Mol. Sci.* **2011**, *1*, 869.
- [105] G. Frenking, R. Tonner, *Pure Appl. Chem.* **2009**, *81*.
- [106] a) L. Zhao, C. Chai, W. Petz, G. Frenking, *Molecules* **2020**, *25*; b) H. Schmidbaur, O. Gasser, *Angew. Chem., Int. Ed. Engl.* **1976**, *15*, 502.
- [107] N. Wiberg, H.-W. Lerner, S.-K. Vasisht, S. Wagner, K. Karaghiosoff, H. Nöth, W. Ponikwar, *Chem. Ber.* **1999**, *1999*, 1211.
- [108] P. K. Majhi, T. Sasamori, *Chem. Lett.* **2018**, *24*, 9441.
- [109] S. Yao, Y. Xiong, M. Driess, *Acc. Chem. Res.* **2017**, *50*, 2026.
- [110] S. Ishida, T. Iwamoto, C. Kabuto, M. Kira, *Nature* **2003**, *421*, 725.
- [111] K. C. Mondal, H. W. Roesky, M. C. Schwarzer, G. Frenking, B. Niepötter, H. Wolf, R. Herbst-Irmer, D. Stalke, *Angew. Chem., Int. Ed. Engl.* **2013**, *52*, 2963.
- [112] a) B. Niepötter, R. Herbst-Irmer, D. Kratzert, P. P. Samuel, K. C. Mondal, H. W. Roesky, P. Jerabek, G. Frenking, D. Stalke, *Angew. Chem., Int. Ed. Engl.* **2014**, *53*, 2766; b) K. C. Mondal, H. W. Roesky, M. C. Schwarzer, G. Frenking, I. Tkach, H. Wolf, D. Kratzert, R. Herbst-Irmer, B. Niepötter, D. Stalke, *Angew. Chem., Int. Ed. Engl.* **2013**, *52*, 1801; c) K. C. Mondal, P. P. Samuel, M. Tretiakov, A. P. Singh, H. W. Roesky, A. C. Stückl, B. Niepötter, E. Carl, H. Wolf, R. Herbst-Irmer et al., *Inorg. Chem.* **2013**, *52*, 4736.
- [113] S. Yao, A. Kostenko, Y. Xiong, A. Ruzicka, M. Driess, *J. Am. Chem. Soc.* **2020**, *142*, 12608.
- [114] J. Keuter, A. Hepp, C. Mück-Lichtenfeld, F. Lips, *Angew. Chem., Int. Ed. Engl.* **2019**, *58*, 4395.
- [115] T. Sugahara, T. Sasamori, N. Tokitoh, *Angew. Chem., Int. Ed. Engl.* **2017**, *56*, 9920.
- [116] a) K. C. Mondal, P. P. Samuel, H. W. Roesky, R. R. Aysin, L. A. Leites, S. Neudeck, J. Lübben, B. Dittrich, N. Holzmann, M. Hermann et al., *J. Am. Chem. Soc.* **2014**, *136*, 8919; b) S. Roy, K. C. Mondal, L. Krause, P. Stollberg, R. Herbst-Irmer, D. Stalke, J. Meyer, A. C. Stückl, B. Maity, D. Koley et al., *J. Am. Chem. Soc.* **2014**, *136*, 16776.
- [117] a) A. Burchert, S. Yao, R. Müller, C. Schattenberg, Y. Xiong, M. Kaupp, M. Driess, *Angew. Chem., Int. Ed. Engl.* **2017**, *56*, 1894; b) Y. Xiong, S. Yao, R. Müller, M. Kaupp, M. Driess, *Angew. Chem., Int. Ed. Engl.* **2015**, *54*, 10254.
- [118] H.-X. Yeong, Y. Li, C.-W. So, *Organometallics* **2014**, *33*, 3636.
- [119] a) P. Frisch, S. Inoue, *Dalton Trans.* **2020**, *49*, 6176; b) P. Frisch, T. Szilvási, S. Inoue, *Chem. Eur. J.* **2020**, *26*, 6271; c) P. Frisch, S. Inoue, *Chem. Commun.* **2018**, *54*, 13658.

- [120] P. Frisch, T. Szilvási, A. Porzelt, S. Inoue, *Inorg. Chem.* **2019**, *58*, 14931.
- [121] N. C. Breit, T. Szilvási, T. Suzuki, D. Gallego, S. Inoue, *J. Am. Chem. Soc.* **2013**, *135*, 17958.
- [122] C. Zybill, D. L. Wilkinson, G. Müller, *Angew. Chem., Int. Ed. Engl.* **1988**, *100*, 574.
- [123] N. Kuhn, T. Kratz, D. Bläser, R. Boese, *Chem. Ber.* **1995**, *128*, 245.
- [124] C. Eisenhut, *Synthese und Reaktivität eines neuartigen NHC-stabilisierten Hydridosilylens*, Technische Universität Berlin, **2016**.
- [125] T. J. Hadlington, M. Driess, C. Jones, *Chem Soc Rev* **2018**, *47*, 4176.
- [126] J. Oetzel, C. Bruhn, U. Siemeling, *Z. anorg. allg. Chem.* **2018**, *644*, 935.
- [127] M. T. Whited, A. M. Deetz, J. W. Boerma, D. E. DeRocha, D. E. Janzen, *Organometallics* **2014**, *33*, 5070.
- [128] F. Hanusch, D. Munz, J. Sutter, K. Meyer, S. Inoue, *Angew. Chem., Int. Ed. Engl.* **2021**, *60*, 23274-23280.
- [129] G. P. Junor, J. Lorkowski, C. M. Weinstein, R. Jazzar, C. Pietraszuk, G. Bertrand, *Angew. Chem., Int. Ed. Engl.* **2020**, *59*, 22028.
- [130] K. Verlinden, H. Buhl, W. Frank, C. Ganter, *Eur. J. Inorg. Chem.* **2015**, *2015*, 2416.
- [131] A. Liske, K. Verlinden, H. Buhl, K. Schaper, C. Ganter, *Organometallics* **2013**, *32*, 5269.
- [132] S. R. Alvarado, I. A. Shortt, H.-J. Fan, J. Vela, *Organometallics* **2015**, *34*, 4023.
- [133] S. Takahashi, A. Ishii, N. Nakata, *Chem. Commun.* **2021**, *57*, 3203.
- [134] A. Burchert, R. Müller, S. Yao, C. Schattenberg, Y. Xiong, M. Kaupp, M. Driess, *Angew. Chem., Int. Ed. Engl.* **2017**, *56*, 6298.
- [135] R. Tacke, C. Kobelt, J. A. Baus, R. Bertermann, C. Burschka, *Dalton Trans.* **2015**, *44*, 14959.
- [136] A. Mitra, J. P. Wojcik, D. Lecoanet, T. Müller, R. West, *Angew. Chem., Int. Ed. Engl.* **2009**, *48*, 4069.
- [137] a) S. Yao, Y. Xiong, M. Driess, *Chem. Eur. J.* **2010**, *16*, 1281; b) C. W. So, H. W. Roesky, R. B. Oswald, A. Pal, P. G. Jones, *Dalton Trans.* **2007**, 5241; c) A. Meltzer, S. Inoue, C. Präsang, M. Driess, *J. Am. Chem. Soc.* **2010**, *132*, 3038; d) S. Yao, Y. Xiong, M. Brym, M. Driess, *Chem. Asian J.* **2008**, *3*, 113; e) S. H. Zhang, H. X. Yeong, C. W. So, *Chem. Eur. J.* **2011**, *17*, 3490.
- [138] a) Y. Wang, M. Karni, S. Yao, Y. Apeloig, M. Driess, *J. Am. Chem. Soc.* **2018**; b) Y.-P. Zhou, M. Karni, S. Yao, Y. Apeloig, M. Driess, *Angew. Chem., Int. Ed. Engl.* **2016**, *55*, 15096.
- [139] R. Azhakar, R. S. Ghadwal, H. W. Roesky, H. Wolf, D. Stalke, *J. Am. Chem. Soc.* **2012**, *134*, 2423.
- [140] a) M. Sankar, Q. He, R. V. Engel, M. A. Sainna, A. J. Logsdail, A. Roldan, D. J. Willock, N. Agarwal, C. J. Kiely, G. J. Hutchings, *Chem. Rev.* **2020**, *120*, 3890; b) A. Fürstner, *ACS Cent. Sci.* **2016**, *2*, 778; c) P. Buchwalter, J. Rosé, P. Braunstein, *Chem. Rev.* **2015**, *115*, 28; d) S. Yamazoe, K. Koyasu, T. Tsukuda, *Acc. Chem. Res.* **2014**, *47*, 816; e) Y. Mikami, A. Dhakshinamoorthy, M. Alvaro, H. García, *Catal. Sci. Technol.* **2013**, *3*, 58.
- [141] a) B. Berti, M. Bortoluzzi, C. Cesari, C. Femoni, M. C. Iapalucci, R. Mazzoni, S. Zacchini, *Eur. J. Inorg. Chem.* **2020**, *2020*, 2191; b) B. Berti, M. Bortoluzzi, C. Cesari, C. Femoni, M. C. Iapalucci, R. Mazzoni, F. Vacca, S. Zacchini, *Eur. J. Inorg. Chem.* **2019**, *2019*, 3084; c) M. Bortoluzzi, C. Cesari, I. Ciabatti, C. Femoni, M. Hayatifar, M. C. Iapalucci, R. Mazzoni, S. Zacchini, *J. Clust. Sci.* **2017**, *28*, 703; d) G. Wang, T. T. Ponduru, Q. Wang, L. Zhao, G. Frenking, H. V. R. Dias, *Chem. Lett.* **2017**, *23*, 17222; e) P. Braunstein, M. Knorr, A. Tiripicchio, M. Tiripicchio Camellini, *Inorg. Chem.* **1992**, *31*, 3685; f) U. Schubert, E. Kunz, M. Knorr, J. Müller, *Chem. Ber.* **1987**, *120*, 1079; g) C. E. Briant, K. P. Hall, D. M. P. Mingos, *J. Chem. Soc., Chem. Commun.* **1983**, 843; h) B. G. Cooper, J. W. Napoline, C. M. Thomas, *Catal. Rev.* **2012**, *54*, 1; i) S. Albonetti, R. Bonelli, J. Epoupa Mengou, C. Femoni, C. Tiozzo, S. Zacchini, F. Trifirò, *Catal. Today* **2008**, *137*, 483.
- [142] S. S. Batsanov, *Inorg. Mater.* **2001**, *37*, 871.

- [143] a) H. Darmandeh, J. Löffler, N. V. Tzouras, B. Dereli, T. Scherpf, K.-S. Feichtner, S. Vanden Broeck, K. van Hecke, M. Saab, C. S. J. Cazin et al., *Angew. Chem., Int. Ed. Engl.* **2021**, *60*, 21014; b) M. Rigoulet, S. Massou, E. D. Sosa Carrizo, S. Mallet-Ladeira, A. Amgoune, K. Miqueu, D. Bourissou, *Proc. Natl. Acad. Sci. U.S.A.* **2019**, *116*, 46; c) F. Rekhroukh, L. Estévez, C. Bijani, K. Miqueu, A. Amgoune, D. Bourissou, *Angew. Chem., Int. Ed. Engl.* **2016**, *55*, 3414; d) H. Schmidbaur, H. G. Raubenheimer, L. Dobrzańska, *Chem Soc Rev* **2014**, *43*, 345.
- [144] a) G. Dos Passos Gomes, G. Xu, X. Zhu, L.-M. Chamoreau, Y. Zhang, O. Bistri-Aslanoff, S. Roland, I. V. Alabugin, M. Sollogoub, *Chem. Eur. J.* **2021**, *27*, 8127; b) M. Kumar, J. S. Francisco, *J. Am. Chem. Soc.* **2020**, *142*, 6001; c) W. Scherer, A. C. Dunbar, J. E. Barquera-Lozada, D. Schmitz, G. Eickerling, D. Kratzert, D. Stalke, A. Lanza, P. Macchi, N. P. M. Casati et al., *Angew. Chem., Int. Ed. Engl.* **2015**, *54*, 2505.
- [145] B. Huang, M. Hu, F. D. Toste, *Trends in Chemistry* **2020**, *2*, 707.
- [146] J. Schröder, D. Himmel, D. Kratzert, V. Radtke, S. Richert, S. Weber, T. Böttcher, *Chem. Commun.* **2019**, *55*, 1322.
- [147] M. Muhr, P. Heiß, M. Schütz, R. Bühler, C. Gemel, M. H. Linden, H. B. Linden, R. A. Fischer, *Dalton Trans.* **2021**, *50*, 9031.
- [148] a) G. J. Kubas, G. Kiss, C. D. Hoff, *Organometallics* **1991**, *10*, 2870; b) P. Kalck, R. Pince, R. Poilblanc, J. Roussel, *J. Organomet. Chem.* **1970**, *24*, 445.
- [149] *APEX suite of crystallographic software*, Bruker AXS Inc, Madison, Wisconsin, USA, **2015**.
- [150] *SAINT and SADABS*, Bruker AXS Inc, Madison, Wisconsin, USA, **2008**.
- [151] G. M. Sheldrick, *SHELXL-2014*, University of Göttingen, Göttingen, Germany, **2014**.
- [152] C. B. Hübschle, G. M. Sheldrick, B. Dittrich, *J. Appl. Crystallogr.* **2011**, *44*, 1281.
- [153] G. M. Sheldrick, *SHELXL-97*, University of Göttingen, Göttingen, Germany, **1998**.
- [154] A. J. C. Wilson, V. Geist, *International Tables for Crystallography. Volume C: Mathematical, Physical and Chemical Tables.*, **1992**, Dordrecht/Boston/London, Tables 6.1.1.4 (pp 500-502), 4.2.6.8 (pp. 219-222) and 4.2.4.2 (pp. 193-199).
- [155] C. F. Macrae, I. J. Bruno, J. A. Chisholm, P. R. Edgington, P. McCabe, E. Pidcock, L. Rodriguez-Monge, R. Taylor, J. van de Streek, P. A. Wood, *J. Appl. Crystallogr.* **2008**, *41*, 466.
- [156] a) F. Neese, *Wiley Interdiscip. Rev. Comput. Mol. Sci.* **2018**, *8*; b) F. Neese, *Wiley Interdiscip. Rev. Comput. Mol. Sci.* **2012**, *2*, 73.
- [157] a) C. Adamo, V. Barone, *J. Chem. Phys.* **1999**, *110*, 6158; b) J. P. Perdew, M. Ernzerhof, K. Burke, *J. Chem. Phys.* **1996**, *105*, 9982.
- [158] a) S. Grimme, S. Ehrlich, L. Goerigk, *J. Comput. Chem.* **2011**, *32*, 1456; b) S. Grimme, J. Antony, S. Ehrlich, H. Krieg, *J. Chem. Phys.* **2010**, *132*, 154104.
- [159] F. Weigend, R. Ahlrichs, *Phys. Chem. Chem. Phys.* **2005**, *7*, 3297.
- [160] a) K. Eichkorn, F. Weigend, O. Treutler, R. Ahlrichs, *Theoret. Chim. Acta* **1997**, *97*, 119; b) D. Andrae, U. Huermann, M. Dolg, H. Stoll, H. Preu, *Theoret. Chim. Acta* **1990**, *77*, 123.
- [161] G. Knizia, J. E. M. N. Klein, *Angew. Chem., Int. Ed. Engl.* **2015**, *54*, 5518.
- [162] R. Bjornsson, F. Neese, S. DeBeer, *Inorg. Chem.* **2017**, *56*, 1470.
- [163] M. Römel, S. Ye, F. Neese, *Inorg. Chem.* **2009**, *48*, 784.
- [164] F. Neese, *Inorg. Chim. Acta* **2002**, *337*, 181.
- [165] A. Wolf, M. Reiher, B. A. Hess, *J. Chem. Phys.* **2002**, *117*, 9215.
- [166] T. V. Harris, R. K. Szilagy, *Inorg. Chem.* **2011**, *50*, 4811.
- [167] a) C. van Wüllen, *J. Chem. Phys.* **1998**, *109*, 392; b) E. van Lenthe, E. J. Baerends, J. G. Snijders, *J. Chem. Phys.* **1993**, *99*, 4597.
- [168] I. M. Alecu, J. Zheng, Y. Zhao, D. G. Truhlar, *J. Chem. Theory Comput.* **2010**, *6*, 2872.

## 8 Appendix

### Crystallographic Details

General considerations: Single crystal diffraction data were recorded on *Bruker* instruments equipped with a Helios optic monochromator and a Mo IMS microsource ( $\lambda = 0.71073 \text{ \AA}$ ) with CMOS / Photon area detector or a Mo TXS rotating anode source ( $\lambda = 0.71073 \text{ \AA}$ ) with CMOS / Photon area detector. The data collection was performed, using the APEX III software package<sup>[149]</sup> on single crystals coated with Fomblin ® Y as perfluorinated ether. The single crystals were mounted on a micro sampler, transferred to the diffractometer and measured frozen under a stream of cold nitrogen. A matrix scan was used to determine the initial lattice parameters. Reflections were merged and corrected for Lorentz and polarization effects, scan speed, and background using SAINT.<sup>[150]</sup> Absorption corrections, including odd and even ordered spherical harmonics were performed using SADABS.<sup>[150]</sup> Space group assignments were based upon systematic absences, E statistics, and successful refinement of the structures. Structures were solved by direct methods with the aid of successive difference Fourier maps, and were refined against all data using the APEX III software in conjunction with SHELXL-2014<sup>[151]</sup> and SHELXLE.<sup>[152]</sup> H atoms were placed in calculated positions and refined using a riding model, with methylene and aromatic C–H distances of 0.99 and 0.95 Å, respectively, and  $U_{\text{iso}}(\text{H}) = 1.2 \cdot U_{\text{eq}}(\text{C})$ . Non-hydrogen atoms were refined with anisotropic displacement parameters. Full-matrix least-squares refinements were carried out by minimizing  $\sum w(F_o^2 - F_c^2)^2$  with the SHELXL-97 weighting scheme.<sup>[153]</sup> Neutral atom scattering factors for all atoms and anomalous dispersion corrections for the non-hydrogen atoms were taken from International Tables for Crystallography.<sup>[154]</sup> The images of the crystal structures were generated by Mercury.<sup>[155]</sup> The CCDC numbers CCDC- (2085156 - 2085158) contain the supplementary crystallographic data for the structures **P1**, **P8** and **P17**. These data can be obtained free of charge from the Cambridge Crystallographic Data Centre via <https://www.ccdc.cam.ac.uk/structures/>.

Table S 1. Crystal data and structure refinement for compound P1, P4, P7.

Compound #	P1	P4	P7
Chemical formula	C <sub>44</sub> H <sub>52</sub> Cl <sub>2</sub> N <sub>6</sub> Si, 2(C <sub>6</sub> H <sub>4</sub> F <sub>2</sub> )	2(C <sub>44</sub> H <sub>52</sub> Cl <sub>3</sub> N <sub>6</sub> Si), 2(Cl), 2(C <sub>4</sub> H <sub>10</sub> O), 7(C <sub>2</sub> H <sub>3</sub> N)	C <sub>44</sub> H <sub>54</sub> N <sub>6</sub> Si, 2(I)
Formula weight	992.09 g/mol	2105.23 g/mol	948.82 g/mol
Temperature	100 K	100 K	100 K
Wavelength	0.71073 Å	0.71073 Å	0.71073 Å
Crystal size	0.378 x 0.296 x 0.130 mm	0.254 x 0.113 x 0.101 mm	0.355 x 0.137 x 0.118 mm
Crystal habit	clear colorless fragment	clear colorless fragment	clear colorless fragment
Crystal system	triclinic	monoclinic	triclinic
Space group	<i>P</i> -1	<i>P</i> 2 <sub>1</sub> / <i>c</i>	<i>P</i> -1
Unit cell dimensions	a = 14.0779(12) Å; α = 76.724(4)° b = 14.3401(12) Å; β = 71.447(4)° c = 14.7770(12) Å; γ = 67.418(4)°	a = 19.649(2) Å; α = 90° b = 27.963(3) Å; β = 90.277(4)° c = 21.220(3) Å; γ = 90°	a = 11.7048(9) Å; α = 82.688(3)° b = 16.0873(14) Å; β = 69.690(3)° c = 16.8481(15) Å; γ = 68.662(3)°
Volume	2591.5(4) Å <sup>3</sup>	11659(2) Å <sup>3</sup>	2771.3(4) Å <sup>3</sup>
Z	2	4	2
Density (calculated)	1.271 g/cm <sup>3</sup>	1.199 g/cm <sup>3</sup>	1.137 g/cm <sup>3</sup>
Radiation source	TXS rotating anode	IMS microsource	IMS microsource
Theta range for data collection	2.26 to 25.39°	2.03 to 25.36°	1.98 to 25.35°
Index ranges	-16 ≤ h ≤ 16, -17 ≤ k ≤ 17, -17 ≤ l ≤ 17	-23 ≤ h ≤ 21, -33 ≤ k ≤ 33, -23 ≤ l ≤ 25	-14 ≤ h ≤ 14, -19 ≤ k ≤ 19, -20 ≤ l ≤ 20
Reflections collected	45078	83104	39683
Independent reflections	9486	21321	10122
Completeness	0.996	0.996	0.996
Absorption correction	Multi-Scan	Multi-Scan	Multi-Scan
Max. and min. transmission	0.7452 and 0.5463	0.7453 and 0.6888	0.7452 and 0.6561
Refinement method	Full-matrix least-squares on F <sup>2</sup>	Full-matrix least-squares on F <sup>2</sup>	Full-matrix least-squares on F <sup>2</sup>
Function minimized	Σ w(F <sub>o</sub> <sup>2</sup> - F <sub>c</sub> <sup>2</sup> ) <sup>2</sup>	Σ w(F <sub>o</sub> <sup>2</sup> - F <sub>c</sub> <sup>2</sup> ) <sup>2</sup>	Σ w(F <sub>o</sub> <sup>2</sup> - F <sub>c</sub> <sup>2</sup> ) <sup>2</sup>
Data / restraints / parameters	9486 / 0 / 634	21321 / 813 / 1524	10122 / 204 / 539
Goodness-of-fit on F <sup>2</sup>	1.028	1.031	1.025
Final R indices [I > 2σ(I)]	R1 = 0.0457, wR2 = 0.0981	R1 = 0.0645, wR2 = 0.1514	R1 = 0.0355, wR2 = 0.0865
R indices (all data)	R1 = 0.0747, wR2 = 0.1092	R1 = 0.1078, wR2 = 0.1783	R1 = 0.0460, wR2 = 0.0923
Largest diff. peak and hole	0.324 and -0.352 eÅ <sup>-3</sup>	0.455 and -0.604 eÅ <sup>-3</sup>	0.716 and -0.802 eÅ <sup>-3</sup>

Table S 2. Crystal data and structure refinement for compound **P8**, **P17**, **P18**.

Compound #	<b>P8</b>	<b>P17</b>	<b>P18</b>
Chemical formula	C <sub>44</sub> H <sub>52</sub> Cl <sub>2</sub> N <sub>6</sub> S Si, 3 (C <sub>2</sub> H <sub>3</sub> N)	C <sub>48</sub> H <sub>52</sub> Au Cl Fe N <sub>6</sub> O <sub>4</sub> Si	C <sub>106</sub> H <sub>114</sub> Au <sub>2</sub> Fe <sub>2</sub> N <sub>14</sub> O <sub>8</sub> Si <sub>2</sub>
Formula weight	919.13 g/mol	1093.32 g/mol	2273.94 g/mol
Temperature	100 K	100 K	100 K
Wavelength	0.71073 Å	0.71073 Å	0.71073 Å
Crystal size	0.273 x 0.211 x 0.182 mm	0.176 x 0.165 x 0.091 mm	0.218 x 0.180 x 0.155 mm
Crystal habit	clear colorless fragment	clear light yellow fragment	clear yellow block
Crystal system	triclinic	monoclinic	monoclinic
Space group	<i>P</i> -1	<i>C</i> <sub>2</sub> / <i>c</i>	<i>P</i> <sub>2</sub> <sub>1</sub> / <i>c</i>
Unit cell dimensions	a = 12.2139(11) Å; α = 70.258(3)° b = 14.4858(13) Å; β = 84.626(3)° c = 15.2925(13) Å; γ = 80.130(3)°	a = 30.060(2) Å; α = 90° b = 16.7584(11) Å; β = 121.366(2)° c = 23.3357(16) Å; γ = 90°	a = 14.4735(12) Å; α = 90° b = 18.7683(13) Å; β = 93.953(3)° c = 24.6240(18) Å; γ = 90°
Volume	2507.1(4) Å <sup>3</sup>	10037.6(12) Å <sup>3</sup>	6673.0(9) Å <sup>3</sup>
Z	2	8	2
Density (calculated)	1.218 g/cm <sup>3</sup>	1.447 g/cm <sup>3</sup>	1.132 g/cm <sup>3</sup>
Radiation source	TXS rotating anode	IMS microsource	IMS microsource
Theta range for data collection	2.39 to 25.42°	2.00 to 25.35°	1.92 to 25.35°
Index ranges	-14 ≤ h ≤ 14, -17 ≤ k ≤ 17, -18 ≤ l ≤ 18	-36 ≤ h ≤ 36, -20 ≤ k ≤ 20, -28 ≤ l ≤ 28	-17 ≤ h ≤ 16, -22 ≤ k ≤ 22, -29 ≤ l ≤ 28
Reflections collected	131380	149934	64332
Independent reflections	9241	9204	12205
Completeness	0.998	0.999	0.997
Absorption correction	Multi-Scan	Multi-Scan	Multi-Scan
Max. and min. transmission	0.7452 and 0.7144	0.7452 and 0.6606	0.7453 and 0.5624
Refinement method	Full-matrix least-squares on F <sup>2</sup>	Full-matrix least-squares on F <sup>2</sup>	Full-matrix least-squares on F <sup>2</sup>
Function minimized	Σ w(F <sub>o</sub> <sup>2</sup> - F <sub>c</sub> <sup>2</sup> ) <sup>2</sup>	Σ w(F <sub>o</sub> <sup>2</sup> - F <sub>c</sub> <sup>2</sup> ) <sup>2</sup>	Σ w(F <sub>o</sub> <sup>2</sup> - F <sub>c</sub> <sup>2</sup> ) <sup>2</sup>
Data / restraints / parameters	9241 / 0 / 583	9204 / 0 / 571	12205 / 253 / 690
Goodness-of-fit on F <sup>2</sup>	1.038	1.139	1.059
Final R indices [I > 2σ(I)]	R1 = 0.0346, wR2 = 0.0930	R1 = 0.0213, wR2 = 0.0467	R1 = 0.0705, wR2 = 0.1700
R indices (all data)	R1 = 0.0386, wR2 = 0.0961	R1 = 0.0312, wR2 = 0.0533	R1 = 0.0942, wR2 = 0.1859
Largest diff. peak and hole	0.313 and -0.351 eÅ <sup>-3</sup>	0.957 and -0.682 eÅ <sup>-3</sup>	6.596 and -2.211 eÅ <sup>-3</sup>

Table S 3. Crystal data and structure refinement for compound P21, P22, P23.

Compound #	P21	P22	P23
Chemical formula	C <sub>48</sub> H <sub>52</sub> Fe N <sub>6</sub> O <sub>4</sub> Si, C <sub>4</sub> H <sub>10</sub> O	C <sub>48</sub> H <sub>53</sub> Fe N <sub>6</sub> O <sub>4</sub> Si, C <sub>4</sub> H Fe O <sub>4</sub>	C <sub>48</sub> H <sub>52</sub> Cl Fe N <sub>6</sub> O <sub>4</sub> Si, C <sub>4</sub> H Fe O <sub>4</sub> , C <sub>4</sub> H <sub>10</sub> O
Formula weight	935.02 g/mol	1030.80 g/mol	1139.36 g/mol
Temperature	100 K	100 K	100 K
Wavelength	0.71073 Å	0.71073 Å	0.71073 Å
Crystal size	0.273 x 0.240 x 0.175 mm	0.145 x 0.134 x 0.108 mm	0.244 x 0.217 x 0.136 mm
Crystal habit	clear colorless fragment	clear colorless block	clear light orange block
Crystal system	monoclinic	monoclinic	triclinic
Space group	<i>P</i> 2 <sub>1</sub> / <i>c</i>	<i>P</i> 2 <sub>1</sub> / <i>c</i>	<i>P</i> -1
Unit cell dimensions	a = 12.1472(6) Å; α = 90° b = 18.4259(9) Å; β = 99.409(2)° c = 22.6851(11) Å; γ = 90°	a = 11.2653(5) Å; α = 90° b = 26.7561(11) Å; β = 95.477(1)° c = 17.0043(6) Å; γ = 90°	a = 13.6114(10) Å; α = 107.339(3)° b = 14.9329(13) Å; β = 96.927(3)° c = 16.0582(14) Å; γ = 90.121(3)°
Volume	5009.1(4) Å <sup>3</sup>	5102.0(4) Å <sup>3</sup>	3090.4(4) Å <sup>3</sup>
Z	4	4	2
Density (calculated)	1.240 g/cm <sup>3</sup>	1.342 g/cm <sup>3</sup>	1.224 g/cm <sup>3</sup>
Radiation source	TXS rotating anode	IMS microsource	IMS microsource
Theta range for data collection	2.03 to 25.35°	1.94 to 25.35°	2.04 to 25.36°
Index ranges	-14 ≤ h ≤ 14, -22 ≤ k ≤ 22, -27 ≤ l ≤ 27	-13 ≤ h ≤ 13, -32 ≤ k ≤ 32, -19 ≤ l ≤ 20	-16 ≤ h ≤ 16, -17 ≤ k ≤ 17, -19 ≤ l ≤ 19
Reflections collected	107117	106093	129944
Independent reflections	9167	9349	11312
Completeness	0.999	1.000	0.999
Absorption correction	Multi-Scan	Multi-Scan	Multi-Scan
Max. and min. transmission	0.7453 and 0.7141	0.7452 and 0.7096	0.7452 and 0.6879
Refinement method	Full-matrix least-squares on F <sup>2</sup>	Full-matrix least-squares on F <sup>2</sup>	Full-matrix least-squares on F <sup>2</sup>
Function minimized	Σ w(F <sub>o</sub> <sup>2</sup> - F <sub>c</sub> <sup>2</sup> ) <sup>2</sup>	Σ w(F <sub>o</sub> <sup>2</sup> - F <sub>c</sub> <sup>2</sup> ) <sup>2</sup>	Σ w(F <sub>o</sub> <sup>2</sup> - F <sub>c</sub> <sup>2</sup> ) <sup>2</sup>
Data / restraints / parameters	9167 / 133 / 651	9349 / 0 / 662	11312 / 143 / 750
Goodness-of-fit on F <sup>2</sup>	1.021	1.089	1.008
Final R indices [I > 2σ(I)]	R1 = 0.0426, wR2 = 0.1186	R1 = 0.0633, wR2 = 0.1461	R1 = 0.0442, wR2 = 0.1180
R indices (all data)	R1 = 0.0465, wR2 = 0.1222	R1 = 0.0772, wR2 = 0.1539	R1 = 0.0510, wR2 = 0.1228
Largest diff. peak and hole	0.657 and -0.619 eÅ <sup>-3</sup>	1.921 and -1.549 eÅ <sup>-3</sup>	0.839 and -0.609 eÅ <sup>-3</sup>

Table S 4. Crystal data and structure refinement for compound [Dip<sup>n</sup>NHI<sup>nBu</sup>H][BF<sub>4</sub>], [bis<sup>Ph</sup>-NHI<sup>Mes</sup>H][BF<sub>4</sub>].

Compound #	[Dip <sup>n</sup> NHI <sup>nBu</sup> H][BF <sub>4</sub> ]	[bis <sup>Ph</sup> -NHI <sup>Mes</sup> H][BF <sub>4</sub> ]
Chemical formula	C <sub>31</sub> H <sub>46</sub> N <sub>3</sub> , B F <sub>4</sub>	C <sub>48</sub> H <sub>53</sub> N <sub>6</sub> , B F <sub>4</sub> , 2(CH Cl <sub>3</sub> )
Formula weight	547.52 g/mol	1039.51 g/mol
Temperature	100 K	100 K
Wavelength	0.71073 Å	0.71073 Å
Crystal size	0.612 x 0.211 x 0.173 mm	0.315 x 0.141 x 0.106 mm
Crystal habit	clear colorless fragment	clear colorless fragment
Crystal system	monoclinic	monoclinic
Space group	<i>P</i> 2 <sub>1</sub> / <i>c</i>	<i>P</i> 2 <sub>1</sub> / <i>c</i>
Unit cell dimensions	a = 10.738(6) Å; α = 90° b = 23.104(16) Å; β = 91.21(2)° c = 12.364(7) Å; γ = 90°	a = 15.229(9) Å; α = 90° b = 14.764(8) Å; β = 95.654(17)° c = 23.635(13) Å; γ = 90°
Volume	3067(3) Å <sup>3</sup>	5288(5) Å <sup>3</sup>
Z	4	4
Density (calculated)	1.186 g/cm <sup>3</sup>	1.306 g/cm <sup>3</sup>
Radiation source	TXS rotating anode	TXS rotating anode
Theta range for data collection	2.41 to 25.69°	1.926 to 25.349°
Index ranges	-12<=h<=12, -28<=k<=23, -14<=l<=12	-18<=h<=18, -17<=k<=17, -28<=l<=28
Reflections collected	11176	229228
Independent reflections	5493	9737
Completeness	0.943	0.968
Absorption correction	Multi-Scan	Multi-Scan
Max. and min. transmission	0.7453 and 0.6409	0.7452 and 0.6874
Refinement method	Full-matrix least-squares on F <sup>2</sup>	Full-matrix least-squares on F <sup>2</sup>
Function minimized	Σ w(F <sub>o</sub> <sup>2</sup> - F <sub>c</sub> <sup>2</sup> ) <sup>2</sup>	Σ w(F <sub>o</sub> <sup>2</sup> - F <sub>c</sub> <sup>2</sup> ) <sup>2</sup>
Data / restraints / parameters	5493 / 0 / 361	9737 / 0 / 623
Goodness-of-fit on F <sup>2</sup>	1.036	2.073
Final R indices [I>2σ(I)]	R1 = 0.0647, wR2 = 0.1502	R1 = 0.1148, wR2 = 0.4029
R indices (all data)	R1 = 0.0965, wR2 = 0.1667	R1 = 0.1242, wR2 = 0.4202
Largest diff. peak and hole	0.270 and -0.347 eÅ <sup>-3</sup>	1.42 and -1.24 eÅ <sup>-3</sup>

**checkCIF/PLATON report**

Structure factors have been supplied for datablock(s) I

THIS REPORT IS FOR GUIDANCE ONLY. IF USED AS PART OF A REVIEW PROCEDURE FOR PUBLICATION, IT SHOULD NOT REPLACE THE EXPERTISE OF AN EXPERIENCED CRYSTALLOGRAPHIC REFEREE.

No syntax errors found.      CIF dictionary      Interpreting this report

**Datablock: P1**


---

Bond precision:    C-C = 0.0036 Å                      Wavelength=0.71073

Cell:                      a=14.0779 (12)              b=14.3401 (12)              c=14.7770 (12)  
                                     alpha=76.724 (4)              beta=71.447 (4)              gamma=67.418 (4)

Temperature:    100 K

	Calculated	Reported
Volume	2591.5 (4)	2591.5 (4)
Space group	P -1	P -1
Hall group	-P 1	-P 1
Moiety formula	C <sub>44</sub> H <sub>52</sub> Cl N <sub>6</sub> Si, 2(C <sub>6</sub> H <sub>4</sub> F <sub>2</sub> ), Cl	C <sub>44</sub> H <sub>52</sub> Cl N <sub>6</sub> Si, 2(C <sub>6</sub> H <sub>4</sub> F <sub>2</sub> ), Cl
Sum formula	C <sub>56</sub> H <sub>60</sub> Cl <sub>2</sub> F <sub>4</sub> N <sub>6</sub> Si	C <sub>56</sub> H <sub>60</sub> Cl <sub>2</sub> F <sub>4</sub> N <sub>6</sub> Si
Mr	992.09	992.09
Dx, g cm <sup>-3</sup>	1.271	1.271
Z	2	2
Mu (mm <sup>-1</sup> )	0.206	0.206
F000	1044.0	1044.0
F000'	1045.17	
h, k, lmax	16, 17, 17	16, 17, 17
Nref	9519	9486
Tmin, Tmax	0.929, 0.974	0.546, 0.745
Tmin'	0.925	

Correction method= # Reported T Limits: Tmin=0.546 Tmax=0.745  
 AbsCorr = MULTI-SCAN

Data completeness= 0.997                      Theta(max)= 25.390

R(reflections)= 0.0457( 6937)              wR2(reflections)= 0.1092( 9486)

S = 1.028                                      Npar= 634

---

The following ALERTS were generated. Each ALERT has the format

**test-name\_ALERT\_alert-type\_alert-level.**

Click on the hyperlinks for more details of the test.

---

**Alert level C**

PLAT334_ALERT_2_C	Small Average Benzene C-C Dist. C45 -C50	1.37	Ang.
PLAT334_ALERT_2_C	Small Average Benzene C-C Dist. C51 -C56	1.37	Ang.
PLAT906_ALERT_3_C	Large K value in the Analysis of Variance .....	2.526	Check
PLAT910_ALERT_3_C	Missing # of FCF Reflection(s) Below Theta(Min)	7	Note
PLAT911_ALERT_3_C	Missing # FCF Refl Between THmin & STh/L= 0.600	7	Report

---

**Alert level G**

PLAT154_ALERT_1_G	The s.u.'s on the Cell Angles are Equal ..(Note)	0.004	Degree
PLAT300_ALERT_4_G	Atom Site Occupancy of *H16A is Constrained at	0.5	Check
PLAT300_ALERT_4_G	Atom Site Occupancy of *H16B is Constrained at	0.5	Check
PLAT300_ALERT_4_G	Atom Site Occupancy of *H16C is Constrained at	0.5	Check
PLAT300_ALERT_4_G	Atom Site Occupancy of *H16D is Constrained at	0.5	Check
PLAT300_ALERT_4_G	Atom Site Occupancy of *H16E is Constrained at	0.5	Check
PLAT300_ALERT_4_G	Atom Site Occupancy of *H16F is Constrained at	0.5	Check
PLAT300_ALERT_4_G	Atom Site Occupancy of *H24A is Constrained at	0.5	Check
PLAT300_ALERT_4_G	Atom Site Occupancy of *H24B is Constrained at	0.5	Check
PLAT300_ALERT_4_G	Atom Site Occupancy of *H24C is Constrained at	0.5	Check
PLAT300_ALERT_4_G	Atom Site Occupancy of *H24D is Constrained at	0.5	Check
PLAT300_ALERT_4_G	Atom Site Occupancy of *H24E is Constrained at	0.5	Check
PLAT300_ALERT_4_G	Atom Site Occupancy of *H24F is Constrained at	0.5	Check
PLAT300_ALERT_4_G	Atom Site Occupancy of *H34A is Constrained at	0.5	Check
PLAT300_ALERT_4_G	Atom Site Occupancy of *H34B is Constrained at	0.5	Check
PLAT300_ALERT_4_G	Atom Site Occupancy of *H34C is Constrained at	0.5	Check
PLAT300_ALERT_4_G	Atom Site Occupancy of *H34D is Constrained at	0.5	Check
PLAT300_ALERT_4_G	Atom Site Occupancy of *H34E is Constrained at	0.5	Check
PLAT300_ALERT_4_G	Atom Site Occupancy of *H34F is Constrained at	0.5	Check
PLAT790_ALERT_4_G	Centre of Gravity not Within Unit Cell: Resd. # C6 H4 F2	3	Note
PLAT912_ALERT_4_G	Missing # of FCF Reflections Above STh/L= 0.600	25	Note
PLAT978_ALERT_2_G	Number C-C Bonds with Positive Residual Density	3	Note

---

- 0 **ALERT level A** = Most likely a serious problem - resolve or explain  
 0 **ALERT level B** = A potentially serious problem, consider carefully  
 5 **ALERT level C** = Check. Ensure it is not caused by an omission or oversight  
 22 **ALERT level G** = General information/check it is not something unexpected
- 1 ALERT type 1 CIF construction/syntax error, inconsistent or missing data  
 3 ALERT type 2 Indicator that the structure model may be wrong or deficient  
 3 ALERT type 3 Indicator that the structure quality may be low  
 20 ALERT type 4 Improvement, methodology, query or suggestion  
 0 ALERT type 5 Informative message, check
-

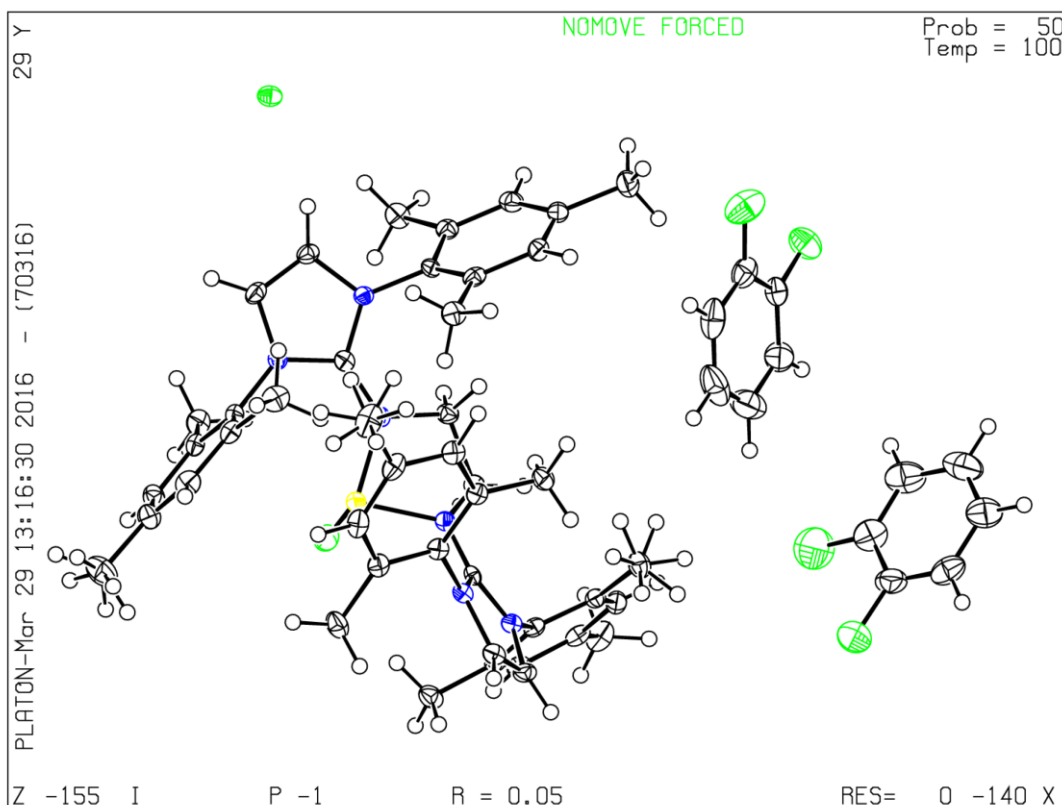
## Publication of your CIF

You should attempt to resolve as many as possible of the alerts in all categories. Often the minor alerts point to easily fixed oversights, errors and omissions in your CIF or refinement strategy, so attention to these fine details can be worthwhile. In order to resolve some of the more serious problems it may be necessary to carry out additional measurements or structure refinements. However, the nature of your study may justify the reported deviations from journal submission requirements and the more serious of these should be commented upon in the discussion or experimental section of a paper or in the "special\_details" fields of the CIF. *checkCIF* was carefully designed to identify outliers and unusual parameters, but every test has its limitations and alerts that are not important in a particular case may appear. Conversely, the absence of alerts does not guarantee there are no aspects of the results needing attention. It is up to the individual to critically assess their own results and, if necessary, seek expert advice.

If you wish to submit your CIF for publication in Acta Crystallographica Section C or E, you should upload your CIF via the web. If you wish to submit your CIF for publication in IUCrData you should upload your CIF via the web. If your CIF is to form part of a submission to another IUCr journal, you will be asked, either during electronic submission or by the Co-editor handling your paper, to upload your CIF via our web site.

## PLATON version of 07/03/2016; check.def file version of 02/03/2016

Datablock 1 - ellipsoid plot



**checkCIF/PLATON report**

Structure factors have been supplied for datablock(s) HanFr8\_fine

THIS REPORT IS FOR GUIDANCE ONLY. IF USED AS PART OF A REVIEW PROCEDURE FOR PUBLICATION, IT SHOULD NOT REPLACE THE EXPERTISE OF AN EXPERIENCED CRYSTALLOGRAPHIC REFEREE.

No syntax errors found.      CIF dictionary      Interpreting this report

**Datablock: P4**


---

Bond precision:    C-C = 0.0085 A                      Wavelength=0.71073

Cell:                      a=19.649(2)              b=27.963(3)              c=21.220(3)  
                                     alpha=90                      beta=90.277(4)              gamma=90

Temperature:              100 K

	Calculated	Reported
Volume	11659(2)	11659(2)
Space group	P 21/n	P 21/n
Hall group	-P 2yn	-P 2yn
Moiety formula	2(C44 H52 Cl3 N6 Si), 2(C4 H10 O), 7(C2 H3 N), 2(Cl)	2(C44 H52 Cl3 N6 Si), 2(C4 H10 O), 7(C2 H3 N), 2(Cl)
Sum formula	C110 H145 Cl8 N19 O2 Si2	C110 H145 Cl8 N19 O2 Si2
Mr	2105.23	2105.23
Dx, g cm <sup>-3</sup>	1.199	1.199
Z	4	4
Mu (mm <sup>-1</sup> )	0.269	0.269
F000	4472.0	4472.0
F000'	4478.61	
h,k,lmax	23,33,25	23,33,25
Nref	21392	21321
Tmin,Tmax	0.964,0.973	0.689,0.745
Tmin'	0.934	

Correction method= # Reported T Limits: Tmin=0.689 Tmax=0.745  
 AbsCorr = MULTI-SCAN

Data completeness= 0.997                      Theta(max) = 25.360

R(reflections)= 0.0645( 15311)              wR2(reflections)= 0.1783( 21321)

S = 1.031                      Npar= 1524

---

The following ALERTS were generated. Each ALERT has the format

**test-name\_ALERT\_alert-type\_alert-level.**

Click on the hyperlinks for more details of the test.

### ● Alert level C

PLAT230_ALERT_2_C	Hirshfeld Test Diff for	N11	--C45	.	5.7	s.u.
PLAT244_ALERT_4_C	Low	'Solvent' Ueq as Compared to Neighbors of			C95	Check
PLAT244_ALERT_4_C	Low	'Solvent' Ueq as Compared to Neighbors of			C97	Check
PLAT244_ALERT_4_C	Low	'Solvent' Ueq as Compared to Neighbors of			C101	Check
PLAT244_ALERT_4_C	Low	'Solvent' Ueq as Compared to Neighbors of			C103	Check
PLAT250_ALERT_2_C	Large	U3/U1 Ratio for Average U(i,j) Tensor	....		2.2	Note
PLAT260_ALERT_2_C	Large	Average Ueq of Residue Including		N18	0.101	Check
PLAT340_ALERT_3_C	Low	Bond Precision on C-C Bonds	.....		0.00854	Ang.
PLAT910_ALERT_3_C	Missing # of FCF Reflection(s) Below Theta(Min).				10	Note
PLAT911_ALERT_3_C	Missing FCF Refl Between Thmin & STh/L=		0.600		22	Report

### ● Alert level G

PLAT002_ALERT_2_G	Number of Distance or Angle Restraints on AtSite				46	Note
PLAT003_ALERT_2_G	Number of Uiso or Uij Restrained non-H Atoms	...			46	Report
PLAT013_ALERT_1_G	N.O.K. _shelx_hkl_checksum Found in CIF	.....			Please	Check
PLAT083_ALERT_2_G	SHELXL Second Parameter in WGHT	Unusually Large			10.06	Why ?
PLAT175_ALERT_4_G	The CIF-Embedded .res File Contains SAME Records				3	Report
PLAT177_ALERT_4_G	The CIF-Embedded .res File Contains DELU Records				3	Report
PLAT178_ALERT_4_G	The CIF-Embedded .res File Contains SIMU Records				3	Report
PLAT301_ALERT_3_G	Main Residue Disorder	.....(Resd 1 )			17%	Note
PLAT301_ALERT_3_G	Main Residue Disorder	.....(Resd 2 )			17%	Note
PLAT302_ALERT_4_G	Anion/Solvent/Minor-Residue Disorder	(Resd 4 )			100%	Note
PLAT302_ALERT_4_G	Anion/Solvent/Minor-Residue Disorder	(Resd 5 )			100%	Note
PLAT304_ALERT_4_G	Non-Integer Number of Atoms in	..... (Resd 4 )			9.63	Check
PLAT304_ALERT_4_G	Non-Integer Number of Atoms in	..... (Resd 5 )			5.37	Check
PLAT411_ALERT_2_G	Short Inter H...H Contact	H64	..H20	.	2.12	Ang.
			1-x,-y,1-z =		3_656	Check
PLAT412_ALERT_2_G	Short Intra XH3 .. XHn	H8A	..H26D	.	2.10	Ang.
			x,y,z =		1_555	Check
PLAT860_ALERT_3_G	Number of Least-Squares Restraints	.....			813	Note
PLAT870_ALERT_4_G	ALERTS Related to Twinning Effects Suppressed	..			!	Info
PLAT883_ALERT_1_G	No Info/Value for _atom_sites_solution_primary	.			Please	Do !
PLAT912_ALERT_4_G	Missing # of FCF Reflections Above STh/L=	0.600			48	Note
PLAT913_ALERT_3_G	Missing # of Very Strong Reflections in FCF	....			1	Note
PLAT931_ALERT_5_G	CIFcalcFCF Twin Law	[ 0 0 1]	Est.d BASF		0.39	Check
PLAT941_ALERT_3_G	Average HKL Measurement Multiplicity	.....			3.9	Low

0 **ALERT level A** = Most likely a serious problem - resolve or explain  
 0 **ALERT level B** = A potentially serious problem, consider carefully  
 10 **ALERT level C** = Check. Ensure it is not caused by an omission or oversight  
 22 **ALERT level G** = General information/check it is not something unexpected

2 ALERT type 1 CIF construction/syntax error, inconsistent or missing data  
 8 ALERT type 2 Indicator that the structure model may be wrong or deficient  
 8 ALERT type 3 Indicator that the structure quality may be low  
 13 ALERT type 4 Improvement, methodology, query or suggestion  
 1 ALERT type 5 Informative message, check

It is advisable to attempt to resolve as many as possible of the alerts in all categories. Often the minor alerts point to easily fixed oversights, errors and omissions in your CIF or refinement strategy, so attention to these fine details can be worthwhile. In order to resolve some of the more serious problems it may be necessary to carry out additional measurements or structure refinements. However, the purpose of your study may justify the reported deviations and the more serious of these should normally be commented upon in the discussion or experimental section of a paper or in the "special\_details" fields of the CIF. checkCIF was carefully designed to identify outliers and unusual parameters, but every test has its limitations and alerts that are not important in a particular case may appear. Conversely, the absence of alerts does not guarantee there are no aspects of the results needing attention. It is up to the individual to critically assess their own results and, if necessary, seek expert advice.

### Publication of your CIF in IUCr journals

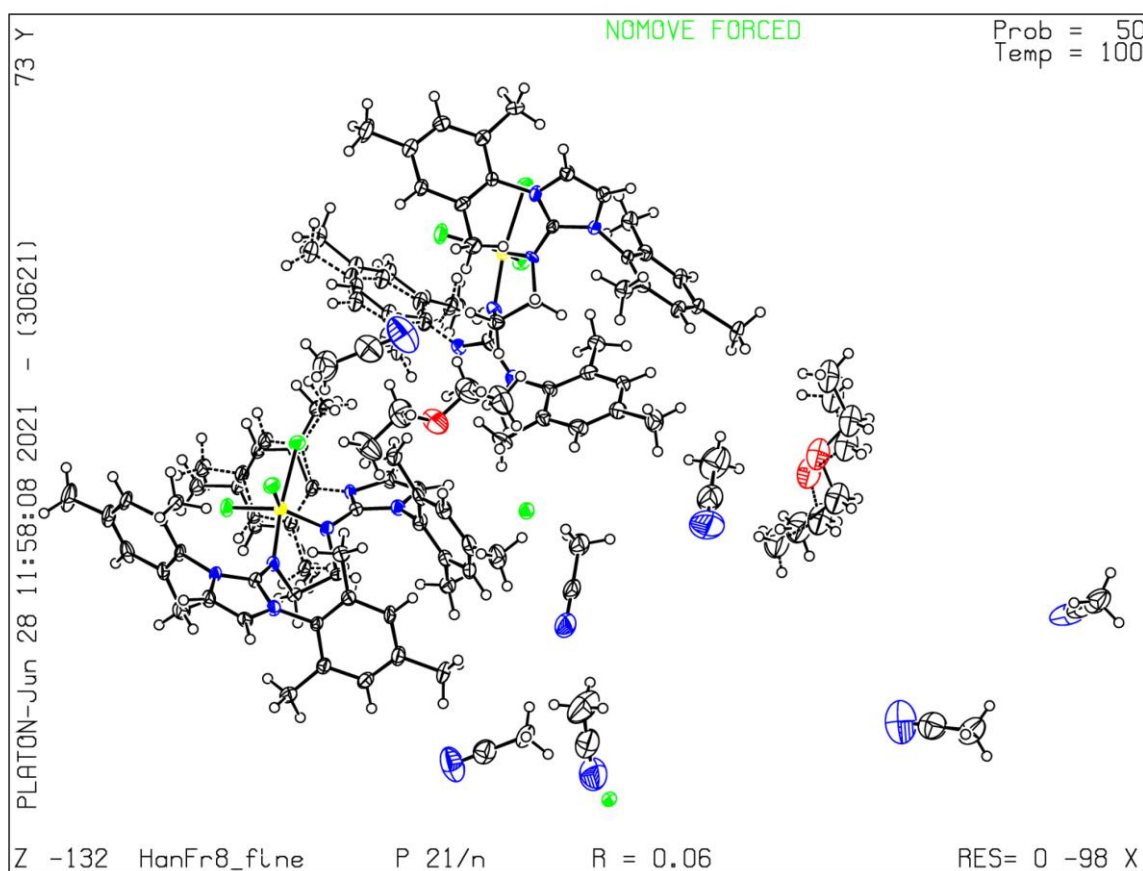
A basic structural check has been run on your CIF. These basic checks will be run on all CIFs submitted for publication in IUCr journals (*Acta Crystallographica*, *Journal of Applied Crystallography*, *Journal of Synchrotron Radiation*); however, if you intend to submit to *Acta Crystallographica Section C* or *E* or *IUCrData*, you should make sure that full publication checks are run on the final version of your CIF prior to submission.

### Publication of your CIF in other journals

Please refer to the *Notes for Authors* of the relevant journal for any special instructions relating to CIF submission.

PLATON version of 03/06/2021; check.def file version of 02/06/2021

Datablock HanFr8\_fine - ellipsoid plot



## checkCIF/PLATON report

Structure factors have been supplied for datablock(s) HanFr34\_sq\_fine

THIS REPORT IS FOR GUIDANCE ONLY. IF USED AS PART OF A REVIEW PROCEDURE FOR PUBLICATION, IT SHOULD NOT REPLACE THE EXPERTISE OF AN EXPERIENCED CRYSTALLOGRAPHIC REFEREE.

No syntax errors found.      CIF dictionary      Interpreting this report

### Datablock: P7

Bond precision:	C-C = 0.0076 Å	Wavelength=0.71073	
Cell:	a=11.7048 (9)	b=16.0873 (14)	c=16.8481 (15)
	alpha=82.688 (3)	beta=69.690 (3)	gamma=68.662 (3)
Temperature:	100 K		
	Calculated	Reported	
Volume	2771.3 (4)	2771.3 (4)	
Space group	P -1	P -1	
Hall group	-P 1	-P 1	
Moiety formula	C44 H54 N6 Si, 2(I) [+ solvent]	C44 H54 N6 Si, 2(I)	
Sum formula	C44 H54 I2 N6 Si [+ solvent]	C44 H54 I2 N6 Si	
Mr	948.82	948.82	
Dx, g cm <sup>-3</sup>	1.137	1.137	
Z	2	2	
Mu (mm <sup>-1</sup> )	1.186	1.186	
F000	960.0	960.0	
F000'	958.52		
h, k, lmax	14, 19, 20	14, 19, 20	
Nref	10156	10122	
Tmin, Tmax	0.823, 0.869	0.656, 0.745	
Tmin'	0.656		

Correction method= # Reported T Limits: Tmin=0.656 Tmax=0.745  
AbsCorr = MULTII-SCAN

Data completeness= 0.997                      Theta(max)= 25.350

---

R(reflections)= 0.0355( 8273) wR2(reflections)=  
0.0923( 10122)  
S = 1.025 Npar= 539

---

The following ALERTS were generated. Each ALERT has the format  
**test-name\_ALERT\_alert-type\_alert-level.**  
Click on the hyperlinks for more details of the test.

---

 **Alert level B**

PLAT112\_ALERT\_2\_B ADDSYM Detects New (Pseudo) Symm. Elem n 100 %Fit

**Author Response: The data was carefully checked for higher symmetry. Orthorhombic and monoclinic spacegroups were tested, but resulted in unstable and/or unfavorable refinements. This alerts may be caused by twinning and/or disorder of the crystal.**

PLAT112\_ALERT\_2\_B ADDSYM Detects New (Pseudo) Symm. Elem c 100 %Fit

**Author Response: The data was carefully checked for higher symmetry. Orthorhombic and monoclinic spacegroups were tested, but resulted in unstable and/or unfavorable refinements. This alerts may be caused by twinning and/or disorder of the crystal.**

PLAT112\_ALERT\_2\_B ADDSYM Detects New (Pseudo) Symm. Elem n 100 %Fit

**Author Response: The data was carefully checked for higher symmetry. Orthorhombic and monoclinic spacegroups were tested, but resulted in unstable and/or unfavorable refinements. This alerts may be caused by twinning and/or disorder of the crystal.**

PLAT113\_ALERT\_2\_B ADDSYM Suggests Possible Pseudo/New Space Group Fddd Check

**Author Response: The data was carefully checked for higher symmetry. Orthorhombic and monoclinic spacegroups were tested, but resulted in unstable and/or unfavorable refinements. This alerts may be caused by twinning and/or disorder of the crystal.**

---

 **Alert level C**

PLAT155_ALERT_4_C The Triclinic Unitcell is NOT Reduced .....	Please Do !
PLAT250_ALERT_2_C Large U3/U1 Ratio for Average U(i,j) Tensor ....	2.7 Note
PLAT420_ALERT_2_C D-H Bond Without Acceptor Si1D --H01D .	Please Check
PLAT420_ALERT_2_C D-H Bond Without Acceptor Si1D --H02D .	Please Check
PLAT906_ALERT_3_C Large K Value in the Analysis of Variance .....	4.972 Check
PLAT911_ALERT_3_C Missing FCF Refl Between Thmin & STh/L= 0.600	30 Report

---

**Alert level G**

PLAT003_ALERT_2_G	Number of Uiso or Uij Restrained non-H Atoms ...	10	Report
PLAT083_ALERT_2_G	SHELXL Second Parameter in WGHT Unusually Large	5.85	Why ?
PLAT154_ALERT_1_G	The s.u.'s on the Cell Angles are Equal ..(Note)	0.003	Degree
PLAT178_ALERT_4_G	The CIF-Embedded .res File Contains SIMU Records	1	Report
PLAT187_ALERT_4_G	The CIF-Embedded .res File Contains RIGU Records	1	Report
PLAT301_ALERT_3_G	Main Residue Disorder .....(Resd 1 )	10%	Note
PLAT380_ALERT_4_G	Incorrectly? Oriented X(sp2)-Methyl Moiety .....	C25	Check
PLAT380_ALERT_4_G	Incorrectly? Oriented X(sp2)-Methyl Moiety .....	C34	Check
PLAT606_ALERT_4_G	Solvent Accessible VOID(S) in Structure .....	!	Info
PLAT720_ALERT_4_G	Number of Unusual/Non-Standard Labels .....	9	Note
PLAT790_ALERT_4_G	Centre of Gravity not Within Unit Cell: Resd. # I	2	Note
PLAT790_ALERT_4_G	Centre of Gravity not Within Unit Cell: Resd. # I	3	Note
PLAT860_ALERT_3_G	Number of Least-Squares Restraints .....	204	Note
PLAT869_ALERT_4_G	ALERTS Related to the Use of SQUEEZE Suppressed	!	Info
PLAT883_ALERT_1_G	No Info/Value for _atom_sites_solution_primary .	Please	Do !
PLAT910_ALERT_3_G	Missing # of FCF Reflection(s) Below Theta(Min).	4	Note
PLAT912_ALERT_4_G	Missing # of FCF Reflections Above STh/L= 0.600	2	Note
PLAT933_ALERT_2_G	Number of OMIT Records in Embedded .res File ...	5	Note
PLAT941_ALERT_3_G	Average HKL Measurement Multiplicity .....	3.9	Low
PLAT978_ALERT_2_G	Number C-C Bonds with Positive Residual Density.	1	Info

- 
- 0 **ALERT level A** = Most likely a serious problem - resolve or explain  
4 **ALERT level B** = A potentially serious problem, consider carefully  
6 **ALERT level C** = Check. Ensure it is not caused by an omission or oversight  
20 **ALERT level G** = General information/check it is not something unexpected
- 2 ALERT type 1 CIF construction/syntax error, inconsistent or missing data  
11 ALERT type 2 Indicator that the structure model may be wrong or deficient  
6 ALERT type 3 Indicator that the structure quality may be low  
11 ALERT type 4 Improvement, methodology, query or suggestion  
0 ALERT type 5 Informative message, check
-

It is advisable to attempt to resolve as many as possible of the alerts in all categories. Often the minor alerts point to easily fixed oversights, errors and omissions in your CIF or refinement strategy, so attention to these fine details can be worthwhile. In order to resolve some of the more serious problems it may be necessary to carry out additional measurements or structure refinements. However, the purpose of your study may justify the reported deviations and the more serious of these should normally be commented upon in the discussion or experimental section of a paper or in the "special\_details" fields of the CIF. checkCIF was carefully designed to identify outliers and unusual parameters, but every test has its limitations and alerts that are not important in a particular case may appear. Conversely, the absence of alerts does not guarantee there are no aspects of the results needing attention. It is up to the individual to critically assess their own results and, if necessary, seek expert advice.

#### Publication of your CIF in IUCr journals

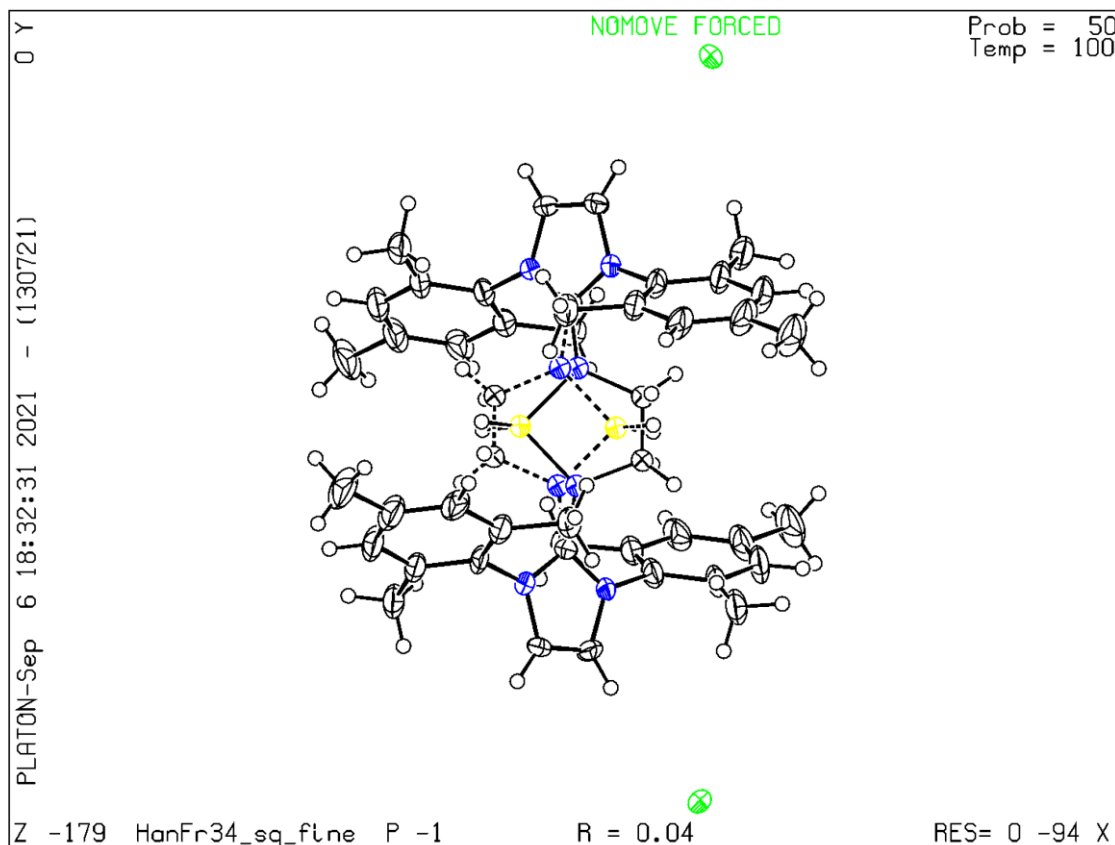
A basic structural check has been run on your CIF. These basic checks will be run on all CIFs submitted for publication in IUCr journals (*Acta Crystallographica*, *Journal of Applied Crystallography*, *Journal of Synchrotron Radiation*); however, if you intend to submit to *Acta Crystallographica Section C* or *E* or *IUCrData*, you should make sure that full publication checks are run on the final version of your CIF prior to submission.

#### Publication of your CIF in other journals

Please refer to the *Notes for Authors* of the relevant journal for any special instructions relating to CIF submission.

PLATON version of 13/07/2021; check.def file version of 13/07/2021

Datablock HanFr34\_sq\_fine - ellipsoid plot



## checkCIF/PLATON report

Structure factors have been supplied for datablock(s) I

THIS REPORT IS FOR GUIDANCE ONLY. IF USED AS PART OF A REVIEW PROCEDURE FOR PUBLICATION, IT SHOULD NOT REPLACE THE EXPERTISE OF AN EXPERIENCED CRYSTALLOGRAPHIC REFEREE.

No syntax errors found.      CIF dictionary      Interpreting this report

### Datablock: P8

---

Bond precision:    C-C = 0.0023 A                      Wavelength=0.71073

Cell:                      a=12.2139(11)              b=14.4858(13)              c=15.2925(13)  
                                     alpha=70.258(3)              beta=84.626(3)              gamma=80.130(3)

Temperature:    100 K

	Calculated	Reported
Volume	2507.1(4)	2507.1(4)
Space group	P -1	P -1
Hall group	-P 1	-P 1
Moiety formula	C44 H52 Cl N6 S Si, 3(C2 H3 N), Cl	C44 H52 Cl N6 S Si, 3(C2 H3 N), Cl
Sum formula	C50 H61 Cl2 N9 S Si	C50 H61 Cl2 N9 S Si
Mr	919.13	919.13
Dx, g cm-3	1.218	1.218
Z	2	2
Mu (mm-1)	0.238	0.238
F000	976.0	976.0
F000'	977.26	
h,k,lmax	14,17,18	14,17,18
Nref	9250	9241
Tmin,Tmax	0.942,0.958	0.714,0.745
Tmin'	0.937	

Correction method= # Reported T Limits: Tmin=0.714 Tmax=0.745  
 AbsCorr = MULTI-SCAN

Data completeness= 0.999                      Theta(max)= 25.420

R(reflections)= 0.0346( 8416)                      wR2(reflections)= 0.0961( 9241)

S = 1.038                                      Npar= 583

---

The following ALERTS were generated. Each ALERT has the format  
**test-name\_ALERT\_alert-type\_alert-level**.  
 Click on the hyperlinks for more details of the test.

---

● <b>Alert level C</b>		
PLAT910_ALERT_3_C	Missing # of FCF Reflection(s) Below Theta(Min).	8 Note

---

● <b>Alert level G</b>		
PLAT154_ALERT_1_G	The s.u.'s on the Cell Angles are Equal ..(Note)	0.003 Degree
PLAT720_ALERT_4_G	Number of Unusual/Non-Standard Labels .....	2 Note
PLAT790_ALERT_4_G	Centre of Gravity not Within Unit Cell: Resd. # C2 H3 N	4 Note
PLAT790_ALERT_4_G	Centre of Gravity not Within Unit Cell: Resd. # C1	5 Note
PLAT883_ALERT_1_G	No Info/Value for _atom_sites_solution_primary .	Please Do !
PLAT912_ALERT_4_G	Missing # of FCF Reflections Above STh/L= 0.600	7 Note
PLAT933_ALERT_2_G	Number of OMIT Records in Embedded .res File ...	5 Note
PLAT978_ALERT_2_G	Number C-C Bonds with Positive Residual Density.	10 Info

---

0 **ALERT level A** = Most likely a serious problem - resolve or explain  
 0 **ALERT level B** = A potentially serious problem, consider carefully  
 1 **ALERT level C** = Check. Ensure it is not caused by an omission or oversight  
 8 **ALERT level G** = General information/check it is not something unexpected

2 ALERT type 1 CIF construction/syntax error, inconsistent or missing data  
 2 ALERT type 2 Indicator that the structure model may be wrong or deficient  
 1 ALERT type 3 Indicator that the structure quality may be low  
 4 ALERT type 4 Improvement, methodology, query or suggestion  
 0 ALERT type 5 Informative message, check

---

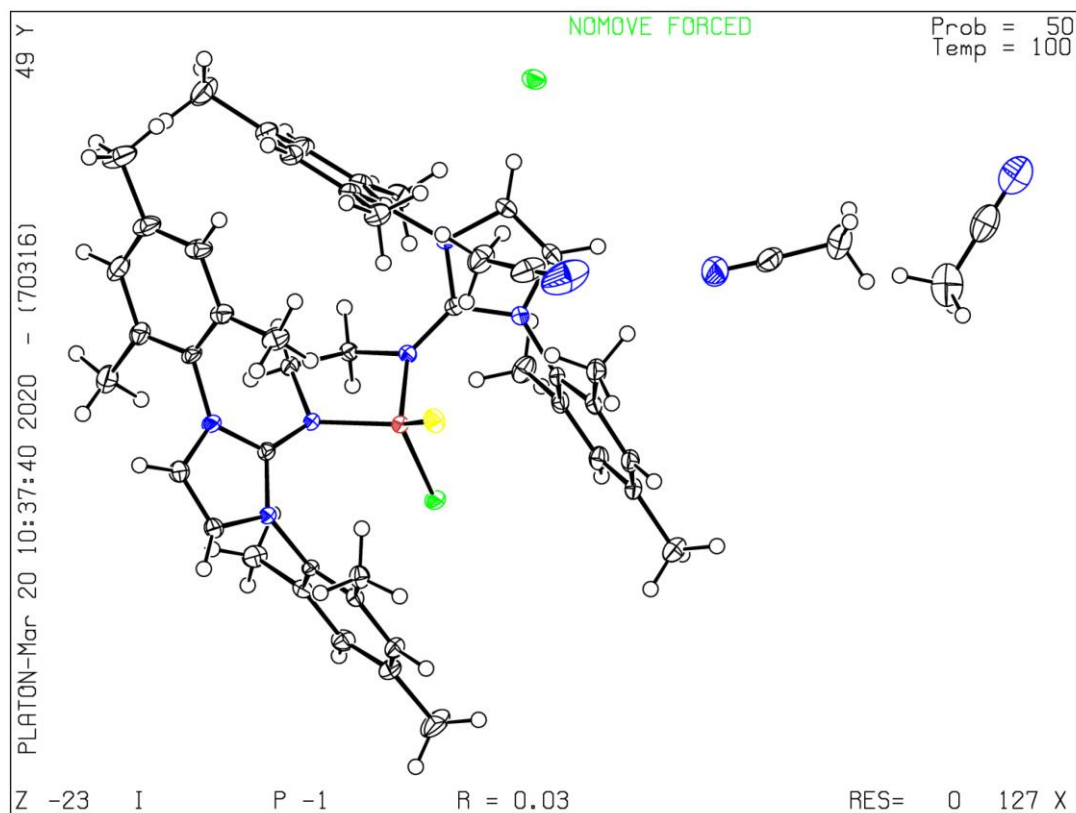
### Publication of your CIF

You should attempt to resolve as many as possible of the alerts in all categories. Often the minor alerts point to easily fixed oversights, errors and omissions in your CIF or refinement strategy, so attention to these fine details can be worthwhile. In order to resolve some of the more serious problems it may be necessary to carry out additional measurements or structure refinements. However, the nature of your study may justify the reported deviations from journal submission requirements and the more serious of these should be commented upon in the discussion or experimental section of a paper or in the "special\_details" fields of the CIF. *checkCIF* was carefully designed to identify outliers and unusual parameters, but every test has its limitations and alerts that are not important in a particular case may appear. Conversely, the absence of alerts does not guarantee there are no aspects of the results needing attention. It is up to the individual to critically assess their own results and, if necessary, seek expert advice.

If you wish to submit your CIF for publication in Acta Crystallographica Section C or E, you should upload your CIF via the web. If you wish to submit your CIF for publication in IUCrData you should upload your CIF via the web. If your CIF is to form part of a submission to another IUCr journal, you will be asked, either during electronic submission or by the Co-editor handling your paper, to upload your CIF via our web site.

## PLATON version of 22/12/2019; check.def file version of 13/12/2019

Datablock I - ellipsoid plot



**checkCIF/PLATON report**

Structure factors have been supplied for datablock(s) HanFr13\_fine

THIS REPORT IS FOR GUIDANCE ONLY. IF USED AS PART OF A REVIEW PROCEDURE FOR PUBLICATION, IT SHOULD NOT REPLACE THE EXPERTISE OF AN EXPERIENCED CRYSTALLOGRAPHIC REFEREE.

No syntax errors found.      CIF dictionary      Interpreting this report

**Datablock: P17**


---

Bond precision:    C-C = 0.0049 Å                      Wavelength=0.71073

Cell:                      a=30.060(2)              b=16.7584(11)              c=23.3357(16)  
                                     alpha=90                      beta=121.366(2)              gamma=90

Temperature:              100 K

	Calculated	Reported
Volume	10037.6(12)	10037.6(12)
Space group	C 2/c	C 2/c
Hall group	-C 2yc	-C 2yc
Moiety formula	C48 H52 Au Cl Fe N6 O4 Si [+ solvent]	C48 H52 Au Cl Fe N6 O4 Si
Sum formula	C48 H52 Au Cl Fe N6 O4 Si [+ solvent]	C48 H52 Au Cl Fe N6 O4 Si1
Mr	1093.32	1093.32
Dx, g cm <sup>-3</sup>	1.447	1.447
Z	8	8
Mu (mm <sup>-1</sup> )	3.332	3.332
F000	4400.0	4400.0
F000'	4390.09	
h,k,lmax	36,20,28	36,20,28
Nref	9210	9204
Tmin,Tmax	0.562,0.738	0.661,0.745
Tmin'	0.551	

Correction method= # Reported T Limits: Tmin=0.661 Tmax=0.745  
 AbsCorr = MULTI-SCAN

Data completeness= 0.999                      Theta(max)= 25.350

R(reflections)= 0.0213( 8071)                      wR2(reflections)= 0.0533( 9204)

S = 1.139                                      Npar= 571

---

The following ALERTS were generated. Each ALERT has the format

**test-name\_ALERT\_alert-type\_alert-level.**

Click on the hyperlinks for more details of the test.

---

### ● Alert level C

PLAT220_ALERT_2_C	NonSolvent Resd 1 C	Ueq(max) / Ueq(min) Range	3.7 Ratio
PLAT222_ALERT_3_C	NonSolvent Resd 1 H	Uiso(max)/Uiso(min) Range	4.2 Ratio
PLAT905_ALERT_3_C	Negative K value in the Analysis of Variance ...		-0.198 Report

---

### ● Alert level G

PLAT013_ALERT_1_G	N.O.K. _shelx_hkl_checksum Found in CIF .....		Please Check
PLAT083_ALERT_2_G	SHELXL Second Parameter in WGHT Unusually Large	35.84	Why ?
PLAT128_ALERT_4_G	Alternate Setting for Input Space Group C2/c		I2/a Note
PLAT230_ALERT_2_G	Hirshfeld Test Diff for O1 --C45 .	8.0	s.u.
PLAT232_ALERT_2_G	Hirshfeld Test Diff (M-X) Fe1 --C45 .	7.3	s.u.
PLAT605_ALERT_4_G	Largest Solvent Accessible VOID in the Structure	352	A**3
PLAT720_ALERT_4_G	Number of Unusual/Non-Standard Labels .....	2	Note
PLAT869_ALERT_4_G	ALERTS Related to the Use of SQUEEZE Suppressed		! Info
PLAT883_ALERT_1_G	No Info/Value for _atom_sites_solution_primary .		Please Do !
PLAT910_ALERT_3_G	Missing # of FCF Reflection(s) Below Theta(Min).	4	Note
PLAT978_ALERT_2_G	Number C-C Bonds with Positive Residual Density.	1	Info

- 
- 0 **ALERT level A** = Most likely a serious problem - resolve or explain
  - 0 **ALERT level B** = A potentially serious problem, consider carefully
  - 3 **ALERT level C** = Check. Ensure it is not caused by an omission or oversight
  - 11 **ALERT level G** = General information/check it is not something unexpected
- 
- 2 ALERT type 1 CIF construction/syntax error, inconsistent or missing data
  - 5 ALERT type 2 Indicator that the structure model may be wrong or deficient
  - 3 ALERT type 3 Indicator that the structure quality may be low
  - 4 ALERT type 4 Improvement, methodology, query or suggestion
  - 0 ALERT type 5 Informative message, check
-

It is advisable to attempt to resolve as many as possible of the alerts in all categories. Often the minor alerts point to easily fixed oversights, errors and omissions in your CIF or refinement strategy, so attention to these fine details can be worthwhile. In order to resolve some of the more serious problems it may be necessary to carry out additional measurements or structure refinements. However, the purpose of your study may justify the reported deviations and the more serious of these should normally be commented upon in the discussion or experimental section of a paper or in the "special\_details" fields of the CIF. checkCIF was carefully designed to identify outliers and unusual parameters, but every test has its limitations and alerts that are not important in a particular case may appear. Conversely, the absence of alerts does not guarantee there are no aspects of the results needing attention. It is up to the individual to critically assess their own results and, if necessary, seek expert advice.

#### Publication of your CIF in IUCr journals

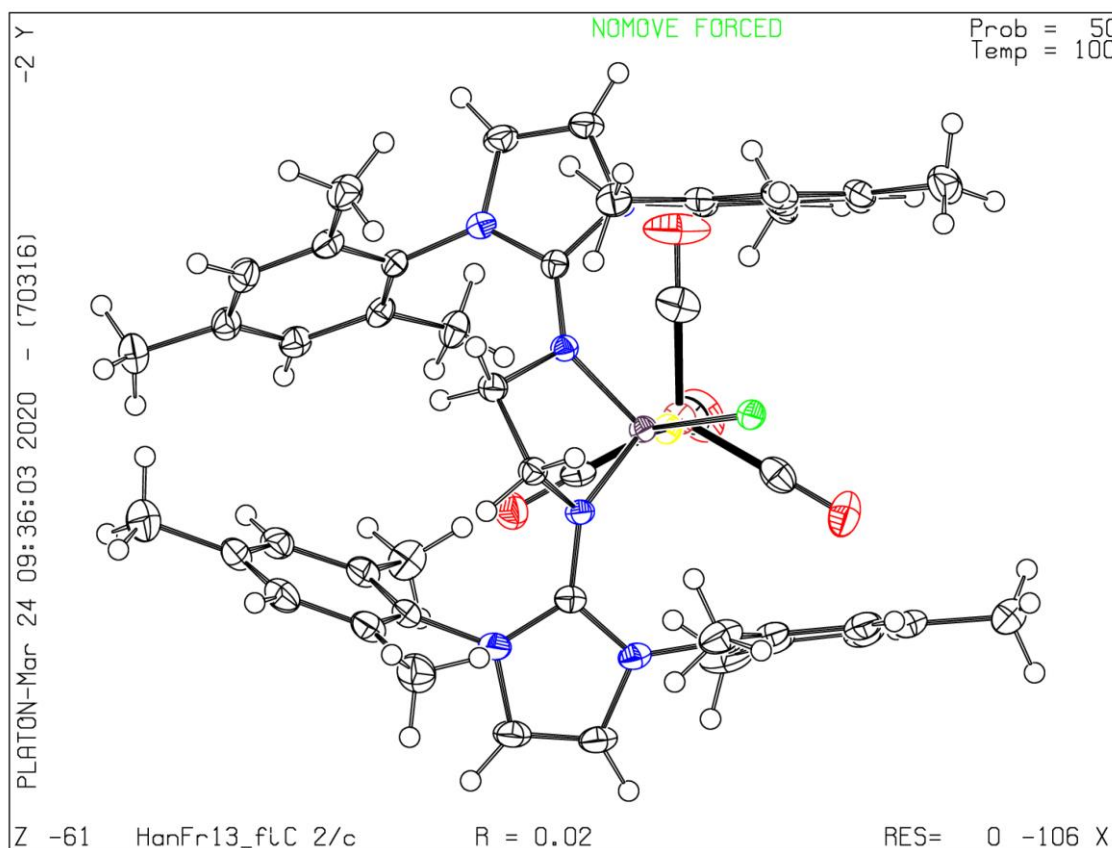
A basic structural check has been run on your CIF. These basic checks will be run on all CIFs submitted for publication in IUCr journals (*Acta Crystallographica*, *Journal of Applied Crystallography*, *Journal of Synchrotron Radiation*); however, if you intend to submit to *Acta Crystallographica Section C* or *E* or *IUCrData*, you should make sure that full publication checks are run on the final version of your CIF prior to submission.

#### Publication of your CIF in other journals

Please refer to the *Notes for Authors* of the relevant journal for any special instructions relating to CIF submission.

PLATON version of 22/12/2019; check.def file version of 13/12/2019

Datablock HanFr13\_fine - ellipsoid plot





The following ALERTS were generated. Each ALERT has the format

**test-name\_ALERT\_alert-type\_alert-level.**

Click on the hyperlinks for more details of the test.

### ● Alert level C

DIFMX02_ALERT_1_C	The maximum difference density is > 0.1*ZMAX*0.75 The relevant atom site should be identified.		
PLAT094_ALERT_2_C	Ratio of Maximum / Minimum Residual Density ....	2.98	Report
PLAT097_ALERT_2_C	Large Reported Max. (Positive) Residual Density	6.60	eA-3
PLAT234_ALERT_4_C	Large Hirshfeld Difference Fe1 --C45 .	0.16	Ang.
PLAT234_ALERT_4_C	Large Hirshfeld Difference C37 --C38 .	0.20	Ang.
PLAT234_ALERT_4_C	Large Hirshfeld Difference C38 --C39 .	0.17	Ang.
PLAT234_ALERT_4_C	Large Hirshfeld Difference C39 --C43 .	0.16	Ang.
PLAT241_ALERT_2_C	High 'MainMol' Ueq as Compared to Neighbors of		C2 Check
PLAT242_ALERT_2_C	Low 'MainMol' Ueq as Compared to Neighbors of		Fe1 Check
PLAT334_ALERT_2_C	Small Aver. Benzene C-C Dist C9 -C14	1.37	Ang.
PLAT342_ALERT_3_C	Low Bond Precision on C-C Bonds .....	0.01605	Ang.
PLAT911_ALERT_3_C	Missing FCF Refl Between Thmin & STh/L= 0.600		33 Report
PLAT973_ALERT_2_C	Check Calcd Positive Resid. Density on Aul	1.17	eA-3

### ● Alert level G

PLAT002_ALERT_2_G	Number of Distance or Angle Restraints on AtSite	16	Note
PLAT003_ALERT_2_G	Number of Uiso or Uij Restrained non-H Atoms ...	16	Report
PLAT083_ALERT_2_G	SHELXL Second Parameter in WGHT Unusually Large	68.03	Why ?
PLAT175_ALERT_4_G	The CIF-Embedded .res File Contains SAME Records	2	Report
PLAT178_ALERT_4_G	The CIF-Embedded .res File Contains SIMU Records	2	Report
PLAT186_ALERT_4_G	The CIF-Embedded .res File Contains ISOR Records	1	Report
PLAT232_ALERT_2_G	Hirshfeld Test Diff (M-X) Fe1 --C45D .	5.6	s.u.
PLAT301_ALERT_3_G	Main Residue Disorder .....(Resd 1 )	12%	Note
PLAT410_ALERT_2_G	Short Intra H...H Contact H8B ..H53D .	1.97	Ang.
	x,y,z = 1_555		Check
PLAT410_ALERT_2_G	Short Intra H...H Contact H40 ..H51D .	2.10	Ang.
	x,y,z = 1_555		Check
PLAT606_ALERT_4_G	Solvent Accessible VOID(S) in Structure .....	!	Info
PLAT860_ALERT_3_G	Number of Least-Squares Restraints .....	253	Note
PLAT869_ALERT_4_G	ALERTS Related to the Use of SQUEEZE Suppressed	!	Info
PLAT883_ALERT_1_G	No Info/Value for _atom_sites_solution_primary .		Please Do !
PLAT910_ALERT_3_G	Missing # of FCF Reflection(s) Below Theta(Min).	4	Note
PLAT912_ALERT_4_G	Missing # of FCF Reflections Above STh/L= 0.600	2	Note
PLAT913_ALERT_3_G	Missing # of Very Strong Reflections in FCF ....	1	Note
PLAT933_ALERT_2_G	Number of OMIT Records in Embedded .res File ...	3	Note
PLAT978_ALERT_2_G	Number C-C Bonds with Positive Residual Density.	1	Info

- 
- 0 **ALERT level A** = Most likely a serious problem - resolve or explain  
 0 **ALERT level B** = A potentially serious problem, consider carefully  
 13 **ALERT level C** = Check. Ensure it is not caused by an omission or oversight  
 19 **ALERT level G** = General information/check it is not something unexpected
- 2 ALERT type 1 CIF construction/syntax error, inconsistent or missing data  
 14 ALERT type 2 Indicator that the structure model may be wrong or deficient  
 6 ALERT type 3 Indicator that the structure quality may be low  
 10 ALERT type 4 Improvement, methodology, query or suggestion  
 0 ALERT type 5 Informative message, check
-

It is advisable to attempt to resolve as many as possible of the alerts in all categories. Often the minor alerts point to easily fixed oversights, errors and omissions in your CIF or refinement strategy, so attention to these fine details can be worthwhile. In order to resolve some of the more serious problems it may be necessary to carry out additional measurements or structure refinements. However, the purpose of your study may justify the reported deviations and the more serious of these should normally be commented upon in the discussion or experimental section of a paper or in the "special\_details" fields of the CIF. checkCIF was carefully designed to identify outliers and unusual parameters, but every test has its limitations and alerts that are not important in a particular case may appear. Conversely, the absence of alerts does not guarantee there are no aspects of the results needing attention. It is up to the individual to critically assess their own results and, if necessary, seek expert advice.

#### Publication of your CIF in IUCr journals

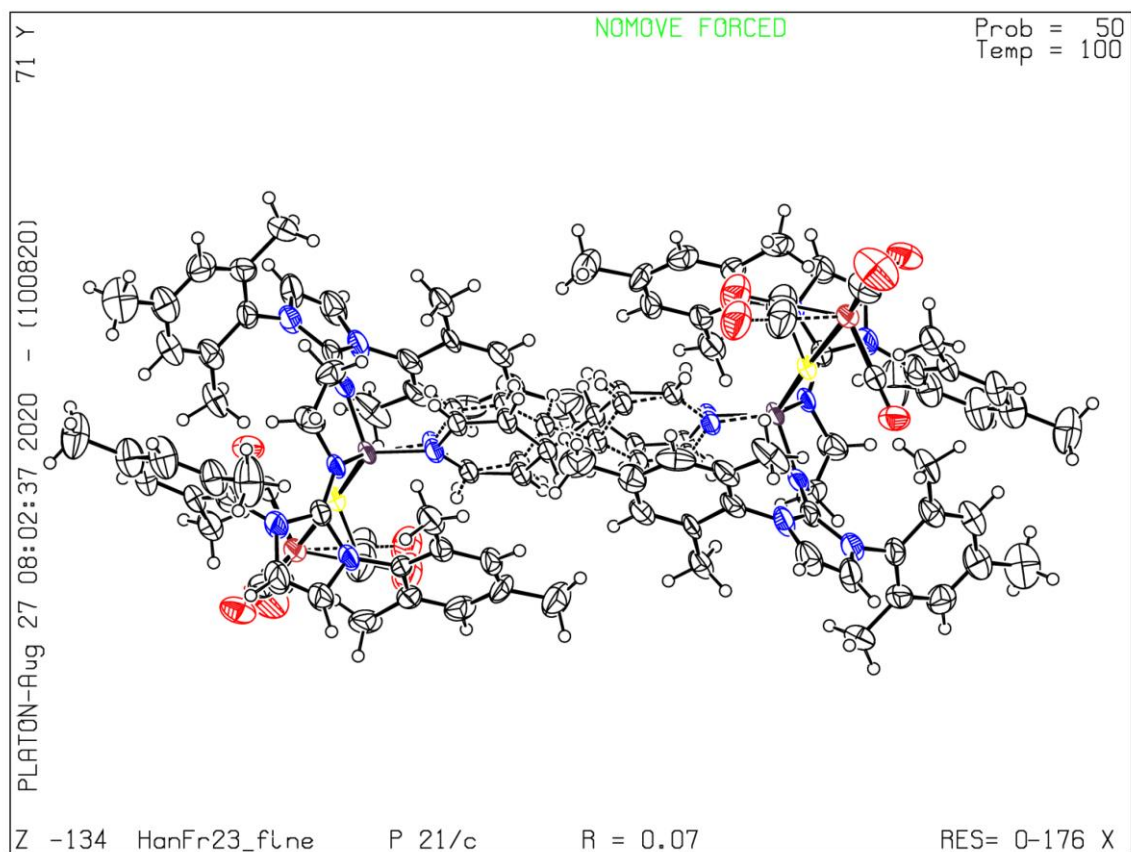
A basic structural check has been run on your CIF. These basic checks will be run on all CIFs submitted for publication in IUCr journals (*Acta Crystallographica*, *Journal of Applied Crystallography*, *Journal of Synchrotron Radiation*); however, if you intend to submit to *Acta Crystallographica Section C* or *E* or *IUCrData*, you should make sure that full publication checks are run on the final version of your CIF prior to submission.

#### Publication of your CIF in other journals

Please refer to the *Notes for Authors* of the relevant journal for any special instructions relating to CIF submission.

PLATON version of 10/08/2020; check.def file version of 06/08/2020

Datablock HanFr23\_fine - ellipsoid plot



**checkCIF/PLATON report**

Structure factors have been supplied for datablock(s) HanFr35\_fine

THIS REPORT IS FOR GUIDANCE ONLY. IF USED AS PART OF A REVIEW PROCEDURE FOR PUBLICATION, IT SHOULD NOT REPLACE THE EXPERTISE OF AN EXPERIENCED CRYSTALLOGRAPHIC REFEREE.

No syntax errors found.      CIF dictionary      Interpreting this report

**Datablock: P21**

Bond precision:	C-C = 0.0031 A	Wavelength=0.71073	
Cell:	a=12.1472 (6)	b=18.4259 (9)	c=22.6851 (11)
	alpha=90	beta=99.409 (2)	gamma=90
Temperature:	100 K		
	Calculated	Reported	
Volume	5009.1 (4)	5009.1 (4)	
Space group	P 21/n	P 21/n	
Hall group	-P 2yn	-P 2yn	
Moiety formula	C48 H52 Fe N6 O4 Si, C4 H10 O	C48 H52 Fe N6 O4 Si, C4 H10 O	
Sum formula	C52 H62 Fe N6 O5 Si	C52 H62 Fe N6 O5 Si	
Mr	935.02	935.02	
D <sub>x</sub> , g cm <sup>-3</sup>	1.240	1.240	
Z	4	4	
Mu (mm <sup>-1</sup> )	0.377	0.377	
F000	1984.0	1984.0	
F000'	1986.39		
h, k, lmax	14, 22, 27	14, 22, 27	
Nref	9173	9167	
Tmin, Tmax	0.902, 0.936	0.714, 0.745	
Tmin'	0.902		

Correction method= # Reported T Limits: Tmin=0.714 Tmax=0.745  
AbsCorr = MULTI-SCAN

Data completeness= 0.999      Theta(max)= 25.350

R(reflections)= 0.0426 ( 8396)      wR2(reflections)=  
0.1222 ( 9167)

S = 1.021      Npar= 651

The following ALERTS were generated. Each ALERT has the format

**test-name\_ALERT\_alert-type\_alert-level.**

Click on the hyperlinks for more details of the test.

### ● Alert level C

PLAT420_ALERT_2_C	D-H Bond Without Acceptor Sil	--H1	.	Please Check
PLAT906_ALERT_3_C	Large K Value in the Analysis of Variance	.....		2.197 Check
PLAT911_ALERT_3_C	Missing FCF Refl Between Thmin & STh/L=	0.600		4 Report

### ● Alert level G

PLAT002_ALERT_2_G	Number of Distance or Angle Restraints on AtSite			10 Note
PLAT003_ALERT_2_G	Number of Uiso or Uij Restrained non-H Atoms ...			10 Report
PLAT013_ALERT_1_G	N.O.K. _shelx_hkl_checksum Found in CIF	.....		Please Check
PLAT083_ALERT_2_G	SHELXL Second Parameter in WGHT Unusually Large			6.32 Why ?
PLAT175_ALERT_4_G	The CIF-Embedded .res File Contains SAME Records			1 Report
PLAT178_ALERT_4_G	The CIF-Embedded .res File Contains SIMU Records			1 Report
PLAT230_ALERT_2_G	Hirshfeld Test Diff for O2	--C46	.	6.9 s.u.
PLAT232_ALERT_2_G	Hirshfeld Test Diff (M-X) Fel	--C45	.	7.2 s.u.
PLAT232_ALERT_2_G	Hirshfeld Test Diff (M-X) Fel	--C46	.	10.7 s.u.
PLAT232_ALERT_2_G	Hirshfeld Test Diff (M-X) Fel	--C47	.	6.5 s.u.
PLAT232_ALERT_2_G	Hirshfeld Test Diff (M-X) Fel	--C48	.	7.5 s.u.
PLAT302_ALERT_4_G	Anion/Solvent/Minor-Residue Disorder (Resd 2 )			100% Note
PLAT302_ALERT_4_G	Anion/Solvent/Minor-Residue Disorder (Resd 3 )			100% Note
PLAT304_ALERT_4_G	Non-Integer Number of Atoms in ..... (Resd 2 )			11.58 Check
PLAT304_ALERT_4_G	Non-Integer Number of Atoms in ..... (Resd 3 )			3.42 Check
PLAT380_ALERT_4_G	Incorrectly? Oriented X(sp <sup>2</sup> )-Methyl Moiety	.....		C43 Check
PLAT411_ALERT_2_G	Short Inter H...H Contact H2	..H50C	.	1.46 Ang.
		x,y,z =		1_555 Check
PLAT413_ALERT_2_G	Short Inter XH3 .. XHn H2	..H52D	.	1.40 Ang.
		x,y,z =		1_555 Check
PLAT432_ALERT_2_G	Short Inter X...Y Contact C2	..C52D	.	3.19 Ang.
		x,y,z =		1_555 Check
PLAT720_ALERT_4_G	Number of Unusual/Non-Standard Labels	.....		2 Note
PLAT793_ALERT_4_G	Model has Chirality at Sil (Centro SPGR)			R Verify
PLAT860_ALERT_3_G	Number of Least-Squares Restraints	.....		133 Note
PLAT883_ALERT_1_G	No Info/Value for _atom_sites_solution_primary	.		Please Do !
PLAT910_ALERT_3_G	Missing # of FCF Reflection(s) Below Theta(Min).			3 Note
PLAT933_ALERT_2_G	Number of OMIT Records in Embedded .res File	...		2 Note
PLAT978_ALERT_2_G	Number C-C Bonds with Positive Residual Density.			5 Info

0 **ALERT level A** = Most likely a serious problem - resolve or explain  
 0 **ALERT level B** = A potentially serious problem, consider carefully  
 3 **ALERT level C** = Check. Ensure it is not caused by an omission or oversight  
 26 **ALERT level G** = General information/check it is not something unexpected

2 ALERT type 1 CIF construction/syntax error, inconsistent or missing data  
 14 ALERT type 2 Indicator that the structure model may be wrong or deficient  
 4 ALERT type 3 Indicator that the structure quality may be low  
 9 ALERT type 4 Improvement, methodology, query or suggestion  
 0 ALERT type 5 Informative message, check

It is advisable to attempt to resolve as many as possible of the alerts in all categories. Often the minor alerts point to easily fixed oversights, errors and omissions in your CIF or refinement strategy, so attention to these fine details can be worthwhile. In order to resolve some of the more serious problems it may be necessary to carry out additional measurements or structure refinements. However, the purpose of your study may justify the reported deviations and the more serious of these should normally be commented upon in the discussion or experimental section of a paper or in the "special\_details" fields of the CIF. checkCIF was carefully designed to identify outliers and unusual parameters, but every test has its limitations and alerts that are not important in a particular case may appear. Conversely, the absence of alerts does not guarantee there are no aspects of the results needing attention. It is up to the individual to critically assess their own results and, if necessary, seek expert advice.

#### Publication of your CIF in IUCr journals

A basic structural check has been run on your CIF. These basic checks will be run on all CIFs submitted for publication in IUCr journals (*Acta Crystallographica*, *Journal of Applied Crystallography*, *Journal of Synchrotron Radiation*); however, if you intend to submit to *Acta Crystallographica Section C* or *E* or *IUCrData*, you should make sure that full publication checks are run on the final version of your CIF prior to submission.

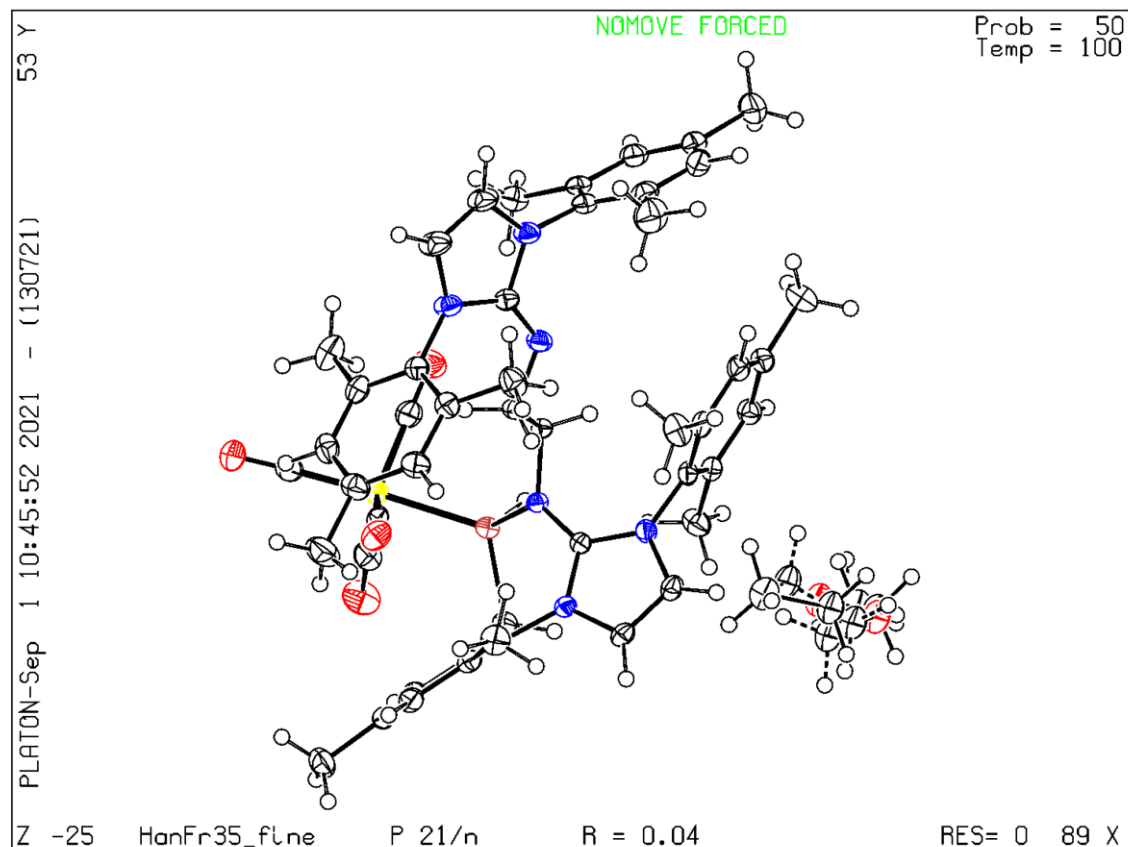
#### Publication of your CIF in other journals

Please refer to the *Notes for Authors* of the relevant journal for any special instructions relating to CIF submission.

---

PLATON version of 13/07/2021; check.def file version of 13/07/2021

Datablock HanFr35\_fine - ellipsoid plot





The following ALERTS were generated. Each ALERT has the format

**test-name\_ALERT\_alert-type\_alert-level.**

Click on the hyperlinks for more details of the test.

### ● Alert level C

PLAT220_ALERT_2_C	NonSolvent	Resd 1	C	Ueq(max)/Ueq(min)	Range	3.9	Ratio
PLAT222_ALERT_3_C	NonSolvent	Resd 1	H	Uiso(max)/Uiso(min)	Range	5.2	Ratio
PLAT234_ALERT_4_C	Large Hirshfeld	Difference	O8	--C52	.	0.16	Ang.
PLAT420_ALERT_2_C	D-H Without	Acceptor	Si1	--H1	.		Please Check
PLAT906_ALERT_3_C	Large K Value	in the Analysis	of Variance	.....		5.810	Check

### ● Alert level G

PLAT083_ALERT_2_G	SHELXL	Second Parameter	in WGHT	Unusually Large		14.48	Why ?
PLAT232_ALERT_2_G	Hirshfeld	Test Diff (M-X)	Fe1	--C45	.	5.4	s.u.
PLAT233_ALERT_4_G	Hirshfeld (M-X	Solvent)	Fe2	--C52	.	5.5	s.u.
PLAT301_ALERT_3_G	Main Residue	Disorder	.....(Resd 1	)		3%	Note
PLAT412_ALERT_2_G	Short Intra	XH3 .. XHn	H8D	..H42B	.	1.92	Ang.
				x,y,z =		1_555	Check
PLAT412_ALERT_2_G	Short Intra	XH3 .. XHn	H24A	..H7A	.	2.00	Ang.
				x,y,z =		1_555	Check
PLAT432_ALERT_2_G	Short Inter	X...Y Contact	O4	..C7D		3.00	Ang.
				x,1/2-y,-1/2+z =		4_554	Check
PLAT605_ALERT_4_G	Largest Solvent	Accessible VOID	in the Structure			84	A**3
PLAT794_ALERT_5_G	Tentative Bond	Valency for Fe2	(II)	.		1.95	Info
PLAT869_ALERT_4_G	ALERTS Related	to the Use of SQUEEZE	Suppressed			!	Info
PLAT883_ALERT_1_G	No Info/Value	for _atom_sites_solution_primary	.			Please	Do !
PLAT910_ALERT_3_G	Missing # of	FCF Reflection(s)	Below Theta(Min)	.		3	Note
PLAT978_ALERT_2_G	Number C-C	Bonds with Positive	Residual Density	.		5	Info

0 **ALERT level A** = Most likely a serious problem - resolve or explain  
 0 **ALERT level B** = A potentially serious problem, consider carefully  
 5 **ALERT level C** = Check. Ensure it is not caused by an omission or oversight  
 13 **ALERT level G** = General information/check it is not something unexpected

1 ALERT type 1 CIF construction/syntax error, inconsistent or missing data  
 8 ALERT type 2 Indicator that the structure model may be wrong or deficient  
 4 ALERT type 3 Indicator that the structure quality may be low  
 4 ALERT type 4 Improvement, methodology, query or suggestion  
 1 ALERT type 5 Informative message, check

It is advisable to attempt to resolve as many as possible of the alerts in all categories. Often the minor alerts point to easily fixed oversights, errors and omissions in your CIF or refinement strategy, so attention to these fine details can be worthwhile. In order to resolve some of the more serious problems it may be necessary to carry out additional measurements or structure refinements. However, the purpose of your study may justify the reported deviations and the more serious of these should normally be commented upon in the discussion or experimental section of a paper or in the "special\_details" fields of the CIF. checkCIF was carefully designed to identify outliers and unusual parameters, but every test has its limitations and alerts that are not important in a particular case may appear. Conversely, the absence of alerts does not guarantee there are no aspects of the results needing attention. It is up to the individual to critically assess their own results and, if necessary, seek expert advice.

### Publication of your CIF in IUCr journals

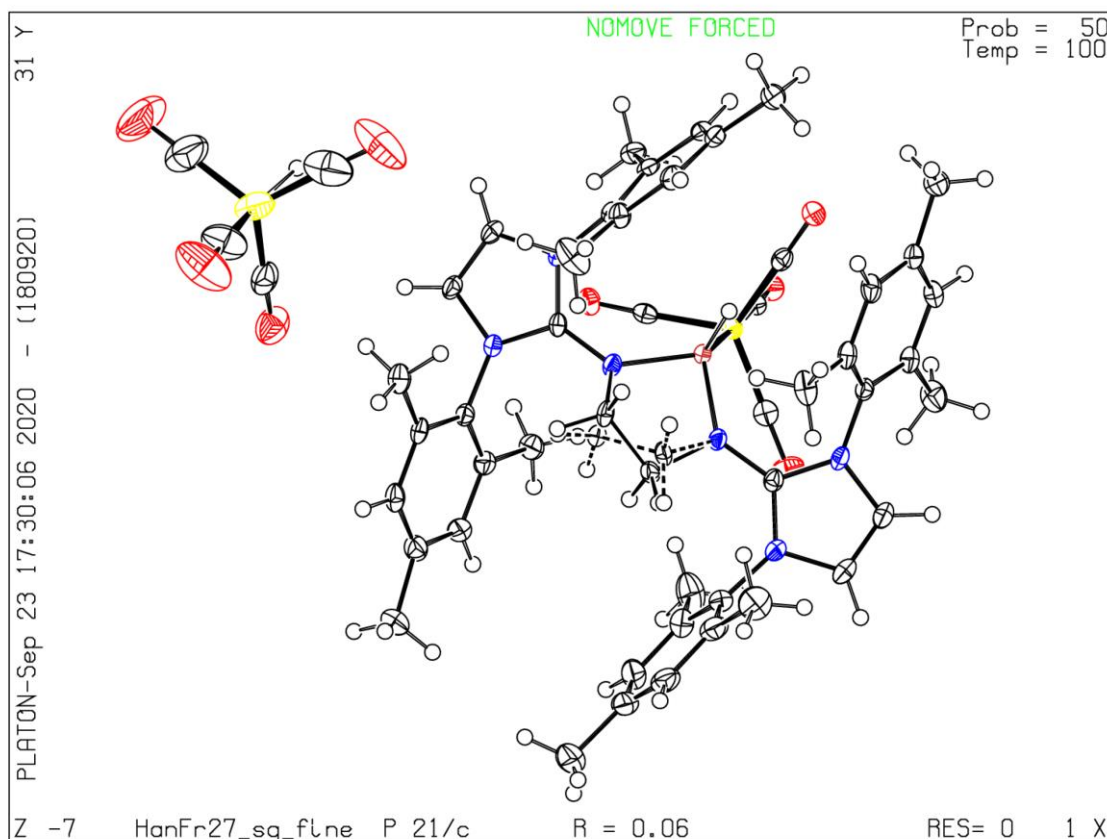
A basic structural check has been run on your CIF. These basic checks will be run on all CIFs submitted for publication in IUCr journals (*Acta Crystallographica*, *Journal of Applied Crystallography*, *Journal of Synchrotron Radiation*); however, if you intend to submit to *Acta Crystallographica Section C* or *E* or *IUCrData*, you should make sure that full publication checks are run on the final version of your CIF prior to submission.

### Publication of your CIF in other journals

Please refer to the *Notes for Authors* of the relevant journal for any special instructions relating to CIF submission.

PLATON version of 18/09/2020; check.def file version of 20/08/2020

Datablock HanFr27\_sq\_fine - ellipsoid plot



**checkCIF/PLATON report**

Structure factors have been supplied for datablock(s) HanFr16\_fine

THIS REPORT IS FOR GUIDANCE ONLY. IF USED AS PART OF A REVIEW PROCEDURE FOR PUBLICATION, IT SHOULD NOT REPLACE THE EXPERTISE OF AN EXPERIENCED CRYSTALLOGRAPHIC REFEREE.

No syntax errors found.      CIF dictionary      Interpreting this report

**Datablock: P23**

Bond precision:	C-C = 0.0041 A	Wavelength=0.71073	
Cell:	a=13.6114(10)	b=14.9329(13)	c=16.0582(14)
	alpha=107.339(3)	beta=96.927(3)	gamma=90.121(3)
Temperature:	100 K		
	Calculated	Reported	
Volume	3090.4(4)	3090.4(4)	
Space group	P -1	P -1	
Hall group	-P 1	-P 1	
Moiety formula	C48 H52 Cl Fe N6 O4 Si, C4 H Fe O4, C4 H10 O [+ solvent]	C48 H52 Cl Fe N6 O4 Si, C4 H Fe O4, C4 H10 O	
Sum formula	C56 H63 Cl Fe2 N6 O9 Si [+ solvent]	C56 H63 Cl Fe2 N6 O9 Si	
Mr	1139.36	1139.36	
Dx, g cm <sup>-3</sup>	1.224	1.224	
Z	2	2	
Mu (mm <sup>-1</sup> )	0.586	0.586	
F000	1192.0	1192.0	
F000'	1194.27		
h, k, lmax	16, 17, 19	16, 17, 19	
Nref	11324	11312	
Tmin, Tmax	0.867, 0.923	0.688, 0.745	
Tmin'	0.867		

Correction method= # Reported T Limits: Tmin=0.688 Tmax=0.745

AbsCorr = MULTI-SCAN

Data completeness= 0.999

Theta(max)= 25.360

R(reflections) = 0.0442 ( 9922)

wR2(reflections) =  
0.1228 ( 11312)

S = 1.008

Npar = 750

The following ALERTS were generated. Each ALERT has the format

**test-name\_ALERT\_alert-type\_alert-level.**

Click on the hyperlinks for more details of the test.

### Alert level C

PLAT220_ALERT_2_C	NonSolvent	Resd 1	C	Ueq(max)/Ueq(min) Range	3.8	Ratio
PLAT222_ALERT_3_C	NonSolvent	Resd 1	H	Uiso(max)/Uiso(min) Range	4.7	Ratio
PLAT244_ALERT_4_C	Low	'Solvent'		Ueq as Compared to Neighbors of	Fe2	Check
PLAT250_ALERT_2_C	Large	U3/U1		Ratio for Average U(i,j) Tensor ...	2.1	Note
PLAT906_ALERT_3_C	Large	K		Value in the Analysis of Variance .....	2.057	Check
PLAT910_ALERT_3_C	Missing	#		of FCF Reflection(s) Below Theta(Min).	5	Note

### Alert level G

PLAT002_ALERT_2_G	Number of Distance or Angle	Restraints on AtSite	4	Note
PLAT003_ALERT_2_G	Number of Uiso or Uij	Restrained non-H Atoms ...	12	Report
PLAT013_ALERT_1_G	N.O.K.	_shelx_hkl_checksum Found in CIF .....	Please	Check
PLAT154_ALERT_1_G	The s.u.'s on the Cell	Angles are Equal ..(Note)	0.003	Degree
PLAT175_ALERT_4_G	The CIF-Embedded .res	File Contains SAME Records	1	Report
PLAT177_ALERT_4_G	The CIF-Embedded .res	File Contains DELU Records	1	Report
PLAT178_ALERT_4_G	The CIF-Embedded .res	File Contains SIMU Records	2	Report
PLAT230_ALERT_2_G	Hirshfeld Test Diff for	O2 --C46	7.3	s.u.
PLAT230_ALERT_2_G	Hirshfeld Test Diff for	O3 --C47	5.5	s.u.
PLAT232_ALERT_2_G	Hirshfeld Test Diff (M-X)	Fe1 --C45	7.2	s.u.
PLAT232_ALERT_2_G	Hirshfeld Test Diff (M-X)	Fe1 --C46	9.9	s.u.
PLAT232_ALERT_2_G	Hirshfeld Test Diff (M-X)	Fe1 --C47	8.2	s.u.
PLAT232_ALERT_2_G	Hirshfeld Test Diff (M-X)	Fe1 --C48	6.5	s.u.
PLAT233_ALERT_4_G	Hirshfeld (M-X Solvent)	Fe2 --C49	5.1	s.u.
PLAT233_ALERT_4_G	Hirshfeld (M-X Solvent)	Fe2 --C52	6.0	s.u.
PLAT301_ALERT_3_G	Main Residue Disorder .....	(Resd 1)	7%	Note
PLAT302_ALERT_4_G	Anion/Solvent/Minor-Residue	Disorder (Resd 2)	22%	Note
PLAT412_ALERT_2_G	Short Intra XH3 .. XHn	H7DB ..H26C	2.00	Ang.
		x,y,z =	1_555	Check
PLAT412_ALERT_2_G	Short Intra XH3 .. XHn	H8A ..H42A	2.00	Ang.
		x,y,z =	1_555	Check
PLAT606_ALERT_4_G	Solvent Accessible VOID(S)	in Structure .....	!	Info
PLAT720_ALERT_4_G	Number of Unusual/Non-Standard	Labels .....	6	Note
PLAT790_ALERT_4_G	Centre of Gravity not Within	Unit Cell: Resd. #	3	Note
	C4 H10 O			
PLAT860_ALERT_3_G	Number of Least-Squares	Restraints .....	143	Note
PLAT869_ALERT_4_G	ALERTS Related to the Use of	SQUEEZE Suppressed	!	Info
PLAT883_ALERT_1_G	No Info/Value for _atom_sites_	solution_primary	Please	Do !
PLAT912_ALERT_4_G	Missing # of FCF Reflections	Above STh/L= 0.600	7	Note
PLAT978_ALERT_2_G	Number C-C Bonds with Positive	Residual Density.	2	Info

0 **ALERT level A** = Most likely a serious problem - resolve or explain

0 **ALERT level B** = A potentially serious problem, consider carefully

6 **ALERT level C** = Check. Ensure it is not caused by an omission or oversight

27 **ALERT level G** = General information/check it is not something unexpected

```

3 ALERT type 1 CIF construction/syntax error, inconsistent or missing data
13 ALERT type 2 Indicator that the structure model may be wrong or deficient
5 ALERT type 3 Indicator that the structure quality may be low
12 ALERT type 4 Improvement, methodology, query or suggestion
0 ALERT type 5 Informative message, check

```

It is advisable to attempt to resolve as many as possible of the alerts in all categories. Often the minor alerts point to easily fixed oversights, errors and omissions in your CIF or refinement strategy, so attention to these fine details can be worthwhile. In order to resolve some of the more serious problems it may be necessary to carry out additional measurements or structure refinements. However, the purpose of your study may justify the reported deviations and the more serious of these should normally be commented upon in the discussion or experimental section of a paper or in the "special\_details" fields of the CIF. checkCIF was carefully designed to identify outliers and unusual parameters, but every test has its limitations and alerts that are not important in a particular case may appear. Conversely, the absence of alerts does not guarantee there are no aspects of the results needing attention. It is up to the individual to critically assess their own results and, if necessary, seek expert advice.

### Publication of your CIF in IUCr journals

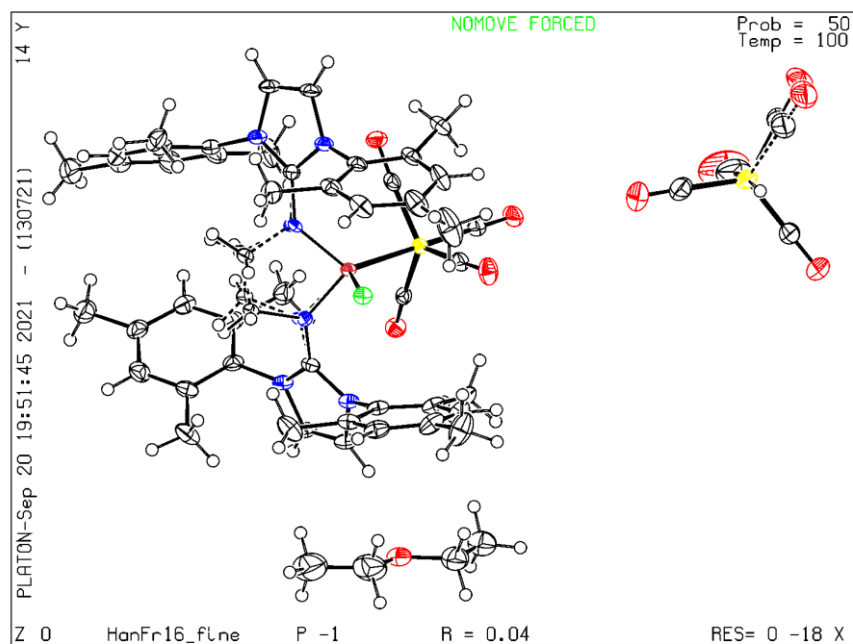
A basic structural check has been run on your CIF. These basic checks will be run on all CIFs submitted for publication in IUCr journals (*Acta Crystallographica*, *Journal of Applied Crystallography*, *Journal of Synchrotron Radiation*); however, if you intend to submit to *Acta Crystallographica Section C* or *E* or *IUCrData*, you should make sure that full publication checks are run on the final version of your CIF prior to submission.

### Publication of your CIF in other journals

Please refer to the *Notes for Authors* of the relevant journal for any special instructions relating to CIF submission.

PLATON version of 13/07/2021; check.def file version of 13/07/2021

Datablock HanFr16\_fine - ellipsoid plot



**checkCIF/PLATON report**

Structure factors have been supplied for datablock(s) deifr12\_0m

THIS REPORT IS FOR GUIDANCE ONLY. IF USED AS PART OF A REVIEW PROCEDURE FOR PUBLICATION, IT SHOULD NOT REPLACE THE EXPERTISE OF AN EXPERIENCED CRYSTALLOGRAPHIC REFEREE.

No syntax errors found. CIF dictionary Interpreting this report

**Datablock: Dip<sub>NH</sub>nBu**

Bond precision: C-C = 0.0041 Å Wavelength=0.71073  
 Cell: a=10.738 (6) b=23.104 (16) c=12.364 (7)  
 alpha=90 beta=91.21 (2) gamma=90  
 Temperature: 100 K

	Calculated	Reported
Volume	3067 (3)	3067 (3)
Space group	P 21/n	P 21/n
Hall group	-P 2yn	-P 2yn
Moiety formula	C31 H46 N3, B F4	C31 H46 N3, B F4
Sum formula	C31 H46 B F4 N3	C31 H46 B F4 N3
Mr	547.52	547.52
D <sub>x</sub> , g cm <sup>-3</sup>	1.186	1.186
Z	4	4
Mu (mm <sup>-1</sup> )	0.086	0.086
F000	1176.0	1176.0
F000'	1176.57	
h, k, lmax	13, 28, 15	12, 28, 14
Nref	5825	5493
Tmin, Tmax	0.978, 0.985	0.641, 0.745
Tmin'	0.949	

Correction method= # Reported T Limits: Tmin=0.641 Tmax=0.745  
 AbsCorr = MULTI-SCAN

Data completeness= 0.943 Theta (max)= 25.690

R(reflections)= 0.0647 ( 3981) wR2(reflections)=  
 0.1667 ( 5493)  
 S = 1.036 Npar= 361

The following ALERTS were generated. Each ALERT has the format

**test-name\_ALERT\_alert-type\_alert-level.**

Click on the hyperlinks for more details of the test.

### Alert level B

PLAT029\_ALERT\_3\_B \_diffn\_measured\_fraction\_theta\_full value Low . 0.954 Why?

### Alert level C

PLAT220_ALERT_2_B	NonSolvent	Resd 1 C	Ueq(max)/Ueq(min) Range	3.9	Ratio
PLAT340_ALERT_3_C	Low Bond Precision on C-C Bonds	.....	.....	0.00407	Ang.
PLAT906_ALERT_3_C	Large K Value in the Analysis of Variance	.....	.....	8.891	Check
PLAT906_ALERT_3_C	Large K Value in the Analysis of Variance	.....	.....	2.072	Check
PLAT911_ALERT_3_C	Missing FCF Refl Between Thmin & STh/L=	0.600	.....	250	Report

### Alert level G

PLAT007_ALERT_5_G	Number of Unrefined Donor-H Atoms	.....	.....	1	Report
PLAT013_ALERT_1_G	N.O.K. _shelx_hkl_checksum Found in CIF	.....	.....	Please	Check
PLAT063_ALERT_4_G	Crystal Size Possibly too Large for Beam Size	..	..	0.61	mm
PLAT244_ALERT_4_G	Low 'Solvent' Ueq as Compared to Neighbors of	.....	.....	B1	Check
PLAT883_ALERT_1_G	No Info/Value for _atom_sites_solution_primary	..	..	Please	Do !
PLAT910_ALERT_3_G	Missing # of FCF Reflection(s) Below Theta(Min).	.....	.....	3	Note
PLAT912_ALERT_4_G	Missing # of FCF Reflections Above STh/L=	0.600	.....	63	Note
PLAT933_ALERT_2_G	Number of HKL-OMIT Records in Embedded .res File	.....	.....	3	Note
PLAT941_ALERT_3_G	Average HKL Measurement Multiplicity	.....	.....	2.0	Low
PLAT978_ALERT_2_G	Number C-C Bonds with Positive Residual Density.	.....	.....	2	Info

- 0 **ALERT level A** = Most likely a serious problem - resolve or explain  
 1 **ALERT level B** = A potentially serious problem, consider carefully  
 5 **ALERT level C** = Check. Ensure it is not caused by an omission or oversight  
 10 **ALERT level G** = General information/check it is not something unexpected
- 2 ALERT type 1 CIF construction/syntax error, inconsistent or missing data  
 3 ALERT type 2 Indicator that the structure model may be wrong or deficient  
 7 ALERT type 3 Indicator that the structure quality may be low  
 3 ALERT type 4 Improvement, methodology, query or suggestion  
 1 ALERT type 5 Informative message, check

It is advisable to attempt to resolve as many as possible of the alerts in all categories. Often the minor alerts point to easily fixed oversights, errors and omissions in your CIF or refinement strategy, so attention to these fine details can be worthwhile. In order to resolve some of the more serious problems it may be necessary to carry out additional measurements or structure refinements. However, the purpose of your study may justify the reported deviations and the more serious of these should normally be commented upon in the discussion or experimental section of a paper or in the "special\_details" fields of the CIF. checkCIF was carefully designed to identify outliers and unusual parameters, but every test has its limitations and alerts that are not important in a particular case may appear. Conversely, the absence of alerts does not guarantee there are no aspects of the results needing attention. It is up to the individual to critically assess their own results and, if necessary, seek expert advice.

### Publication of your CIF in IUCr journals

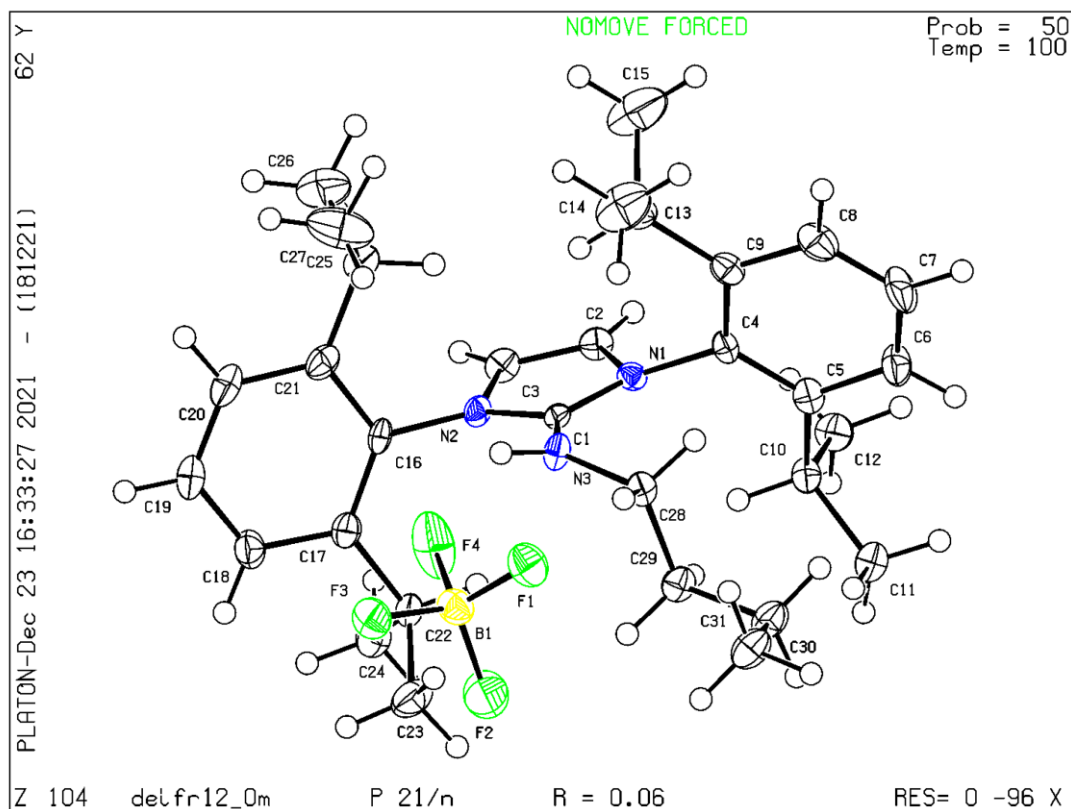
A basic structural check has been run on your CIF. These basic checks will be run on all CIFs submitted for publication in IUCr journals (*Acta Crystallographica*, *Journal of Applied Crystallography*, *Journal of Synchrotron Radiation*); however, if you intend to submit to *Acta Crystallographica Section C* or *E* or *IUCrData*, you should make sure that full publication checks are run on the final version of your CIF prior to submission.

### Publication of your CIF in other journals

Please refer to the *Notes for Authors* of the relevant journal for any special instructions relating to CIF submission.

PLATON version of 18/12/2021; check.def file version of 18/12/2021

Datablock deifr12\_0m - ellipsoid plot



**checkCIF/PLATON report**

Structure factors have been supplied for datablock(s) deifr14\_a

THIS REPORT IS FOR GUIDANCE ONLY. IF USED AS PART OF A REVIEW PROCEDURE FOR PUBLICATION, IT SHOULD NOT REPLACE THE EXPERTISE OF AN EXPERIENCED CRYSTALLOGRAPHIC REFEREE.

No syntax errors found.      CIF dictionary      Interpreting this report

**Datablock: bis<sup>Ph</sup>-NHl<sup>Mes</sup>**

Bond precision:	C-C = 0.0089 A	Wavelength=0.71073
Cell:	a=15.229 (9)      b=14.764 (8)      c=23.635 (13)	
	alpha=90      beta=95.654 (17)      gamma=90	
Temperature:	103 K	
	Calculated	Reported
Volume	5288 (5)	5288 (5)
Space group	P 21/c	P 21/c
Hall group	-P 2ybc	-P 2ybc
Moiety formula	C48 H53 N6, B F4, 2(C H C13)	C48 H53 N6, B F4, 2(C H C13)
Sum formula	C50 H55 B C16 F4 N6	C50 H55 B C16 F4 N6
Mr	1039.51	1039.51
Dx, g cm <sup>-3</sup>	1.306	1.306
Z	4	4
Mu (mm <sup>-1</sup> )	0.379	0.379
F000	2160.0	2160.0
F000'	2164.35	
h, k, lmax	18, 17, 28	18, 17, 28
Nref	9694	9737
Tmin, Tmax	0.938, 0.961	0.687, 0.745
Tmin'	0.887	

Correction method= # Reported T Limits: Tmin=0.687 Tmax=0.745  
AbsCorr = MULTI-SCAN

Data completeness= 1.004      Theta(max)= 25.350

R(reflections)= 0.1148 ( 8663)      wR2(reflections)=  
S = 2.073      Npar= 623      0.4202 ( 9737)

The following ALERTS were generated. Each ALERT has the format

**test-name\_ALERT\_alert-type\_alert-level.**

Click on the hyperlinks for more details of the test.

### Alert level B

PLAT084\_ALERT\_3\_B High wR2 Value (i.e. > 0.25) ..... 0.42 Report

### Alert level C

DIFMX02\_ALERT\_1\_C The maximum difference density is > 0.1\*ZMAX\*0.75

The relevant atom site should be identified.

GOODF01\_ALERT\_2\_C The least squares goodness of fit parameter lies

outside the range 0.80 <> 2.00

Goodness of fit given = 2.073

PLAT082_ALERT_2_C High R1 Value .....	0.11 Report
PLAT087_ALERT_2_C Unsatisfactory S value (Too High) .....	2.07 Check
PLAT097_ALERT_2_C Large Reported Max. (Positive) Residual Density	1.42 eA-3
PLAT220_ALERT_2_C NonSolvent Resd 1 C Ueq(max)/Ueq(min) Range	4.0 Ratio
PLAT244_ALERT_4_C Low 'Solvent' Ueq as Compared to Neighbors of	B1 Check
PLAT244_ALERT_4_C Low 'Solvent' Ueq as Compared to Neighbors of	C49 Check
PLAT244_ALERT_4_C Low 'Solvent' Ueq as Compared to Neighbors of	C50 Check
PLAT340_ALERT_3_C Low Bond Precision on C-C Bonds .....	0.00891 Ang.
PLAT911_ALERT_3_C Missing FCF Refl Between Thmin & STh/L= 0.600	11 Report
PLAT918_ALERT_3_C Reflection(s) with I(obs) much Smaller I(calc) .	23 Check
PLAT939_ALERT_3_C Large Value of Not (SHELXL) Weight Optimized S .	22.83 Check

### Alert level G

PLAT013_ALERT_1_G N.O.K. _shelx_hkl_checksum Found in CIF .....	Please Check
PLAT072_ALERT_2_G SHELXL First Parameter in WGHT Unusually Large	0.20 Report
PLAT380_ALERT_4_G Incorrectly? Oriented X(sp2)-Methyl Moiety .....	C37 Check
PLAT870_ALERT_4_G ALERTS Related to Twinning Effects Suppressed ..	! Info
PLAT883_ALERT_1_G No Info/Value for _atom_sites_solution_primary .	Please Do !
PLAT910_ALERT_3_G Missing # of FCF Reflection(s) Below Theta(Min).	3 Note
PLAT912_ALERT_4_G Missing # of FCF Reflections Above STh/L= 0.600	8 Note
PLAT930_ALERT_2_G FCF-based Twin Law ( 0 0 1) Est.d BASF	0.20 Check
PLAT931_ALERT_5_G CIFcalcFCF Twin Law ( 0 0 1) Est.d BASF	0.24 Check

0 **ALERT level A** = Most likely a serious problem - resolve or explain

1 **ALERT level B** = A potentially serious problem, consider carefully

13 **ALERT level C** = Check. Ensure it is not caused by an omission or oversight

9 **ALERT level G** = General information/check it is not something unexpected

3 ALERT type 1 CIF construction/syntax error, inconsistent or missing data

7 ALERT type 2 Indicator that the structure model may be wrong or deficient

6 ALERT type 3 Indicator that the structure quality may be low

6 ALERT type 4 Improvement, methodology, query or suggestion

1 ALERT type 5 Informative message, check

It is advisable to attempt to resolve as many as possible of the alerts in all categories. Often the minor alerts point to easily fixed oversights, errors and omissions in your CIF or refinement strategy, so attention to these fine details can be worthwhile. In order to resolve some of the more serious problems it may be necessary to carry out additional measurements or structure refinements. However, the purpose of your study may justify the reported deviations and the more serious of these should normally be commented upon in the discussion or experimental section of a paper or in the "special\_details" fields of the CIF. checkCIF was carefully designed to identify outliers and unusual parameters, but every test has its limitations and alerts that are not important in a particular case may appear. Conversely, the absence of alerts does not guarantee there are no aspects of the results needing attention. It is up to the individual to critically assess their own results and, if necessary, seek expert advice.

#### Publication of your CIF in IUCr journals

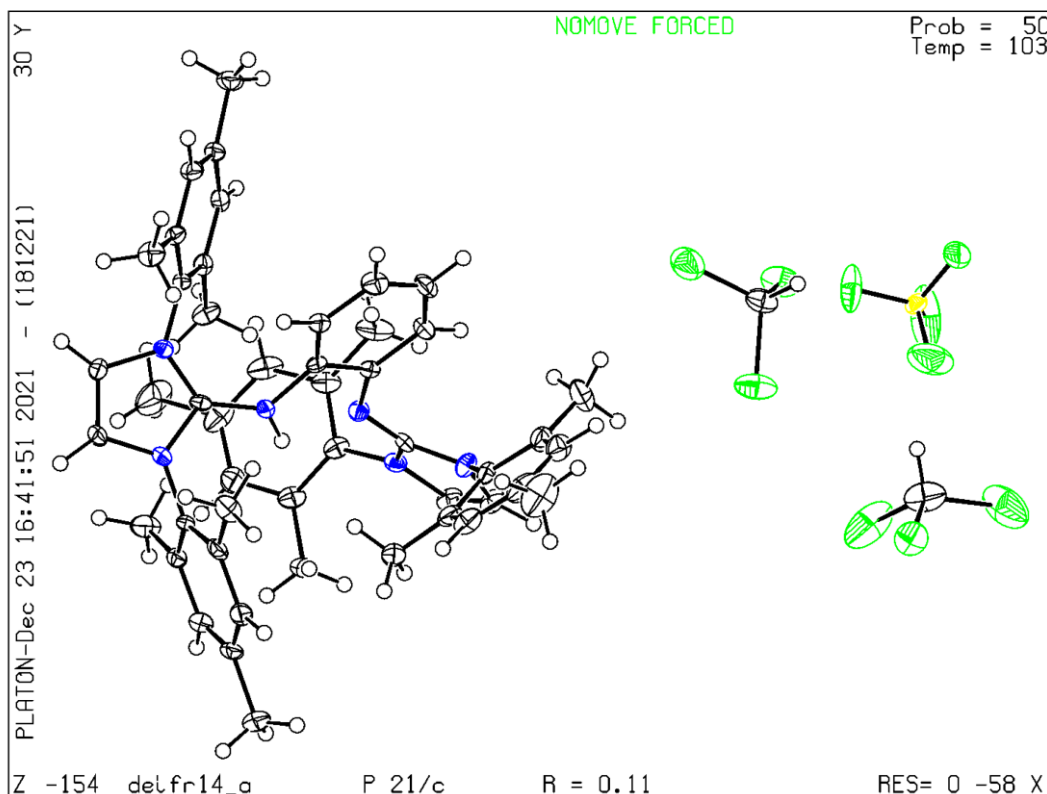
A basic structural check has been run on your CIF. These basic checks will be run on all CIFs submitted for publication in IUCr journals (*Acta Crystallographica*, *Journal of Applied Crystallography*, *Journal of Synchrotron Radiation*); however, if you intend to submit to *Acta Crystallographica Section C* or *E* or *IUCrData*, you should make sure that full publication checks are run on the final version of your CIF prior to submission.

#### Publication of your CIF in other journals

Please refer to the *Notes for Authors* of the relevant journal for any special instructions relating to CIF submission.

PLATON version of 18/12/2021; check.def file version of 18/12/2021

Datablock deifr14\_a - ellipsoid plot



## Computational Details to P17

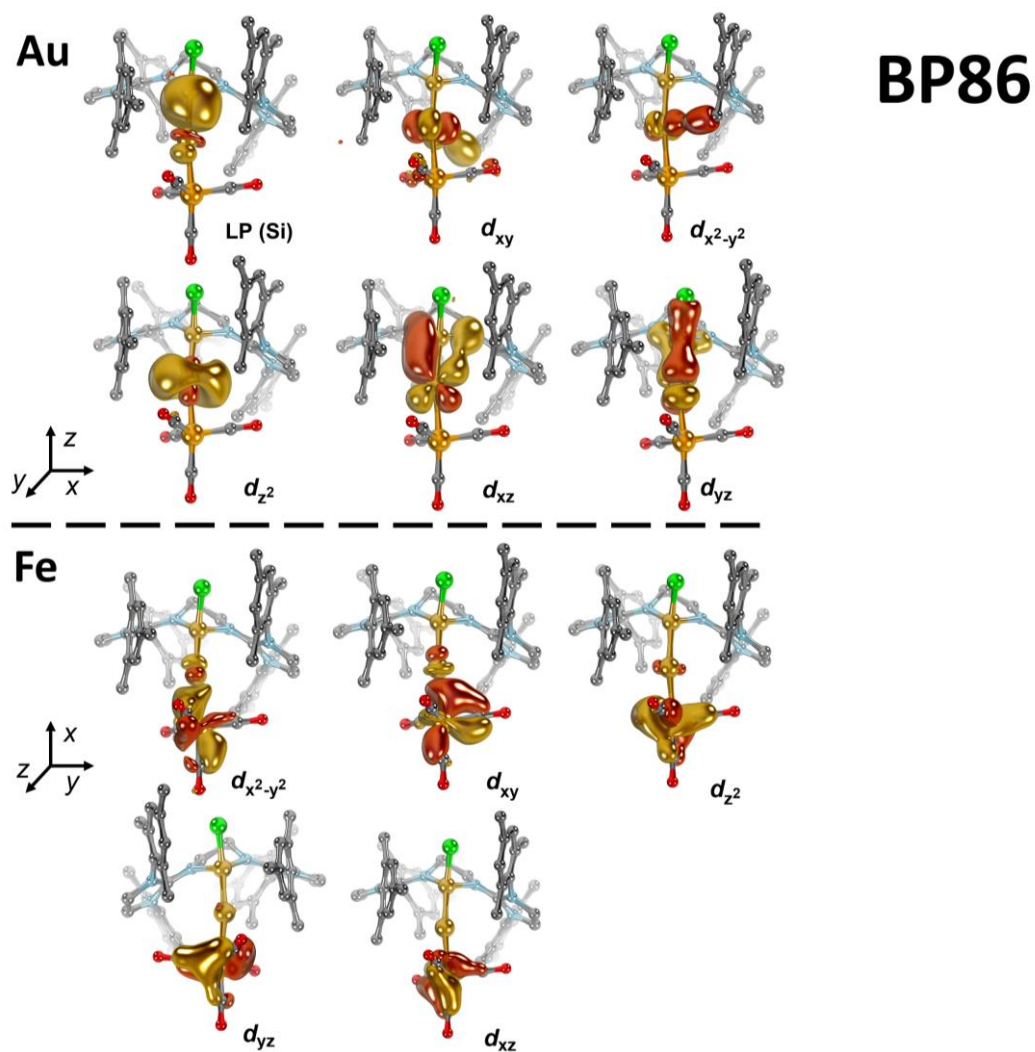
All calculations were performed with ORCA v.4.0.1<sup>[156]</sup> by Prof. Dr. Dominik Munz, as a collaborating scientist. Two computational strategies were applied, which both gave consistent results:

1) The geometric parameters were optimized using the PBE0 functional,<sup>[157]</sup> with dispersion correction D3(BJ)<sup>[158]</sup> and the def2-SVP basis set.<sup>[159]</sup> For Si, Au, and Fe, the def2-TZVP basis set and the def2-ECP (for Au) were used.<sup>[160]</sup> Tighter than default scf (“*tightscf*”) and optimization criteria (“*tightopt*”) were chosen in conjunction with finer than default grid values (“*grid7*”; “*nofinalgrid*”) and WITHOUT the RIJCOSX approximation. The optimized geometric parameters were verified as true minima by the absence of negative eigenvalues in the harmonic vibrational frequency analysis. For the analysis of the electronic structure, single-point calculations were performed (PBE0-D3BJ/def2-TZVPP//PBE0-D3BJ/def2-SVP). The population analysis was performed using Knizia’s Intrinsic Bond Orbitals.<sup>[161]</sup> Other localization methods (Foster-Boys, Pipek-Mezey) led to similar results. The calculations for the Mößbauer parameters followed a procedure developed by F. Neese and coworkers.<sup>[162,163]</sup> The calculation of the <sup>57</sup>Fe Mößbauer parameters was performed with the TPSSh functional and without the RIJCOSX approximation, the core properties basis set CP(PPP)<sup>[164]</sup> for iron and the DKH-def2-TZVPP basis set for all other atoms, the second order Douglas-Kroll-Hess method,<sup>[165]</sup> and even tighter scf (“*verytightscf*”) and grid setting for iron, gold and silicon (“*SpecialGridIntAcc 7*”) and the other atoms (“*grid6*”, “*nofinalgrid*”). The <sup>57</sup>Fe Mößbauer isomer shifts were calibrated using the extended (“whole”) calibration parameters according to F. Neese.<sup>[162]</sup> This calibration set includes previously reported calibration sets.<sup>[163,166]</sup> Modeling of the Mößbauer spectrum with the BP86 and B3LYP functionals led to comparable spectroscopic parameters. Accordingly, similar spectroscopic parameters were obtained for the solid-state structure with optimized positions of hydrogen atoms as coordinates.

2) Scalar relativistic calculations with the Zeroth Order Regular Approximation (ZORA)<sup>[167]</sup> and the BP86 functional were performed (ZORA-BP86-D3BJ/def2-TZVPP//ZORA-BP86-D3BJ/def2-SVP). For Au, and Fe, the SARC all-electron basis set were used, for Si the ZORA-def2-TZVP basis set. A comparable fit as obtained with strategy 1 was obtained for the structural parameters in the solid state (Table S 5), whereas the vibrational spectra (frequencies were scaled by 0.981 according to ref<sup>[168]</sup>) were in better agreement with the experiment and are thus shown in the thesis. The IBOs (Figure S 1), which could not be obtained at the ZORA level, were calculated at the BP86/def2-TZVPP(def2-ECP)//ZORA-BP86-D3BJ/def2-SCP level of theory and are essentially equivalent to the ones obtained with PBE0.

Table S 5. Benchmark of structural parameters of **P17**. Bond lengths are given in [ $\text{\AA}$ ], angles in [ $^\circ$ ].

	Solid State	PBE0	BP86
Si-Cl	2.1076	2.13	2.145
Si-Au	2.2676	2.27	2.261
Au-Fe	2.5305	2.5	2.504
CO-HCH <sub>2</sub> Mes	2.579	2.896	2.51
Si-Au-Fe	173.65	168.6	169.2

Figure S 1. IBOs for **P17** as obtained with BP86.

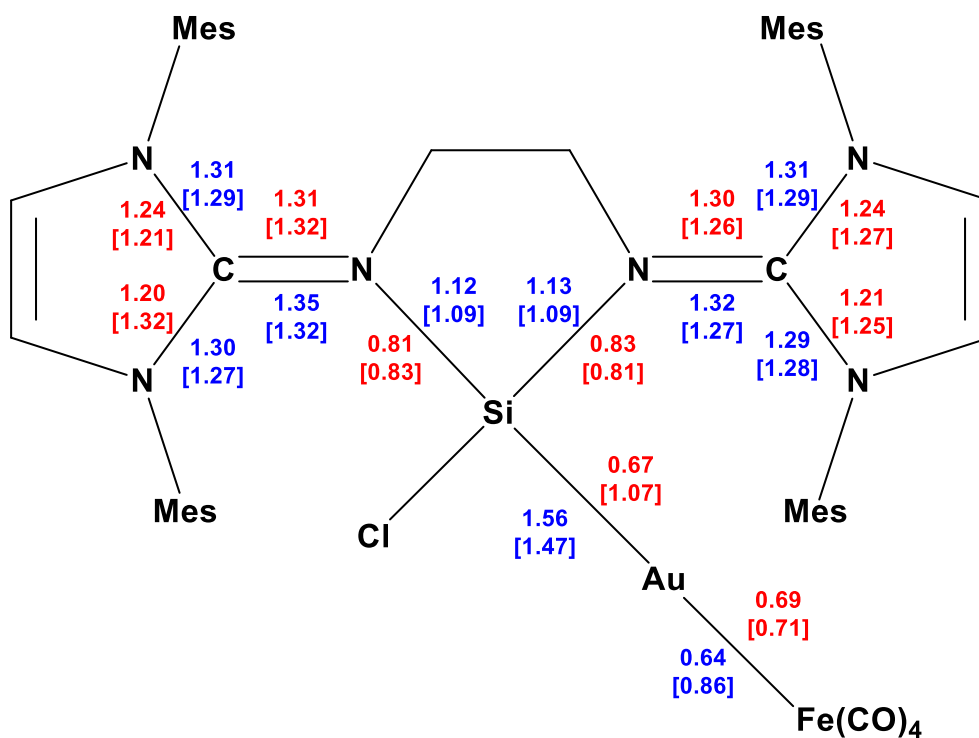


Figure S 2. Bond orders in **P17**. Mayer bond orders in red (PBE0 [ZORA-PB86]) and Löwdin bond orders in blue (PBE0 [ZORA-PB86]).

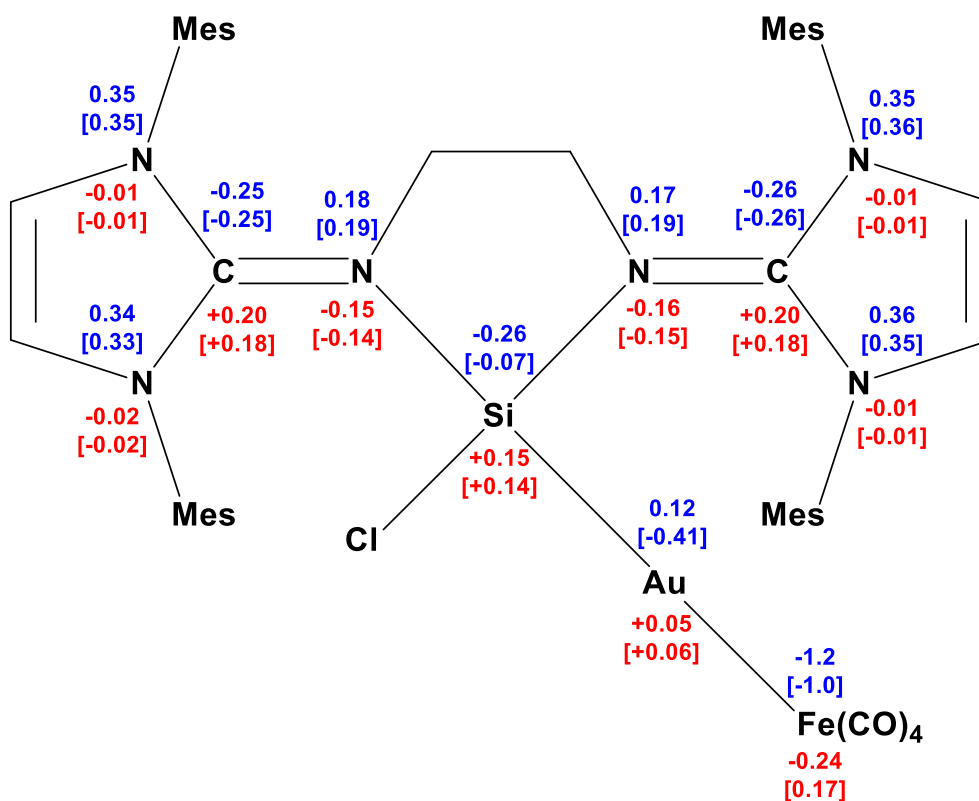


Figure S 3. Calculated partial charges in **P17**. Hirshfeld partial charges in red (PBE0 [ZORA-PB86]) and Löwdin partial charges in blue (PBE0 [ZORA-PB86]).

Table S 6. Energies of calculated compounds.

<b>BP</b>				
<b>Compound</b>	<b>E [Eh]</b>	<b>H [Eh]</b>	<b>G [Eh]</b>	<b>NImag</b>
<b>Fe(CO)<sub>4</sub><sup>2-</sup></b>	-1731.583664	-1731.541484	-1731.585866	0
<b>97</b>	-22334.061991	-22333.602426	-223337.039014	0
<b>NHCMesFe(CO)<sub>4</sub></b>	-2655.992479	-2655.533689	-2655.628490	0
<b>82</b>	-3138.766511	-3138.152546	-3138.263869	0
<b>P17</b>	-24199.554221	-24198.599820	-24198.757207	0
<b>PBE0</b>				
<b>Fe(CO)<sub>4</sub><sup>2-</sup></b>	-1715.978536	-1715.935089	-1715.979077	0
<b>NHCMesFe(CO)<sub>4</sub></b>	-2638.600065	-2638.128933	-2638.222504	0
<b>P17</b>	-4634.120518	-4633.139796	-4,633.294931	0

**XYZ coordinates****NHCMes<sub>4</sub>Fe(CO)<sub>4</sub>\_BP86**

C	-1.13671	0.89300	-2.88598	C	-0.30202	5.83927	-3.83167
C	-1.20232	-0.16370	-2.02235	H	1.78247	5.25517	-3.66505
N	-1.20844	0.37334	-0.73444	H	-2.45147	6.10572	-3.86895
C	-1.15006	1.75225	-0.75487	C	-1.09981	-0.46404	0.42972
N	-1.10469	2.04727	-2.10260	C	-2.25546	-0.88823	1.11506
H	-1.11105	0.94207	-3.97396	C	0.20062	-0.86655	0.81648
H	-1.24641	-1.23899	-2.19132	C	-2.07488	-1.71387	2.24216
Fe	-1.35595	3.00339	0.75967	C	0.32415	-1.69621	1.94021
C	-3.09381	2.85119	0.43966	C	-0.80104	-2.12087	2.67522
O	-4.24747	2.76999	0.25085	H	-2.96260	-2.04748	2.79643
C	-0.51660	1.96259	1.95013	H	1.32769	-2.00170	2.26468
O	0.01807	1.42154	2.83674	C	-3.37314	3.78844	-2.79005
C	-1.72395	4.11458	2.09189	H	-4.01342	4.11381	-3.62831
O	-1.97714	4.84293	2.96362	H	-3.49298	2.70127	-2.66057
C	-0.37188	4.31064	0.03240	H	-3.75995	4.26345	-1.87124
O	0.25266	5.24492	-0.28647	C	0.00466	7.20613	-4.39657
C	-0.86210	3.34162	-2.68064	H	0.85326	7.17310	-5.10250
C	0.48632	3.70119	-2.91582	H	-0.86581	7.63485	-4.92183
C	-1.93817	4.18168	-3.02903	H	0.28145	7.90656	-3.58539
C	0.74076	4.95311	-3.49385	C	1.60915	2.79245	-2.48216
C	-1.62704	5.43183	-3.59925	H	1.61217	2.68427	-1.38113
				H	1.50918	1.77551	-2.90327
				H	2.58682	3.19896	-2.78725
				C	-3.63929	-0.46980	0.68981

H	-3.66862	-0.12270	-0.35509	C	0.34810	-1.84492	0.01610
H	-4.35294	-1.30449	0.80147	C	-2.05931	-1.94879	1.47618
H	-4.00313	0.36563	1.31361	C	0.28538	-2.50802	1.25398
C	1.41325	-0.34917	0.08403	C	-0.90813	-2.56710	1.99912
H	2.33647	-0.80509	0.47645	H	-2.99148	-1.96583	2.05713
H	1.36207	-0.54803	-1.00189	H	1.19862	-2.96632	1.65818
H	1.49527	0.74750	0.20484	C	-3.12276	2.62923	-3.13857
C	-0.63364	-2.96304	3.91786	H	-3.96717	3.22726	-3.52108
H	-1.56048	-3.50582	4.17054	H	-3.22492	1.59529	-3.51145
H	0.17940	-3.70129	3.80208	H	-3.21479	2.59540	-2.03486
H	-0.37526	-2.32544	4.78503	C	-0.37131	6.76874	-4.04045
<b>97_BP86</b>				H	0.50792	7.10219	-4.62006
C	-0.96231	0.00376	-3.86231	H	-1.27743	7.21726	-4.48486
C	-1.03563	-1.05274	-2.98751	H	-0.26964	7.15423	-3.00790
N	-0.77523	-0.53378	-1.71674	C	1.91047	2.26662	-3.61452
C	-0.54048	0.82313	-1.75989	H	2.05183	1.97699	-2.55498
N	-0.65792	1.12916	-3.10047	H	1.86005	1.33078	-4.20056
H	-1.09857	0.05347	-4.94253	H	2.79668	2.83784	-3.93854
H	-1.24845	-2.10928	-3.15005	C	-3.26284	-0.53405	-0.25728
Fe	-1.42533	4.03591	1.16713	H	-3.39071	-0.63524	-1.34916
C	-2.97753	3.37061	0.67985	H	-4.17898	-0.89130	0.24188
O	-4.02981	2.92882	0.34072	H	-3.16531	0.54982	-0.04586
C	-0.43906	3.01104	2.22561	C	1.64254	-1.69599	-0.74424
O	0.19668	2.36395	2.98766	H	2.46101	-2.24496	-0.24920
C	-1.90246	5.28114	2.31022	H	1.55619	-2.05857	-1.78510
O	-2.22377	6.11543	3.08061	H	1.92211	-0.62677	-0.80143
C	-0.64474	5.03400	-0.06609	C	-0.93861	-3.22461	3.36037
O	-0.14531	5.75493	-0.86416	H	-1.91505	-3.70093	3.56023
C	-0.60839	2.50198	-3.52524	H	-0.15201	-3.99350	3.45916
C	0.65405	3.09066	-3.74724	H	-0.77076	-2.47437	4.15706
C	-1.80406	3.25304	-3.51912	Au	-0.64273	2.19625	-0.31186
C	0.70110	4.47412	-3.98126	<b>Fe(CO)<sub>4</sub><sup>2-</sup>_BP86</b>			
C	-1.70250	4.63404	-3.76047	O	2.40120	4.17319	-1.41987
C	-0.46314	5.26499	-3.96679	Fe	3.51635	3.73951	1.25200
H	1.67863	4.95675	-4.11630	O	1.80767	1.99028	2.87049
H	-2.61482	5.24341	-3.71331	O	6.20225	2.66357	0.82925
C	-0.83278	-1.25160	-0.47606	C	2.83629	3.99746	-0.32728
C	-2.04859	-1.27249	0.24222	C	2.50041	2.69275	2.20649

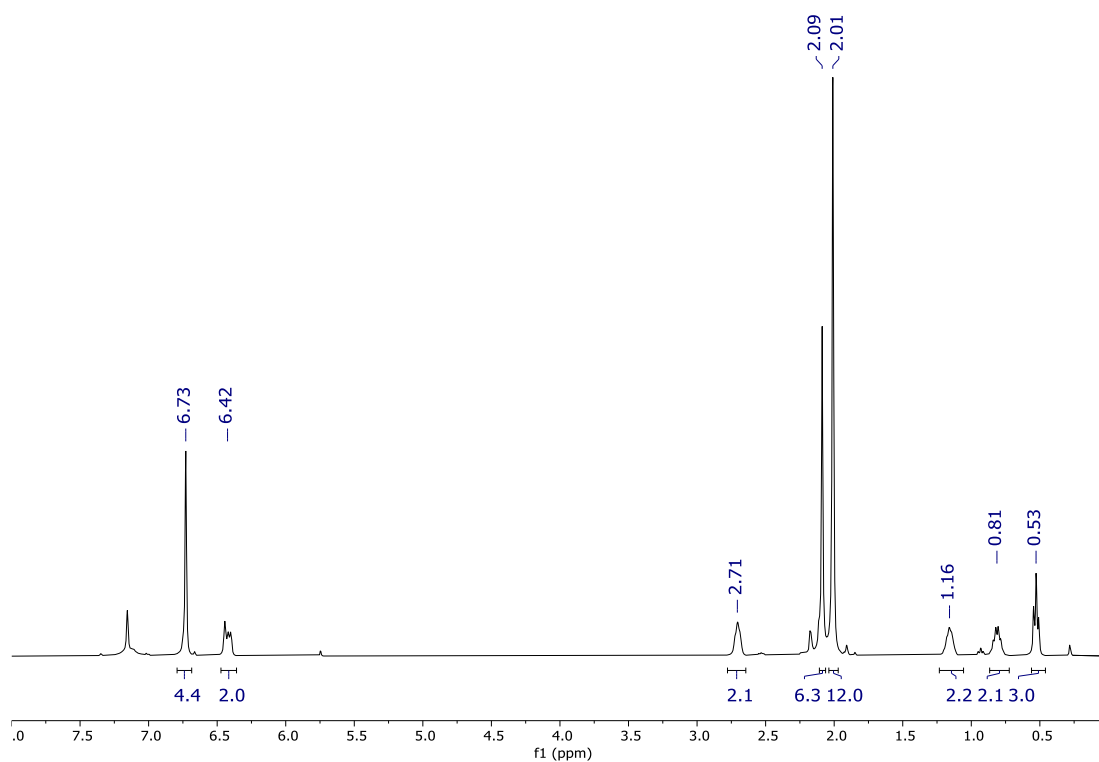
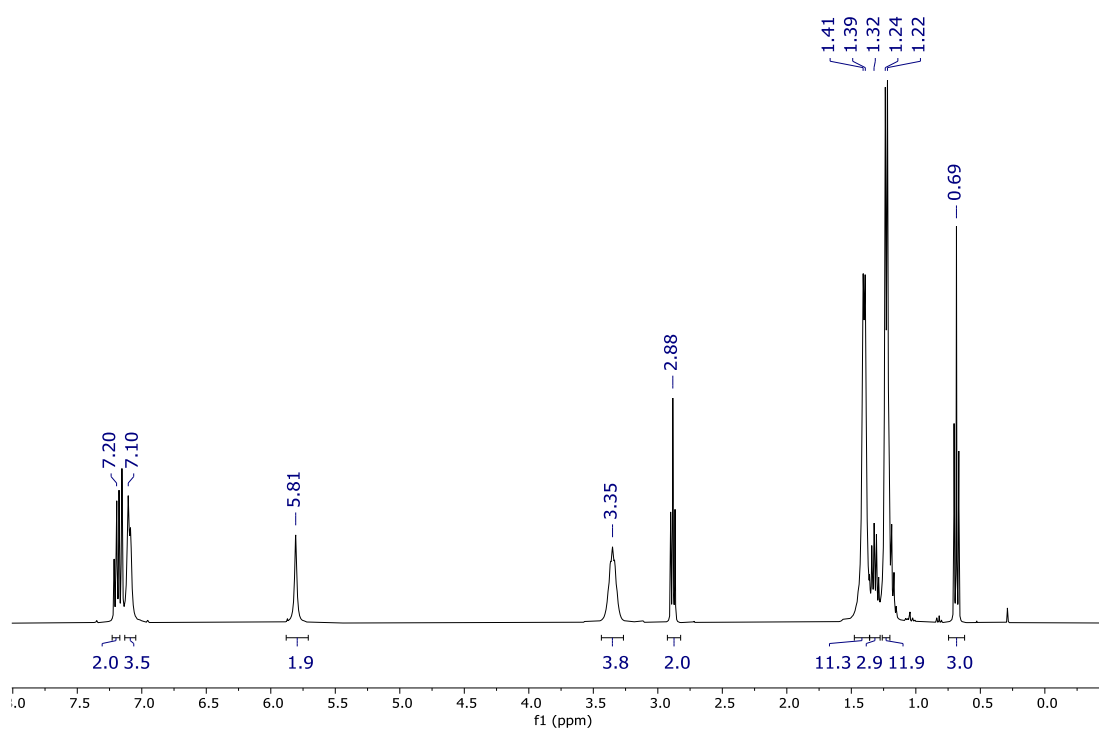
C	5.10384	3.08082	1.01019	C	9.37006	9.45366	4.74709
C	3.70589	5.24208	2.09971	H	9.65766	10.15338	5.54853
O	3.85431	6.26844	2.68067	H	8.61652	9.95004	4.10801
<b>P17_BP86</b>				H	10.25968	9.28855	4.11115
Cl	3.17654	9.33918	2.11010	C	2.81464	3.73722	-0.54333
Si	3.95346	7.38073	2.51336	C	4.93155	2.88635	1.56927
Au	3.63797	5.35049	1.56913	C	2.03206	3.00009	2.20910
O	2.46083	4.22220	-1.56479	C	3.12220	1.27086	0.44605
Fe	3.27458	2.94628	0.96937	<b>NHC<sup>Mes</sup>-Fe(CO)<sub>4</sub>_PBE0</b>			
N	7.07532	7.53591	1.12279	C	-1.07527	0.93520	-2.81878
C	6.83230	7.65862	2.47161	C	-1.16910	-0.10641	-1.96187
N	8.05047	7.48035	3.09619	N	-1.15091	0.42668	-0.68488
O	6.03283	2.79939	2.00579	C	-1.05484	1.79251	-0.70973
C	8.43222	7.27672	0.91328	N	-1.00556	2.08029	-2.04324
H	8.82366	7.14426	-0.09354	H	-1.05113	0.97859	-3.90357
N	1.24379	6.48730	4.23207	H	-1.24764	-1.17574	-2.13431
O	1.19441	3.01412	3.05006	Fe	-1.20591	3.03606	0.83297
C	9.04312	7.25097	2.13204	C	-2.93378	2.99721	0.45270
H	5.84374	2.50086	6.66652	O	-4.05595	2.99243	0.17798
C	8.84594	8.15934	5.32099	C	-0.17286	2.00759	1.86983
C	4.31673	3.92309	6.12274	O	0.53107	1.45085	2.59063
C	7.09395	4.96148	4.05750	C	-1.58179	3.96066	2.29602
H	6.94254	3.99593	4.56022	O	-1.86870	4.53994	3.24350
H	7.71703	4.77611	3.16540	C	-0.33022	4.42668	0.13498
H	6.10633	5.28463	3.67571	O	0.20984	5.39390	-0.17310
C	4.03877	3.32446	4.77821	C	-0.82361	3.36411	-2.64995
H	4.78510	2.56652	4.49798	C	0.48808	3.82878	-2.83216
H	4.01966	4.07815	3.96681	C	-1.93605	4.07437	-3.12393
H	3.03968	2.85381	4.74410	C	0.66499	5.06271	-3.45874
C	8.45702	6.41551	8.72425	C	-1.70346	5.31111	-3.73105
H	8.93071	7.24534	9.27481	C	-0.41785	5.82971	-3.89463
H	9.02585	5.49326	8.94237	H	1.68139	5.44113	-3.60087
H	7.43859	6.26889	9.12812	H	-2.55963	5.88667	-4.09534
C	6.48962	5.10784	-0.36824	C	-1.09502	-0.42725	0.46683
H	6.71942	4.94503	0.69748	C	-2.26007	-0.77190	1.16394
H	7.44367	5.07450	-0.93041	C	0.15913	-0.96149	0.81454
H	5.86843	4.25562	-0.68677	C	-2.13424	-1.64823	2.24859
C	5.49302	8.84356	-0.21513	C	0.22834	-1.82494	1.90410

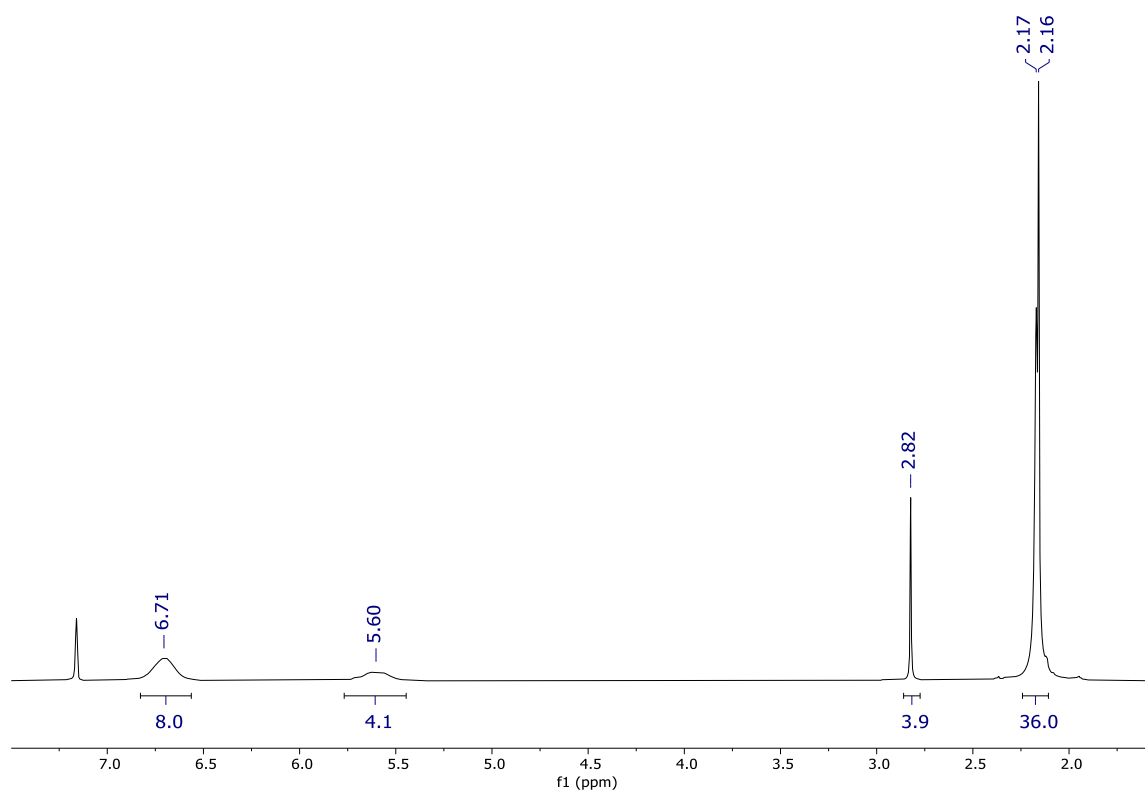
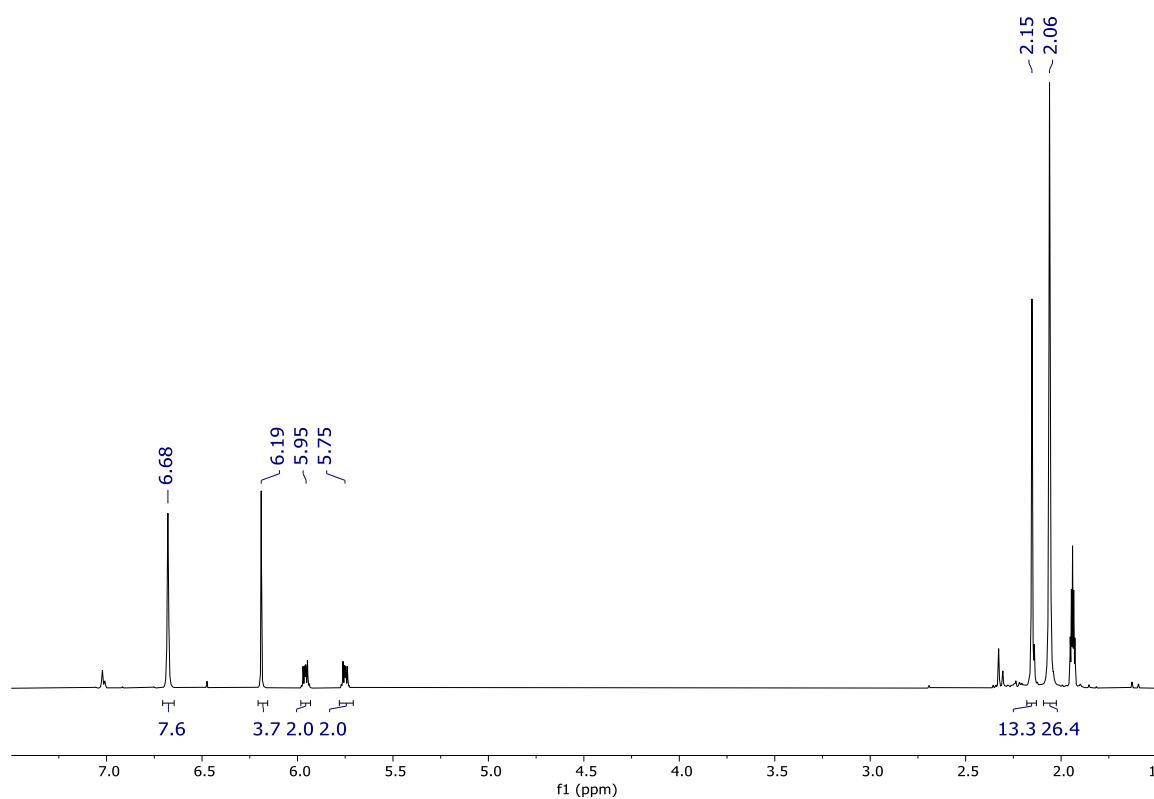
C	-0.90616	-2.17573	2.64157	<b>P17_PBE0</b>			
H	-3.03600	-1.92897	2.80095	Cl	3.16913	9.24315	2.08389
H	1.20127	-2.23318	2.19238	Si	3.93537	7.30548	2.52566
C	-3.33806	3.56246	-2.97883	Au	3.63773	5.27963	1.54579
H	-3.96225	3.89816	-3.81822	O	2.75358	4.10655	-1.65314
H	-3.38256	2.46621	-2.93053	Fe	3.34547	2.87419	0.93223
H	-3.79941	3.93978	-2.05471	N	7.05822	7.54379	1.18235
C	-0.21853	7.19404	-4.48936	C	6.79617	7.62627	2.51344
H	0.79938	7.32563	-4.88403	N	7.99368	7.46158	3.14738
H	-0.92996	7.39153	-5.30415	O	6.05499	2.78073	2.01789
H	-0.38254	7.96987	-3.72310	C	8.41198	7.32088	0.98764
C	1.66426	3.05523	-2.31669	H	8.81958	7.21951	-0.01272
H	1.69114	3.08374	-1.21479	N	1.20211	6.46717	4.23538
H	1.62345	1.99500	-2.61055	O	1.25397	2.97927	2.96235
H	2.60404	3.48093	-2.69237	C	8.99789	7.27960	2.20234
C	-3.61029	-0.23053	0.80941	H	10.02740	7.11497	2.50363
H	-3.66452	0.12484	-0.22788	N	2.43893	5.50770	5.75083
H	-4.38587	-0.99496	0.96208	O	3.10411	0.09190	0.12571
H	-3.85964	0.62761	1.45105	C	2.46187	6.42736	4.74727
C	1.40077	-0.58494	0.06421	N	5.60644	7.83505	3.08398
H	2.27739	-1.08528	0.49529	C	0.40567	5.54326	4.89299
H	1.33930	-0.86475	-0.99963	H	-0.63157	5.39502	4.61273
H	1.57306	0.50217	0.10638	N	3.49247	7.17286	4.31499
C	-0.78374	-3.08036	3.83219	C	1.16569	4.95683	5.83941
H	-1.76214	-3.45108	4.17047	H	0.94903	4.16738	6.55172
H	-0.14714	-3.95014	3.61050	C	5.45893	8.48698	4.38433
H	-0.31832	-2.54379	4.67506	H	4.96730	9.46074	4.21960
<b>Fe(CO)<sub>4</sub><sup>2-</sup>_PBE0</b>				H	6.41292	8.65677	4.89167
O	2.32057	4.21373	-1.44848	C	0.64762	7.49963	3.40612
Fe	3.53460	3.60616	1.16569	C	0.52909	8.78305	3.96429
O	1.80813	1.94038	2.86412	C	1.03381	9.09358	5.34057
O	6.25538	2.56253	0.85713	H	0.58376	10.02032	5.72069
C	2.78911	3.95780	-0.43811	H	2.12675	9.23469	5.32108
C	2.48548	2.58707	2.20233	H	0.81137	8.28799	6.05707
C	5.18225	2.95012	0.98421	C	-0.03886	9.78716	3.18449
C	3.71171	5.37113	2.14870	H	-0.12263	10.79441	3.60196
O	3.84097	6.65917	2.86608	C	4.56303	7.58974	5.21524
				H	5.14430	6.73569	5.59669
				H	4.16731	8.14480	6.08086

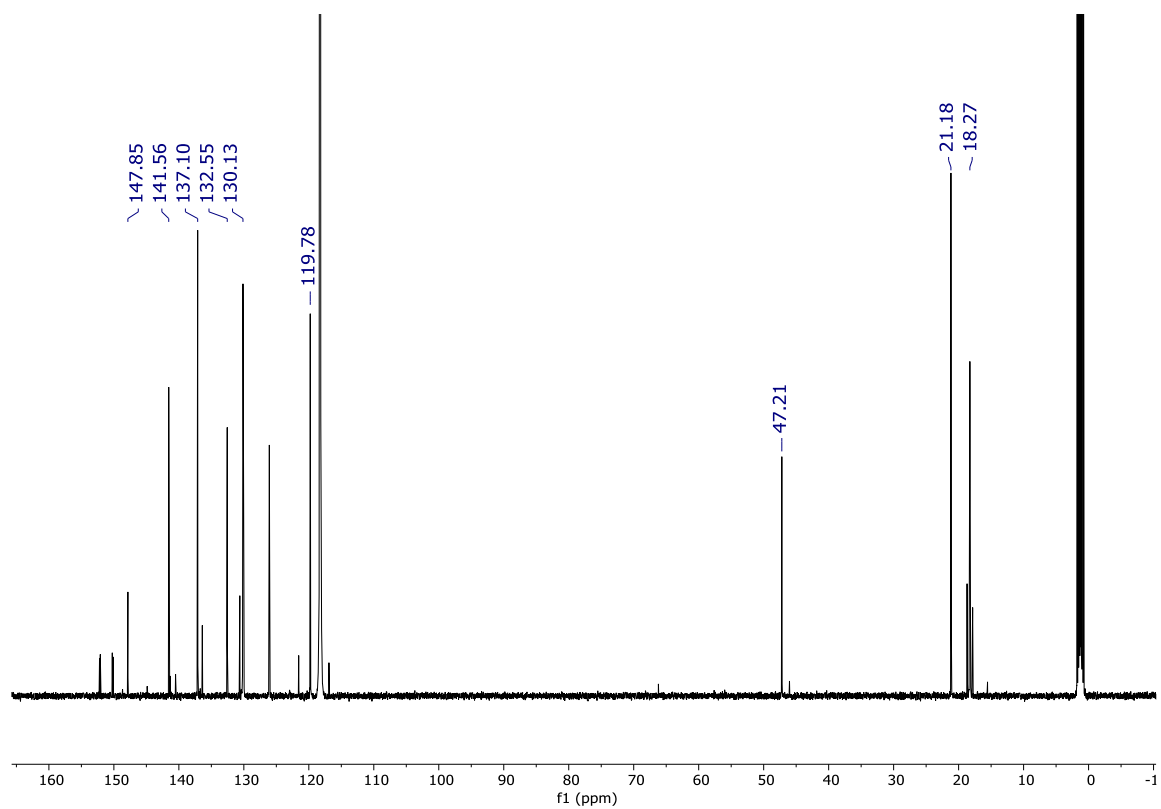
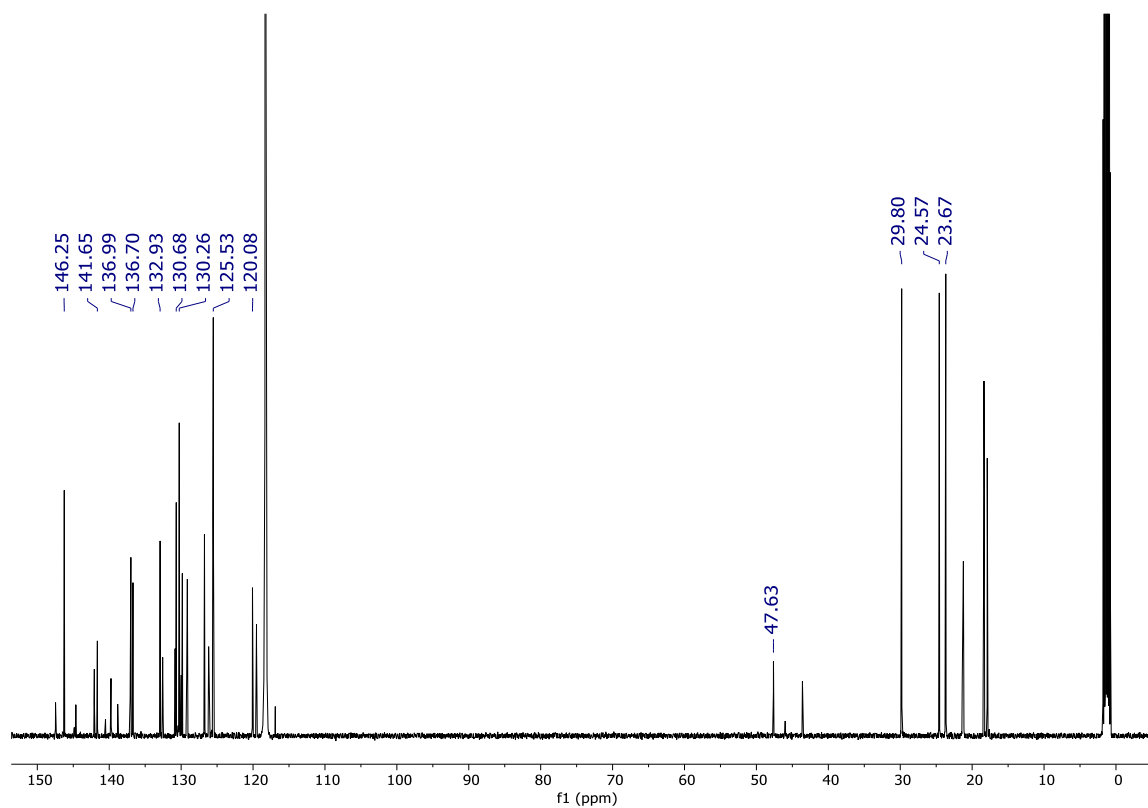
---

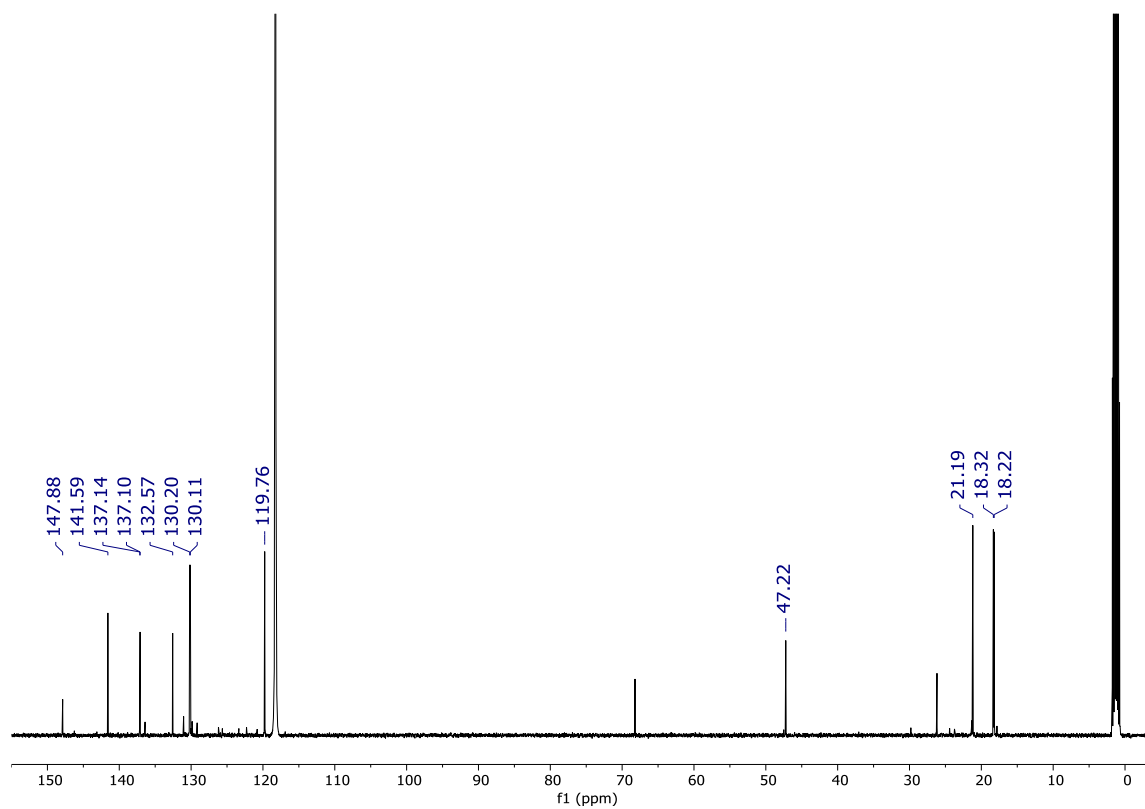
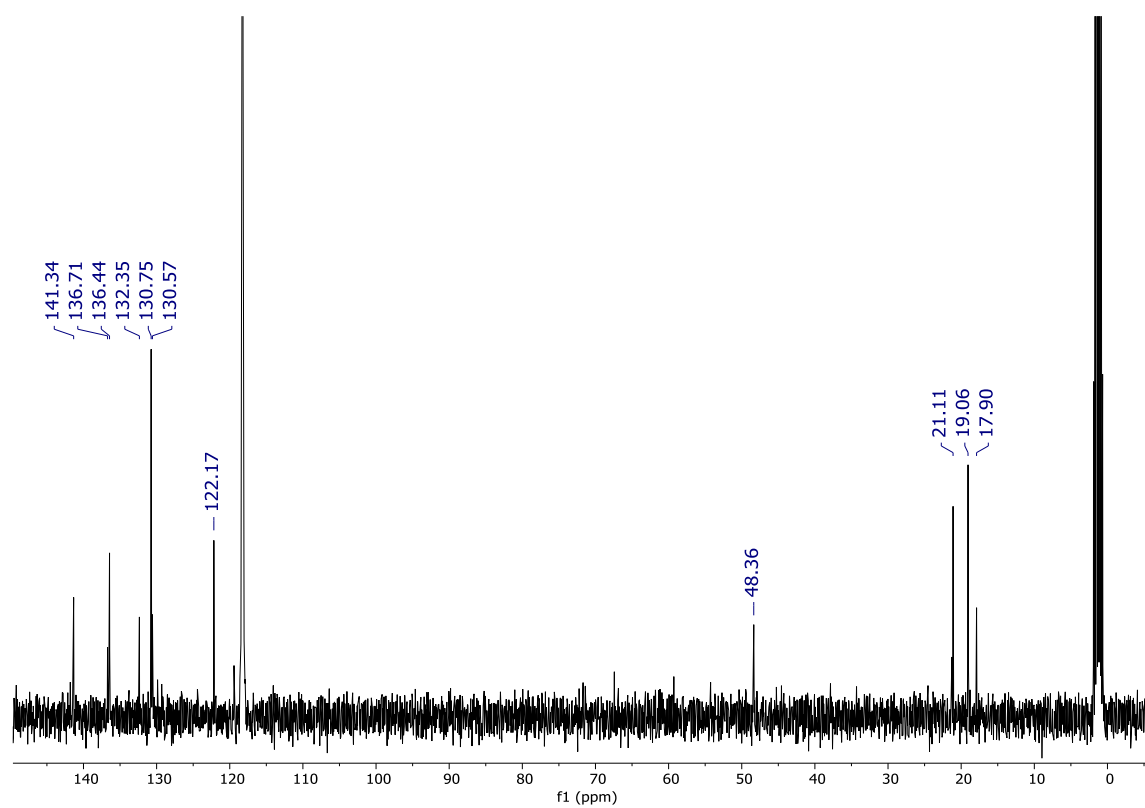
C	-0.48993	9.53998	1.88611	C	5.42075	3.98015	8.30608
C	6.11328	7.64808	0.11219	C	8.49737	6.65194	7.24503
C	-1.02990	10.65116	1.03612	C	6.42545	3.37277	9.24106
H	-1.51891	11.42665	1.64339	H	6.60989	4.01302	10.11467
H	-1.75406	10.28098	0.29658	H	7.38816	3.19088	8.73895
H	-0.21083	11.13677	0.47968	H	6.07091	2.39702	9.61045
C	5.79854	6.48818	-0.61549	C	8.91568	7.87297	6.70830
C	-0.40380	8.23869	1.39287	H	9.36109	8.62496	7.36535
H	-0.77998	8.01886	0.39019	C	5.22112	3.43756	7.03359
C	4.82063	6.60478	-1.60071	H	5.81358	2.57489	6.71523
H	4.50394	5.70546	-2.13275	C	8.77230	8.16452	5.35059
C	0.14752	7.18811	2.13232	C	4.26468	3.94333	6.14962
C	4.18445	7.82069	-1.86911	C	7.19713	4.90207	4.10559
C	0.20079	5.81388	1.55017	H	7.09284	3.93388	4.60766
H	1.22992	5.56383	1.23052	H	7.81745	4.74518	3.21083
H	-0.44756	5.73881	0.66825	H	6.19718	5.18365	3.73828
H	-0.07727	5.02335	2.25911	C	4.02162	3.31983	4.81710
C	4.59660	8.96305	-1.17919	H	4.77475	2.56070	4.57593
H	4.13119	9.92664	-1.40262	H	4.02435	4.05192	3.99327
C	3.50534	5.04030	6.58553	H	3.02922	2.84561	4.77011
C	6.04179	10.13739	0.53153	C	8.61425	6.37178	8.71392
H	5.65705	10.16340	1.56273	H	9.21800	7.13284	9.22692
H	5.67722	11.04108	0.02554	H	9.07083	5.38806	8.89909
H	7.14132	10.18785	0.57453	H	7.61681	6.35711	9.18257
C	3.09020	7.87536	-2.89311	C	6.48969	5.18089	-0.37246
H	2.41392	7.01568	-2.77477	H	6.69766	5.00363	0.69100
H	3.50209	7.82478	-3.91445	H	7.44966	5.13969	-0.91573
H	2.50356	8.80112	-2.81177	H	5.86493	4.34521	-0.71249
C	3.65895	5.60843	7.85777	C	5.57747	8.90654	-0.18786
C	8.18071	7.18921	4.53688	C	9.20264	9.48487	4.78311
C	2.77351	6.72619	8.32485	H	9.51188	10.17328	5.58040
H	3.09069	7.09251	9.30998	H	8.39222	9.96347	4.21019
H	1.72614	6.39454	8.40952	H	10.05073	9.37268	4.08916
H	2.77410	7.57775	7.62816	C	2.99963	3.63569	-0.61244
C	7.77934	5.93493	5.02066	C	4.97441	2.83638	1.56681
C	4.63916	5.07115	8.69580	C	2.08545	2.95031	2.13690
H	4.77418	5.50136	9.69218	C	3.19829	1.19992	0.44308
C	7.94829	5.69596	6.38529				
H	7.63181	4.73096	6.78445				

## Additional NMR spectra

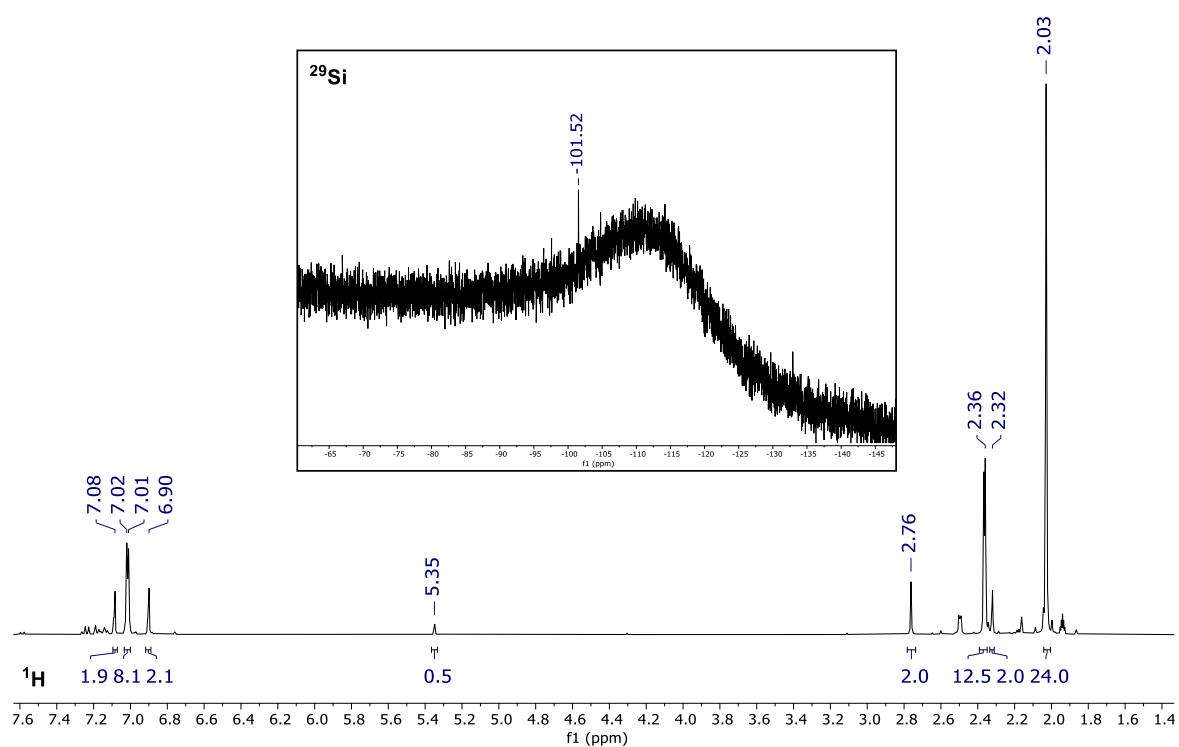
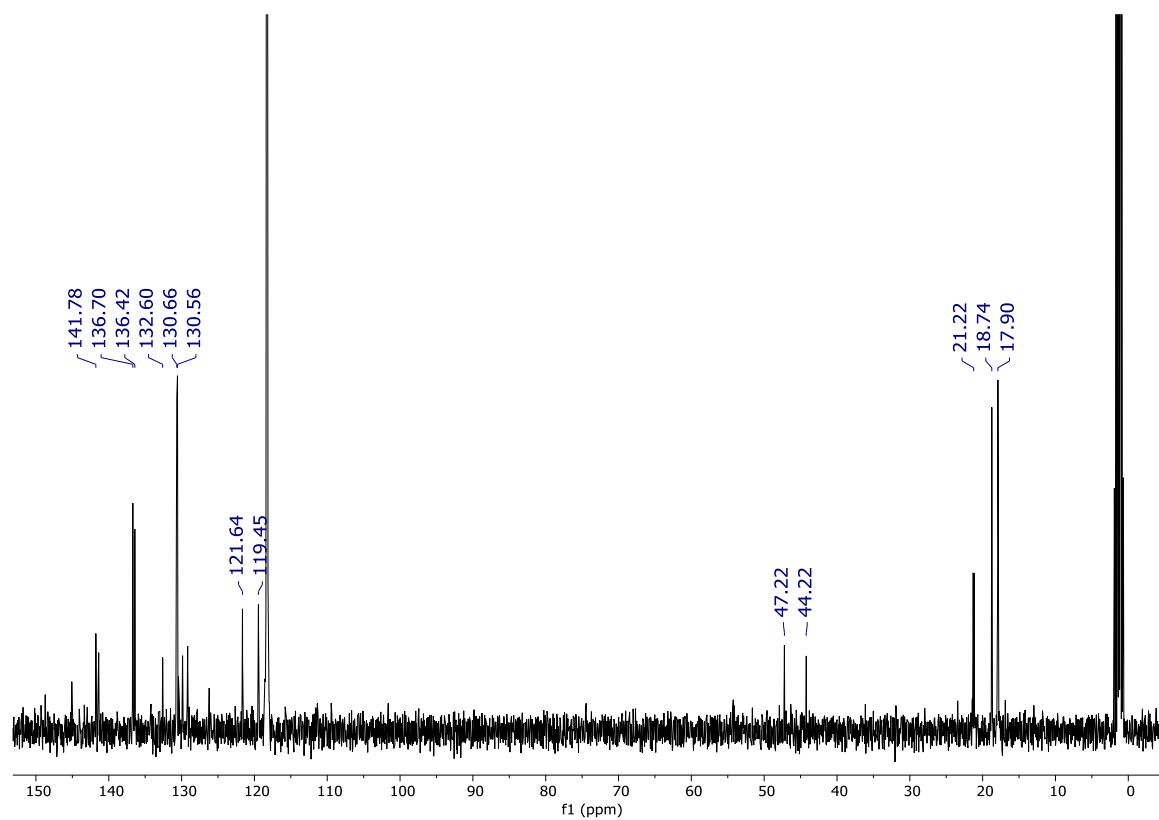
 $\text{MesNHI}^{\text{nBu}}$ Figure S 4.  $^1\text{H-NMR}$  spectrum of  $\text{MesNHI}^{\text{nBu}}$  recorded at 25°C in benzene- $\text{d}_6$ . $\text{DipNHI}^{\text{nBu}}$ Figure S 5.  $^1\text{H-NMR}$  spectrum of  $\text{DipNHI}^{\text{nBu}}$  recorded at 25°C in benzene- $\text{d}_6$ .

**P0**Figure S 6. <sup>1</sup>H-NMR spectrum of bis<sup>Et</sup>-NHIMes (P0) recorded at 25°C in benzene-d<sub>6</sub>.**P0A**Figure S 7. <sup>1</sup>H-NMR spectrum of bis<sup>Ph</sup>-NHIMes (P0A) recorded at 25°C in MeCN-d<sub>3</sub>.

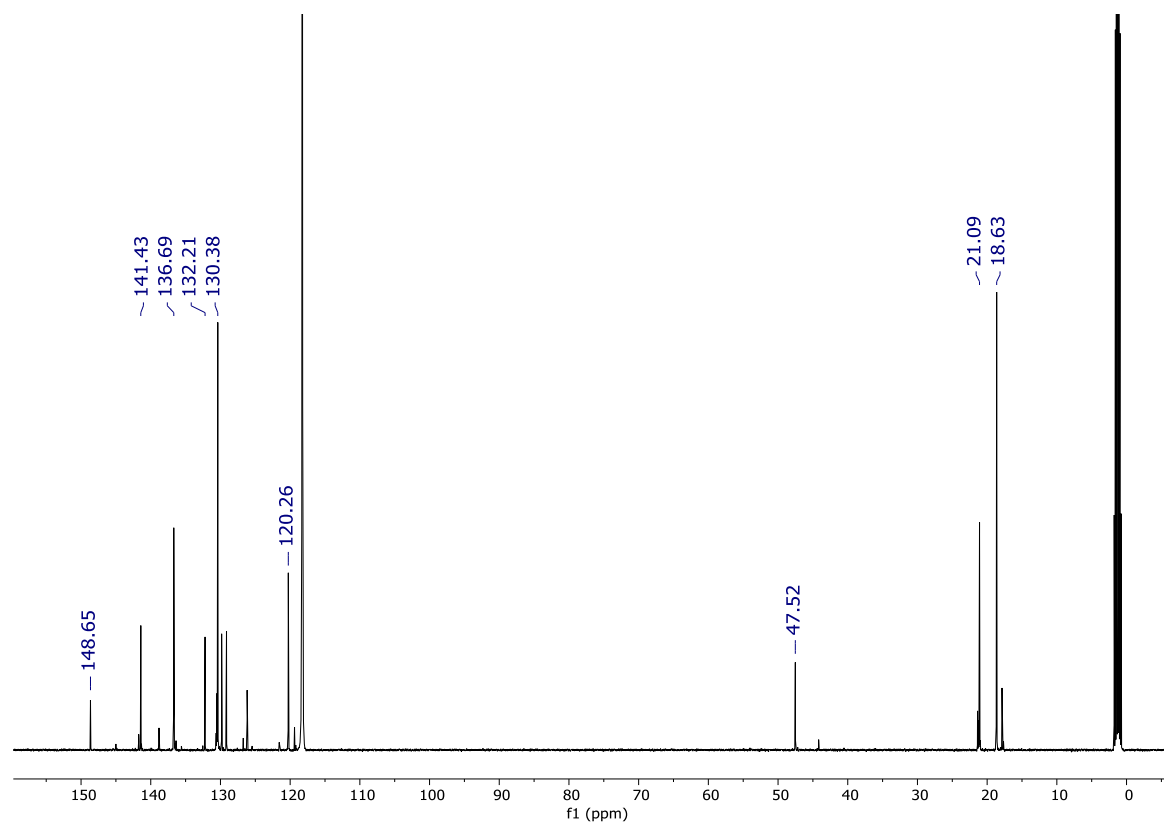
**P1**Figure S 8.  $^{13}\text{C}$ -NMR spectrum of **P1** recorded at 25°C in  $\text{MeCN-d}_3$ .**P2**Figure S 9.  $^{13}\text{C}$ -NMR spectrum of **P2** recorded at 25°C in  $\text{MeCN-d}_3$ .

**P3**Figure S 10. <sup>13</sup>C-NMR spectrum of **P3** recorded at 25°C in MeCN-d<sub>3</sub>.**P4**Figure S 11. <sup>13</sup>C-NMR spectrum of **P4** recorded at 25°C in MeCN-d<sub>3</sub>.

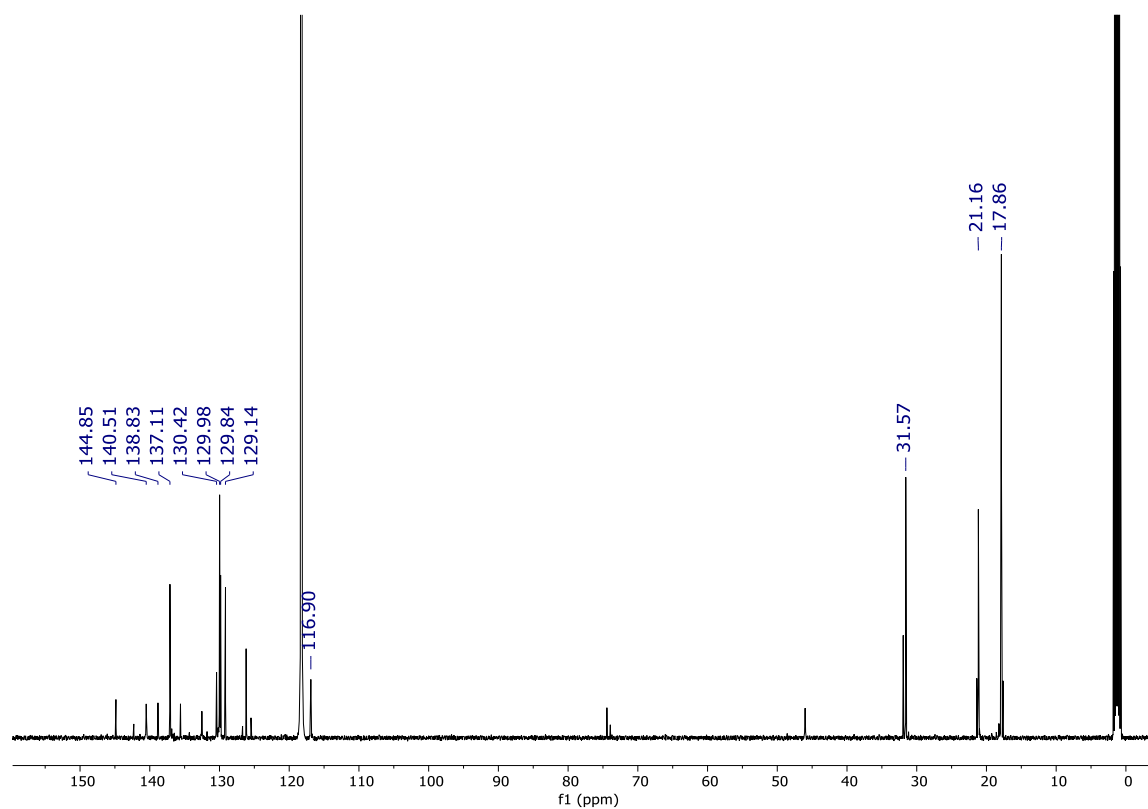
## P5

Figure S 12.  $^1\text{H}$ -NMR (big) and  $^{29}\text{Si}$  (small) spectrum of P5 recorded at 25°C in MeCN- $d_3$ .Figure S 13.  $^{13}\text{C}$ -NMR spectrum of P5 recorded at 25°C in MeCN- $d_3$ .

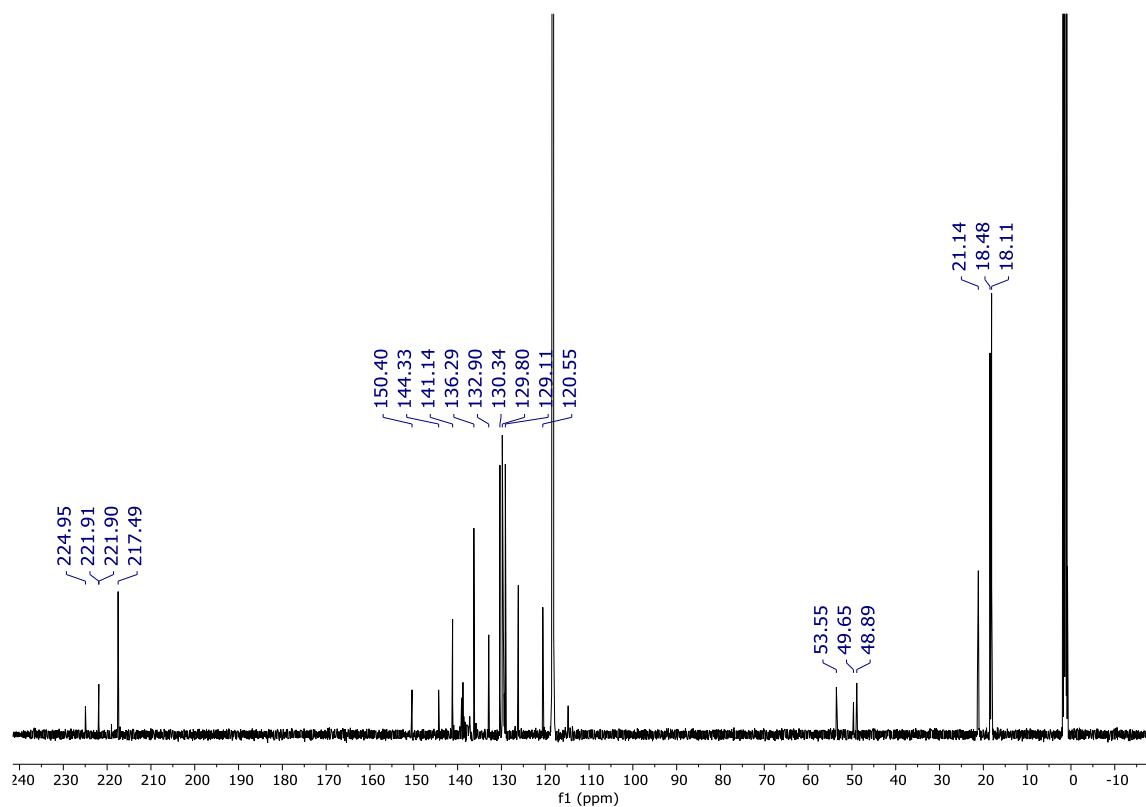
## P6

Figure S 14. <sup>13</sup>C-NMR spectrum of P6 recorded at 25°C in MeCN-d<sub>3</sub>.

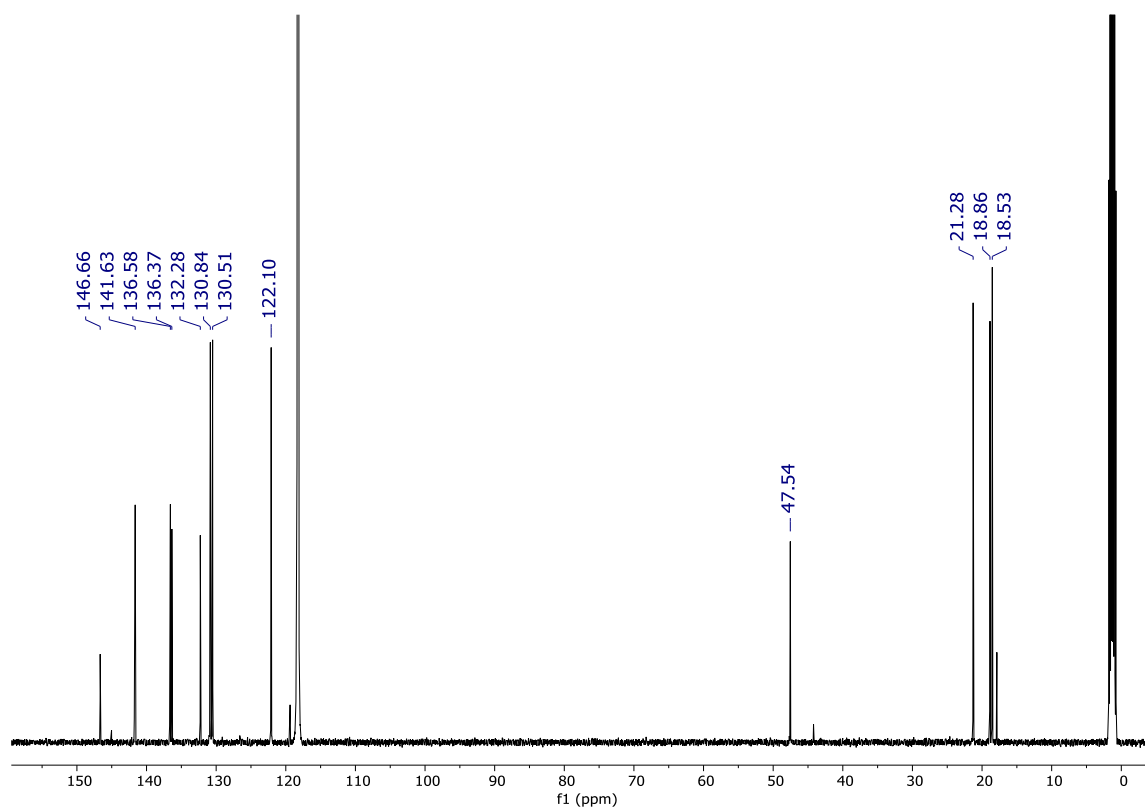
## P6B

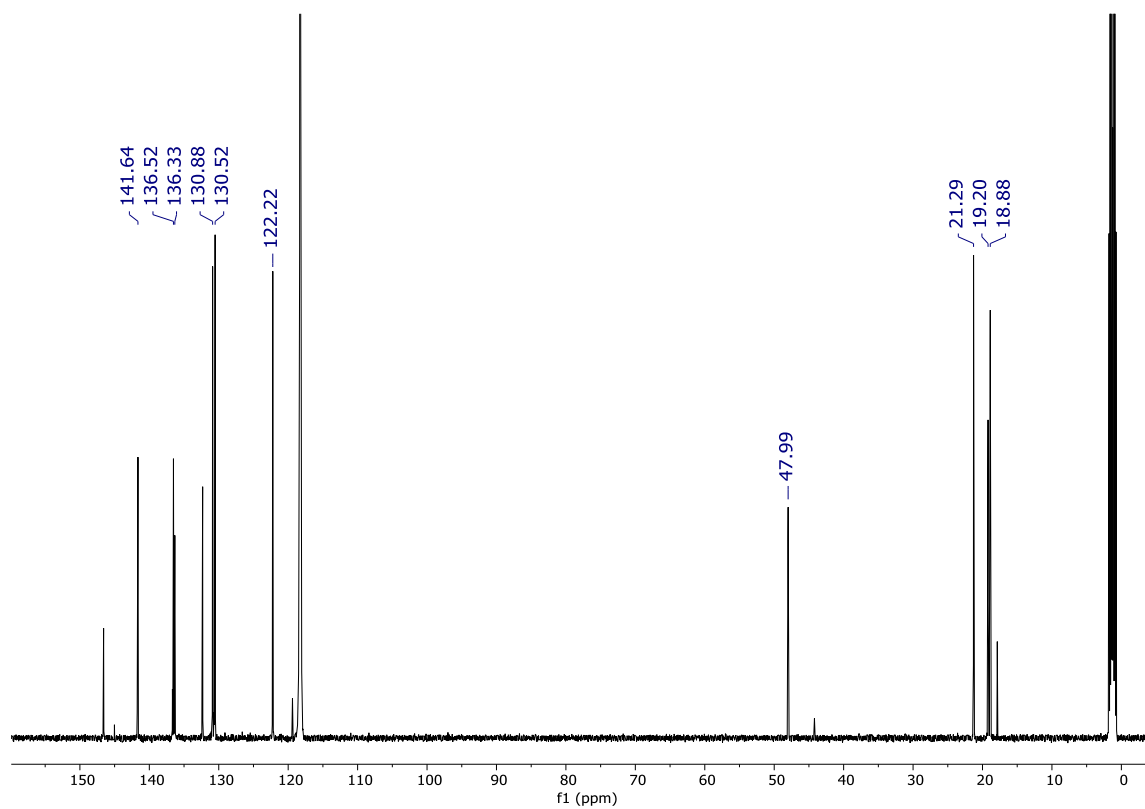
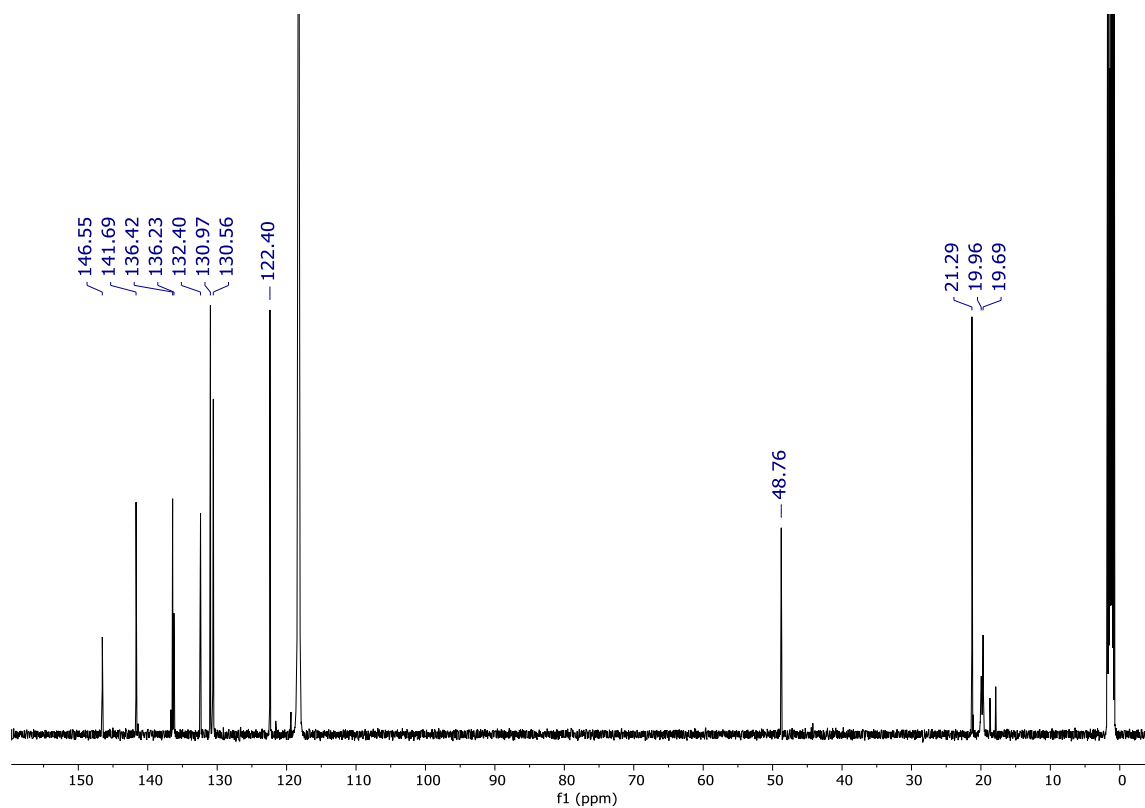
Figure S 15. <sup>13</sup>C-NMR spectrum of P6B recorded at 25°C in MeCN-d<sub>3</sub>.

## P7A

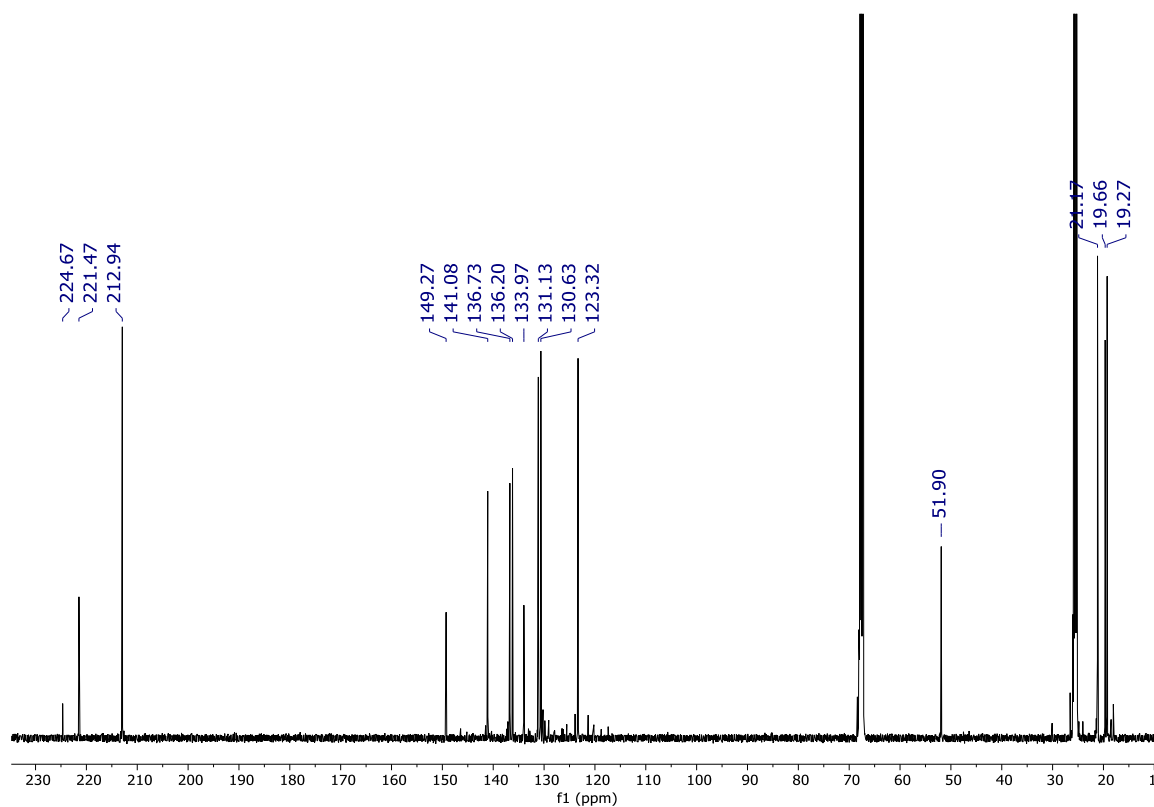
Figure S 16. <sup>13</sup>C-NMR spectrum of P7A recorded at 25°C in MeCN-d<sub>3</sub>.

## P8

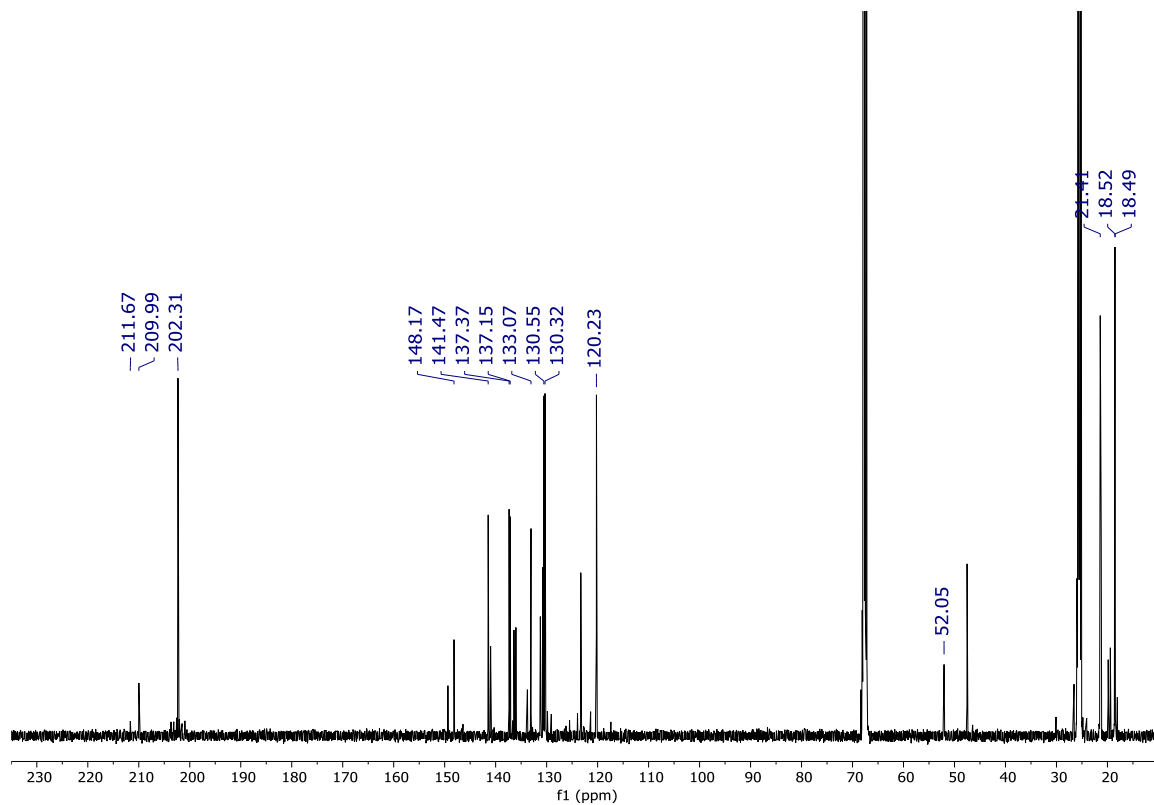
Figure S 17. <sup>13</sup>C-NMR spectrum of P8 recorded at 25°C in MeCN-d<sub>3</sub>.

**P9**Figure S 18. <sup>13</sup>C-NMR spectrum of **P9** recorded at 25°C in MeCN-d<sub>3</sub>.**P10**Figure S 19. <sup>13</sup>C-NMR spectrum of **P10** recorded at 25°C in MeCN-d<sub>3</sub>.

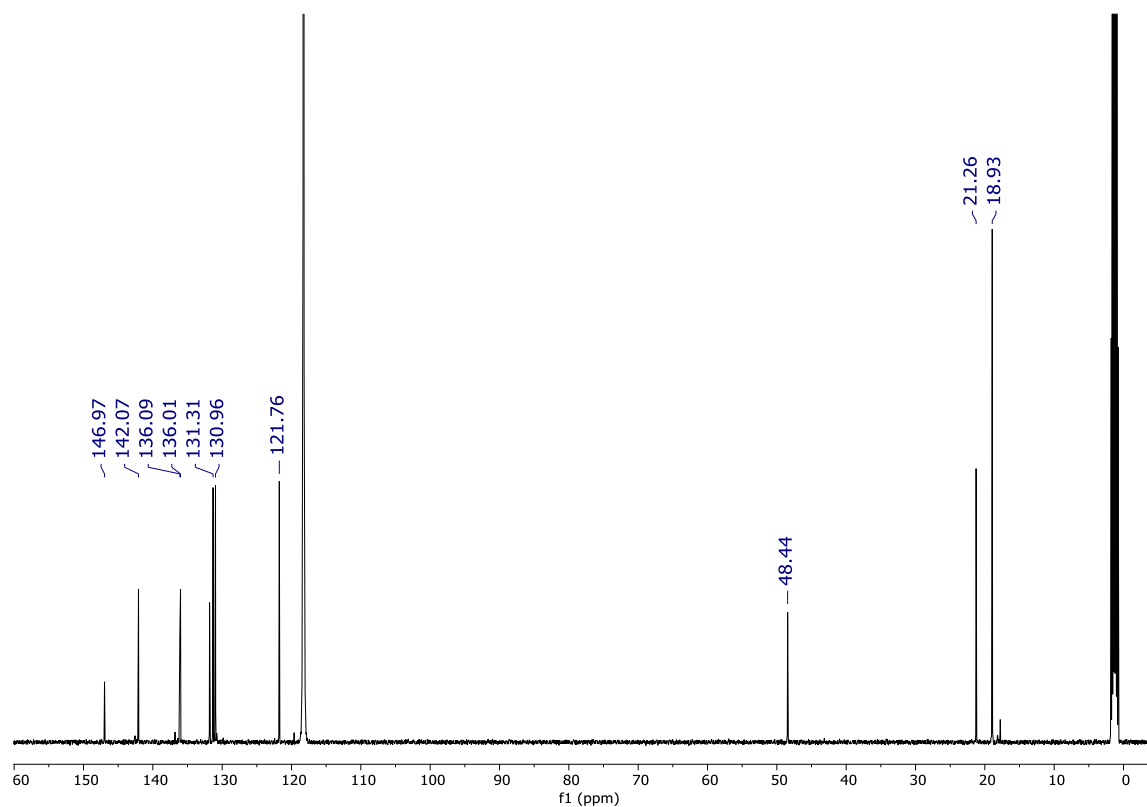
## P11

Figure S 20. <sup>13</sup>C-NMR spectrum of P11 recorded at 25°C in THF-d<sub>8</sub>.

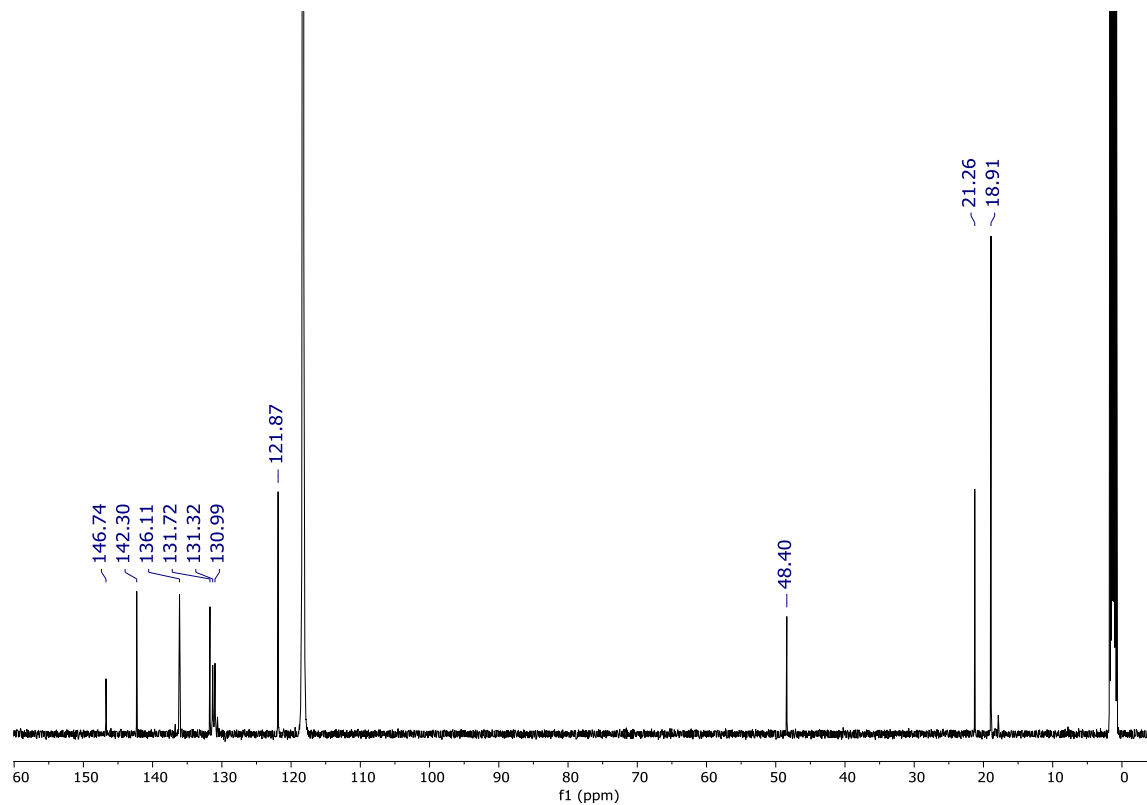
## P12

Figure S 21. <sup>13</sup>C-NMR spectrum of P12 recorded at 25°C in THF-d<sub>8</sub>.

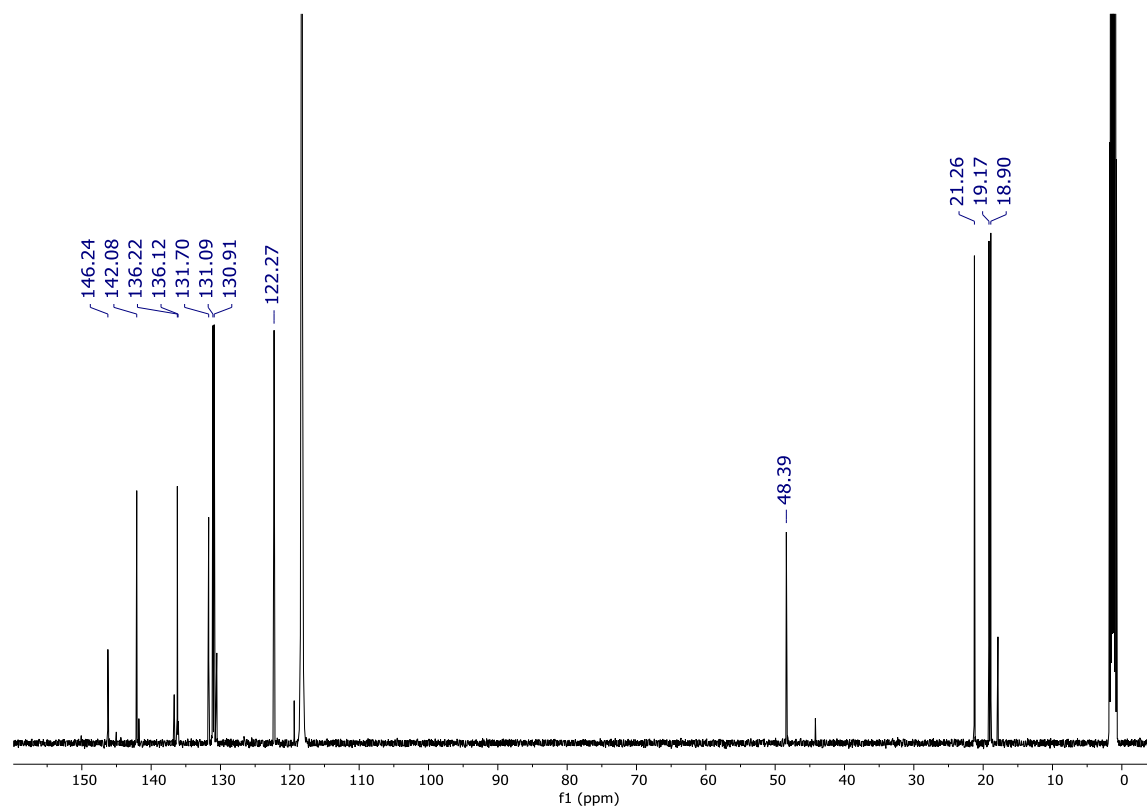
## P13

Figure S 22. <sup>13</sup>C-NMR spectrum of P13 recorded at 25°C in MeCN-d<sub>3</sub>.

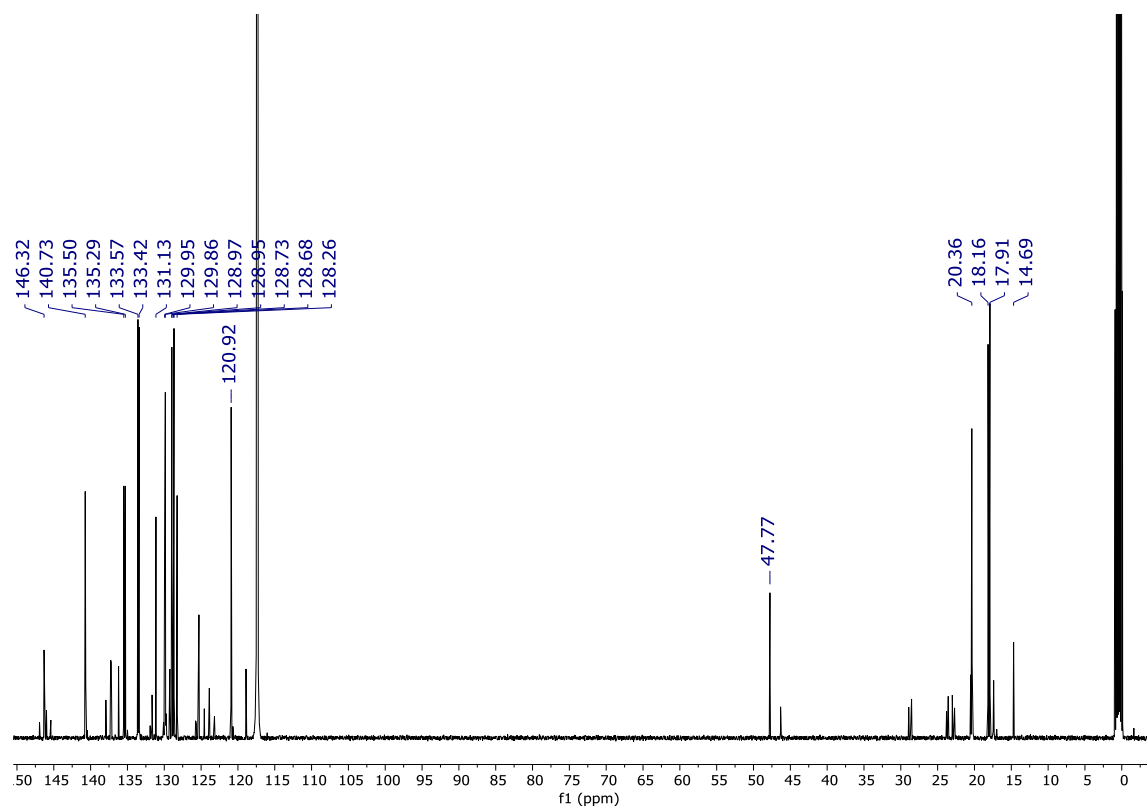
## P14

Figure S 23. <sup>13</sup>C-NMR spectrum of P14 recorded at 25°C in MeCN-d<sub>3</sub>.

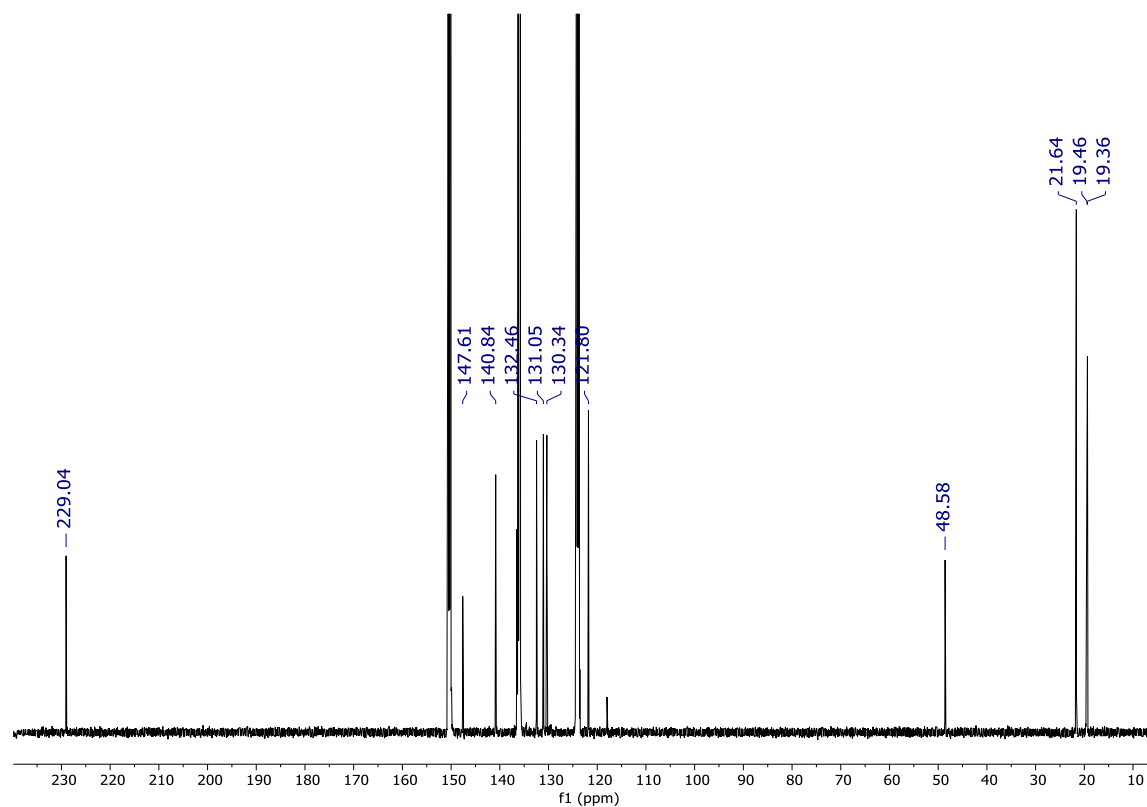
## P15

Figure S 24. <sup>13</sup>C-NMR spectrum of P15 recorded at 25°C in MeCN-d<sub>3</sub>.

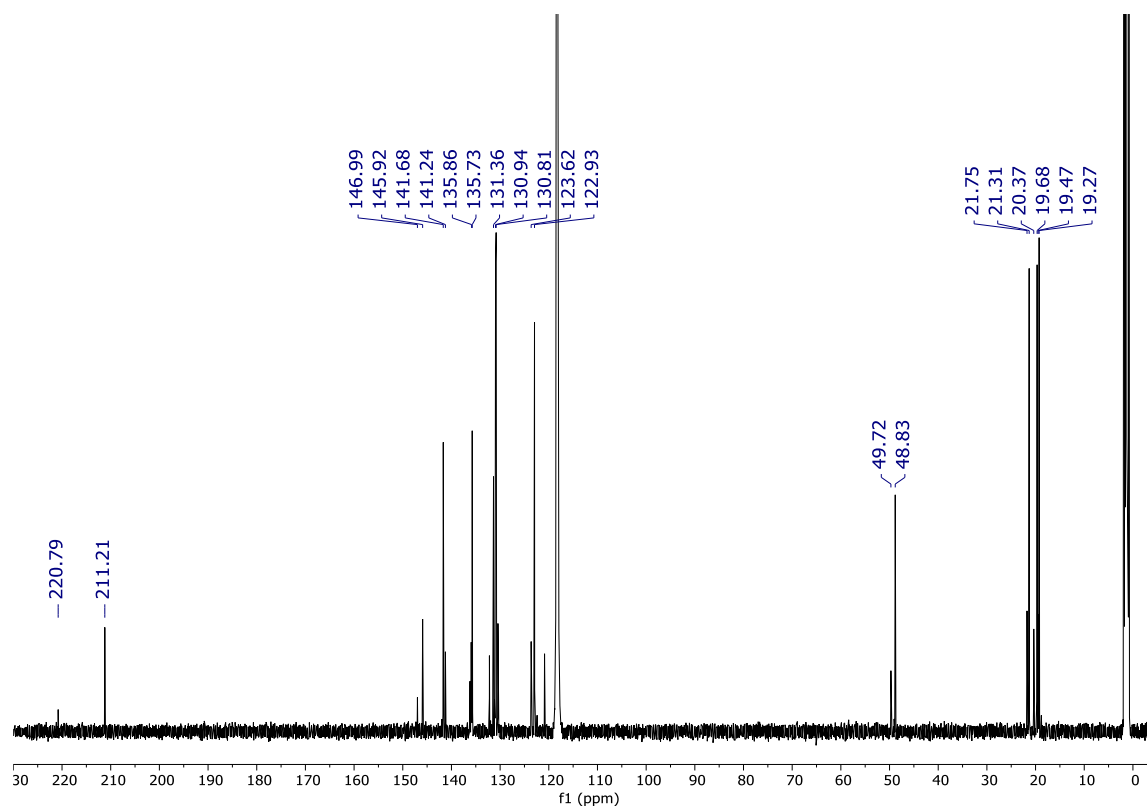
## P16

Figure S 25. <sup>13</sup>C-NMR spectrum of P16 recorded at 25°C in MeCN-d<sub>3</sub>.

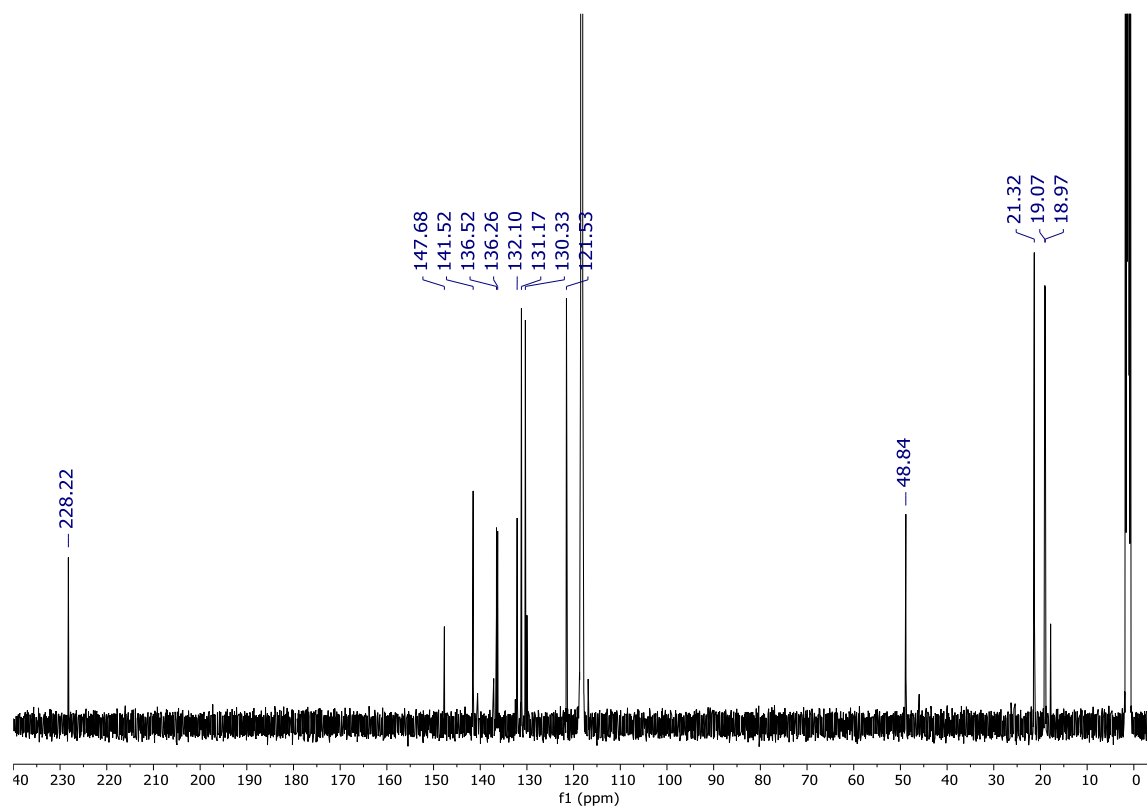
## P17

Figure S 26. <sup>13</sup>C-NMR spectrum of P17 recorded at 25°C in pyridine-d<sub>5</sub>.

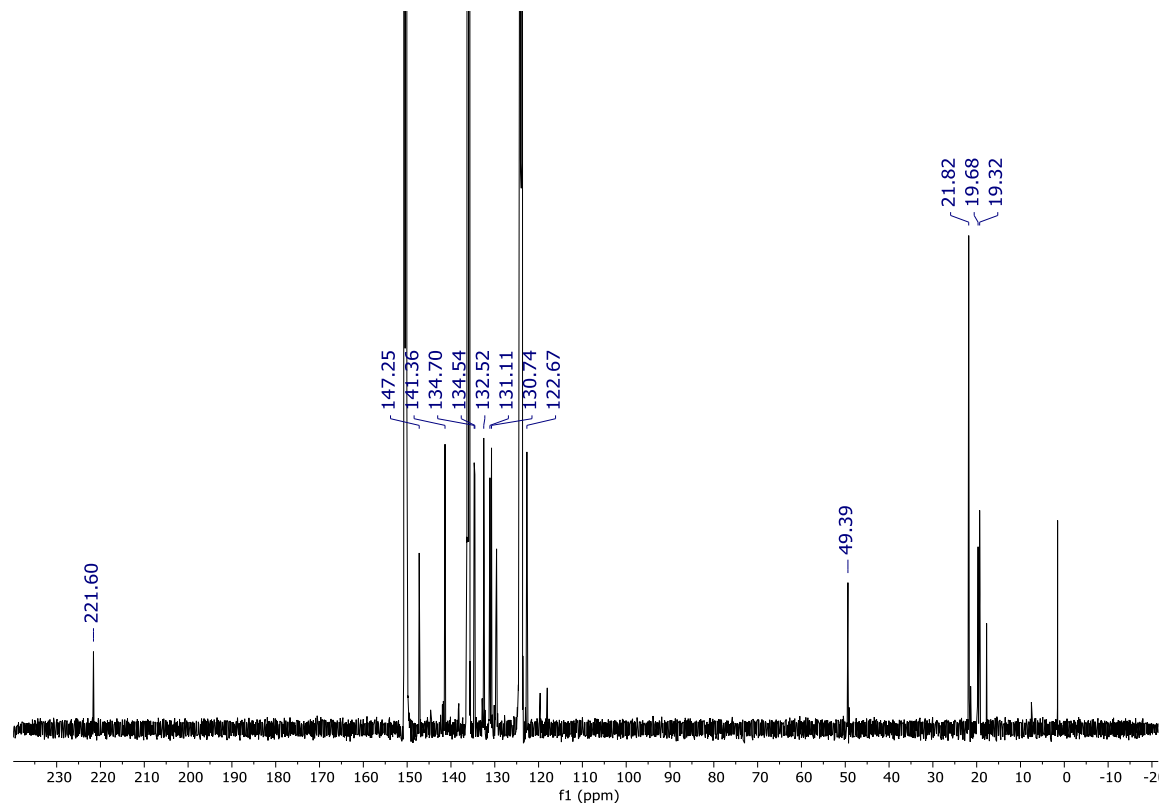
## P17A

Figure S 27. <sup>13</sup>C-NMR spectrum of P17A recorded at 25°C in MeCN-d<sub>3</sub>.

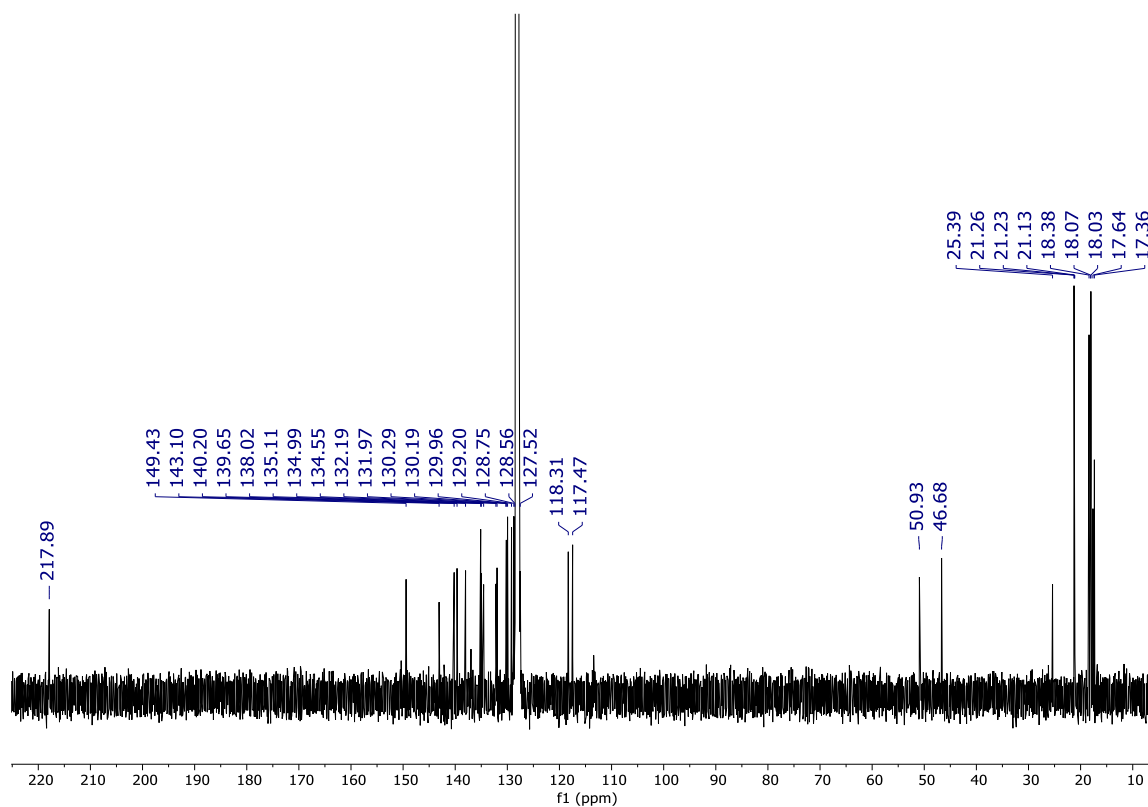
## P19

Figure S 28. <sup>13</sup>C-NMR spectrum of P19 recorded at 25°C in MeCN-d<sub>3</sub>.

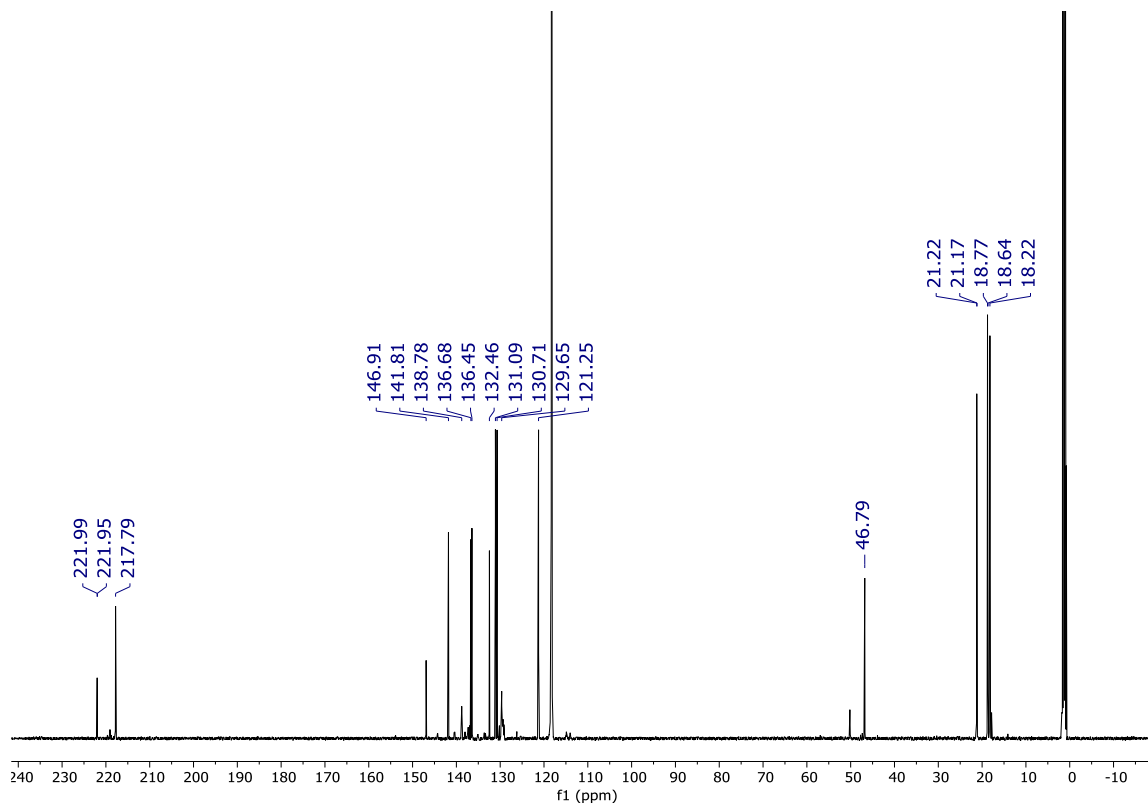
## P20

Figure S 29. <sup>13</sup>C-NMR spectrum of P20 recorded at 25°C in pyridine-d<sub>5</sub>.

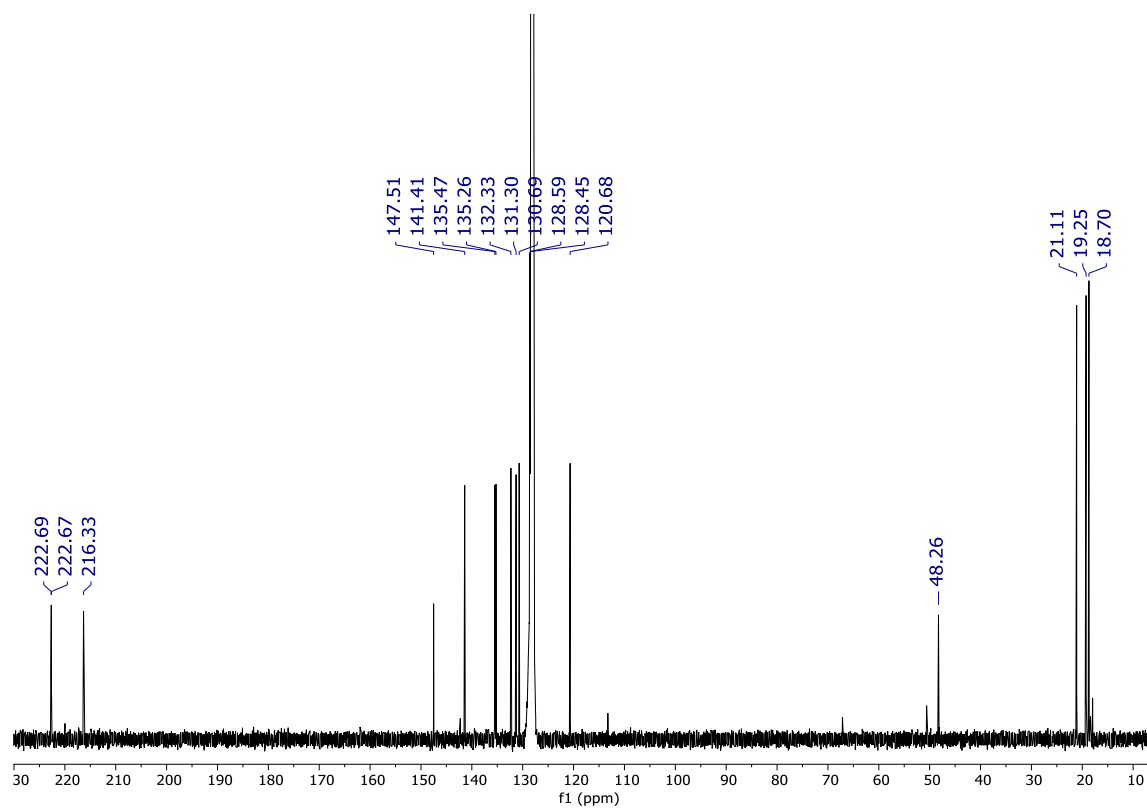
## P21

Figure S 30. <sup>13</sup>C-NMR spectrum of **P21** recorded at 25°C in benzene-d<sub>6</sub>.

## P22

Figure S 31. <sup>13</sup>C-NMR spectrum of **P22** recorded at 25°C in MeCN-d<sub>3</sub>.

## P23

Figure S 32.  $^{13}\text{C}$ -NMR spectrum of P23 recorded at 25°C in benzene- $d_6$ .

## Additional Mass Spectra

### P8

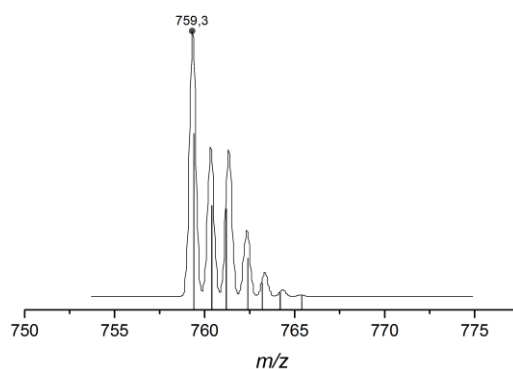


Figure S 33. ESI-MS spectrum (detail view) of **P8** (positive mode, 300 °C, -3500 V; line: measured spectrum; bars: simulated spectrum).

### P9

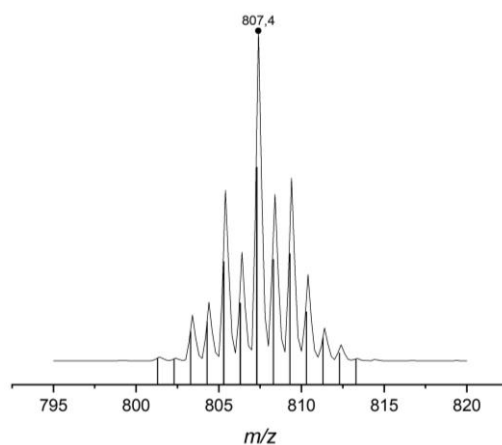


Figure S 34. ESI-MS spectrum (detail view) of **P9** (positive mode, 300 °C, -3500 V; line: measured spectrum; bars: simulated spectrum).

### P10

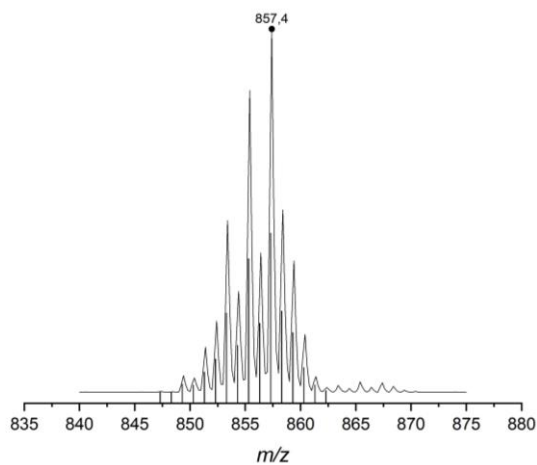


Figure S 35. ESI-MS spectrum (detail view) of **P10** (positive mode, 300 °C, -3500 V; line: measured spectrum; bars: simulated spectrum).

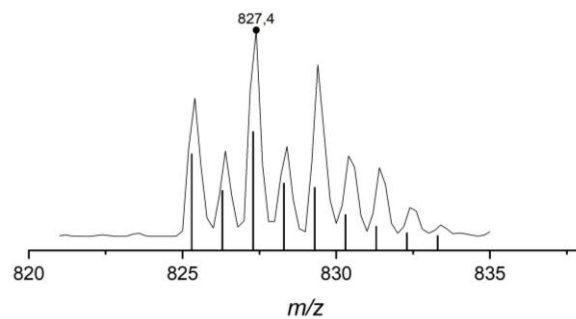
**P13**

Figure S 36. ESI-MS spectrum (detail view) of **P13** (positive mode, 300 °C, -2500 V; line: measured spectrum; bars: simulated spectrum).

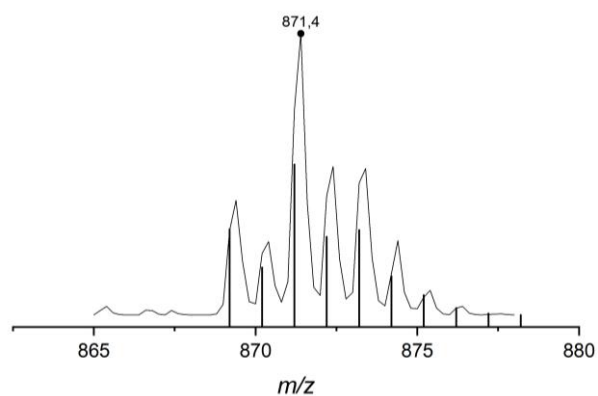
**P14**

Figure S 37. ESI-MS spectrum (detail view) of **P14** (positive mode, 300 °C, -2500 V; line: measured spectrum; bars: simulated spectrum).

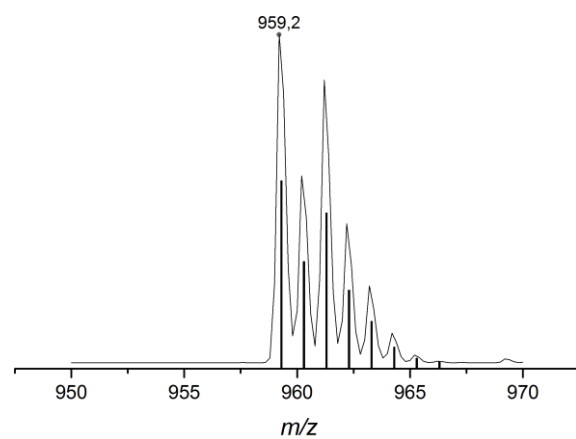
**P15**

Figure S 38. ESI-MS spectrum (detail view) of **P15** (positive mode, 300 °C, -2500 V; line: measured spectrum; bars: simulated spectrum).

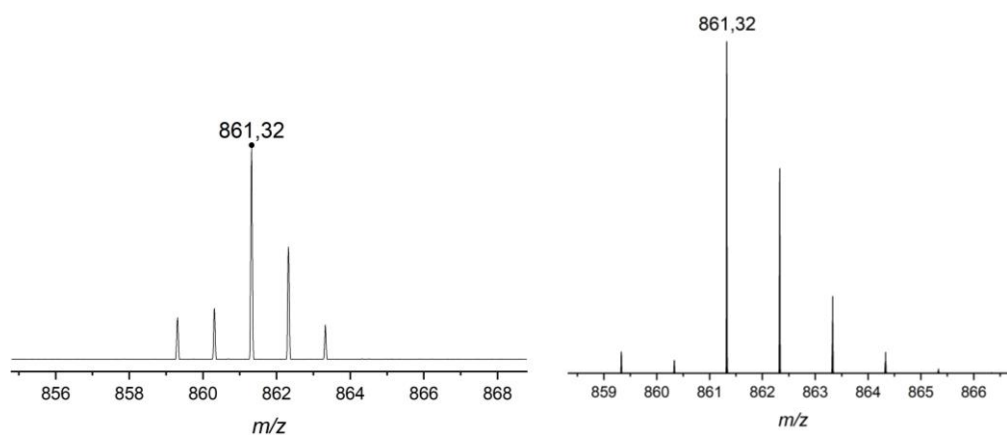
**P21**

Figure S 39. LIFDI-MS spectrum (detail view with isotope pattern) of **P21** (left: measured spectrum; right: simulated spectrum).

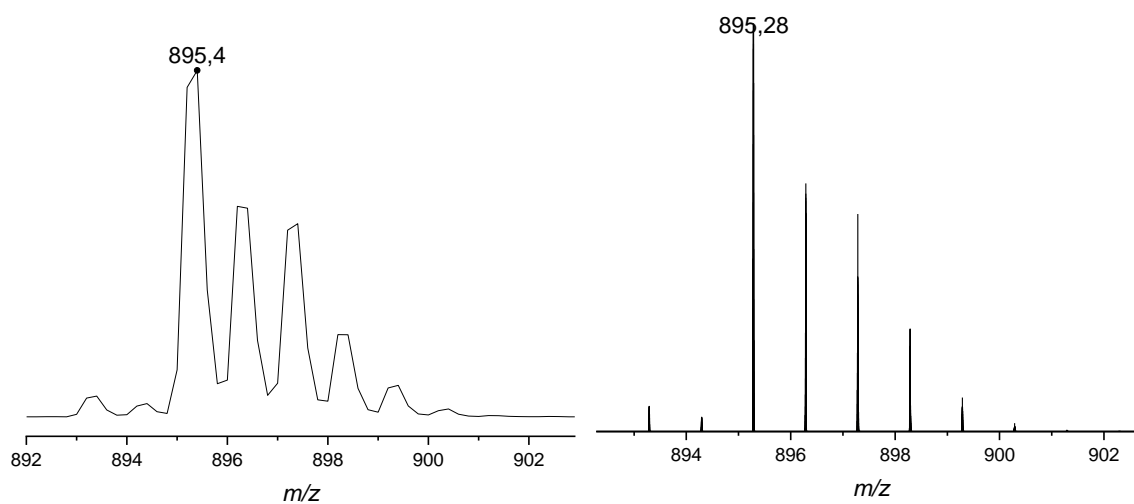
**P23**

Figure S 40. ESI-MS spectrum (detail view) of **P23** (positive mode, 300 °C, -2500 V; left: measured spectrum; right: simulated spectrum).

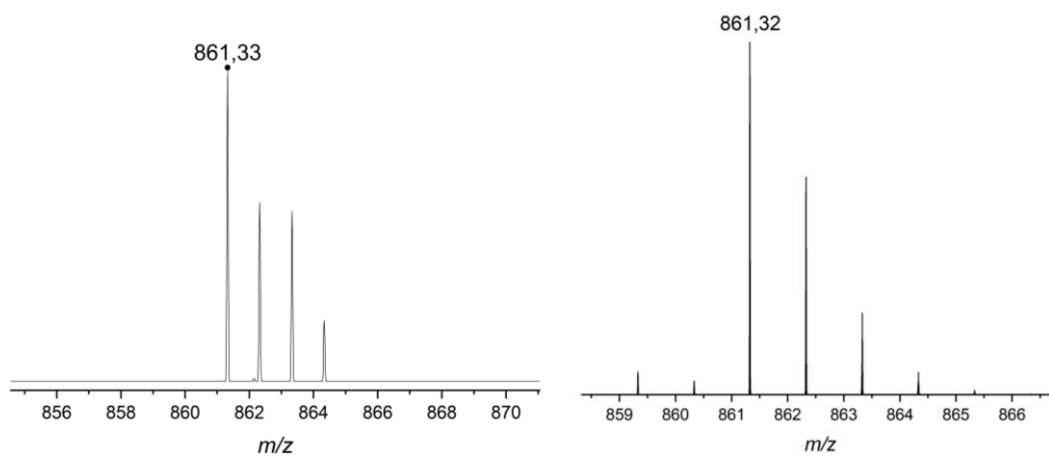
**P7A**

Figure S 41. LIFDI-MS spectrum (detail view with isotope pattern) of **P7A** (left: measured spectrum; right: simulated spectrum).